

**DEVELOPMENT AND EVALUATION OF OPERATIONAL  
STRATEGIES FOR PROVIDING AN INTEGRATED DIAMOND  
INTERCHANGE RAMP-METERING CONTROL SYSTEM**

A Dissertation

by

ZONGZHONG TIAN

Submitted to the Office of Graduate Studies of  
Texas A&M University  
in partial fulfillment of the requirements for the degree of

DOCTOR OF PHILOSOPHY

May 2004

Major Subject: Civil Engineering

**DEVELOPMENT AND EVALUATION OF OPERATIONAL  
STRATEGIES FOR PROVIDING AN INTEGRATED DIAMOND  
INTERCHANGE RAMP-METERING CONTROL SYSTEM**

A Dissertation

by

ZONGZHONG TIAN

Submitted to Texas A&M University  
in partial fulfillment of the requirements  
for the degree of

DOCTOR OF PHILOSOPHY

Approved as to style and content by:

---

Carroll J. Messer  
(Chair of Committee)

---

James Bonneson  
(Member)

---

Paul Nelson  
(Member)

---

Michael Speed  
(Member)

---

Paul Roschke  
(Interim Head of Department)

May 2004

Major Subject: Civil Engineering

**ABSTRACT**

Development and Evaluation of Operational Strategies for  
Providing an Integrated Diamond Interchange Ramp-Metering Control System.

(May 2004)

ZongZhong Tian, B.S., Northern Jiaotong University;

M.S., Northern Jiaotong University;

M.S., University of Idaho

Chair of Advisory Committee: Dr. Carroll J. Messer

Diamond interchanges and their associated ramps are where the surface street arterial system and the freeway system interface. Historically, these two elements of the system have been operated with little or no coordination between the two. Therefore, there is a lack of both analysis tools and operational strategies for considering them as an integrated system. One drawback of operating the ramp-metering system and the diamond interchange system in isolation is that traffic from the ramp, particularly if it is metered, can spill back into the diamond interchange, causing both congestion and safety concerns at the diamond interchange. While flushing the ramp queues by temporarily suspending ramp metering has been the primary strategy for preventing queue spillback, it can result in freeway system breakdown, which would affect the entire system's efficiency.

The aim of this research was to develop operational strategies for managing an integrated diamond interchange ramp-metering system (IDIRMS). Enhanced modeling methodologies were developed for an IDIRMS. A computer model named DRIVE (Diamond Interchange and Ramp Metering Integration Via Evaluation) was developed, which was characterized as a mesoscopic simulation and analysis model. DRIVE incorporated the enhanced modeling methodologies developed in this study and could be used to perform system analysis for an IDIRMS given a set of system input

parameters and variables. DRIVE was validated against a VISSIM microscopic simulation model, and general agreement was found between the two models. System operational characteristics were investigated using DRIVE to gain a better understanding of the system features. Integrated control strategies (ICS) were developed based on the two commonly used diamond interchange phasing schemes, basic three-phase and TTI four-phase.

The ICS were evaluated using VISSIM microscopic simulation under three general traffic demand scenarios: low, medium, and high, as characterized by the volume-to-capacity ratios at the metered ramps. The results of the evaluation indicate that the integrated operations through an adaptive signal control system were most effective under the medium traffic demand scenario by preventing or delaying the onset of ramp-metering queue flush, thereby minimizing freeway breakdown and system delays.

## ACKNOWLEDGMENTS

This research was conducted as part of the TransLink<sup>®</sup> research program and was performed in cooperation with the Texas Department of Transportation and the Federal Highway Administration.

The author wishes to express his sincere appreciation and gratitude to his advisory committee: Dr. Carroll Messer, Dr. James Bonneson, Dr. Paul Nelson, and Dr. Michael Speed. The author would like to express special thanks to Dr. Carroll Messer for serving as chairman of the dissertation committee and for his inspiration and encouragement during the entire course of the dissertation research. Dr. Messer's dedication to academic excellence will certainly have a significant impact on the author in pursuing his future career. Special thanks must also go to Dr. Kevin Balke for his continued guidance and support in developing the research proposal and completing the major research tasks. Many other individuals also contributed to the completion of this dissertation, including Roelof Engelbrecht and Nadeem Chaudhary, friends and colleagues at the TransLink<sup>®</sup> Center.

Finally, the author's gratitude goes to Zhuxin, his lovely wife, and Elli and Emmy, his beautiful daughters who are the main reasons behind his accomplishments.

## TABLE OF CONTENTS

	Page
ABSTRACT .....	iii
ACKNOWLEDGMENTS.....	v
TABLE OF CONTENTS .....	vi
LIST OF FIGURES.....	ix
LIST OF TABLES .....	xvi
CHAPTER I: INTRODUCTION .....	1
Background .....	1
Problem Statement .....	3
Research Objectives .....	4
Scope of Research .....	5
Organization of the Dissertation .....	6
CHAPTER II: STATE OF THE ART.....	8
Diamond Interchange Operations.....	8
Diamond Signal Phasing Schemes .....	8
Calculation of Phase Splits.....	11
Capacity and Delay Calculations .....	15
Freeway Operations and Ramp Metering.....	16
Ramp-metering System Classifications .....	17
Local Traffic-responsive Ramp-metering Algorithms .....	20
Ramp-metering Threshold.....	22
Freeway and Ramp-metering Modeling Methodologies.....	23
The Two-capacity Phenomenon on Freeway Operations .....	27
Integrated Operations .....	34
Microscopic Traffic Simulation Models .....	36
Summary .....	36
CHAPTER III: MODELING METHODOLOGIES .....	38
Integrated System and Its Major Elements .....	38
System Definition and Its Boundaries.....	38
System Variables and Parameters .....	39
Origin-destination Estimation .....	41

	Page
Enhanced Diamond Interchange Modeling.....	46
Delay and Queue Modeling for the External Movements.....	46
Delays and Queues for the Internal Movements.....	50
Freeway and Ramp-metering Operations.....	61
Ramp-metering Threshold.....	62
Freeway and Ramp Metering.....	70
Ramp Arrival Flow Profiles.....	73
Modeling Ramp Queue Spillback.....	78
Summary.....	85
 CHAPTER IV: DEVELOPMENT OF THE DRIVE SOFTWARE.....	 87
Software Features.....	87
Modules and Flow Chart.....	89
Flow Generation.....	89
A Sample Case Analysis.....	94
Summary.....	102
 CHAPTER V: DRIVE MODEL CALIBRATION AND VALIDATION.....	 104
VISSIM Model Development and Calibration.....	104
The Two-capacity Phenomenon in VISSIM.....	106
Calibration and Validation for DRIVE.....	114
Under-saturated Conditions.....	117
Over-saturated Conditions.....	122
Summary.....	128
 CHAPTER VI: ANALYSES OF SYSTEM OPERATIONAL CHARACTERISTICS.....	  130
Effect of Random Flow Variation.....	131
Effect of Ramp-metering Operation.....	133
Effect of Diamond Phasing Scheme.....	136
Effect of Controlled Arterial Right-turn.....	142
Effect of Phase Split.....	144
Effect of Cycle Length.....	146
Effect of Ramp Flow Split.....	149
Summary.....	151
 CHAPTER VII: DEVELOPMENT AND EVALUATION OF INTEGRATED CONTROL STRATEGIES (ICS).....	  153
Resource Management Philosophy.....	153

	Page
The System's Operating Objectives .....	155
Development of ICS .....	156
Low-level Integration .....	156
Non-recurring Congestion .....	157
Recurring Congestion .....	159
ICS Under Recurring Congestion .....	160
A Demand Reduction Model for Spillback Control .....	160
Basic System Requirements for Adaptive Control .....	165
Strategies with Three-Phase .....	168
Strategies with Four-Phase .....	172
ICS's Ramp-metering Component .....	173
Other Considerations for IDIRMS Components .....	175
Evaluation of ICS under Recurring Congestion .....	176
Freeway Mainline Delays and Variations .....	180
Ramp Performance .....	183
Vehicle Delays .....	195
Results with Fixed Metering .....	211
A Framework for Implementing ICS .....	213
Summary .....	217
 CHAPTER VIII: SUMMARY AND CONCLUSIONS .....	 219
Summary of Major Tasks Performed .....	219
Major Findings and Conclusions .....	220
System Operational Features and Characteristics .....	220
Model Calibration and Validation .....	221
ICS Development and Evaluation .....	222
Future Research .....	223
 REFERENCES .....	 225
 APPENDIX A: GLOSSARY .....	 235
 APPENDIX B: VAP CODE .....	 243
 APPENDIX C: TRAFFIC DEMAND SCENARIOS .....	 254
 APPENDIX D: FUNCTIONAL DIAGRAMS OF THE ICS ALGORITHM .....	 257
 VITA .....	 265



## LIST OF FIGURES

	Page
FIGURE 1 Queue spillback at a diamond interchange with ramp metering.....	2
FIGURE 2 Proposed integrated system and its boundaries. ....	6
FIGURE 3 Diamond interchange standard phase design. ....	9
FIGURE 4 Three-phase and traffic progression diagram. ....	9
FIGURE 5 Four-phase and traffic progression diagram. ....	10
FIGURE 6 Design elements for a ramp-metering system.....	17
FIGURE 7 Ramp-metering system classifications.....	18
FIGURE 8 Cumulative arrival and departure method for freeway and ramp-metering modeling.....	25
FIGURE 9 Occupancy-flow diagram.....	28
FIGURE 10 Time series flow-speed diagram.....	29
FIGURE 11 Freeway and ramp traffic demand profile.....	32
FIGURE 12 Selected numbering convention for IDIRMS. ....	39
FIGURE 13 Comparison between assumed counts and estimated flows. ....	45
FIGURE 14 Profile with residual queue and spillback (case 1). ....	47
FIGURE 15 Profile with spillback but no residual queue (case 2). ....	47
FIGURE 16 Profile without residual queue and no spillback (case 3). ....	48
FIGURE 17 Profile with residual queue and no spillback (case 4). ....	48
FIGURE 18 Arrival flow profile for the internal through movement ( <i>MA</i> ): three-phase.....	52
FIGURE 19 Arrival/departure flow profiles for the internal through movement ( <i>MA</i> ): three-phase. ....	52
FIGURE 20 Arrival flow profile for the internal left-turn movement ( <i>MIO</i> ): three-phase. ....	55

	Page
FIGURE 21 Arrival/departure flow profile for the internal left-turn movement ( <i>M10</i> ) with ramp queue spillback: three-phase.....	56
FIGURE 22 Arrival flow profile for the internal through movement ( <i>MB</i> ): three-phase.....	58
FIGURE 23 Arrival flow profile for the internal left-turn movement ( <i>M4</i> ): three-phase.....	58
FIGURE 24 Arrival flow profile for the internal through movement ( <i>MA</i> ): four-phase.....	59
FIGURE 25 Arrival flow profile for the internal left-turn movement ( <i>M10</i> ): four-phase.....	60
FIGURE 26 Arrival flow profile for the internal through movement ( <i>MB</i> ): four-phase.....	60
FIGURE 27 Arrival flow profile for the internal left-turn movement ( <i>M4</i> ): four-phase.....	61
FIGURE 28 Freeway merge and gap conditions without disturbance.....	63
FIGURE 29 Lane flow distribution: two-lane freeway.....	66
FIGURE 30 Lane flow distribution: three-lane freeway.....	66
FIGURE 31 Probabilities of no disruption.....	69
FIGURE 32 Probability of no disruption with random ramp arrival.....	69
FIGURE 33 Ramp arrival flow profile without right-turn control: three-phase.....	74
FIGURE 34 Ramp arrival flow profile without right-turn control: four-phase.....	75
FIGURE 35 Ramp arrival flow profile with right-turn control: three-phase.....	77
FIGURE 36 Ramp arrival flow profile with right-turn control: four-phase.....	78
FIGURE 37 DRIVE modules and functions.....	90
FIGURE 38 DRIVE workflow chart.....	91
FIGURE 39 Probability density functions for Poisson distribution with different $\lambda$ .....	92

	Page
FIGURE 40 Freeway mainline random demands. ....	93
FIGURE 41 Diamond interchange traffic movement random demands. ....	93
FIGURE 42 Traffic demand data for the sample case analysis. ....	95
FIGURE 43 Ramp arrival flow profiles without arterial right-turn control. ....	99
FIGURE 44 Ramp arrival flow profiles with arterial right-turn control. ....	100
FIGURE 45 Simulated ramp-metering rates. ....	101
FIGURE 46 Simulated ramp queues. ....	101
FIGURE 47 Simulated freeway capacities for the case analysis. ....	102
FIGURE 48 Traffic demand profile for achieving the two-capacity phenomenon. ....	107
FIGURE 49 Flow-occupancy diagram from VISSIM. ....	109
FIGURE 50 Speed-flow diagram from VISSIM with 20-second intervals. ....	109
FIGURE 51 Speed-flow diagram from VISSIM with 5-minute intervals. ....	110
FIGURE 52 Speed-flow diagrams from different VISSIM runs. ....	110
FIGURE 53 Capacity values from 10 VISSIM runs. ....	111
FIGURE 54 Flow-speed diagram from VISSIM without ramp metering. ....	112
FIGURE 55 Flow-speed diagram from VISSIM with ramp metering and no queue flush. ....	112
FIGURE 56 Flow-speed diagram from VISSIM with ramp metering and queue flush. ....	113
FIGURE 57 Delays with three-phase and under-saturated conditions. ....	118
FIGURE 58 Delays with four-phase and under-saturated conditions. ....	118
FIGURE 59 Freeway mainline delays with three-phase: under-saturated conditions (with queue flush). ....	121
FIGURE 60 Freeway mainline delays with four-phase: under-saturated conditions (with queue flush). ....	122

	Page
FIGURE 61 Delays with three-phase and over-saturated conditions. ....	123
FIGURE 62 Delays with four-phase and over-saturated conditions. ....	123
FIGURE 63 Freeway mainline delays with three-phase: over-saturated conditions (no queue flush). ....	127
FIGURE 64 Freeway mainline delays with four-phase: over-saturated conditions (no queue flush). ....	127
FIGURE 65 Ramp arrival and departure flows with a fixed demand. ....	132
FIGURE 66 Ramp arrival and departure flows with a stochastic demand. ....	132
FIGURE 67 Freeway throughput flows from DRIVE with traffic-responsive metering and no queue flush. ....	134
FIGURE 68 Freeway throughput flows from DRIVE with traffic-responsive metering and queue flush. ....	134
FIGURE 69 Freeway throughput flows from DRIVE with fixed metering and no queue flush. ....	135
FIGURE 70 Ramp flow profile with the three-phase scheme. ....	137
FIGURE 71 Ramp flow profile with the four-phase scheme. ....	137
FIGURE 72 Ramp queue length results with three-phase and four-phase schemes. ....	138
FIGURE 73 Traffic demands evolution during over-saturated ramp conditions: three-phase. ....	139
FIGURE 74 Traffic demands evolution during over-saturated ramp conditions: four-phase. ....	139
FIGURE 75 Residual queues from ramp spillback: three-phase. ....	140
FIGURE 76 Residual queues from ramp spillback: four-phase. ....	141
FIGURE 77 Queue length results with and without arterial right-turn movement control. ....	143
FIGURE 78 Relationship between green splits and saturated portion of green. ....	145
FIGURE 79 Queue lengths with/without phase split adjustment. ....	146

	Page
FIGURE 80 Queue length distribution histograms: 60-second cycle. ....	147
FIGURE 81 Queue length distribution histograms: 120-second cycle. ....	148
FIGURE 82 Effect of cycle length on ramp queue length. ....	149
FIGURE 83 Effect of ramp flow split on ramp queue length. ....	150
FIGURE 84 Incident within interchange. ....	158
FIGURE 85 Incident downstream of interchange. ....	158
FIGURE 86 Smoothed ramp demand profile through diamond control. ....	164
FIGURE 87 Enhanced detection system and detector layouts. ....	166
FIGURE 88 Hold internal phases with three-phase. ....	168
FIGURE 89 Hold arterial phases with three-phase. ....	169
FIGURE 90 Hold frontage road phase with three-phase and conditional service. ....	169
FIGURE 91 ICS logic and flow chart with three-phase operation. ....	171
FIGURE 92 Hold $\phi 8$ to control left-side ramp entry with four-phase. ....	172
FIGURE 93 Hold $\phi 2$ to control left-side ramp entry with four-phase. ....	173
FIGURE 94 ICS logic and flow chart with four-phase operation. ....	174
FIGURE 95 Ramp-metering component in ICS. ....	175
FIGURE 96 Freeway mainline delays and variations: medium demand. ....	181
FIGURE 97 Freeway mainline delays and variations: high demand. ....	182
FIGURE 98 Relationship between freeway breakdown and queue flush: low demand. ....	184
FIGURE 99 Relationship between freeway breakdown and queue flush: medium demand. ....	185
FIGURE 100 Relationship between freeway breakdown and queue flush: high demand. ....	186

	Page
FIGURE 101 Percent queue flush time: low demand. ....	187
FIGURE 102 Queue flush rate: low demand. ....	187
FIGURE 103 Percent queue flush time: medium demand. ....	189
FIGURE 104 Queue flush rate: medium demand. ....	189
FIGURE 105 Percent queue flush time: high demand (case A). ....	191
FIGURE 106 Queue flush rate: high demand (case A). ....	191
FIGURE 107 Percent queue flush time: high demand (case B). ....	193
FIGURE 108 Queue flush rate: high demand (case B). ....	193
FIGURE 109 Average vehicle delays with ALINEA metering: low demand. ....	196
FIGURE 110 Average vehicle delays with ALINEA metering: medium demand. ....	198
FIGURE 111 No breakdown with ICS and reduced system delay (case 1). ....	200
FIGURE 112 With breakdown and increased system delay (case 2). ....	201
FIGURE 113 Delayed breakdown and identical system delay (case 3). ....	202
FIGURE 114 Average vehicle delays with ALINEA: high demand (case A). ....	204
FIGURE 115 Average vehicle delays with ALINEA: high demand (case B). ....	206
FIGURE 116 Percent queue flush time by demand levels and control strategies: ramp 1. ....	208
FIGURE 117 Queue flush rates by demand levels and control strategies: ramp 1. ....	208
FIGURE 118 Percent flush time by demand levels and control strategies: ramp 2. ....	209
FIGURE 119 Queue flush rates by demand levels and control strategies: ramp 2. ....	209
FIGURE 120 Peak-direction freeway mainline delays by demand levels and control strategies. ....	210
FIGURE 121 System-wide delays by demand levels and control strategies. ....	211

	Page
FIGURE 122 Peak-direction freeway mainline delays by demand levels and control strategies with fixed metering.....	212
FIGURE 123 System-wide delays by demand levels and control strategies with fixed metering.....	213
FIGURE 124 IDIRMS architecture.....	215
FIGURE 125 Diagram of data flow of the proposed ICS algorithm. ....	216
FIGURE 126 Low demand scenario. ....	254
FIGURE 127 Medium demand scenario.....	255
FIGURE 128 High demand scenario. ....	256
FIGURE 129 Top level function diagram of the proposed ICS algorithm. ....	258
FIGURE 130 Diagram of functions for getting and processing detector information.....	259
FIGURE 131 Diagram of functions for determining need for integration control. ....	260
FIGURE 132 Diagram of functions for determining integration control strategy. ....	262
FIGURE 133 Diagram of functions for implementing integration strategy. ....	264

## LIST OF TABLES

	Page
TABLE 1 Ramp-metering thresholds in U.S. applications.....	23
TABLE 2 Delays with/without ramp metering and with different capacity scenarios.....	33
TABLE 3 Calculation of traffic movement demands .....	40
TABLE 4 Calculation of proportion of ramp traffic .....	41
TABLE 5 Origin-destination estimation results.....	45
TABLE 6 Determination of $V_{Mr}(t)$ values.....	80
TABLE 7 Input/output information for DRIVE .....	88
TABLE 8 Input parameters for sample calculations.....	96
TABLE 9 Output performance measures for the sample calculations.....	97
TABLE 10 Traffic demands from DRIVE and VISSIM and statistical test results .....	116
TABLE 11 Validation results for under-saturated conditions .....	120
TABLE 12 Validation results for over-saturated conditions .....	124
TABLE 13 Traffic demand scenarios for ICS evaluation.....	177
TABLE 14 Naming scheme of traffic scenarios and experimental runs.....	178
TABLE 15 Quantitative description of the traffic demand scenarios.....	178
TABLE 16 t-statistical tests comparing ramp performances: low demand.....	188
TABLE 17 t-statistical tests comparing ramp performances: medium demand .....	190
TABLE 18 t-statistical tests comparing ramp performance: high demand (case A) .....	192
TABLE 19 t-statistical tests comparing ramp performances: high demand (case B) .....	194
TABLE 20 t-statistical tests for comparing delays: low demand.....	197
TABLE 21 t-statistical tests for comparing delays: medium demand .....	199



	Page
TABLE 22 t-statistical tests comparing delays: high demand (case A).....	205
TABLE 23 t-statistical tests comparing average delays: high demand (case B).....	207

## CHAPTER I

### INTRODUCTION

#### BACKGROUND

Freeway interchanges establish interconnections between freeway systems and surface street arterials and provide the backbone of highway transportation networks. One of the most commonly used interchange types is the *tight urban diamond interchange (TUDI)*, where two traffic signals are installed on the arterial street to control the interchanging traffic (1, 2). Diamond interchanges are often characterized by complex traffic flow patterns, especially high turning movements and limited spacing between the signals, which make managing their operations difficult. To complicate matters, the majority of freeway ramp meters are located in the vicinity of freeway interchanges such as diamond interchanges. As a result, diamond interchange locations are often sources of operational bottlenecks for both surface street arterials and freeways.

One operational issue existing today is that the diamond interchange and ramp metering are primarily treated as independent elements, primarily due to jurisdictional responsibilities where the surface street arterial is managed by city or county agencies while the freeway and ramp-metering system is managed by the state department of transportation. Traffic engineers and planners typically do not consider the interactions between these two elements, nor do they consider the potential benefits that can be derived from coordinating their operations. The lack of system integration or coordination between the diamond signals and ramp metering often creates major operational concerns, among which queue spillback from the metered ramp is the most obvious. This situation is illustrated in Figure 1.

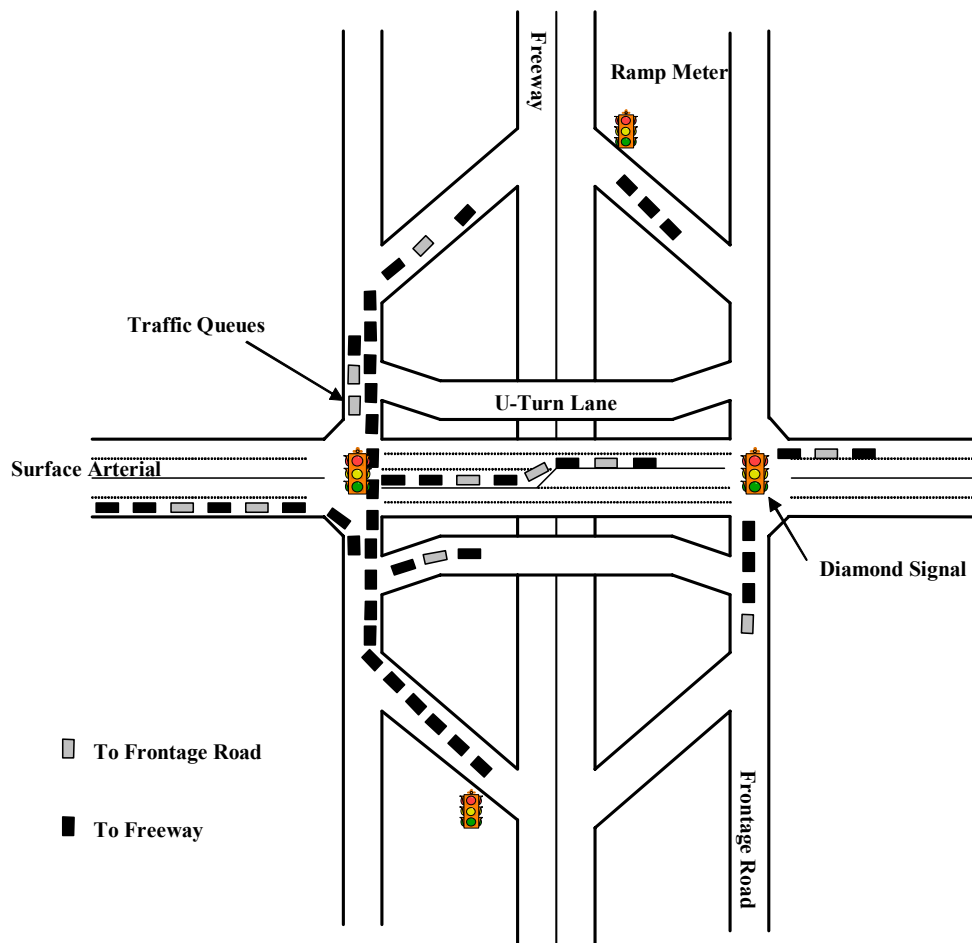


**FIGURE 1 Queue spillback at a diamond interchange with ramp metering.**

During typical rush hours, high traffic demands on the freeway often require restricted entry of traffic from the metered ramp, thus resulting in long queues on the ramp. The fact that the traffic released from the upstream diamond signal arrives in platoons also exacerbates the queue spillback effect, where limited storage spacing on the ramp cannot accommodate the short-term surge of large platoon arrivals. Unless the signal controller at the upstream diamond interchange has some way to sense the queue buildup, traffic would continue to flow to the ramp, until the queue spills back to the surface street (e.g., frontage road or the diamond signal location). Such queue spillback occurrences would interfere with the surface street operation and cause serious safety concerns.

Suggested strategies to control queue spillback generally involve some queue override policies to flush the ramp queues by either increasing the metering rate or terminating metering operations (3). However, such an operation may lead to freeway *breakdown*, a phenomenon indicated by a sudden drop in speed and perhaps in flow. Freeway breakdown results in longer vehicle delays and affects the efficiencies of the entire system. Therefore, it is of significance to explore whether providing integrated operations between a diamond interchange and ramp meters could eliminate the deficiencies of the current independent system operations.

### **PROBLEM STATEMENT**

Current operations at a diamond interchange and ramp meters lack system coordination between the two components. The lack of system coordination is reflected by the fact that little consideration is currently given to diamond operational strategies that minimize or eliminate ramp queue spillback when ramp metering is in operation. Existing diamond interchange strategies focus on serving traffic demands monitored by various traffic sensors on the diamond interchange approaches. Appropriate signal phasing and timing are then developed to best serve the traffic demands (4, 5). However, existing diamond operations completely ignore the constraints imposed by the downstream ramp meter. Excessive and non-controlled release of traffic from the diamond often results in queue spillback at the ramp meter (6).

Queue spillback resulting from the lack of coordination between the ramp meter and diamond interchange creates serious operational concerns on the diamond interchange and the surface street arterial. Although queue override policies currently being used at ramp meters can eliminate queue spillback, frequent queue flushes can lead to freeway breakdown and diminish the main purpose of ramp metering. Therefore, a need exists to address the diamond interchange, ramp-metering, and freeway components in an integrated and coordinated manner to eliminate the deficiencies of the current operations. A need exists to develop modeling methodologies and analytical procedures for analyzing the two components as an integrated system so that system performances can be adequately assessed. Integrated control strategies (ICS) need to be

developed to minimize queue spillback occurrences at the ramp meter while maintaining efficient operations for the system.

## **RESEARCH OBJECTIVES**

The goals of this research are (a) to develop modeling methodologies and analytical procedures for the integrated diamond interchange ramp-metering system (IDIRMS), and (b) to investigate strategies for operating diamond interchanges and ramp-metering systems in an integrated fashion that would reduce the deficiencies of the current operations. Specific objectives of this research include the following:

- Develop modeling methodologies and analytical procedures for estimating various performance measures (e.g., ramp queue length and system delays) for an IDIRMS, given a set of system variables and parameters (e.g., ramp-metering rates, traffic demand profile on both freeway and diamond interchange approaches, diamond signal timing, and geometric information such as spacing between the diamond and ramp meter). The overall methodology can be applied for system operations analysis, development, and evaluation of ICS aimed at minimizing queue spillback occurrences on the metered ramp.
- Use VISSIM (7), a well-calibrated microscopic simulation model, to validate the analytical procedures by comparing the performance measures produced from both the analytical procedures and microscopic simulation model.
- Identify viable ICS for IDIRMS based on a set of established system operating objectives and priorities. One example of such an operational strategy is to apply special signal timing at the diamond interchange to control traffic demands at the ramp, thus minimizing queue spillback and ramp-meter flush occurrences. The ICS should take into account the close interactions between the diamond interchange signals and the ramp meter.
- Conduct proof-of-concept evaluations, in a simulation environment, on the applicability and effectiveness of the ICS under various traffic flow conditions.

- Establish a framework for potential field implementation of the ICS at an IDIRMS, including detailed description of the system architecture, data flows, and system functions.

### **SCOPE OF RESEARCH**

This research's aim was to explore whether traffic control strategies could be developed to better manage the operations between a diamond interchange and the ramp meters immediately adjacent to that diamond interchange in an integrated fashion. This research was focused on identifying the basic relationships and developing analytical tools that could be used in the future to assess operating diamond interchanges and ramp meters as an integrated system. Development and evaluations of the ICS are limited to a simulation environment. While development of a framework for potential implementation of the control system was one of the objectives of this research, no field implementation and testing are proposed within the scope of this research.

The system configuration and its boundaries to be studied are defined in Figure 2. This is a type of diamond interchange with one-way frontage roads, typically seen in urban highways in Texas and some other states. The study also assumes that U-turn lanes are provided for both directions at the diamond interchange. The system includes a segment of freeway mainlines, ramp meters, and a signalized diamond interchange.

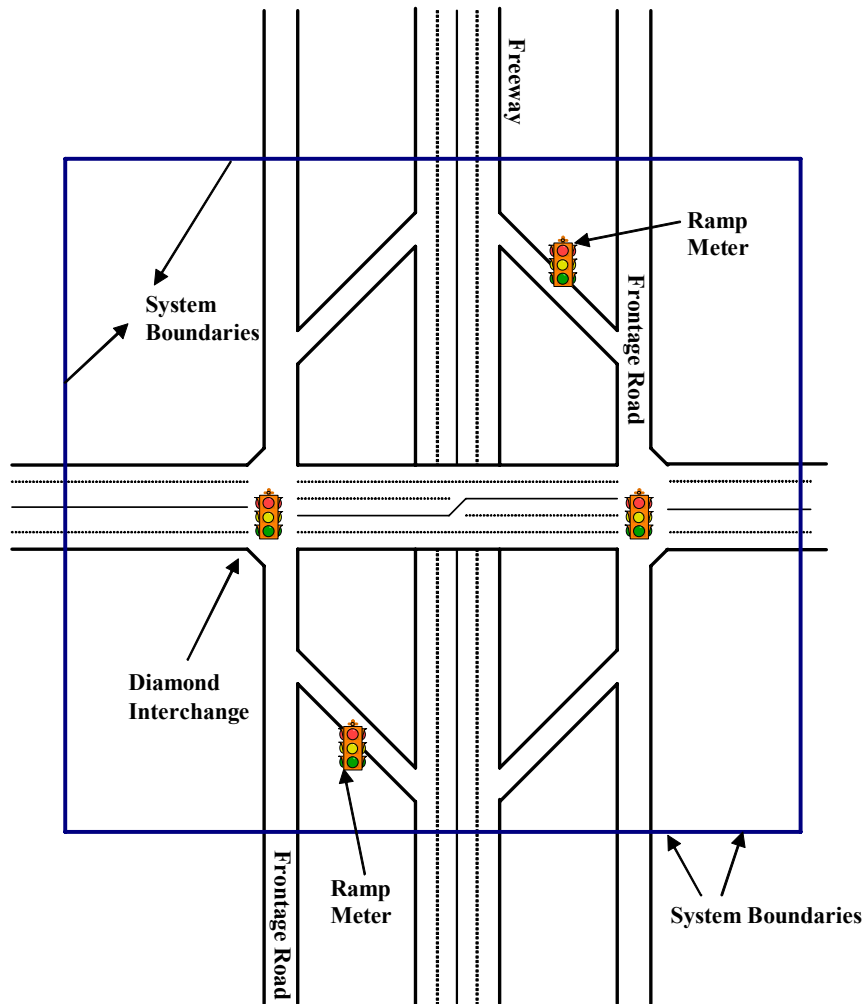


**FIGURE 2 Proposed integrated system and its boundaries.**

## **ORGANIZATION OF THE DISSERTATION**

This dissertation includes a total of eight chapters, including this introductory chapter. Chapter II includes a literature review of state-of-the-art technologies in modeling the operations of a diamond interchange, freeway, and ramp metering. Chapter III documents the enhanced modeling methodologies developed in this research for studying the IDIRMS. Chapter IV documents the development of DRIVE, a computer model that implements the modeling methodologies described in Chapter III. Chapter V provides DRIVE model calibration and validation results against both VISSIM

microscopic simulation and PASSER III (8) software. Chapter VI includes some system operational characteristics obtained from the investigations using the DRIVE software. The purpose of such investigations was to gain a better understanding of the system features to facilitate the development of ICS. Chapter VII documents the development of ICS and the evaluations of the applicability and effectiveness of the ICS using the VISSIM simulation model. Finally, Chapter VIII provides a summary and major conclusions resulting from this research.



## CHAPTER II

### STATE OF THE ART

This chapter provides a state-of-the-art literature review on studies related to modeling diamond interchanges together with freeway and ramp-metering operations. The major principle for diamond interchange operations is summarized, including phasing scheme, capacity, queue, and delay calculations. Documentation of ramp-metering practice and theory includes the ALINEA local traffic-responsive ramp-metering algorithm. The two-capacity phenomenon of freeway operations and its related studies are noted. Research on integrated operations between diamond interchange and ramp metering is provided. Finally, the applications of microscopic simulation models in studying ramp-metering issues are discussed.

### DIAMOND INTERCHANGE OPERATIONS

#### Diamond Signal Phasing Schemes

At a diamond interchange, the two traffic signals are typically controlled by a single signal controller. Figure 3 shows the standard signal phase design, which includes the standard eight phases (except for  $\phi_3$  and  $\phi_7$ ), as most signal controllers possess. Each signal phase controls a particular traffic movement. The two internal through movements are controlled using overlap phases, *A* and *B*. For example, overlap phase *A* controls the internal through movement, which receives green whenever  $\phi_1$  or  $\phi_2$  is green. A diamond interchange also applies unique signal phasing schemes to control its operations, defining the changing sequence of the signal phases and their associated traffic movements.

The two most commonly used diamond phasing schemes are basic three-phase and TTI four-phase (9), as shown in Figure 4 and Figure 5. The two phasing schemes will be simply referred to as three-phase and four-phase in the remaining chapters of the dissertation. Some signal controllers such as those manufactured by Naztec, Inc., (10)

and Eagle Traffic Control Systems, Inc., (11) have built-in functions and specifications to operate these two types of signal phasing schemes.

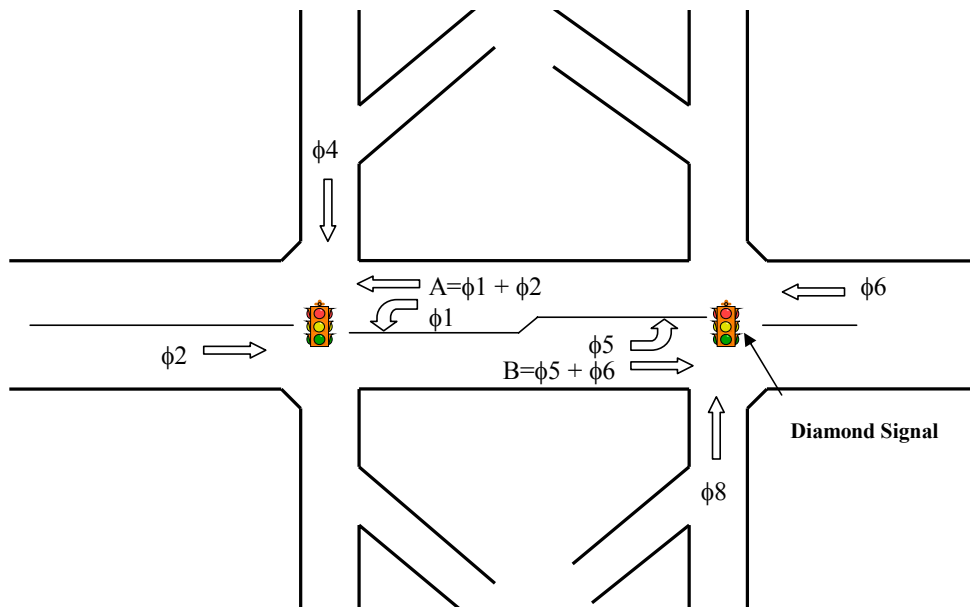


**FIGURE 3 Diamond interchange standard phase design.**

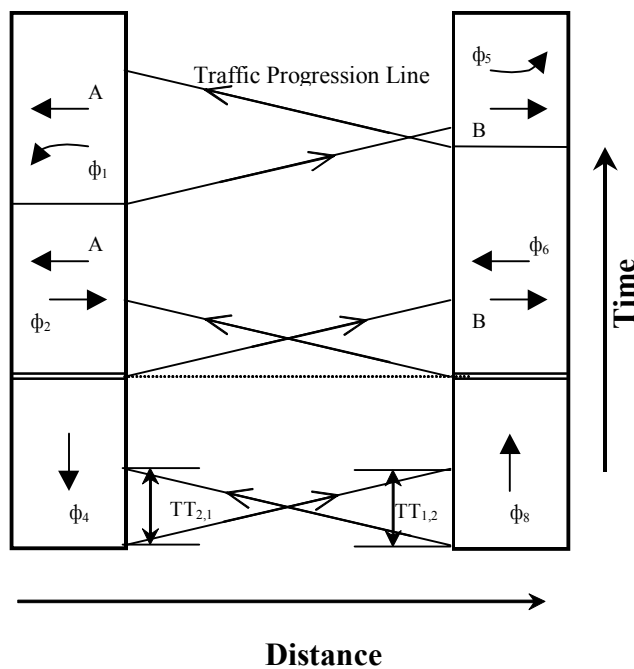


**FIGURE 4 Three-phase and traffic progression diagram.**

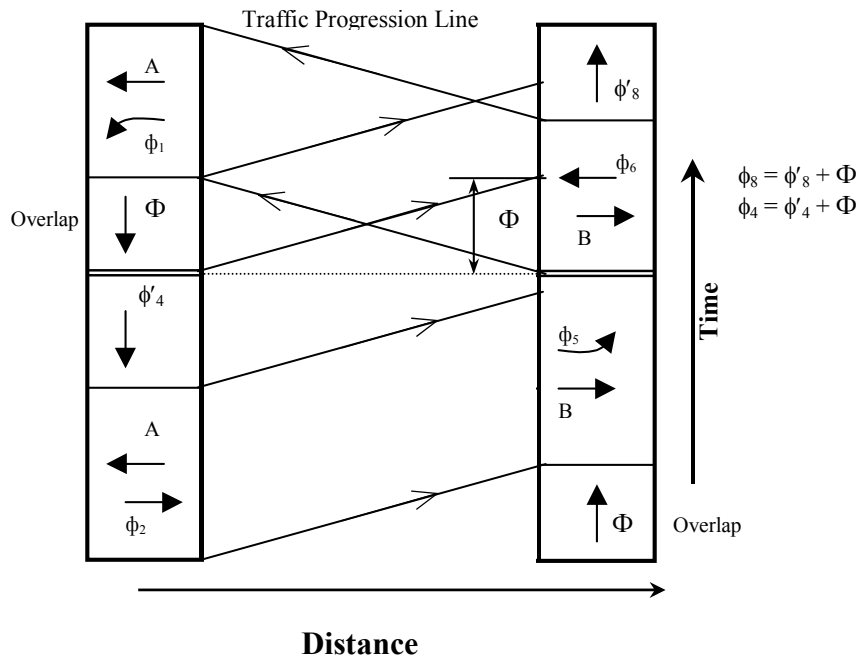


**FIGURE 5 Four-phase and traffic progression diagram.**

Three-phase uses a lag-lag phasing sequence, i.e., the arterial left-turn movement lags the through movement on both sides of the interchange and emphasizes progression for the arterial through traffic. The frontage road/ramp phases ( $\phi_4$  and  $\phi_8$ ) start and end at the same time, followed by the arterial through ( $\phi_2$  and  $\phi_6$ ) and the internal left-turn movement phases ( $\phi_1$  and  $\phi_5$ ). Three-phase operation maintains progression for the arterial through traffic, i.e., the arterial traffic going through the interchange would not stop. The arterial left-turn traffic will be stopped but can normally be cleared by the end of the cycle given sufficient green time for  $\phi_1$  and  $\phi_5$ . Some of the frontage road traffic may be stopped depending on the spacing of the interchange and the frontage road phase duration. For example, the frontage road traffic would have to stop when the phase time ( $\phi_4$  or  $\phi_8$ ) is longer than the travel time,  $TT_{1,2}$  or  $TT_{2,1}$  (see Figure 4). With the increase of spacing and travel time, the proportion of frontage road traffic to be stopped will be reduced. Therefore, three-phase is appropriate

when the frontage roads have balanced traffic demands and there are longer spacing and storage spaces for the internal left-turn vehicles.

Four-phase uses a lead-lead phasing sequence, i.e., the left-turn movements lead the through movements on both sides of the interchange, and it is aimed at minimizing internal queues. Note that the term “overlap” used in describing the four-phase scheme (see Figure 5) has a different meaning than in Figure 3. Overlap in the four-phase scheme is a dummy phase used for the purpose of efficiency while still guaranteeing traffic progression. This phasing scheme is suitable for diamond interchanges that are closely spaced. If timed appropriately, the queues in the internal interchange can be completely eliminated with U-turn lanes. There are some conditions, however, when traffic might stop. For example, the arterial through movement will not stop only if  $\phi_5$  is at least the length of  $\phi_2$ . The frontage road phase ( $\phi_4$ ) traffic will not stop only if  $\phi_6$  is at least  $2\Phi$  long.

Several computer programs are available for analyzing diamond interchange operations, among which PASSER III is specially designed for analyzing diamond interchange operations. The modeling methodologies used in PASSER III are documented next, including signal timing, capacity, and delay calculations.

### **Calculation of Phase Splits**

A well-known methodology based on the equal-degree-of-saturation principle is often used in determining phase splits at signalized intersections. The methodology was originally developed by Webster and Cobbe (12, 13), also aimed at minimizing delays at signalized intersections. The methodology has been adopted in standard procedures such as the *Highway Capacity Manual 2000* (HCM) (14) and PASSER III. A brief description of the method is given below.

Suppose there are  $n$  phases with a phase length of  $\phi_i$  for phase  $i$ . The available time to allocate among these  $n$  phases is the cycle length,  $C$ , in seconds. Phase  $i$  has a lost time of  $l_i = l$ .

$$\sum_{i=1}^n \phi_i = \phi_1 + \phi_2 + \dots + \phi_n = C \quad (1)$$

The capacity of movement  $m$  with phase  $i$  is then:

$$c_m = \frac{g_i}{C} S_m = \frac{\phi_i - l}{C} S_m \quad (2)$$

The degree of saturation for movement  $m$  with phase  $i$  is:

$$x_m = \frac{V_m}{c_m} = \frac{V_m}{S_m} \frac{C}{\phi_i - l} = y_m \frac{C}{\phi_i - l} \quad (3)$$

$$y_m = \frac{v_m}{S_m} \quad (4)$$

To achieve an equal degree of saturation:

$$X_{Cl} = x_m = y_m \frac{C}{\phi_i - l_i} \quad (5)$$

Here,  $y_m$  is taken as the critical movement in phase  $i$ , i.e., the movement in phase  $i$  that has the highest  $y_m$  value. From Equation 5 we have:

$$g_i = \phi_i - l = y_m \frac{C}{X_{Cl}} \quad (6)$$

$$\sum_{i=1}^n g_i = \sum_{i=1}^n (\phi_i - l) = C - nl = \sum_{i=1}^n y_m \frac{C}{X_{Cl}} = \frac{C}{X_{Cl}} \sum_{i=1}^n y_m = \frac{C}{X_{Cl}} Y \quad (7)$$

$$X_{cl} = \frac{C}{C - nl} Y \quad (8)$$

The green split for phase  $i$ ,  $g_i$ , can then be determined based on Equation 9, which would yield an equal degree of saturation (i.e., volume-to-capacity ratio) for the critical movements in each phase:

$$g_i = \frac{y_m}{Y} (C - nl) \quad (9)$$

### ***Phase Splits with Three-Phase***

Based on the equal-degree-of-saturation methodology described above, the phase splits with a three-phase scheme can be determined based on the following equations:

$$\phi_1 + \phi_2 + \phi_4 = C \quad (10)$$

$$\phi_5 + \phi_6 + \phi_8 = C \quad (11)$$

$$g_4 = g_8 = \max\left[\frac{y_4}{y_1 + y_2 + y_4} \times (C - 3l), \frac{y_8}{y_5 + y_6 + y_8} \times (C - 3l)\right] \quad (12)$$

$$g_i = \begin{cases} \frac{y_i}{y_1 + y_2} \times (C - g_4 - 3l), & \text{for } i = 1, 2 \\ \frac{y_i}{y_5 + y_6} \times (C - g_8 - 3l), & \text{for } i = 5, 6 \end{cases} \quad (13)$$

### ***Phase Splits with Four-Phase***

With a four-phase scheme, the phase splits are determined based on the following equations:

$$\phi_2 + \phi_4 + \phi_6 + \phi_8 = C + \Phi + \Phi = C + 2\Phi \quad (14)$$

$$\phi_1 + \phi_5 = C - \Phi \quad (15)$$

$$\phi_1 + \phi_2 + \phi_4 + \phi_5 + \phi_6 + \phi_8 = 2C \quad (16)$$

$$\phi_1 + \phi_2 + \phi_4 = \phi_5 + \phi_6 + \phi_8 = C \quad (17)$$

$$g_i = \frac{y_i}{y_2 + y_4 + y_6 + y_8} \times (C + 2\Phi - 4l) = \frac{y_i}{Y} \times (C + 2\Phi - 4l), \quad \text{for } i = 2,4,6,8 \quad (18)$$

Once  $\phi_2$ ,  $\phi_4$ ,  $\phi_6$ , and  $\phi_8$  are determined based on Equation 18 for an equal volume-to-capacity ratio,  $\phi_1$  and  $\phi_5$  are calculated by the following equations:

$$g_1 = C - \phi_2 - \phi_4 - l \quad (19)$$

$$g_5 = C - \phi_6 - \phi_8 - l \quad (20)$$

## Capacity and Delay Calculations

### *External Movements*

The basic capacity model for the external movement  $m$  with phase  $i$  is calculated using Equation 2, and the basic deterministic delay model for movement  $m$  is calculated by:

$$d_m = d_1 + d_2 + d_3 \quad (21)$$

In Equation 21,  $d_1$  is the first-term uniform delay determined based on the so-called cumulative arrival and departure method<sup>1</sup> (15, 16). This method calculates the total areas bounded by the cumulative arrival and departure curves. The cumulative arrival and departure method is the major modeling method used in this research, and the details of this method will be addressed later in the dissertation.

$$d_1 = \frac{0.5C(1 - g_i / C)^2}{(1 - \frac{g_i}{C} x_m)} \quad (22)$$

$d_2$  is the second-term incremental and over-saturation delay, counting the effects of over-saturation and assuming random arrival flow.

$$d_2 = 225 \left[ (x_m - 1) + \sqrt{(x_m - 1)^2 + 16 \frac{x_m}{c_m}} \right] \quad (23)$$

$d_3$  is the third-term delay due to an initial queue at the beginning of the analysis period.  $d_3$  would only be accurately estimated when the analysis is carried out for multiple cycles; therefore, it is often not counted in deterministic analysis procedures such as PASSER III and HCM.

---

<sup>1</sup> The cumulative arrival and departure method has also been referred to as *queue polygon* method, *supply and demand* method, *input and output* method.



### ***Internal Movements***

The traffic movements within the internal interchange have special arrival and departure patterns directly associated with the diamond interchange's type of phasing scheme. The HCM type delay model as shown in Equation 22 cannot be applied to provide accurate delay estimates. PASSER III employs a method called delay-difference-of-offset, originally developed by Wagner et al. (17, 18). The method predicts downstream vehicle arrivals on a second-by-second basis based on the offset and distance between the two signals. The delays and queues are then calculated based on the cumulative arrival and departure queue polygon method. The original paper provided a graphical description of the method. A description of the method in mathematical formulas will be provided later in the dissertation.

In general, the existing methodologies to determine diamond interchange timing, capacity, and delay are limited to analyzing an isolated interchange. No consideration on queue spillback from ramp metering is given. A number of studies have been conducted to address the impact of over-saturation and queue spillback due to adjacent signals in the arterial street (19, 20); however, no modeling procedures are available to address the potential impact of queue spillback from ramp metering on the diamond interchange operations.

### **FREEWAY OPERATIONS AND RAMP METERING**

The first ramp-metering application appeared in the early 1960s in the United States, mainly as a demonstration project (21). Major implementation of ramp metering occurred during the next decade due to ever-growing urban congestion. Currently, there are more than 20 metropolitan areas in the United States where ramp metering has been implemented (3, 22). Other countries that have also implemented ramp metering include Great Britain, Canada, Denmark, France, Germany, Japan, the Netherlands, New Zealand, and Sweden (3, 23).

Ramp metering offers several operational features for improving freeway traffic flow, safety, and air quality by regulating the flows onto the freeway system. A ramp

signal is installed on an entrance ramp, which operates in a green-yellow-red cycle or only on a green-red cycle. A metering cycle typically includes a fixed green interval, which would allow one vehicle entry per cycle. By varying the red interval, different metering cycles would result and the amount of traffic entering the freeway would be controlled. Figure 6 shows a typical ramp-metering design used in the United States. Major elements of a ramp-metering system include mainline and ramp detectors, a ramp-metering signal, and advanced warning devices. The primary (also called *excessive* or *advance*) queue detector is used as a means of implementing queue flush policies. Ramp metering operation is suspended and the ramp queue is *flushed* whenever the primary queue detector detects a queue, as specified by an occupancy threshold level. In actual field operations, there is usually a transition period after queue flush before resuming normal metering operations. During the transition period, the ramp meter would be essentially still in the queue-flush mode. However, in the modeling process to be addressed in this research, the transition period is not specifically modeled.

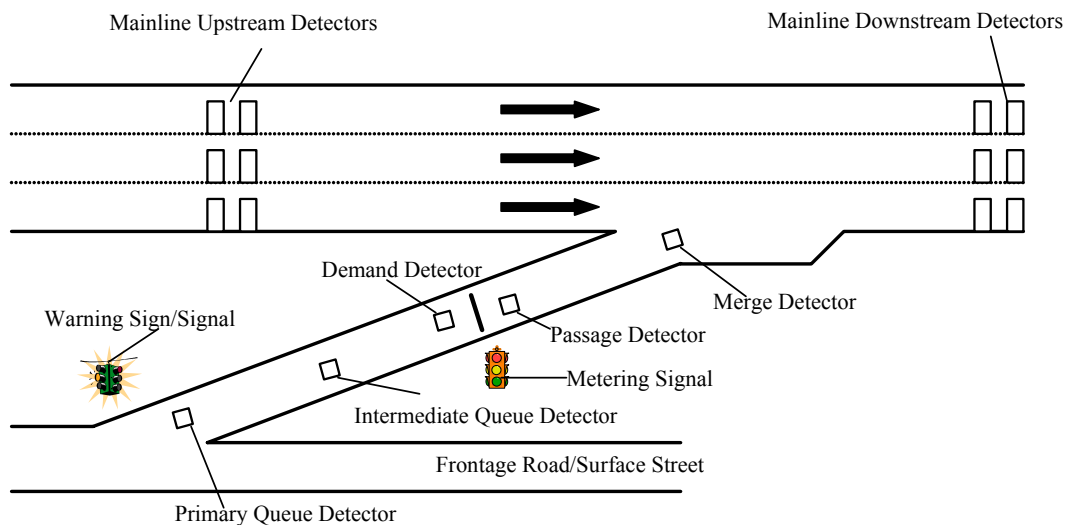


**FIGURE 6 Design elements for a ramp-metering system.**

### Ramp-Metering System Classifications

Ramp metering can be classified into various types from different perspectives. Figure 7

provides a comprehensive classification of the ramp-metering systems.

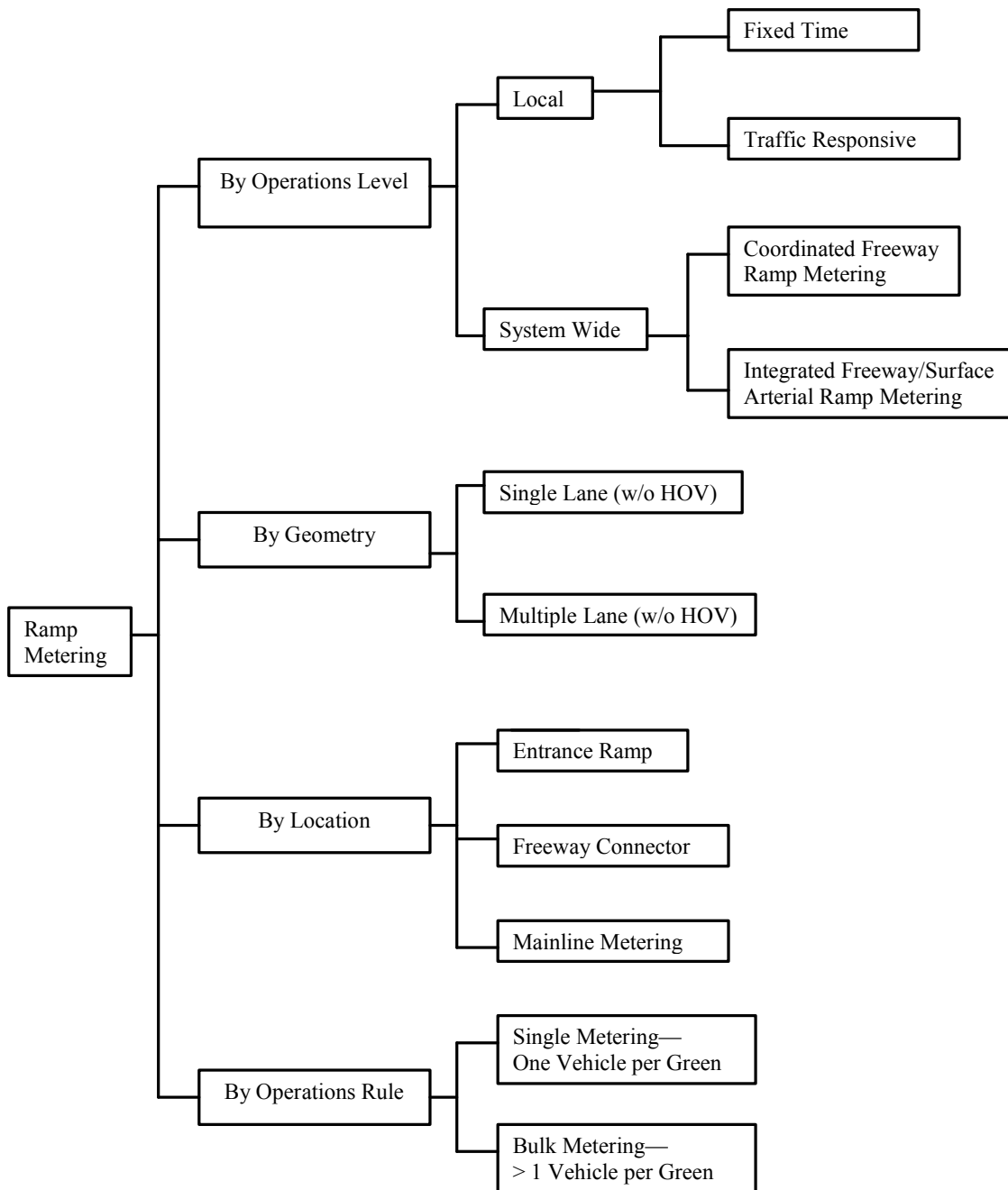


**FIGURE 7 Ramp-metering system classifications.**

There are basically four types of ramp-metering operations based on the level of complexity of the control algorithm: fixed time, local traffic responsive, coordinated freeway ramp metering, and integrated freeway/surface street system. Fixed-time metering is the simplest form and operates at a constant metering cycle. Fixed-time metering mainly serves to break up the platoons of entering vehicles into single vehicle entries, which would provide smooth freeway merge and reduce the accidents related to merging conflicts. This strategy is mostly used where traffic conditions are predictable. The major drawback of fixed-time metering is that the operations cannot react to temporary traffic fluctuations on the freeway mainline. When freeway mainline flow is low and does not warrant ramp-metering operations, ramp traffic may incur unnecessary queues and delays.

Local traffic-responsive ramp metering can automatically adjust the ramp-metering rate based on current traffic conditions in the vicinity of the ramp. Local traffic-responsive ramp metering requires detector installation on the freeway mainline. Controller electronics and software algorithms can select an appropriate metering rate based on occupancy or flow data from the ramp and mainline detectors; therefore, traffic-responsive ramp-metering systems can generally deliver better results than fixed-time metering. More detailed discussions on local traffic-responsive ramp metering are provided later in the chapter.

The coordinated freeway ramp-metering system seeks to optimize a multiple-ramp section of freeway, often with the control of a bottleneck as the ultimate goal (24, 25). Typically a centralized computer supervises numerous ramps and implements control features which can override local metering instructions. This centralized configuration allows the metering rate at any ramp to be influenced by conditions at other locations within the network. In addition to recurring congestion, system-wide ramp metering can also manage freeway incidents, with more restrictive metering upstream and less restrictive metering downstream of the incident. Such a metering system usually places higher priorities on managing freeway operations with little consideration of the surface street traffic.

The integrated freeway/surface street ramp-metering system is the highest-level ramp-metering system and has drawn significant interest in studying this subject area (6, 26, 27, 28, 29, 30, 31). Such a system attempts to maintain optimal operations for the entire corridor, which includes the freeway ramp-metering system and the adjacent surface street arterial system. Due to the fact that freeway ramp metering directly affects surface street operations, the close interaction between the ramp-metering signal and the surface street arterial signal (normally interchange signal) must be taken into consideration. As a result, the hardware requirements for this mode of operation are the most complex, requiring detectors upstream and downstream of the ramp, as well as a communication medium and central computer linked to the ramp signals and surface street signals.

In our study, the IDIRMS is better classified as a hybrid between the integrated freeway/surface street system and the local traffic-responsive system. Only a single ramp-metering location (one meter per direction) is considered, but the close interaction between the ramp-metering signal and the surface street diamond interchange signal needs to be addressed.

### **Local Traffic-Responsive Ramp-metering Algorithms**

The basic principle behind traffic-responsive metering is that real-time data are used to set the metering rate. The term “real time” actually refers to data retrieved from the previous time interval (e.g., 1-minute interval) but not at an instant. The data can be occupancy, speed, and traffic volume, as collected by mainline detectors. Various local traffic-responsive ramp-metering algorithms have been developed. The most common traffic-responsive ramp-metering algorithm is based on the concept of the demand-capacity relationship. The ramp-metering rate is regulated so that the total mainline and ramp traffic demand would not exceed the freeway bottleneck capacity at the merge or somewhere downstream of the merge. Messer (32) describes the metering algorithm in the following equations:

$$M_r(t) = \omega[c_{Fr} - F''(t)] \quad (24)$$

Applying the basic flow-density relationship, and assuming a linear relationship between density and occupancy, Equation 24 becomes:

$$M_r(t) = c_{Fr} - 2.51f_\rho\pi(t) \quad (25)$$

The algorithm now relates metering rate to occupancy, which can be directly obtained from mainline detectors. To implement the ramp-metering algorithm shown in Equation 25, a set of metering plans can be established and stored in a ramp-metering controller, with each plan having a metering rate associated with a range of occupancy values. While various metering algorithms may exist in different forms, they normally follow a similar demand-capacity principle.

The most well-known traffic-responsive ramp-metering algorithm is probably the ALINEA algorithm proposed by Papageorgiou et al. (33). The algorithm was developed based on the feedback concept of automatic control. A number of studies have also led to various modified ALINEA algorithms (34, 35). While ALINEA has been widely used in European countries, its applications in the United States is somewhat limited (23, 36, 37). The original ALINEA algorithm is described in Equation 26 to determine  $M_r(t)$ , the ramp-metering rate for the time interval  $t$ :

$$M_r(t) = M_r(t-1) + K_R[\pi_m - \pi(t)] \quad (26)$$

The ALINEA algorithm described in Equation 26 can smoothly react to traffic flow changes in the freeway mainline under both free-flow and congested conditions. The occupancy is directly related to traffic conditions. When the measured occupancy,  $\pi(t)$ , is less than the target occupancy,  $\pi_m$ , a positive value results for the second term on the right-side equation. As a result, the metering rate will be increased to allow more vehicles to enter the freeway. Similarly, the metering rate will be reduced when the measured occupancy exceeds the target occupancy value. The ALINEA algorithm also

has the advantage of easy field implementation and calibration because only the two parameters,  $K_R$  and  $\pi_m$ , need to be calibrated.

### **Ramp-Metering Threshold**

The main purpose of ramp metering is to prevent or minimize congestion on the freeway, thus reducing traffic delays. However, it is believed that ramp metering would be necessary and effective only when the freeway demand reaches a threshold value. When the freeway demand is so low that traffic from the on-ramp has no difficulty finding gaps to merge, ramp metering would not really improve freeway performance in terms of reducing congestion and delay. Therefore, there exist threshold values to warrant ramp-metering installation and to determine when ramp metering should be turned on during different time periods of the day.

In practice, the majority of U.S. cities where local traffic-responsive ramp metering has been implemented use time-of-day plans to determine the time to operate ramp metering, i.e., to turn on/off ramp meters based on preset times of the day (typically peak periods) regardless of the freeway conditions. Based on a recent survey of some major metropolitan areas where ramp metering has been implemented, only a few cities apply some kind of threshold to determine the conditions to operate ramp metering. These thresholds are shown in Table 1.

The majority of these thresholds were determined based on past experience and field observations. As can be seen, the ramp-metering thresholds used in Denver, Colorado, are actually close to capacity conditions, which might be too high to implement ramp metering. To the author's best knowledge, no literature is available to address the ramp-metering threshold from a theoretical point of view. As a part of this research, a gap-acceptance-based model was developed and will be presented in Chapter III to explore the ramp-metering threshold issue.

**TABLE 1 Ramp-metering thresholds in U.S. applications**

<b>Location</b>	<b>Metering Threshold</b>
Chicago, Illinois	Upstream Mainline Occupancy, 11.7%
Denver, Colorado	Any of the following for three consecutive minutes:  Volume: 1900 vphpl Occupancy: 20% Speed: $\leq 35$ mph
Seattle, Washington	Volume: 1200 vphpl Occupancy: 12%
Milwaukee, Wisconsin	Volume to capacity ratio (v/c): Urban area: 0.7 Rural area: 0.6~0.65

### **Freeway and Ramp-metering Modeling Methodologies**

The modeling methodologies for freeway operations with ramp metering can be classified into two major categories. The first category relates to the modeling methodologies based on the cumulative arrival and departure method (15, 16, 38, 39).

The cumulative arrival and departure method is also referred to as the demand and supply method (40) or the input and output method (16). The method has been widely used in modeling queue and delay measures at different traffic facilities. Equations 27 through 31 provide a generalized description of the cumulative arrival and departure method in a similar manner as described by Gartner (41). Given the traffic demand,  $V(t)$ , and the capacity of the facility,  $c$ , the cumulative arrival function,  $A(t)$ , the departure rate,  $O(t)$ , and the cumulative departure function,  $D(t)$ , can be determined. Subsequently, the performance measures of queue length,  $q(t)$ , and total delay,  $TD$ , can be obtained.

$$\frac{dA}{dt} = V(t) \quad (27)$$



$$\frac{dD}{dt} = O(t) = \begin{cases} c, & \text{if } A(t) > D(t) \\ V(t), & \text{otherwise} \end{cases} \quad (28)$$

$$q(t) = A(t) - D(t) \quad (29)$$

$$\frac{dq}{dt} = V(t) - O(t) \quad (30)$$

$$\frac{dTD}{dt} = q(t) \quad (31)$$

The cumulative arrival and departure method is illustrated in Figure 8 for applications in modeling freeway and ramp-metering operations. The basic principle of the cumulative arrival and departure method is to plot the cumulative vehicle arrival and departure curves. The horizontal offset between the two curves represents the delay for an individual vehicle, and the vertical offset represents the queue length at an instant in terms of the number of vehicles. The total area bounded by the two curves represents the total vehicle delays in vehicle-hour or vehicle-second.

Mathematical expressions are given in Equation 32 through Equation 34 for calculating the total delays for the freeway,  $TD_{Fr}$ , and for the ramp,  $TD_{Rr}$ , shown in Figure 8:

$$TD_{Fr} = \int [A_{Fr}(t) + D_{Rr}(t) - D_{Fr}(t)] dt \quad (32)$$

$$TD_{Rr} = \int [A_{Rr}(t) - D_{Rr}(t)] dt \quad (33)$$

$$TD_{Tr} = TD_{Fr} + TD_{Rr} \quad (34)$$

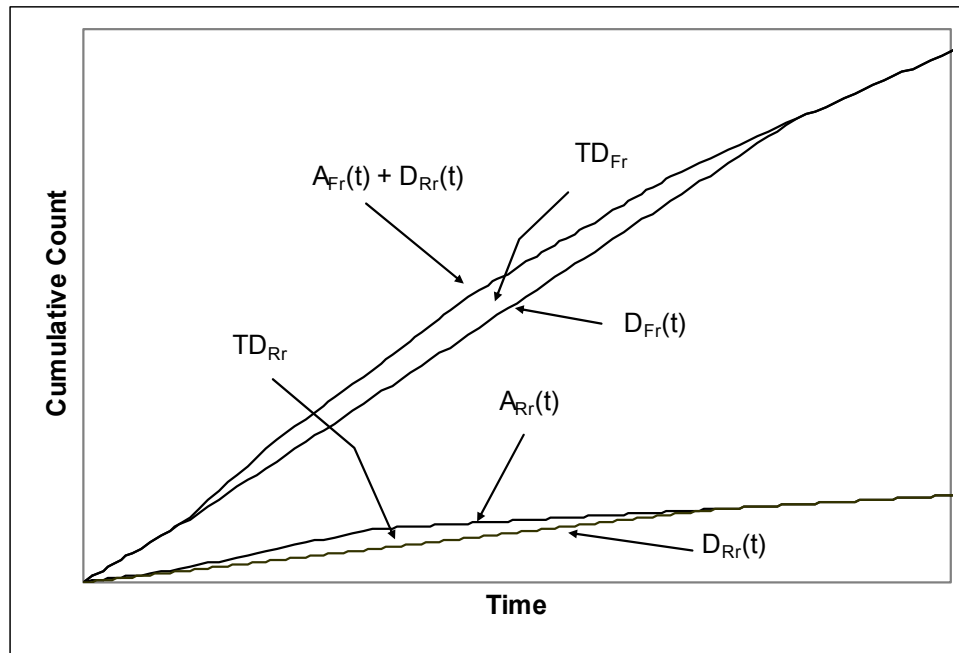


**FIGURE 8 Cumulative arrival and departure method for freeway and ramp-metering modeling.**

The cumulative arrival and departure method described above is presented in the form of continuous functions. The discrete form of the method is often used when modeling freeway operations using time steps, which will be discussed in Chapter III. The cumulative arrival and departure method can be applied to model queues and delays at any type of traffic facility. However, different facilities would have different arrival and departure patterns. For example, the departure of a traffic movement at a signalized intersection is not continuous. The arrival of traffic at a ramp meter has a platoon structure if an upstream signal exists, such as a diamond interchange signal.

The other category is related to the macroscopic models applying fluid dynamic traffic flow theories and the shockwave analysis technique (42, 43, 44, 45, 46, 47, 48, 49). The shockwave-based macroscopic models were established based on the mass conservation principle of the fluid dynamics theory, which is expressed in Equation 35:

$$\frac{\partial \rho}{\partial t} + \frac{\partial v}{\partial b} = M_r(t) - M_o(t) \quad (35)$$

In Equation 35, the relationship between traffic density,  $\rho$ , and flow rate,  $v$ , is expressed on a continuous time and space domain using the partial differential equation. The flow conservation law is maintained by considering the on-ramp flow,  $M_r(t)$ , and the off-ramp flow,  $M_o(t)$ . Equation 35 can also be expressed in the following discrete form:

$$n_k(t+1) = n_k(t) + \Delta T[v_{k-1}(t) - v_k(t) + M_{r,k}(t) - M_{o,k}(t)] \quad (36)$$

Divide both sides by the segment length  $\Delta_k$ :

$$\rho_k(t+1) = \rho_k(t) + \frac{\Delta T}{\Delta_k}[v_{k-1}(t) - v_k(t) + M_{r,k}(t) - M_{o,k}(t)] \quad (37)$$

If the flow-density relationship is known, i.e., the flow  $v_k(t)$  can be expressed by the densities such as in the form  $V[\rho_k(t), \rho_{k+1}(t)]$ , the above equation becomes a complete traffic flow model and can be solved iteratively given the initial condition of the value of  $\rho_0(0)$ . The shockwave speed at the position of segment  $k$  and time  $t$ ,  $\mu_{s,k}(t)$  is expressed by:

$$\mu_{s,k}(t) = \frac{V[\rho_{k+1}(t)] - V[\rho_k(t)]}{\rho_{k+1} - \rho_k} \quad (38)$$

Alternatively, a traffic flow model can be established if the flow-speed relationship is known, such as in the form  $\mu_k(t) = U[\rho_k(t)]$ . Then, the flow rate can be derived based on the fundamental relationship among flow, speed, and density:

$$v_k(t) = \rho_k(t) \cdot \mu_k(t) = \rho_k(t) \cdot U[\rho_k(t)] \quad (39)$$

The flow-density relationship and the speed-density relationship have drawn significant research interest and have resulted in various traffic flow models for freeway operations with ramp metering. In this research, the cumulative arrival and departure method was used in modeling the freeway and ramp-metering components in the IDIRMS. Therefore, the details of the shockwave-based models are not further documented.

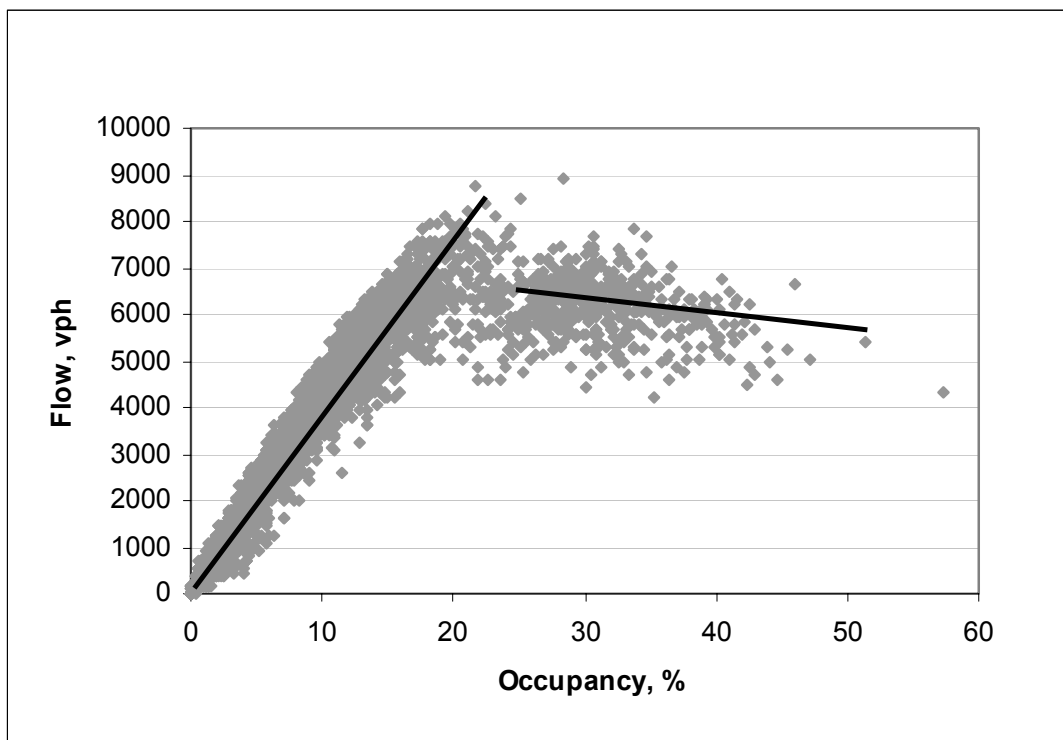
While the cumulative arrival and departure method and the shockwave-based method would yield different queue length estimations, several researchers have demonstrated the compatibility of the two methods in estimating travel time and delays on freeway facilities (16, 50). The cumulative arrival and departure method is the primary modeling methodology used in this research.

### **The Two-Capacity Phenomenon on Freeway Operations**

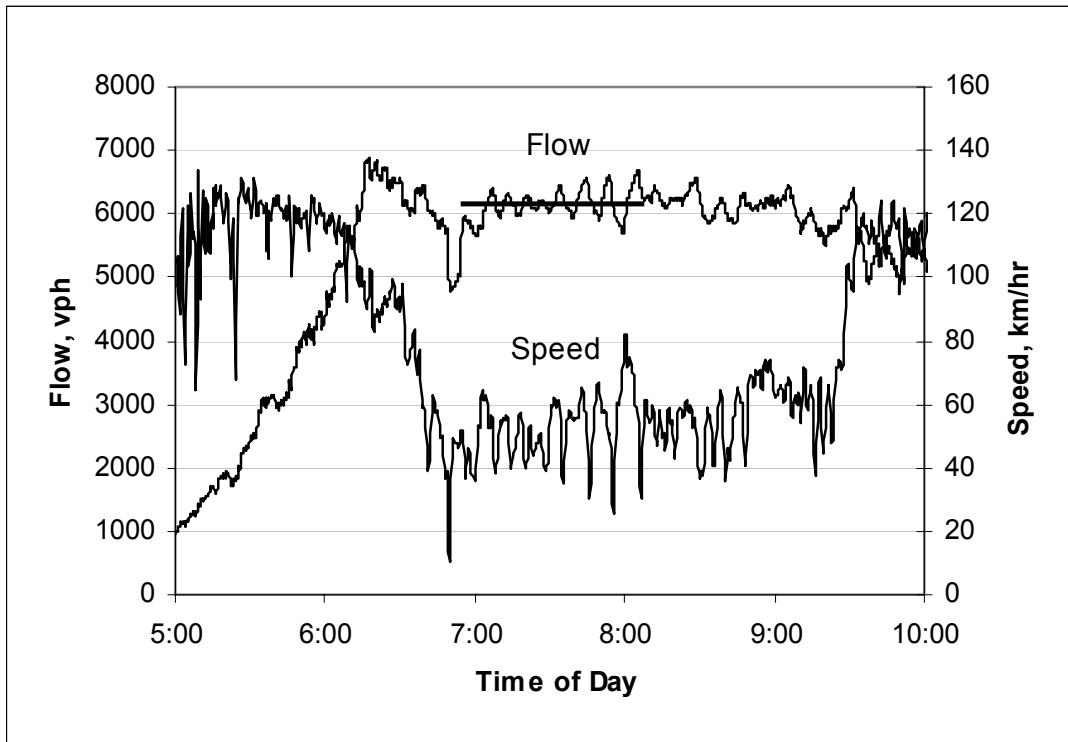
Unlike other traffic facilities, freeways have a unique operational feature described as the two-capacity phenomenon, suggesting that freeway capacity has two distinctive regimes: the capacity value during free flow and the capacity value during congested flow measured at an *active bottleneck* location (51, 52). An active bottleneck, as originally defined by Daganzo (53) is a bottleneck that is not influenced by another bottleneck further downstream. The two capacities are defined as the free-flow capacity,  $c_F$ , and the queue-discharge capacity,  $c_Q$ . The transition from the free-flow condition to the congested condition is often referred to as freeway *breakdown*, characterized by a sudden speed drop, an increase in density, and perhaps a drop in flow rate (54).

Figure 9 and Figure 10 illustrate the breakdown scenario and the two-capacity phenomenon, which are based on field detector data collected by the Ministry of Transportation of Ontario, Canada, upstream of an active freeway merge bottleneck near the Cawthra Rd./Queen Elizabeth Way interchange (55). Figure 9 is a plot of occupancy versus flow. Two distinctive regions, the free-flow region and the congested region, can be clearly seen. A disconnection between the two regions can also be

observed. Lower flow rates can be noticed under the congested region than the highest flows that can be achieved under the free-flow region. Figure 10 is a time series plot of the flow and speed. At about 6:20 a.m., the freeway experienced a sudden drop in speed, indicating the start of breakdown. A lower flow rate under breakdown can be clearly seen. While much higher flows can be achieved with 20-second aggregation, the capacity flow is often measured at a much longer time interval, for example, a 15-minute period as defined in the HCM.



**FIGURE 9 Occupancy-flow diagram.**



**FIGURE 10 Time series flow-speed diagram.**

A significant number of publications have been devoted to studying the two-capacity phenomenon. While the majority of the studies have confirmed the two-capacity phenomenon, there has been disagreement on the level of capacity reduction once breakdown occurs. Hall and Agyemang-Duah (51) emphasize the importance of how the flows should be measured. Firstly, the bottleneck location where flow is measured has to be free from downstream congestion, i.e., any queuing and flow drop should be solely caused by the freeway merge itself, not the congestion from another downstream bottleneck. Secondly, the flow measurement location should not be upstream of the merge because it would not reflect the true capacity due to part of the capacity being consumed by the ramp traffic. Thirdly, the time interval for flow measurement is also critical. Although much higher flows could be achievable within a shorter time period, the flow rate for determining the capacity should be measured over a prolonged period, such as at least 15 minutes as defined in the HCM for capacity flow.

Another important point that Hall and Agyemang-Duah made was that the measurement of pre-breakdown flow should be restricted to the period when demand is close to capacity.

Complying with the above conditions, Hall and Agyemang-Duah selected a freeway merge site in Toronto, Canada, and concluded that the two-capacity phenomenon does exist and the capacity drop after breakdown is about six percent based on the study site. The literature that supports the two-capacity phenomenon includes studies by Cassidy and Bertini (56), Persaud et al. (54, 57), Lorenz and Elefteriadou (58), and Zhang and Levinson (59). These studies report that the range of capacity drops between two percent and 16 percent once breakdown occurs. There are also many unpublished documents based on field observations to support the two-capacity phenomenon (60, 61, 62).

On the other hand, literature was also found to dispute the two-capacity phenomenon, among the most prominent of which is probably the papers by Banks (52, 63). He studied the two-capacity issue using the data collected at four sites in San Diego, California. Although he supported the existence of the two-capacity phenomenon while examining the flows on individual lanes, he concluded that there is no evidence that the flows are significantly different once breakdown occurs when looking at traffic across all the lanes. He actually found that the flows increased after breakdown occurred in three out of the four sites examined. Ringert and Urbanik (64) studied the freeway breakdown issue at three freeway merge locations in Texas. They found that the queue-discharge flow was higher at one site, lower at one site, and no different at another site.

By examining the methodologies used in these studies, a few factors are suspected to have led to their conclusions. For example, Banks used a data collection point upstream of the merge (i.e., a location that does not include the ramp flows), which may not have reflected the true freeway capacity. The higher queue-discharge flows may be due to the measurement of pre-breakdown flow that had not reached its

capacity level, which might be encountered often. Strictly speaking, the true free-flow capacity should not be lower than the queue-discharge capacity if the two-capacity phenomenon exists.

Nonetheless, all the literature tends to agree that freeway breakdown is probabilistic in nature, i.e., freeway breakdown could occur at different flow levels (54, 57, 58, 65). Random variations exist for the flows under both free-flow and queue-discharge-flow conditions. Generally, the variations in the queue-discharge flows are smaller than those before breakdown.

One of the major purposes of ramp metering is to maintain the freeway in the free-flow region by controlling vehicle entry to the freeway so that freeway demand does not exceed its bottleneck capacity. In fact, it is the two-capacity phenomenon that determines the significance of ramp-metering applications. If no two-capacity phenomenon exists and freeway capacity is a single value, ramp metering itself would not achieve any reduction on overall system delay.

Consider the case when the total freeway demand without ramp metering (i.e., mainline demand,  $V_{Fr}$ , plus ramp demand,  $R_r$ ) is greater than the freeway capacity, but the total demand with ramp metering (i.e., mainline demand,  $V_{Fr}$ , plus ramp metering rate,  $M_r$ ) is less than the freeway capacity. When ramp metering is in operation, the freeway would actually have a throughput of  $V_{Fr} + M_r$ , which is lower than the throughput of  $c_{Fr}$  when metering is not present. With ramp metering in operation, the freeway capacity may be under-utilized, thus resulting in higher overall delays for the entire system. The excessive delays would be primarily imposed on the ramp traffic. A numerical example is given below to illustrate this point.

Figure 11 illustrates a 1-hour traffic demand profile at the freeway mainline and the ramp. A single regime capacity of 6500 vehicles per hour (vph) is assumed for the freeway bottleneck location, and a fixed ramp-metering rate of 1200 vph is also assumed. The illustrated traffic demand profile indicates that during the initial ten minutes of the analysis period, the freeway mainline demand of 5000 vph plus the ramp



demand of 2000 vph exceed the freeway bottleneck capacity of 6500 vph. Without ramp metering, the throughput at the freeway bottleneck would equal its capacity of 6500 vph. Assuming that the ramp traffic and the mainline traffic have the same priority to be serviced, the delay would then occur to both the mainline traffic and the ramp traffic. However, with ramp metering in operation, the total demand at the freeway bottleneck would be the mainline demand 5000 vph plus the ramp-metering rate 1200 vph, which is less than the freeway bottleneck capacity 6500 vph, resulting in under-utilization of the freeway capacity. In this case, delay would occur only to the ramp traffic.

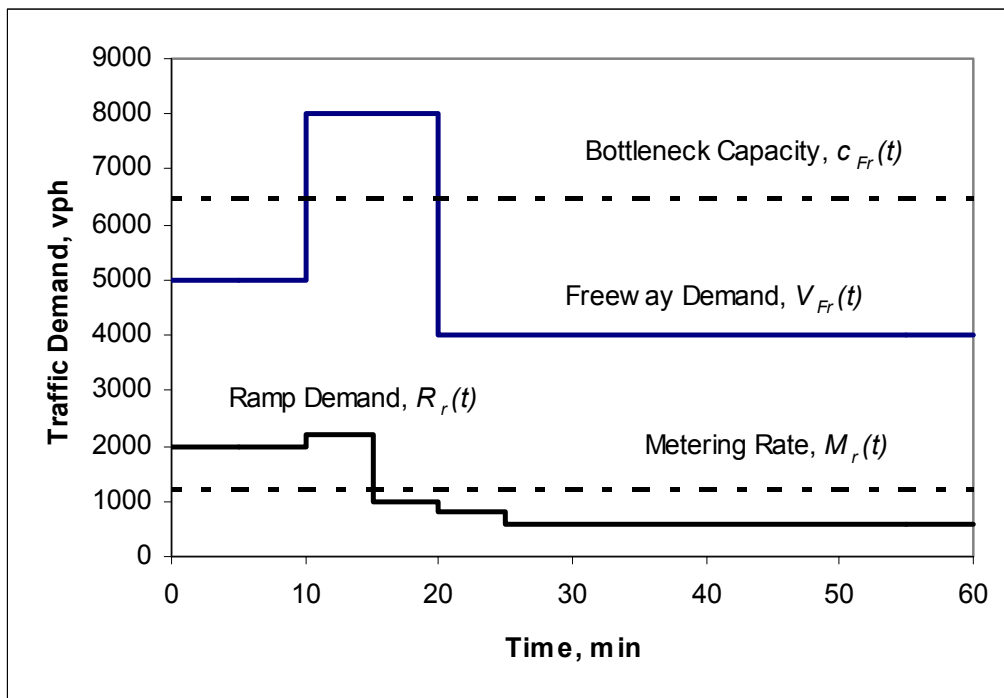


**FIGURE 11 Freeway and ramp traffic demand profile.**

The detailed queue and delay calculations are shown in Table 2 for both a two-capacity regime scenario and a single-capacity regime scenario. The cumulative arrival and departure method introduced earlier was used for the calculations. For the two-capacity regime scenario, the free-flow capacity,  $c_{Fr}$ , was assumed 6600 vph, and the queue-discharge capacity,  $c_{Qr}$ , was assumed 6000 vph. For each 5-min interval, the

freeway and ramp traffic demands, the freeway capacity, the freeway and ramp queues, and the freeway and ramp delays were calculated.

**TABLE 2 Delays with/without ramp metering and with different capacity scenarios**

t (min)	No Metering					With Metering					
	$V_{Fr}(t)$	$R_r(t)$	$c_{Fr}(t)^1$	$q_{Fr}(t)$	$TD_{Fr} + TD_{Rr}$	$O_{Rr}(t)$	$q_{Rr}(t)$	$V_{Fr}(t) + O_{Rr}(t)$	$c_{Fr}(t)^1$	$q_{Fr}(t)$	$TD_{Fr} + TD_{Rr}$
0~5	5000	2000	6000	83	3.5	1200	67	6200	6600	0	2.8
5~10	5000	2000	6000	167	10.4	1200	133	6200	6600	0	8.3
10~15	8000	2200	6000	517	28.5	1200	217	9200	6000	267	25.7
15~20	8000	1000	6000	767	53.5	1200	200	9200	6000	533	50.7
20~25	4000	800	6000	667	59.7	1200	167	5200	6000	467	56.9
25~30	4000	600	6000	550	50.7	1200	117	5200	6000	400	47.9
30~35	4000	600	6000	433	41.0	1200	67	5200	6000	333	38.2
35~40	4000	600	6000	317	31.3	1200	17	5200	6000	267	28.5
40~45	4000	600	6000	200	21.5	800	0	4800	6000	167	18.8
45~50	4000	600	6000	83	11.8	600	0	4600	6000	50	9.0
50~55	4000	600	6000	0	3.5	600	0	4600	6000	0	2.1
55~60	4000	600	6600	0	0.0	600	0	4600	6600	0	0.0
Total Delay	315.3 veh-hr <sup>2</sup>					Total Delay	288.9 veh-hr <sup>2</sup>				
	168.1 veh-hr <sup>3</sup>						197.9 veh-hr <sup>3</sup>				

**Note:** 1. For the two-regime capacity scenario, the freeway capacity,  $c_{Fr}(t)$  is equal to  $c_{Fr}$  if  $q_{Fr}(t-1) = 0$  and  $V_{Fr}(t) + O_{Rr}(t) \leq c_{Fr}$ ; otherwise,  $c_{Fr}(t)$  is equal to  $c_{Qr}$ . For the case of *No Metering*,  $O_{Rr}(t) = R_{Rr}(t)$   
 2. Results with the two-regime capacity:  $c_{Fr} = 6600$  vph,  $c_{Qr} = 6000$  vph;  
 3. Results with the single-regime capacity:  $c_{Fr} = c_{Qr} = 6500$  vph.

As shown in Table 2 that the freeway had a lower capacity (6000 vph) at the beginning of the analysis period without ramp metering, indicating the case of a

breakdown. With ramp metering, however, the freeway was able to maintain at a free-flow condition, thus had a higher capacity (6600 vph) at the beginning of the analysis period. Ramp metering was able to reduce the system delays (from 315.3 veh-hr to 288.9 veh-hr) when the two-capacity regime existed. Similar calculations were carried out assuming a single-regime capacity of 6500 vph. In this case, ramp metering actually increased the system delays (from 168.1 veh-hr to 197.9 veh-hr).

## **INTEGRATED OPERATIONS**

The concept of integrated operations between the surface street signal system and freeway ramp control system dates back to the early 1970s in the context of corridor control (6). Several researchers developed mathematical models for an integrated freeway corridor control system (66, 67, 68). Field implementation and testing have also been conducted in recent years and sought to improve the freeway corridor as a whole, consisting of both the freeway ramp-metering system and the parallel arterial streets (28, 29, 30, 69, 70). However, the majority of the studies on integrated systems often emphasize too broad a range of the network, while not many detailed investigations have been carried out regarding the close interactions between ramp metering and the nearby upstream signalized intersection, such as a diamond interchange. Ignoring the basic integration elements between ramp metering and upstream signals has led to unsuccessful field operations (28, 29).

A limited number of literature sources were found to be related to this research subject. Gordon (71) studied the effect of the ramp-metering sampling interval on ramp queues. One of the conclusions of his study is that queue spillback can be significantly reduced by using a shorter sampling interval, i.e., a more responsive metering operation. His study mainly focused on the ramp metering itself without addressing how the upstream signal timing might affect the ramp queues.

Chaudhary and Messer (72) studied the ramp-metering queues given a fixed ramp-metering rate and stochastic traffic demand at an upstream diamond interchange. Their study was based on simplified assumptions of the diamond interchange timing

and traffic flow, and an empirical equation was developed for estimating the ramp queue length. For example, one of the simplifications was to consider only one side of the diamond interchange, and all the traffic departed from the signal was assumed to arrive at the ramp, which is not the case with the frontage road system.

Han and Reiss (73) studied the relationship between a simple two-phase upstream signal and a ramp meter. They concluded that using a varied ramp-metering rate would be more effective in eliminating the short-term queue spillback that resulted from signal-controlled vehicle arrivals.

Yuan and Kreer (74) addressed the ramp-queuing issue in modeling a coordinated ramp-metering system. In their proposed traffic flow models, they introduced a system constraint for the purpose of balancing the ramp queues among all the metered ramps within the system. However, their study did not consider the effect of an upstream signal on the ramp queue.

Gettman (45) also introduced a system constraint in his non-linear programming model to take into consideration the queue spillback issue, but he did not address how to achieve coordination between the diamond interchange and the ramp-metering signals.

Two studies found in the literature are more closely related to this research topic. One was conducted by Head and Mirchandani (75) to specifically look at the coordination between ramp-metering and diamond interchange operations. Their study sought to develop a real-time adaptive control system that would achieve the coordination between ramp metering and a diamond interchange's operation. Their study focused more on the adaptive feature of the diamond interchange by developing detection and prediction algorithms. Consideration of ramp metering was limited to a fixed ramp-metering rate.

Venglar and Urbanik (76) proposed a system architecture aimed at developing an adaptive control system for a diamond interchange, incorporating various technologies including video detection, a traffic simulator, fiber-optic lane assignment

signing, and communication equipment. The system was intended to integrate various transportation modes and respond to various transportation needs. Unfortunately, ramp metering was not a component of the system.

### **MICROSCOPIC TRAFFIC SIMULATION MODELS**

With the advance of computing technology, microscopic simulation models have been widely used in studying transportation issues such as ramp-metering applications (27, 77, 78, 79). While various traffic simulation models are available, VISSIM (7) and Paramics (80) are two widely used microscopic simulation models for studying traffic problems, such as ramp metering. Unlike other microscopic simulation models such as CORSIM (81), INTEGRATION (82), and SimTraffic (83), both VISSIM and Paramics provide users with the flexibility of developing special signal control logics and algorithms, which are essential in evaluating new control strategies and algorithms. For example, VISSIM is equipped with a *Vehicle Actuated Programming (VAP)* function. VAP is similar to an advanced programming language, which allows users to develop and simulate any signal control algorithm in VISSIM. VAP also provides features such as incident detection and dynamic routing for system monitoring and management purposes. VISSIM was selected in this research as the model for evaluating and testing ICS.

### **SUMMARY**

The state-of-the-art literature review indicates that a significant number of studies have been conducted in the individual areas of diamond interchange operations, freeway operations, and ramp-metering operations. Existing methodologies and models of diamond interchange operations are limited to isolated operations without consideration of the potential impact of ramp-metering queue spillback. A number of studies have also addressed integration between the freeway ramp-metering system and surface street arterial system. However, studies on integrated modeling and operations between a diamond interchange and ramp metering are limited. There are no methodologies and

procedures available to model the interactions between surface street diamond interchange signals and ramp-metering signals.

At most urban transportation networks, freeway ramps and ramp metering often exist in the vicinity of signalized diamond interchanges. As an essential element of either a coordinated freeway ramp-metering system or an integrated freeway/surface street system, ramp metering and its adjacent diamond interchange need to be treated as an integral system due to the close interactions between the ramp-metering signal and the diamond interchange signal. It is important to have a better understanding of the system operational characteristics for better managing system operations when integration strategies are sought. A major challenge of this research is then to build on what has been achieved individually in diamond interchange and ramp-metering operations.

## CHAPTER III

### MODELING METHODOLOGIES

This chapter documents the enhanced modeling methodologies for an IDIRMS. The system boundaries and major elements are defined. Traffic demands at an IDIRMS are given in the form of an origin-destination (OD) matrix. Calculations of the related parameters are discussed, and a model is presented to estimate the OD matrix based on link volume counts. The enhanced modeling methodologies include diamond interchange together with freeway and ramp-metering operations. The methodologies address the close interactions between ramp-metering and diamond interchange operations, particularly the traffic flow profiles at the ramp meters and the impact of ramp queues on diamond interchange operations. A gap-acceptance-based model is also presented to derive the freeway volume thresholds for ramp-metering applications.

Modeling of the traffic queues and delays for freeway, ramp metering, and diamond interchange operations is based on the basic principle of the cumulative arrival and departure method as discussed in Chapter II. However, modeling of the external traffic movements at the diamond interchange is carried out on a cycle-by-cycle basis, where the vehicle arrivals are assumed uniform within the same cycle. Modeling of the freeway and ramp metering operations is carried out on a second-by-second basis, which is expected to provide enough accuracy due to the nature of the macroscopic or mesoscopic level analyses.

### INTEGRATED SYSTEM AND ITS MAJOR ELEMENTS

#### **System Definition and Its Boundaries**

The proposed IDIRMS and its system boundaries were shown previously in Figure 2. This is a type of diamond interchange with one-way frontage road systems, mostly seen in urban highways, such as in Texas. The system includes a diamond interchange, segment of freeway mainlines, and ramp meters on both on-ramps.

### System Variables and Parameters

Figure 12 illustrates the proposed numbering conventions for the traffic movements and demands in an IDIRMS. First, traffic demands in the system are defined by an OD matrix that includes six origins and six destinations, which can be used to derive the 14 turning movements at the diamond interchange, the two freeway mainline flows, and the two on-ramp flows. Table 3 and Table 4 define the relationships among these various traffic flow variables.

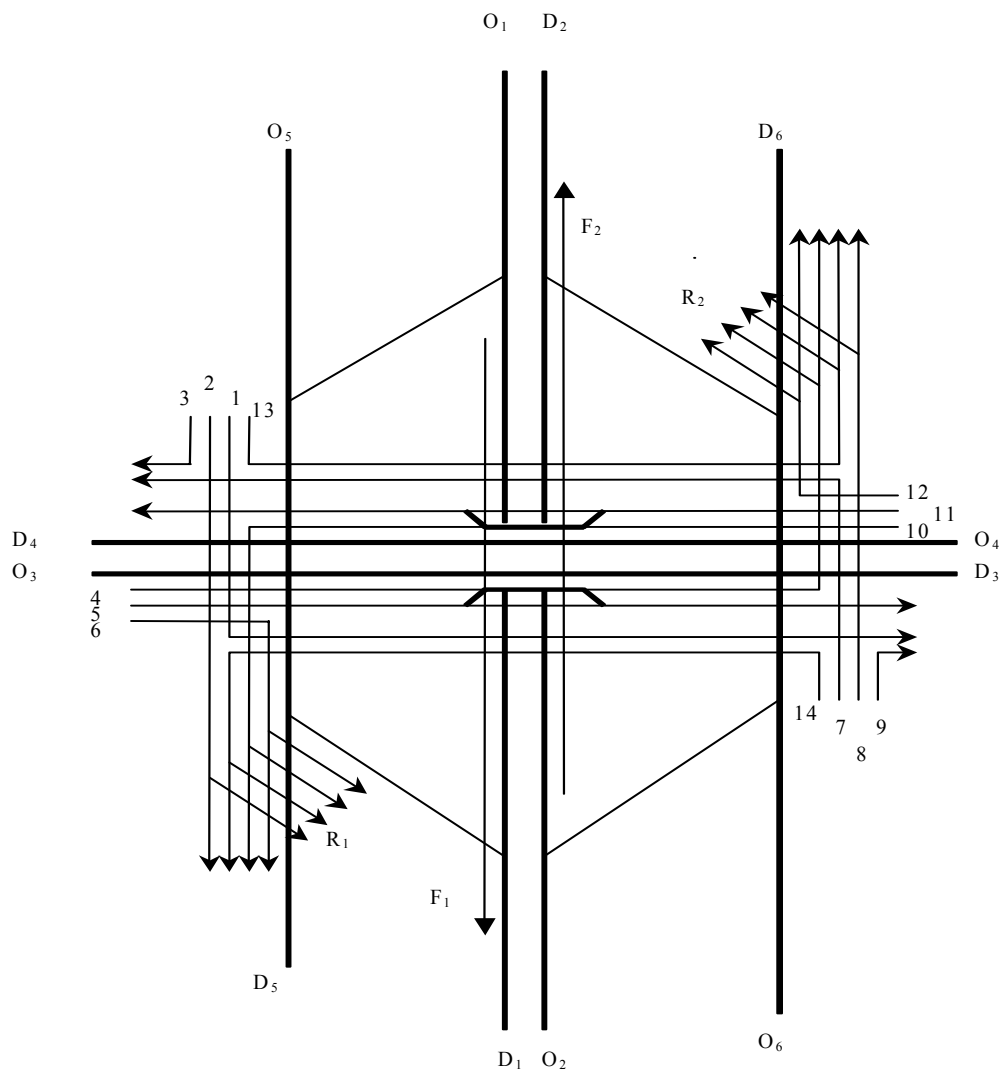


**FIGURE 12 Selected numbering convention for IDIRMS.**



**TABLE 3 Calculation of traffic movement demands**

Diamond/Ramp	Location	Movement	Traffic Movement and OD Flows
<i>Diamond Interchange</i>	Left-Side Frontage Road	LT (M1)	$V_1 = v_{1,3} + v_{5,3}$
		TH (M2)	$V_2 = v_{1,5} + v_{5,5} + v_{5,1}$
		RT (M3)	$V_3 = v_{1,4} + v_{5,4}$
		U (M13)	$V_{13} = v_{5,6} + v_{5,2} + v_{1,6}$
	Arterial A-Direction (Left to Right)	LT (M4)	$V_4 = v_{3,2} + v_{3,6}$
		TH (M5)	$V_5 = v_{3,3}$
		RT (M6)	$V_6 = v_{3,1} + v_{3,5}$
	Right-Side Frontage Road	LT (M7)	$V_7 = v_{6,4} + v_{2,4}$
		TH (M8)	$V_8 = v_{6,6} + v_{6,2} + v_{2,6}$
		RT (M9)	$V_9 = v_{6,3} + v_{2,3}$
		U (M14)	$V_{14} = v_{6,5} + v_{6,1} + v_{2,5}$
	Arterial B-Direction (Right to Left)	LT (M10)	$V_{10} = v_{4,1} + v_{4,5}$
		TH (M11)	$V_{11} = v_{4,4}$
		RT (M12)	$V_{12} = v_{4,6} + v_{4,2}$
<i>On-Ramp</i>	Left-Side Ramp	R1	$R_1 = v_{3,1} + v_{4,1} + v_{5,1} + v_{6,1}$
	Right-Side Ramp	R2	$R_2 = v_{3,2} + v_{4,2} + v_{5,2} + v_{6,2}$

**TABLE 4 Calculation of proportion of ramp traffic**

Ramp	Movement, $m$	Proportion, $p_{m,r}$
R1	M2	$p_{2,1} = \frac{v_{5,1}}{v_{5,1} + v_{5,5} + v_{1,5}}$
	M6	$p_{6,1} = \frac{v_{3,1}}{v_{3,1} + v_{3,5}}$
	M10	$p_{10,1} = \frac{v_{4,1}}{v_{4,1} + v_{4,5}}$
	M14	$p_{14,1} = \frac{v_{6,1}}{v_{6,1} + v_{6,5} + v_{2,5}}$
R2	M8	$p_{8,2} = \frac{v_{6,2}}{v_{6,2} + v_{6,6} + v_{2,6}}$
	M12	$p_{12,2} = \frac{v_{4,2}}{v_{4,2} + v_{4,6}}$
	M4	$p_{4,2} = \frac{v_{3,2}}{v_{3,2} + v_{3,6}}$
	M13	$p_{13,2} = \frac{v_{5,2}}{v_{5,2} + v_{5,6} + v_{1,6}}$

The total traffic demand for on-ramp  $r$ ,  $R_r$ , relates to the diamond interchange turning movements in the following equation:

$$R_r = \sum_m p_{m,r} \cdot U_m = \sum_m p_{m,r} \cdot c_m \text{Min}(x_m, 1), \quad r = 1, 2 \quad (40)$$

### Origin-Destination Estimation

One of the major input data requirements for analyzing an IDIRMS is the OD traffic demand matrix. OD flows can be obtained either from an actual OD survey or can be estimated based on specific link and turning movement counts. OD estimation is a complex subject in itself that has attracted significant research interest (84, 85, 86, 87). However, previous studies usually involved much larger networks with limited sample

link volume count data. Therefore, the estimated OD generally involved large errors and variations. For the system to be analyzed in this research, we have a relatively small-scale network and can normally obtain sufficient traffic volume counts at key locations. A more reliable and accurate OD estimation is likely.

A non-linear optimization model developed in this research is presented below for an OD estimation based on link volume counts. The objective function can be expressed in Equation 41:

$$\text{Min} \sum_{o=1}^6 (VO_o - \sum_{d=1}^6 v_{o,d})^2 + \sum_{d=1}^6 (VD_d - \sum_{o=1}^6 v_{o,d})^2 + \sum_{m=1}^{14} (V_m - V'_m)^2 + \sum_{r=1}^2 (R_r - R'_r)^2 \quad (41)$$

subject to:

$$\left. \begin{aligned} V'_1 &= v_{1,3} + v_{5,3} \\ V'_2 &= v_{1,5} + v_{5,5} + v_{5,1} + v_{1,1} \\ V'_3 &= v_{1,4} + v_{5,4} \\ V'_4 &= v_{3,2} + v_{3,6} \\ V'_5 &= v_{3,3} \\ V'_6 &= v_{3,1} + v_{3,5} \\ V'_7 &= v_{6,4} + v_{2,4} \\ V'_8 &= v_{6,6} + v_{6,2} + v_{2,6} + v_{2,2} \\ V'_9 &= v_{6,3} + v_{2,3} \\ V'_{10} &= v_{4,1} + v_{4,5} \\ V'_{11} &= v_{4,4} \\ V'_{12} &= v_{4,6} + v_{4,2} \\ V'_{13} &= v_{5,6} + v_{5,2} + v_{1,6} \\ V'_{14} &= v_{6,5} + v_{6,1} + v_{2,5} \\ R'_1 &= v_{3,1} + v_{4,1} + v_{5,1} + v_{6,1} \\ R'_2 &= v_{3,2} + v_{4,2} + v_{5,2} + v_{6,2} \end{aligned} \right\} \quad (42)$$

$$\left\{ \begin{array}{l} \alpha_{2,1} \leq (p_{2,1} = \frac{v_{5,1}}{V'_{2}}) \leq \beta_{2,1} \\ \alpha_{10,1} \leq (p_{10,1} = \frac{v_{4,1}}{V'_{10}}) \leq \beta_{10,1} \\ \alpha_{6,1} \leq (p_{6,1} = \frac{v_{3,1}}{V'_{6}}) \leq \beta_{6,1} \\ \alpha_{14,1} \leq (p_{14,1} = \frac{v_{5,1}}{V'_{14}}) \leq \beta_{14,1} \\ \alpha_{8,2} \leq (p_{8,2} = \frac{v_{6,12}}{V'_{8}}) \leq \beta_{8,2} \\ \alpha_{12,2} \leq (p_{12,2} = \frac{v_{6,2}}{V'_{12}}) \leq \beta_{12,2} \\ \alpha_{4,2} \leq (p_{4,2} = \frac{v_{6,12}}{V'_{4}}) \leq \beta_{4,2} \\ \alpha_{13,2} \leq (p_{13,2} = \frac{v_{6,12}}{V'_{13}}) \leq \beta_{13,2} \end{array} \right. \quad (43)$$

$$v_{o,d} \geq 0 \quad (44)$$

The objective function expressed in Equation 41 is to minimize the errors between the estimated variables ( $v_{o,d}$ ,  $V'_m$ ,  $R'_r$ ) and the measured variables ( $VO_o$ ,  $VD_d$ ,  $V_m$ ,  $R_r$ ). The minimization is to take place over all the OD flows,  $v_{i,j}$ , subject to Equations 42 to 44. Equation 42 establishes the relationship between the estimated OD flows and the estimated turning movement flows. Equation 43 establishes an additional set of constrains for  $p_{m,r}$ , the proportion of ramp traffic of each feeding movement. Each  $p_{m,r}$  is subject to the lower boundary,  $\alpha_{m,r}$ , and the higher boundary,  $\beta_{m,r}$ , which would be determined either based on field measurement or estimation. Equation 44 defines that the OD flows must be positive.

The above non-linear programming model can be solved using several optimization algorithms (e.g., the Newton algorithm) included in the *Solver* function of Excel. The following illustrates an example of the OD estimation process and results.

Origin Flows,  $VO_o$ :

$$VO_1 = 7150, VO_2 = 3850, VO_3 = 520, VO_4 = 610, VO_5 = 767, VO_6 = 413$$

Destination Flows,  $VD_d$ :

$$VD_1 = 7430, VD_2 = 3782, VD_3 = 344, VD_4 = 631, VD_5 = 912, VD_6 = 210$$

Turning Movement Counts,  $V_m$ :

$$V_1 = 81, V_2 = 1359, V_3 = 133, V_4 = 130, V_5 = 140, V_6 = 250, V_7 = 329,$$

$$V_8 = 171, V_9 = 124, V_{10} = 340, V_{11} = 170, V_{12} = 100, V_{13} = 9, V_{14} = 58$$

On-Ramp and Off-Ramp Counts,  $R_r, R_{off,r}$ :

$$R_1 = 1095, R_2 = 201, R_{off,1} = 815, R_{off,2} = 269$$

The boundary values of  $\alpha_{m,r}$  and  $\beta_{m,r}$  must be positive numbers, and the range of values can be specified if they can be estimated.

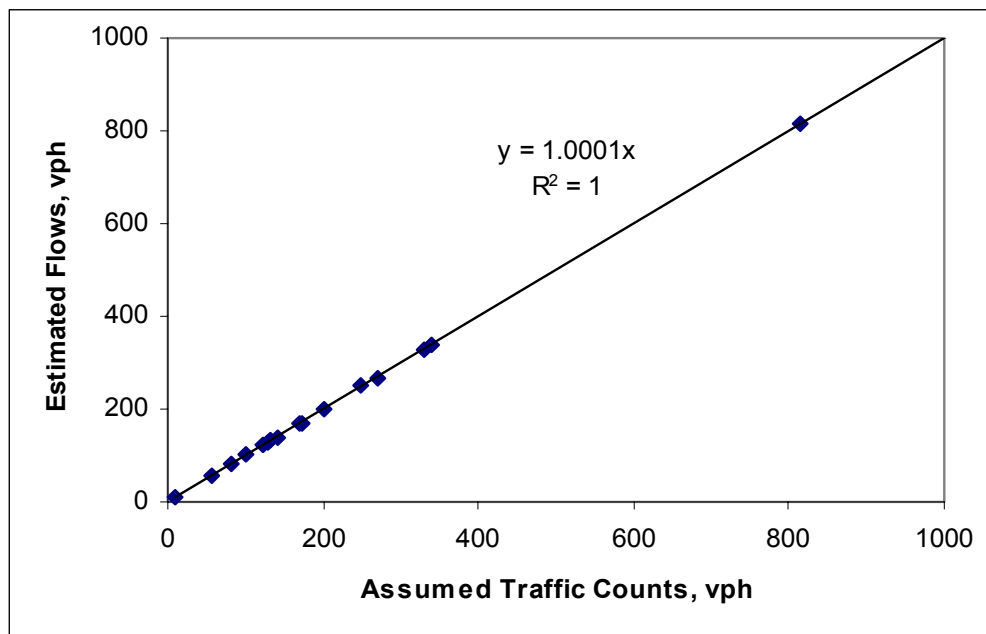
Table 5 is the estimated OD matrix. A comparison between the assumed flows and the estimated flows is shown in Figure 13. A perfect match can be seen between the two flows as indicated by  $R^2 = 1$ . The resulting  $p_{m,r}$  values are given below:

$$p_{2,1} = 0.40, p_{6,1} = 0.83, p_{10,1} = 0.86, p_{14,1} = 0.98,$$

$$p_{8,2} = 0.53, p_{12,2} = 0.33, p_{4,2} = 0.52, p_{13,2} = 1.00$$

**TABLE 5 Origin-destination estimation results**

O/D	$D_1$	$D_2$	$D_3$	$D_4$	$D_5$	$D_6$	$VO_o$	$\hat{VO}_o$
$O_1$	6335	–	79	117	619	0	7150	7150
$O_2$	–	3581	63	159	0	47	3850	3850
$O_3$	207	67	140	–	43	63	520	520
$O_4$	292	33	–	170	48	67	610	610
$O_5$	540	9	1	16	201	0	767	767
$O_6$	57	92	61	170	2	32	413	413
$VD_d$	7430	3782	344	631	912	210	Total = 13310	
$\hat{VD}_d$	7430	3782	344	631	912	210		

**FIGURE 13 Comparison between assumed counts and estimated flows.**

When the complete turning movement and link volume counts are available, the only additional estimates given by the OD estimation process are the  $p_{m,r}$  values. Of course, the same procedure can still be used to provide estimates if only a portion of the volume counts are available. An OD matrix is usually given in a transportation planning process through travel demand forecasting models. In this case, the values of all other traffic flow variables can be derived based on the relationships defined in Table 3 and Table 4.

### **ENHANCED DIAMOND INTERCHANGE MODELING**

As discussed in Chapter II, the existing models for analyzing diamond interchange operations lack consideration of queue spillback from ramp meters. The existing modeling methodologies are also based on deterministic traffic demands without consideration of random traffic flows. An enhanced modeling methodology was developed in this research to overcome the shortcomings of the existing models. The enhanced methodology was designed to perform operational analysis over multiple cycles, with consideration of not only the random traffic flow variations, but also the effect of ramp-metering queue spillback. The modeling methodology is addressed next in separate procedures for the external and internal movements.

#### **Delay and Queue Modeling for the External Movements**

The cumulative arrival and departure method as described in Chapter II was used to model the delays and queues for the external movements at the diamond interchange with consideration of ramp queue spillback. Figure 14 through Figure 17 illustrate various cases for a particular signal cycle where an initial queue, a residual queue, and ramp queue spillback conditions exist. Figure 14 represents a more generalized case and was used in the following discussions to demonstrate how queues and delays were calculated. It is noted that modeling of the external movements at the diamond interchange was carried out on a cycle-by-cycle basis due to the assumption of uniform arrival within a cycle. However, the impeded departure flow,  $S'_m$ , due to ramp queue spillback needs to be obtained based on second-by-second modeling, which will be

addressed in the section of modeling freeway and ramp metering operations.

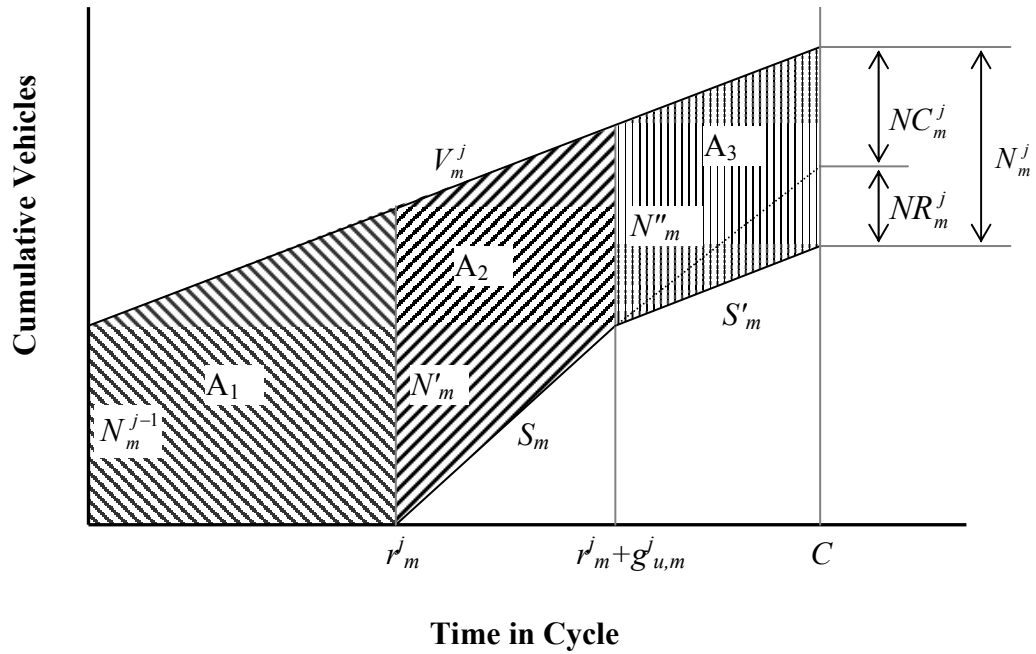


FIGURE 14 Profile with residual queue and spillback (case 1).

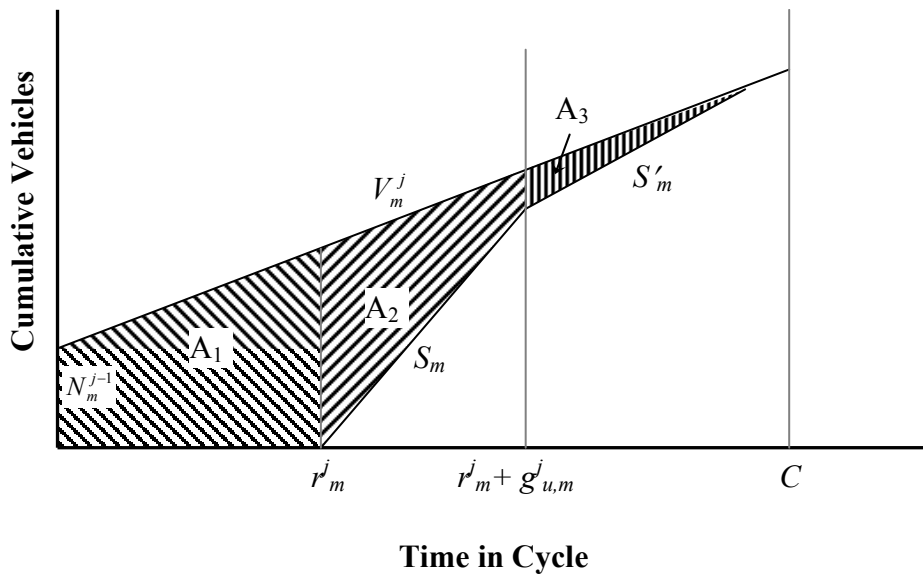


FIGURE 15 Profile with spillback but no residual queue (case 2).



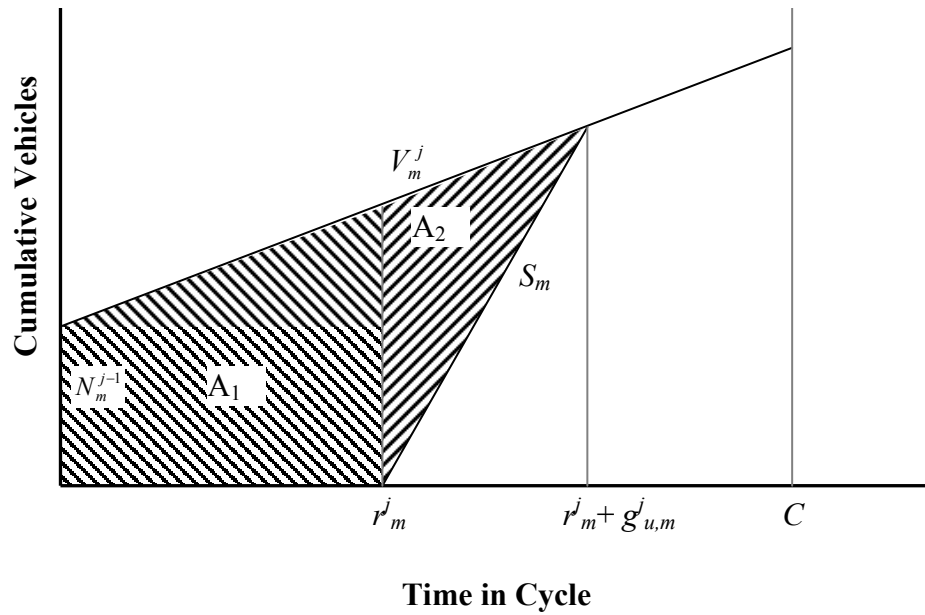


FIGURE 16 Profile without residual queue and no spillback (case 3).

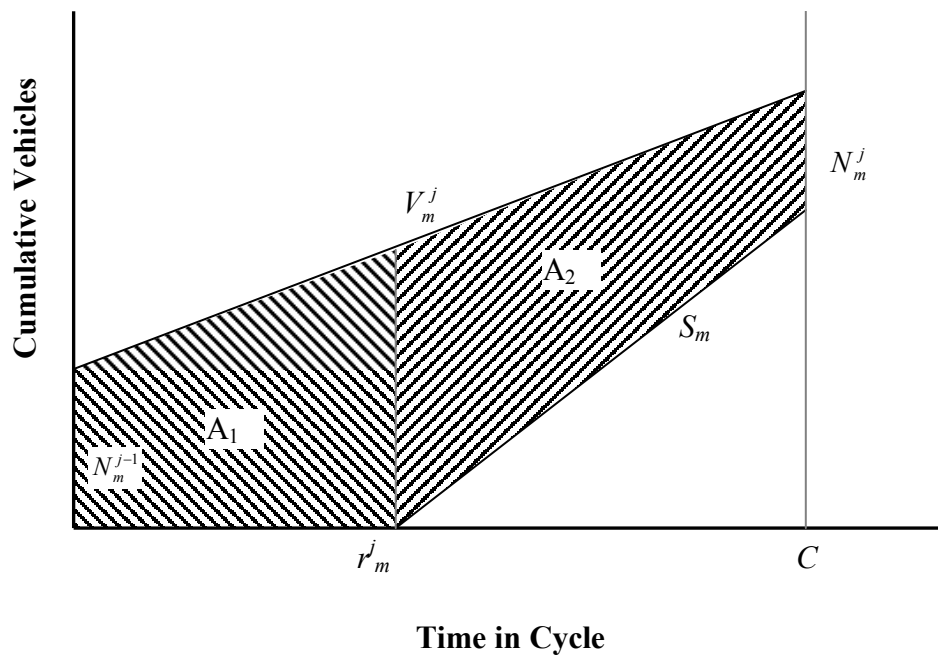


FIGURE 17 Profile with residual queue and no spillback (case 4).

As shown in Figure 14, the average traffic demand for movement  $m$  during a particular cycle  $j$  was assumed to be  $V_m^j$ .  $V_m^j$  was different among cycles for considering the random variations. Traffic would discharge from the interchange approach at saturation flow rate  $S_m$  when no ramp queue spillback occurred, and at a reduced flow rate  $S'_m$  when ramp queue spillback occurred. There may exist both an initial queue,  $N_m^{j-1}$ , and a residual queue,  $N_m^j$ . The residual queue consists of a portion due to signal over-saturation itself ( $NC_m^j$ ) and a portion due to ramp queue spillback ( $NR_m^j$ ). The exact total delay for traffic movement  $m$  during the cycle can be represented by the total areas of the queue polygon (areas of A1, A2, and A3). In fact, if  $NR_m^j$  in Figure 14 could be obtained, the delay calculations could be carried out without having to know  $S'_m$ . The calculation of  $NR_m^j$  will be addressed later in the section on modeling ramp queue spillback.

$NC_m^j$  can be determined based on Equation 45:

$$NC_m^j = \frac{(V_m^j - c_m^j)}{3600} C + N_m^{j-1} \quad (45)$$

$c_m^j$ , the unimpeded capacity of movement  $m$ , can be calculated based on Equation 46:

$$c_m^j = \frac{C - r_m^j}{C} S_m \quad (46)$$

The total shaded areas of the queue polygon represent the total delays experienced by the vehicles arriving in the current cycle  $j$ . The total delays are calculated from the following equations:

$$A_1 = (N_m^{j-1} + N'_m) \frac{r_m^j}{2} \quad (47)$$

$$A_2 = (N'_m + N''_m) \frac{g_{u,m}^j}{2} \quad (48)$$

$$A_3 = (N''_m + N_m^j + \frac{C - r_m^j - g_{u,m}^j}{2}) \quad (49)$$

$$N'_m = N_m^{j-1} + \frac{r_m^j V_m^j}{3600} \quad (50)$$

$$N''_m = N'_m + \frac{(V_m^j - S_m) g_{u,m}^j}{3600} \quad (51)$$

The average delay for movement  $m$  during cycle  $j$  is:

$$d_m^j = \frac{A_1 + A_2 + A_3}{C \frac{V_m^j}{3600}} = 3600 \frac{A_1 + A_2 + A_3}{C V_m^j} \quad (52)$$

The queue length is represented by the vertical distance in the queue polygon in Figure 14. The maximum number of vehicles in the queue usually occurs at the start of the green interval.

### Delays and Queues for the Internal Movements

Modeling of the queues and delays for the internal movements (i.e., the left-turn and through movements within the interchange) is based on the basic principle of the delay-difference-of-offset method as discussed in Chapter II but with consideration of the

impact of ramp-metering queues. The internal movements have unique traffic arrival and departure patterns determined based on the diamond phasing schemes, spacing, and traffic flows. In this section, the flow profiles are depicted for the two types of phasing schemes studied: three-phase and four-phase. Calculations of the related parameters, delays, and queues are then expressed in mathematical form.

### ***Three-Phase***

Figure 18 shows the arrival profile for the internal through movement at the left-side diamond interchange (denoted as  $MA$ ) with three-phase operation, and Figure 19 is the cumulative arrival and departure flow profiles. The time reference zero of the profile is the start of the frontage road phases ( $\phi_4$  and  $\phi_8$ ). Note that  $MA$ , being serviced by the overlap phase  $A$ , has the green indication during the arterial phase ( $\phi_2$ ) and the internal left-turn phase ( $\phi_1$ ). It has the red indication during the frontage road phases ( $\phi_4$  and  $\phi_8$ ).

The first part of the platoon traffic is from  $M7$ , the left-turn movement from the right-side frontage road. It arrives at the left-side diamond interchange at time  $t_1$ , which is equal to the travel time,  $TT_{2,1}$ . After the platoon, the arrival flow becomes the average demand flow of  $V_7$ , represented by the dashed line. The flow drops to zero during the lost time  $l_8$ . For simplicity, the flow depicted in the dashed line was converted into the average flow rate,  $V'_7$ , over the non-saturated portion of phase 8. The next platoon arrival is from  $M11$ , the right-side arterial approach with the average flow of  $V_{11}$ . The end of the arrival profile,  $t_5$ , marks the end of green for phase 6, after which there are no further arrivals.

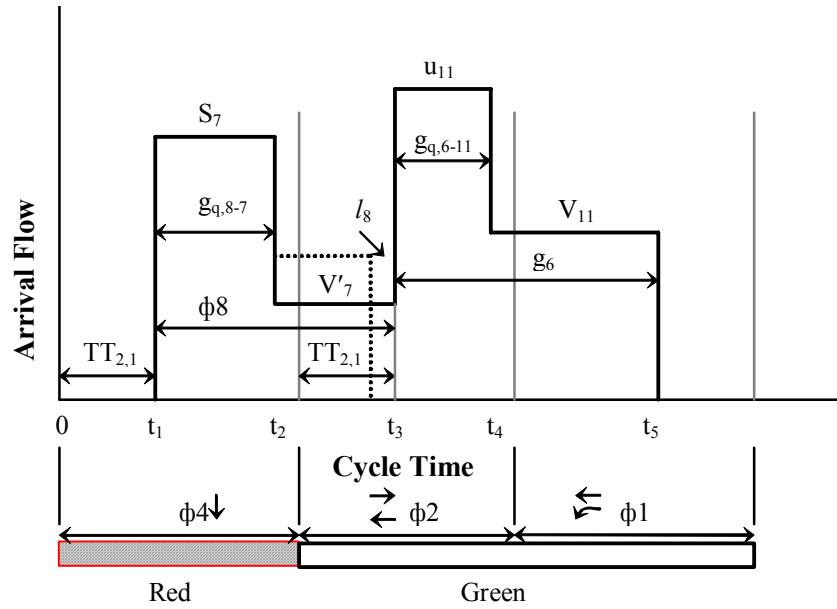


FIGURE 18 Arrival flow profile for the internal through movement (MA): three-phase.

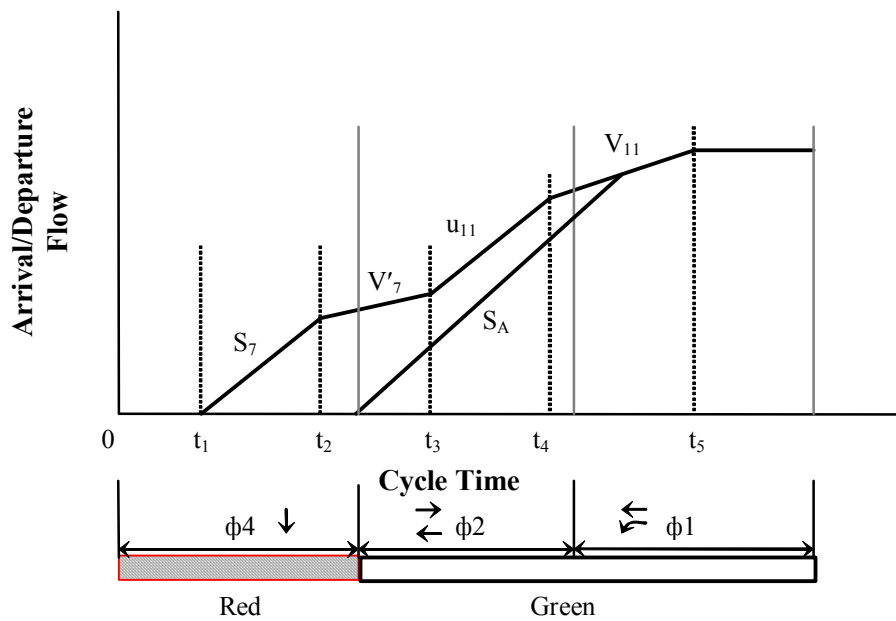


FIGURE 19 Arrival/departure flow profiles for the internal through movement (MA): three-phase.

Equation 53 through Equation 57 describe the calculations of the variables shown in Figure 18. Assume random arrival for the traffic movements (e.g.,  $M7$ ,  $M8$ ) on the frontage road approaches; then:

$$g_{q,8-7} = \frac{3600N_7 + V_7r_8}{S_7 - V_7} \quad (53)$$

$$V_7' = \frac{V_7(\phi_8 - g_{q,8-7} - l_8)}{\phi_8 - g_{q,8-7}} = \frac{V_7(g_8 - g_{q,8-7})}{\phi_8 - g_{q,8-7}} \quad (54)$$

For the arterial approach movements (e.g.,  $M4\_5$ ,  $M10\_11$ ), the random arrival assumption would not be appropriate due to the fact that the diamond interchange is most likely coordinated with adjacent traffic signals. Therefore, the following equations are more appropriate for calculating  $g_{q,6-11}$ :

$$g_{q,6-11} = \begin{cases} \frac{3600(N_{10} + N_{11}) + (V_{10} + V_{11})(1 - P_{10\_11})Cg_6}{S_{10\_11}g_6 - (V_{10} + V_{11})P_{10\_11}C}, & x_{10\_11} < 1 \\ g_6, & x_{10\_11} \geq 1 \end{cases} \quad (55)$$

$$u_{11} = S_{10\_11} \frac{V_{11}}{V_{10} + V_{11}} \quad (56)$$

Note that when an arrival is random,  $P_{10\_11} = g_6/C$  and  $g_{q,6-11}$  can be simplified as:

$$g_{q,6-11} = \begin{cases} \frac{3600(N_{10} + N_{11}) + (V_{10} + V_{11})r_6}{S_{10\_11} - (V_{10} + V_{11})}, & x_{10\_11} < 1 \\ g_6, & x_{10\_11} \geq 1 \end{cases} \quad (57)$$

Equation 58 through Equation 64 describe the calculations of delay and queue for the internal through movement ( $MA$ ):

$$U_{L-T}(t) = \begin{cases} 0, & 0 < t \leq t_1 \\ S_7, & t_1 < t \leq t_2 \\ V_7', & t_2 < t \leq t_3 \\ u_{11}, & t_3 < t \leq t_4 \\ V_{11}, & t_4 < t \leq t_5 \\ 0, & t_5 < t \leq C \end{cases} \quad (58)$$

$$O_{L-T}(t) = \begin{cases} 0, & 0 < t \leq \phi_4 \\ S_A, & \phi_4 < t \leq \phi_4 + g_{q,A} \\ U_{L-T}(t), & \phi_4 + g_{q,A} < t \leq C \end{cases} \quad (59)$$

$g_{q,A}$  is solved from Equation 60:

$$g_{q,A} S_A = \sum_{t=0}^{\phi_4} U_{L-T}(t) + \sum_{t=\phi_4}^{g_{q,A} + \phi_4} U_{L-T}(t) \quad (60)$$

$$\left. \begin{aligned} t_1 &= TT_{2,1} \\ t_2 &= t_1 + g_{q,8-7} \\ t_3 &= t_1 + \phi_8 \\ t_4 &= t_3 + g_{q,6-11} \\ t_5 &= t_3 + g_6 \end{aligned} \right\} \quad (61)$$

$$N_{L-T}(t) = \text{Max}[0, N_{L-T}(t-1) + \frac{U_{L-T}(t) - O_{L-T}(t)}{3600}] \quad (62)$$

$$TD_{L-T} = \sum_{t=1}^c N_{L-T}(t) \quad (63)$$

$$d_{L-T} = \frac{TD_{L-T}}{(V_7 + V_{11})C} 3600 \quad (64)$$

Similarly, the traffic flow profiles for the internal left-turn movement (*M10*) are depicted in Figure 20 and Figure 21.

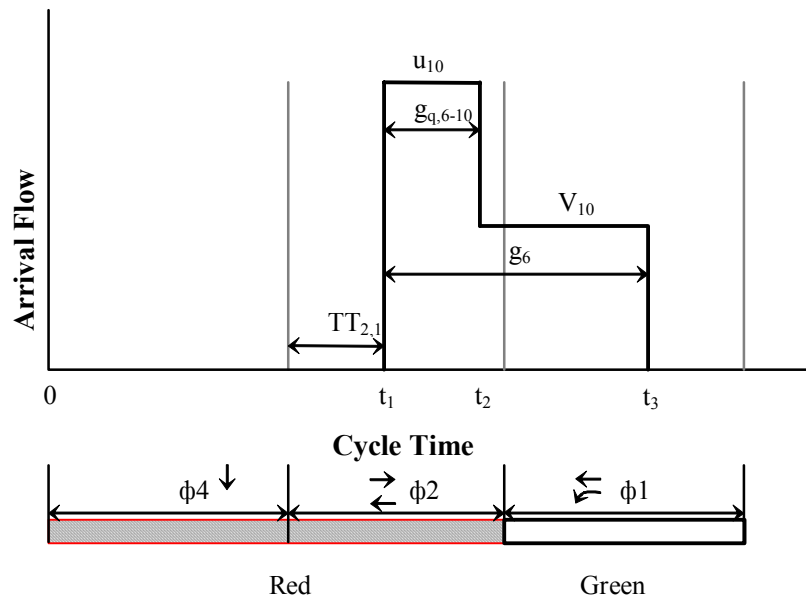


**FIGURE 20** Arrival flow profile for the internal left-turn movement (*M10*): three-phase.



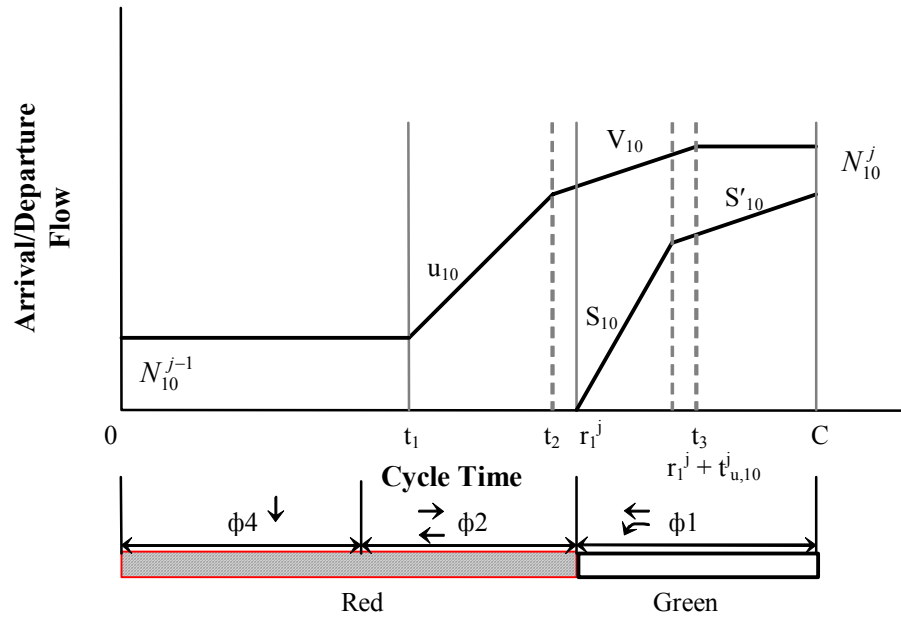


**FIGURE 21** Arrival/departure flow profile for the internal left-turn movement (*M10*) with ramp queue spillback: three-phase.

In Figure 21, the effect of ramp queue spillback is indicated by the reduced saturation flow rate,  $S_{10}'$ . Other related parameters are calculated based on Equation 65 through Equation 70 for the internal left-turn movement (*M10*):

$$u_{10} = S_{10-11} \frac{V_{10}}{V_{10} + V_{11}} \quad (65)$$

Note that  $g_{q,6-10} = g_{q,6-11}$  when *M10* and *M11* are assumed to distribute evenly among all the travel lanes on the arterial approach.

$$U_{L-L}(t) = \begin{cases} 0, & 0 < t \leq t_1 \\ u_{10}, & t_1 < t \leq t_2 \\ V_{10}, & t_2 < t \leq t_3 \\ 0, & t_3 < t \leq C \end{cases} \quad (66)$$

$$O_{L-L}(t) = \begin{cases} 0, & 0 < t \leq r_1^j \\ S_{10}, & r_1^j < t \leq r_1^j + t_{u,10}^j \\ S'_{10}, & r_1^j + t_{u,10}^j < t \leq C \end{cases} \quad (67)$$

$$N_{L-L}(t) = \text{Max}[0, N_{L-L}(t-1) + \frac{U_{L-L}(t) - O_{L-L}(t)}{3600}] \quad (68)$$

$$TD_{L-L} = \sum_{t=1}^C N_{L-L}(t) \quad (69)$$

$$d_{L-L} = \frac{TD_{L-L}}{V_{10}C} 3600 \quad (70)$$

Similarly, the queues and delays for the internal movements at the right-side interchange are depicted in Figure 22 and Figure 23 and in Equation 71 through Equation 74:

$$g_{q,4-1} = \frac{3600N_1 + V_1r_2}{S_1 - V_1} \quad (71)$$

$$V_1' = \frac{V_1(\phi_4 - g_{q,4-1} - l_4)}{\phi_4 - g_{q,4-1}} = \frac{V_1(g_4 - g_{q,4-1})}{\phi_4 - g_{q,4-1}} \quad (72)$$

$$u_4 = S_{4-5} \frac{V_4}{V_4 + V_5} \quad (73)$$

$$g_{q,2-4} = \begin{cases} \frac{3600(N_4 + N_5) + (V_4 + V_5)r_2}{S_{4-5} - (V_4 + V_5)}, & x_{4-5} < 1 \\ g_2, & x_{4-5} \geq 1 \end{cases} \quad (74)$$

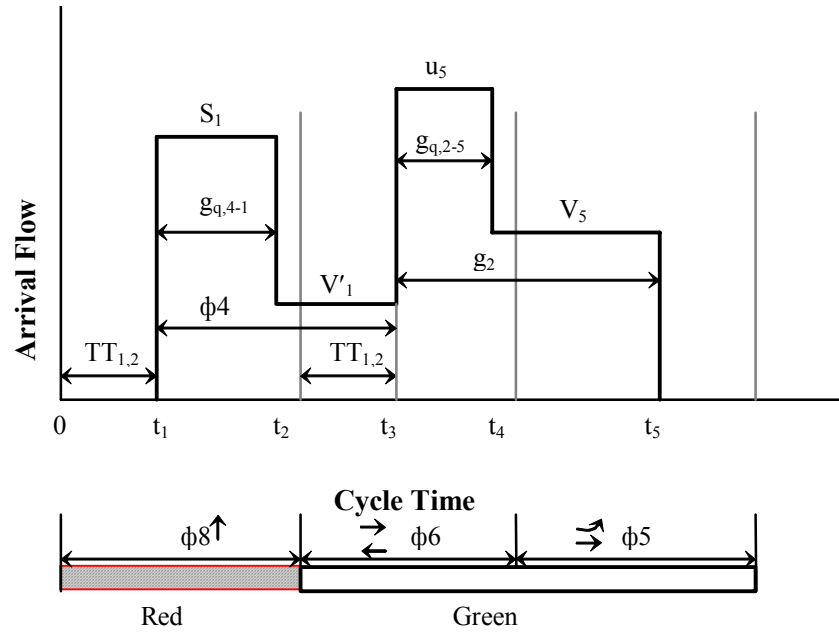


**FIGURE 22** Arrival flow profile for the internal through movement (*MB*): three-phase.

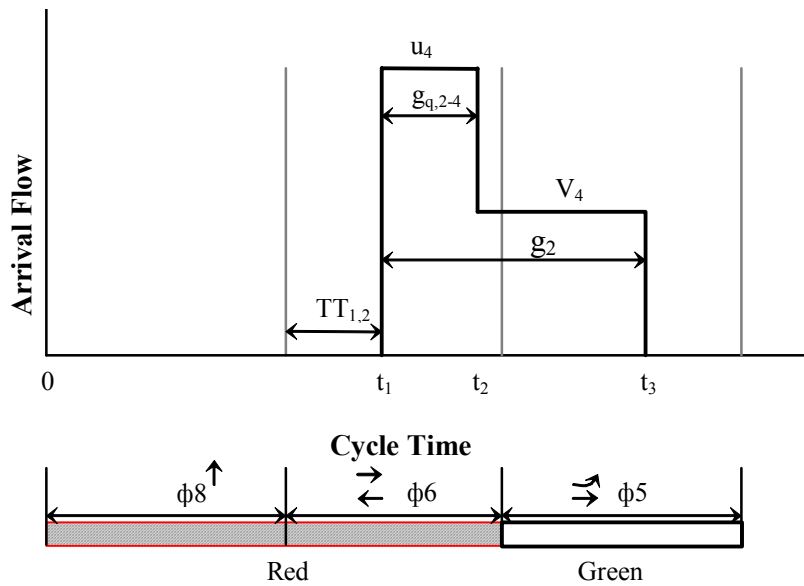


**FIGURE 23** Arrival flow profile for the internal left-turn movement (*M4*): three-phase.

### Four-Phase

With four-phase operation, the traffic flow profiles are depicted in Figure 24 through Figure 27. Note that the start of  $\phi_1$  is referenced as the time zero point. The initial offset  $t_1$  of two seconds for the first platoon arrival (see Figure 24) indicates the 2-second difference between travel time and the overlap phase in four-phase operation, i.e., the platoon from the right-side arterial ( $\phi_6$ ) arrives two seconds after phase 1 starts. Setting the overlap two seconds shorter than the travel time is a common practice to ensure drivers see the signal turning green without incurring significant deceleration. Queues and delays for the internal movements can be calculated using equations similar to those for the three-phase operation.

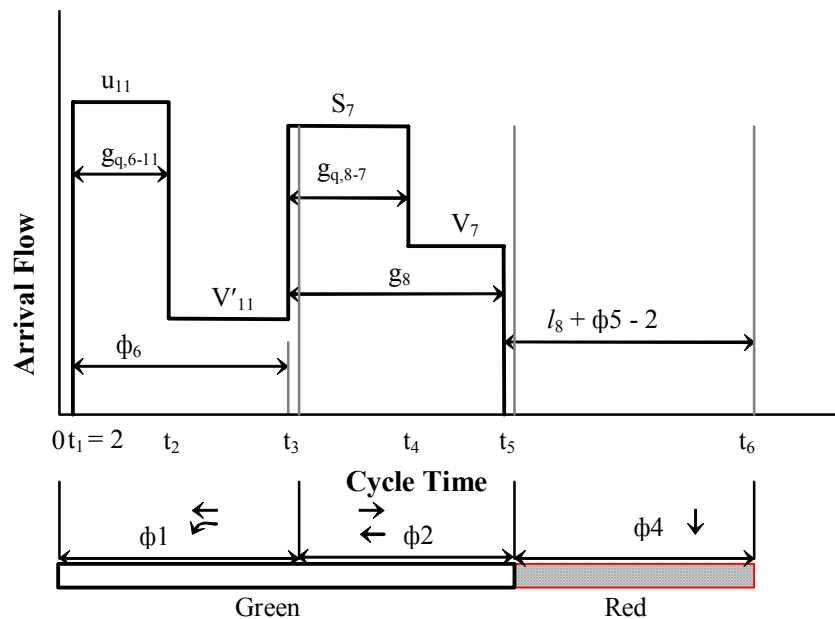


**FIGURE 24** Arrival flow profile for the internal through movement (MA): four-phase.

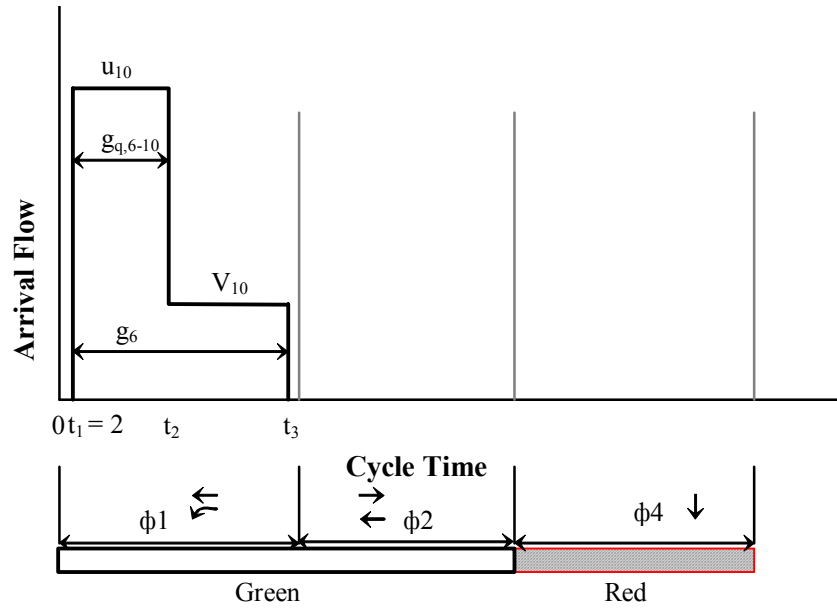


**FIGURE 25** Arrival flow profile for the internal left-turn movement (*M10*): four-phase.

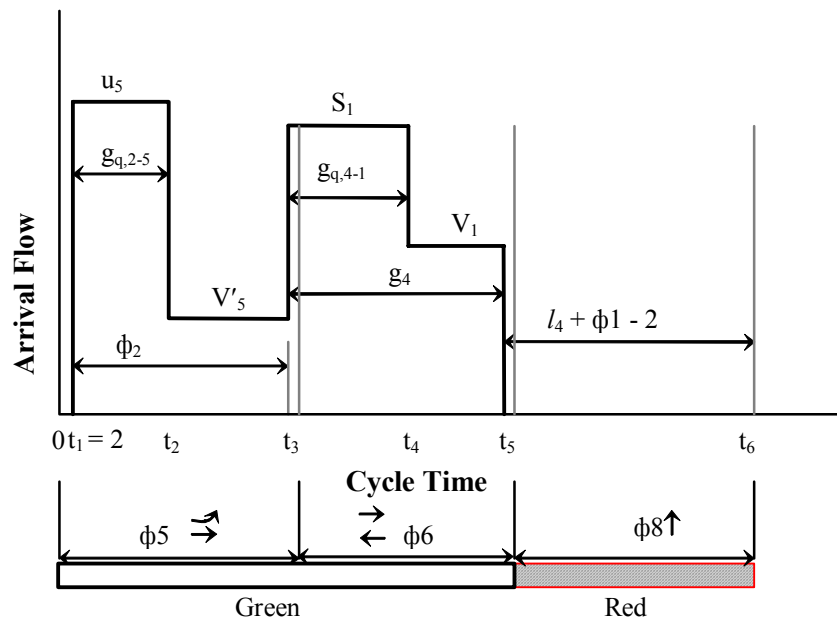


**FIGURE 26** Arrival flow profile for the internal through movement (*MB*): four-phase.

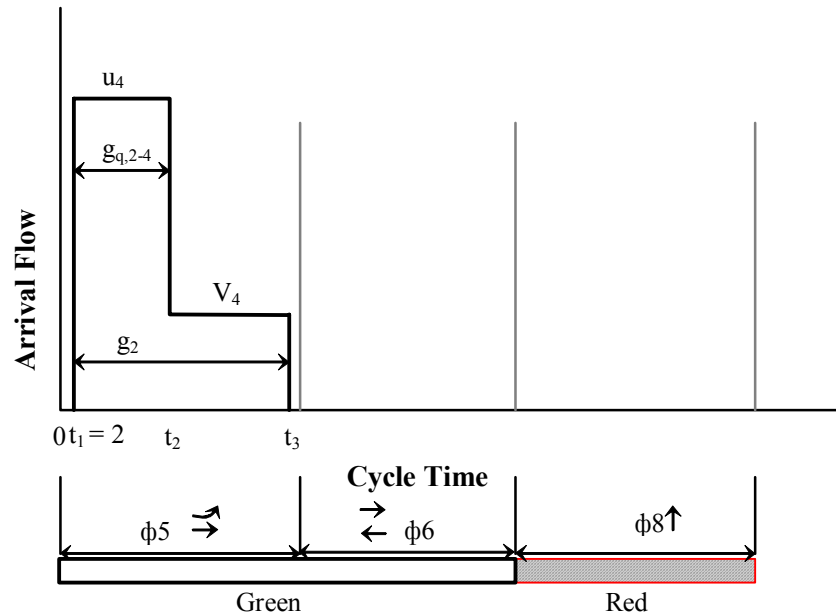


**FIGURE 27** Arrival flow profile for the internal left-turn movement (M4): four-phase.

## **FREEWAY AND RAMP-METERING OPERATIONS**

Modeling of freeway and ramp-metering operations is also based on the cumulative arrival and departure methodology with consideration of stochastic traffic flow on the freeway mainline and the unique arrival flow patterns at the ramp meters that resulted from the upstream diamond interchange signal. The cumulative arrival/departure flows on the freeway mainlines and the ramps are derived for every 1-second interval based on the flow-balance principle (72). First, a gap-acceptance-based model is introduced for determining ramp-metering thresholds. Mathematical formulations are then given to describe the modeling process for freeway operations and ramp metering. Finally, the representation of ramp arrival flow profiles is described.

### Ramp-Metering Threshold

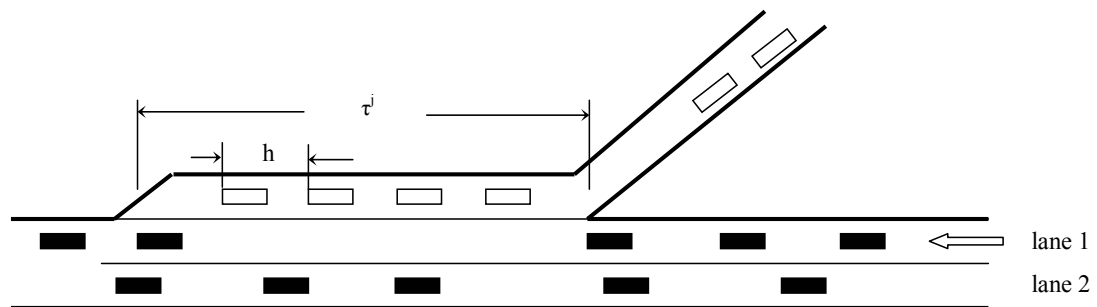
As discussed in Chapter II, ramp metering is effective only when the freeway mainline traffic reaches a minimum threshold value. Currently, most ramp-metering thresholds are empirically derived based on field observations. In this section, a model based on the gap-acceptance theory was presented which explored the characteristics at a freeway merge and the effect of ramp-control strategies. The modeling process also yielded a theoretically derived ramp-metering threshold.

Figure 28 illustrates three cases for a typical freeway merge operation, when no disruption would occur to the freeway mainline traffic: (a) a freeway mainline gap is large enough to handle the ramp traffic; (b) the mainline gap is not large enough, but the vehicle can slow down to yield a large gap; and (c) the mainline gap is not large enough, but the freeway vehicle can make a lane change and yield a large gap. In the figure, a platoon size of four vehicles is shown. These three conditions were used to establish the mainline volume threshold when ramp metering is not necessary. Obviously, the volume threshold is related to the size of the platoon.

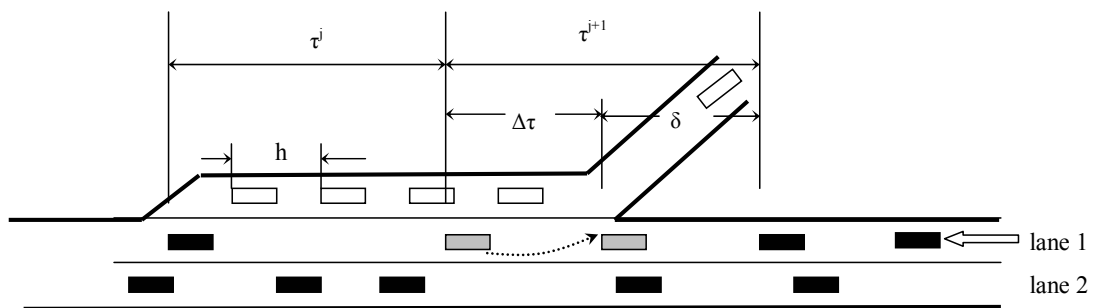
In general, the distribution of the headways/gaps in a traffic stream follows a function  $f(\tau) = f(\tau, V)$ , where  $\tau$  is the length of the headway and  $V$  the traffic volume in vehicles per second. One of the commonly used headway distributions for traffic stream is the Cowan's M3 model (88). Sullivan and Troutbeck (89) proved that the Cowan's M3 model can accurately represent vehicle headways in both freeway and arterial street.

Cowan's M3 model is a dichotomized distribution. Its cumulative density function,  $F(\tau)$ , is given in Equation 75. Cowan's M3 model was evolved from the shifted negative exponential distribution with two additional parameters:  $\varepsilon$ , the proportion of free-moving vehicles, and  $\theta$ , the flow rate within non-bunched vehicles.  $\varepsilon$  and the minimum headway,  $\delta$ , in Equation 75 need to be calibrated based on site locations. For example, the factors affecting  $\varepsilon$  include the flow rate, the number of travel lanes, the traffic composition, and the distance to an upstream signal (90).

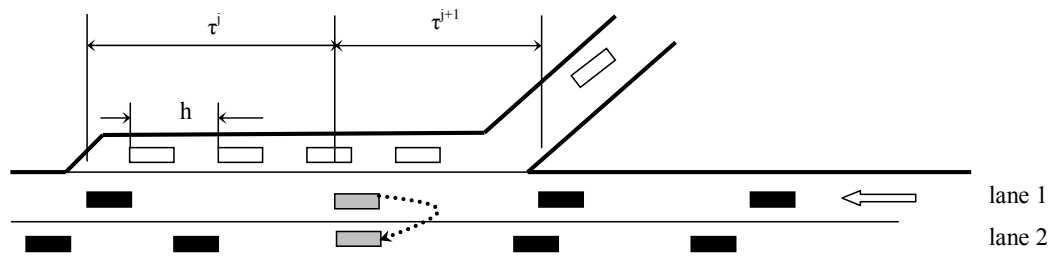
$$F(\tau) = \begin{cases} 1 - \varepsilon e^{-\theta(\tau-\delta)} & \text{for } \tau \geq \delta \\ 0 & \text{for } \tau < \delta \end{cases} \quad (75)$$



(a) Platoon size  $n = 4$  veh. Gap in the merge lane,  $\tau^j$ , is no less than  $(n + 1)$ .



(b) Gap in the first lane is  $\Delta\tau$  shorter than required. The freeway vehicle can slow down by  $\Delta\tau$  without affecting the following vehicle.



(c) Gap in the first lane is smaller than required. The freeway vehicle can make a lane change to the adjacent lane.

**FIGURE 28 Freeway merge and gap conditions without disturbance.**



For normal traffic conditions without impedance of upstream signals such as the freeway traffic, the following equations apply (91):

$$\varepsilon = 1 - V \cdot \delta \quad (76)$$

$$\theta = V \quad (77)$$

Thus, Equation 75 yields:

$$F(\tau) = \begin{cases} 1 - (1 - V\delta)e^{-V(\tau-\delta)} & \text{for } \tau \geq \delta \\ 0 & \text{for } \tau < \delta \end{cases} \quad (78)$$

To further model the ramp-merging process, the traffic volume in the merging lane needs to be known, which can be obtained if the total mainline volume and the lane volume distribution are known. In this research, field data were collected at two site locations for estimating the lane flow distributions. One of the sites is a two-lane freeway section in College Station, Texas. The other site is a three-lane freeway section in Toronto, Canada.

Based on the data from the two-lane freeway in College Station, Texas, the proportion of lane volume distribution,  $p_l$ , has the regression form shown in Equation 79:

$$\begin{cases} p_1 = 0.332 + (1 - 0.332) \cdot e^{-1.440 \cdot V_F^{0.5}} \\ p_2 = 1 - p_1 \end{cases} \quad (79)$$

Based on the field data collected in the three-lane freeway section in Toronto, Canada, the lane volume distribution has the following regression form shown in Equation 80:

$$\begin{cases} p_1 = 0.235 + (1 - 0.235) \cdot e^{-4.758V_F^{0.5}} \\ p_3 = 0.420 \cdot (1 - e^{-2.340 \cdot V_F}) \\ p_2 = 1 - p_1 - p_3 \end{cases} \quad (80)$$

Figure 29 and Figure 30 illustrate the above regression equations. As can be seen from these figures, the proportion of traffic volume in the merge lane (lane 1),  $p_1$ , decreases as the freeway flow increases, which is consistent with the results documented in Figure 3.6 of May's *Traffic Flow Fundamentals* (40). However, this contradicts the results found by Park (92). Park indicates that  $p_1$  increases as freeway volume increases.

Once  $p_l$  is obtained, the traffic flows in each lane can then be calculated:

$$\begin{cases} V_{l1} = p_1 \cdot V_F \\ V_{l2} = p_2 \cdot V_F \\ \dots \\ \dots \end{cases} \quad (81)$$

The probability of no disruption to freeway mainline traffic, as defined in the three cases shown in Figure 28, can be determined and used to determine the ramp-metering threshold based on an assumed acceptable level of probability. For case a, the probability of no disruption,  $P_{ND,a}$ , is equal to the probability that the length of a gap in the mainline traffic stream in lane 1 is larger than the platoon size,  $B$ , measured in seconds. That is, the probability of no disruption in this case is simply the probability of  $\tau \geq B$ .

$$P_{ND,a} = P(\tau \geq B) = 1 - F_\tau(\tau = B) = \varepsilon_1 \cdot e^{-V_{l1} \cdot (B - \delta)} \quad (82)$$

where  $\varepsilon_l$  is the proportion of non-bunched vehicles in lane 1 traffic of the freeway mainline.

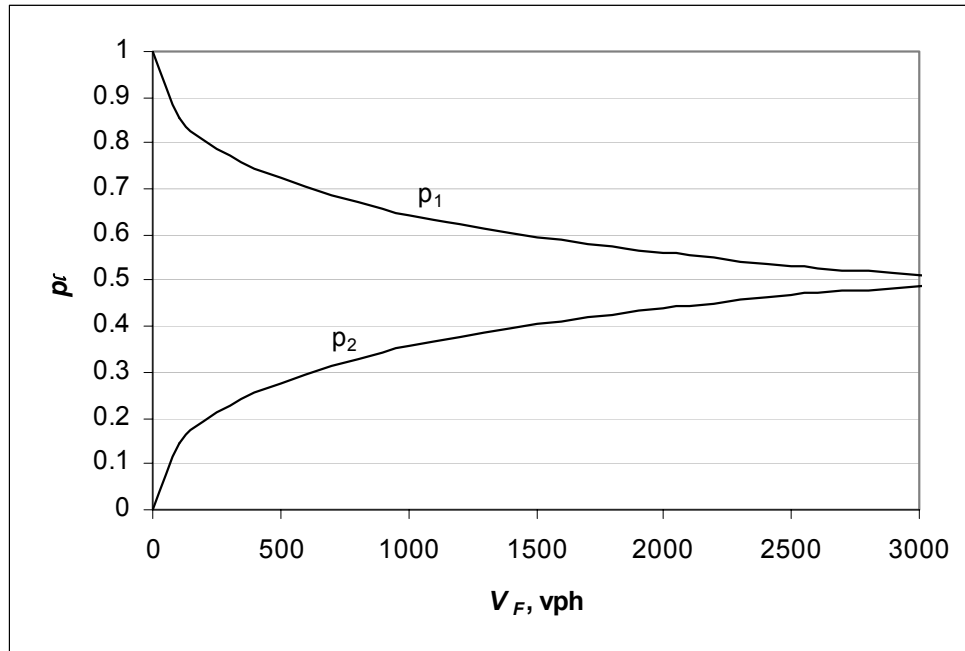


**FIGURE 29** Lane flow distribution: two-lane freeway.

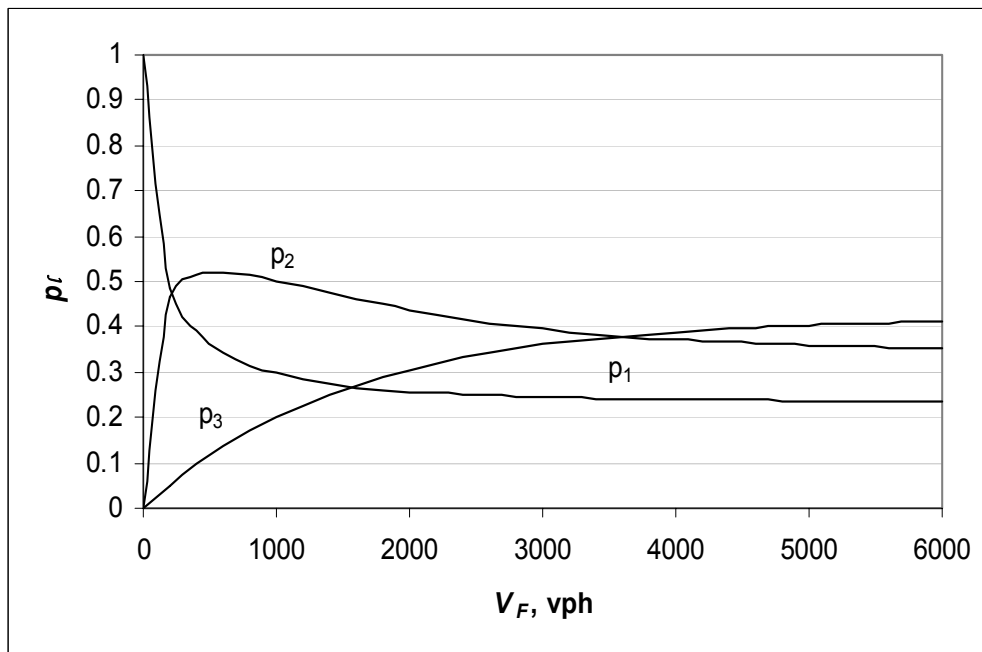


**FIGURE 30** Lane flow distribution: three-lane freeway.

For case b, we are looking for the probability of  $\tau^1 + \tau^2 > B + \delta$  under the condition of  $\tau^1 \leq B$ , where  $\tau^1$  and  $\tau^2$  are two consecutive gaps in the major stream. We can consider the event of  $\tau^1 + \tau^2 > B + \delta$  and the event of  $\tau^1 \leq B$  to be independent; thus, we have:

$$\begin{aligned} P_{ND,b} &= \Pr(\tau^1 + \tau^2 > B + \delta \mid \tau^1 \leq B) \\ &= \Pr(\tau^1 + \tau^2 > B + \delta) \cdot \Pr(\tau^1 \leq B) \end{aligned} \quad (83)$$

Since  $\tau^1 + \tau^2$  obeys the shifted-Erlang distribution (93), we have:

$$F_{\tau^1 + \tau^2}(\tau) = 1 - \varepsilon_1 \cdot e^{-2V_{l1}(\tau - \delta)} \cdot [1 + 2 \cdot V_{l1} \cdot (\tau - \delta)] \quad (84)$$

$$\begin{aligned} P_{ND,b} &= \Pr(\tau^1 + \tau^2 > B + \delta) \cdot \Pr(\tau^1 \leq B) \\ &= [1 - F_{\tau^1 + \tau^2}(B + \delta)] \cdot F_{\tau^1}(B) \\ &= \varepsilon_1 \cdot e^{-2V_{l1}(B + \delta - \delta)} \cdot [1 + 2 \cdot V_{l1} \cdot (B + \delta - \delta)] \cdot [1 - \varepsilon_1 \cdot e^{-V_{l1}(B - \delta)}] \\ &= \varepsilon_1 \cdot e^{-2V_{l1} \cdot B} \cdot (1 + 2 \cdot V_{l1} \cdot B) \cdot [1 - \varepsilon_1 \cdot e^{-V_{l1}(B - \delta)}] \end{aligned} \quad (85)$$

For case c, the probability of no disruption,  $P_{ND,c}$ , is the probability of  $\tau_1 < B$ ,  $\tau_2 > \tau_{c,2}$ , and  $\tau^1 + \tau^2 < B + \delta$ . Thus, the probability of no disruption is:

$$P_{ND,c} = \Pr(\tau_1 < B) \cdot \Pr(\tau_2 > \tau_{c,2}) \cdot \Pr(\tau^1 + \tau^2 < B + \delta) \quad (86)$$

$$\begin{aligned} P_{ND,c} &= \Pr(\tau_1 < B) \cdot \Pr(\tau_2 > \tau_{c,2}) \cdot \Pr(\tau^1 + \tau^2 < B) \\ &= F_{\tau_1}(B) \cdot [1 - F_{\tau_2}(\tau_{c,2})] \cdot F_{\tau^1 + \tau^2}(B) \\ &= [1 - \varepsilon_1 \cdot e^{-V_{l1}(B - \delta)}] \cdot \varepsilon_2 \cdot e^{-V_{l2}(\tau_{c,2} - \delta)} \cdot [1 - \varepsilon_1 \cdot e^{-2V_{l1} \cdot B} \cdot (1 + 2 \cdot V_{l1} \cdot B)] \end{aligned} \quad (87)$$

$$P_{ND} = P_{ND,a} + P_{ND,b} + P_{ND,c} \quad (88)$$

Once the platoon size of the ramp traffic,  $B$ , measured in seconds is known,  $P_{ND}$  can then be obtained from the equations described above. For example, with random arrival (no upstream signal),  $B$  can be estimated by:

$$B = \frac{x_R h}{1 - x_R} \quad (89)$$

Equation 89 indicates that the ramp volume-to-capacity ratio,  $x_R$ , is a major variable to determine the size of the platoon,  $B$ . The capacity of the freeway on-ramp,  $c_{ramp}$ , can be calculated based on either the gap-acceptance model as shown in Equation 90 or based on the HCM linear model as shown in Equation 91:

$$c_{ramp} = \frac{\varepsilon_1}{\tau_f} \cdot e^{-V_{l1}(\tau_{e,1} \frac{\tau_f}{2} - \delta)} \quad (90)$$

$$c_{ramp} = 4600 - (V_{l1} + V_{l2}) \quad (91)$$

Figure 31 illustrates the probabilities of no disruption as defined in Equation 82, Equation 83, Equation 87, and Equation 88 for a three-lane freeway and with random ramp arrivals. The capacity is based on the HCM deterministic capacity formula shown in Equation 91, and the ramp traffic demand is 500 vph. Figure 32 illustrates the probability of no disruption with different ramp demand levels. If the acceptable probability level is assumed to be 0.90, the mainline threshold without disruption is approximately between 3500 vph and 4500 vph for a three-lane freeway. In the next section of this chapter, the modeling of the ramp-metering operations in determining the ramp-metering rate is discussed, which applies the mainline volume threshold to determine whether the meter should be on or off (refer to Equation 95 in the next section).

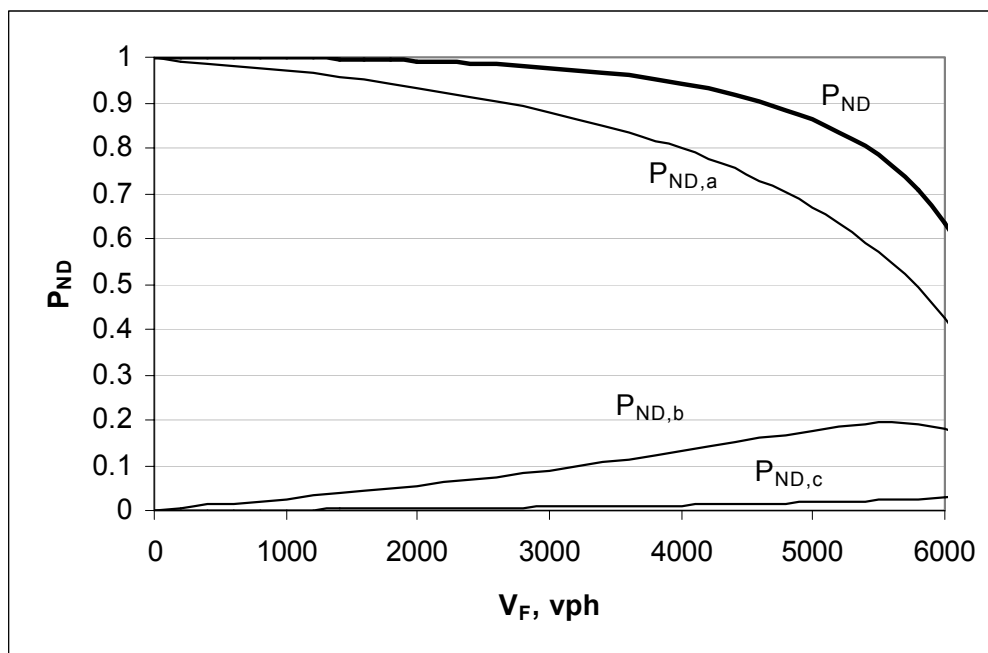


**FIGURE 31 Probabilities of no disruption.**

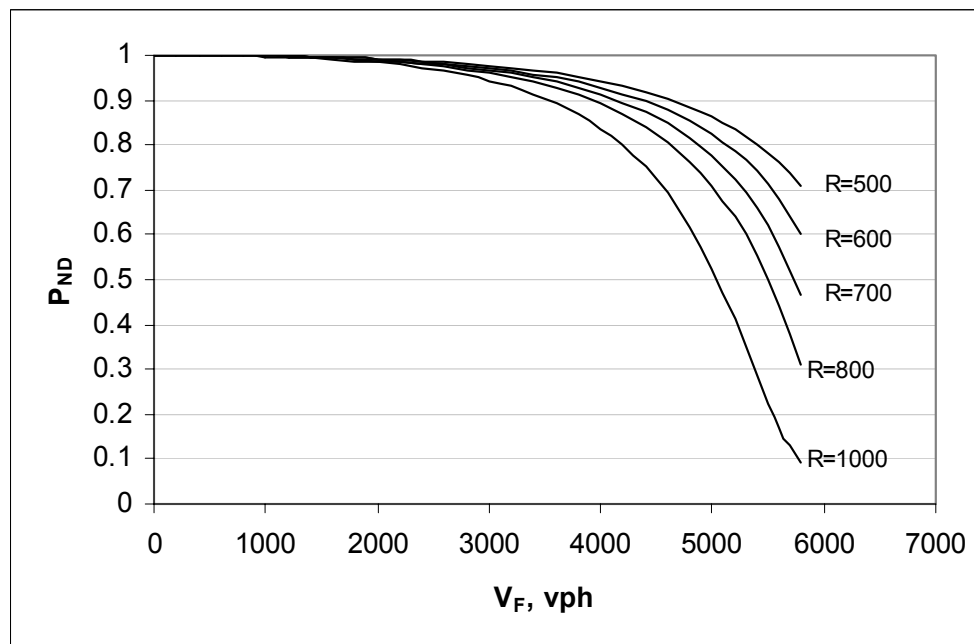


**FIGURE 32 Probability of no disruption with random ramp arrival.**

The above gap-acceptance-based threshold model provides a first step to explore ramp-metering thresholds from the theoretical point of view. The model could be expanded to conduct more detailed investigations on this subject. Further research results can be found in a possible future publication (94).

### Freeway and Ramp Metering

The modeling of freeway and ramp-metering operations in this research consists of procedures for determining traffic-responsive ramp-metering rate, stochastic freeway mainline capacity, queues, and delays on both the ramps and the mainlines. Again, the cumulative arrival/departure method is used to calculate queues and delays. The analysis is carried out on a second-by-second basis, including detailed descriptions of the arrival and departure flow profiles.

Equation 92 through Equation 94 derive the freeway mainline flow expected to arrive immediately upstream of the on-ramp at time interval  $t$ . The initial randomly generated demand,  $F_r(t)$ , is capped at a level that equals a factor  $\gamma$  times the free-flow capacity,  $c_{Fr}$ , representing the maximum flow rate that could get to the ramp merge point.  $F_r'(t)$  is the average flow at time step  $t$  during the ramp-metering interval,  $a$ .  $F_r''(t)$  will be used to determine the ramp-metering rate in Equation 95 so that the same ramp-metering rate would result in the same metering interval.

$$F_r'(t) = \begin{cases} \gamma c_{Fr}, & F_r(t) > \gamma c_{Fr} \\ \text{Min}[F_r(t) + \Delta F_r(t-1), \gamma c_{Fr}], & \text{Otherwise} \end{cases} \quad (92)$$

$$\Delta F_r(t) = \text{Max}[0, \Delta F_r(t-1) + F_r(t) - F_r'(t)] \quad (93)$$

$$F_r''(t) = \frac{1}{a} \sum_{i=\text{int}(\frac{t-1}{a})a+1}^{i+a-1} F_r'(i) \quad (94)$$

$$M_r(t) = \left\{ \begin{array}{ll} M_{r,\min}, & q_{Fr} \left[ \text{int} \left( \frac{t-1}{a} \right) a \right] \geq \frac{c_{Fr}(\eta-1)}{3600} \\ M_{r,\min}, & F_r''(t) + \frac{1}{\omega} M_{r,\min} > c_{Fr} \\ S_{Rr}, & F_r''(t) \leq V_T \\ \text{Min} \{ \omega [c_{Fr} - F_r''(t)], M_{r,\max} \}, & \text{Otherwise} \end{array} \right\} \quad (95)$$

The ramp-metering rate determined from Equation 95 follows the basic demand-capacity principle as described in Equation 24. However, it does have a component of terminating ramp-metering operation if the mainline flow is below the metering threshold,  $V_T$ , where  $S_{Rr}$ , the ramp queue flush rate, would result.

Equations 96 through 99 represent the cumulative arrival and departure method in discrete forms. Equation 96 is the number of cumulative arrivals for the ramp,  $r$ . Equation 97 is the ramp queue length at time  $t$ . Equation 98 is the cumulative departure function at the ramp. Equation 99 is the ramp throughput flow at time  $t$ .

$$A_{Rr}(t) = \sum_{i=1}^t \frac{R_r(i)}{3600} \quad (96)$$

$$q_{Rr}(t) = \text{Max} \left[ 0, q_{Rr}(t-1) + \frac{R_r(t) - M_r(t)}{3600} \right] \quad (97)$$

$$D_{Rr}(t) = A_{Rr}(t) - q_{Rr}(t) \quad (98)$$

$$O_{Rr}(t) = 3600 [D_{Rr}(t) - D_{Rr}(t-1)] \quad (99)$$

Equation 100 determines the freeway mainline capacity at time  $t$ , which has the two-capacity nature with random variations, as given by the random variable generation



function,  $F^{-1}()$ .  $F^{-1}()$  produces a random variable based on the normal distribution with the mean freeway capacity, either  $c_{Qr}$  or  $c_{Fr}$ , and the standard deviation, either  $\sigma_{Qr}$ , or  $\sigma_{Fr}$ , depending on the conditions described in Equation 100. The mean capacities and their standard deviations would have to be obtained either from field studies or through simulation.  $\eta$  in Equation 100 is called the breakdown factor (calibrated at 1.3 later in the dissertation) to reflect that the freeway will break down once the bottleneck demand is 1.3 times or higher than the free-flow capacity,  $c_{Fr}$ . Introducing  $\eta$  in the equation is to allow freeway to maintain at free-flow condition even with marginal queues on the freeway.

$$c_{Fr}(t) = \begin{cases} F^{-1}(RND, c_{Qr}, \sigma_{Qr}), & 3600q_{Fr}(t-1) + F_r''(t) + O_{Rr}(t) > \eta c_{Fr} \\ F^{-1}(RND, c_{Fr}, \sigma_{Fr}), & \text{Otherwise} \end{cases} \quad (100)$$

Equations 101 through 104 represent the modeling process using the discrete form cumulative arrival and departure method for the freeway mainline. Equation 105 and Equation 106 are the total delays in terms of vehicle-hours for the ramp and the mainline, respectively.

$$A_{Fr}(t) = \sum_{i=1}^t \frac{[F_r''(i) + O_{Rr}(i)]}{3600} \quad (101)$$

$$q_{Fr}(t) = \text{Max}[0, q_{Fr}(t-1) + \frac{F_r''(t) + O_{Rr}(t) - c_{Fr}(t)}{3600}] \quad (102)$$

$$D_{Fr}(t) = A_{Fr}(t) - q_{Fr}(t) \quad (103)$$

$$O_{Fr}(t) = 3600[D_{Fr}(t) - D_{Fr}(t-1)] \quad (104)$$

$$TD_{Rr} = \sum_{i=1}^T \frac{q_{Rr}(i)}{3600} \quad (105)$$

$$TD_{Fr} = \sum_{i=1}^T \frac{q_{Fr}(i)}{3600} \quad (106)$$

### **Ramp Arrival Flow Profiles**

Modeling ramp operations using the cumulative arrival and departure method requires adequate description of the traffic arrival and departure flow profiles. With the existence of upstream diamond interchange signals, vehicles arrive at the metered on-ramps with unique flow structures, which are related to the type of control and the signal timing at the diamond interchange signals. Similar to the graphical description of the internal traffic movement profiles, the ramp arrival profiles are created considering the diamond signal phasing, timing, and flow distribution between the ramp and the frontage road. Only the profiles for *R1* are illustrated below to demonstrate the processes for creating the profiles. Profiles for *R2* follow the same procedures. The profiles do not take into account the possible platoon dispersion as traffic moves downstream to the ramp.

#### ***Profiles without Arterial Right-Turn Control***

When the arterial right-turn traffic and the U-turn traffic are not controlled by the diamond signal, uniform arrivals are assumed for the right-turn and U-turn traffic. Figure 33 is the arrival flow profile with the three-phase scheme.

Each traffic movement controlled by the diamond interchange signal (i.e., *M2* and *M10* in this case) would leave the diamond interchange and arrive at the ramp with

two flow regimes: the saturated queue discharge regime and the unsaturated regime. The flow rate ( $W_j$ ) is the actual traffic flow rate arriving at  $RI$ , which does not include the traffic going to the frontage road. For example, during the frontage road phases ( $\phi_4$  and  $\phi_8$ ), the first portion of the flow,  $W_j$ , occurs when the frontage road movement  $M_2$  discharges at its saturation flow rate ( $S_2$ ). Therefore,  $W_j$  is composed of the flows  $S_2$ ,  $V_6$ , and  $V_{14}$ . After the queue of  $M_2$  is cleared, the flow rate reduces to its average demand ( $V_2$ ). After the green interval of  $\phi_4$  and during  $\phi_2$ , the only components of the ramp arrival flows are those from the arterial right-turn movement ( $M_6$ ) and the U-turn movement ( $M_{14}$ ). The relationship between the individual flows should satisfy:

$$R_1 = \frac{1}{C} \sum_{j=1}^5 W_j (t_j - t_{j-1}) \quad (107)$$

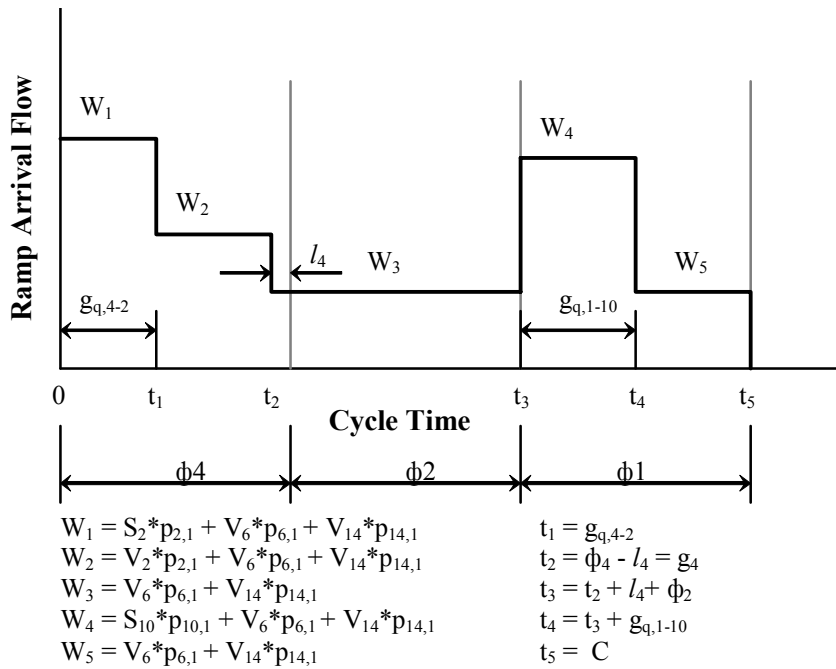


**FIGURE 33 Ramp arrival flow profile without right-turn control: three-phase.**

The related parameters in Figure 33 are calculated in the following equations:

$$g_{q,4-2} = \begin{cases} \frac{3600N_2 + V_2r_4}{S_2 - V_2}, & x_2 < 1 \\ g_4, & x_2 \geq 1 \end{cases} \quad (108)$$

$$g_{q,1-10} = \begin{cases} g_1x_{10} = \frac{3600N_{10} + V_{10}C}{S_{10}}, & q_{M10} < Q_{M10} \\ \frac{Q_{M10}}{S_{10}} 3600, & q_{M10} = Q_{M10} \end{cases} \quad (109)$$

Figure 34 is the ramp arrival flow profile with the four-phase scheme. For the case of four-phase diamond phasing, the profile needs to take into consideration the phases of the other side interchange (i.e.,  $\phi_6$  and  $\phi_8$ ). The dashed line during the period between  $t_1$  and  $t_2$  is a more accurate representation of the actual arrival flow; however, for modeling purposes, the flow profile is simplified by using the average flow rate during the unsaturated green portion and the clearance interval.

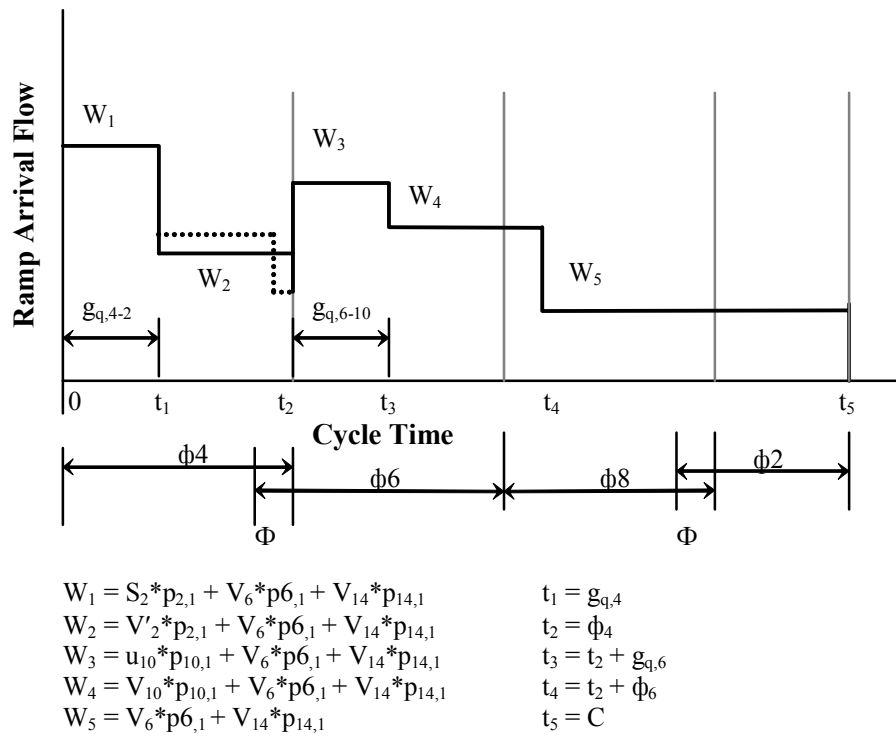


**FIGURE 34 Ramp arrival flow profile without right-turn control: four-phase.**

The related parameters in Figure 34 are calculated in the following equations:

$$g_{q,6-10} = \begin{cases} \frac{3600(N_{10} + N_{11}) + (V_{10} + V_{11})(1 - P_{10-11})Cg_6}{S_{10-11}g_6 - (V_{10} + V_{11})P_{10-11}C}, & x_{10-11} < 1 \\ g_6, & x_{10-11} \geq 1 \end{cases} \quad (110)$$

$$u_{10} = S_{10-11} \frac{V_{10}}{V_{10} + V_{11}} \quad (111)$$

When arterial traffic has random arrival:

$$g_{q,6-10} = \begin{cases} \frac{3600(N_{10} + N_{11}) + (V_{10} + V_{11})r_6}{S_{10-11} - (V_{10} + V_{11})}, & x_{10-11} < 1 \\ g_6, & x_{10-11} \geq 1 \end{cases} \quad (112)$$

$$V_2' = \frac{V_2(\phi_4 - g_{q,4-2} - l)}{\phi_4 - g_{q,4-2}} = \frac{V_2(g_4 - g_{q,4-2})}{\phi_4 - g_{q,4-2}} \quad (113)$$

As shown in Figure 33 and Figure 34, the ramp arrival profiles with both three-phase and four-phase can be represented with five different flow regimes when the arterial right-turn traffic movement is not controlled by the signal.

### ***Profiles with Arterial Right-Turn Control***

When the arterial right-turn movement is controlled with the arterial through movement and with a signal, the profiles will be different. Figure 35 shows the ramp arrival profile with a three-phase phasing scheme, which includes six flow regimes.

The related parameters in Figure 35 are calculated in the following equations:

$$V'_6 = \frac{V_6(\phi_2 - g_{q,2-6} - l)}{\phi_2 - g_{q,2} - 6} = \frac{V_6(g_2 - g_{q,2-6})}{\phi_2 - g_{q,2} - 6} \quad (114)$$

$$u_6 = \begin{cases} S_6, & \text{Exclusive right - turn lane} \\ (S_{4-5} + S_6) \frac{V_6}{V_4 + V_5 + V_6}, & \text{Shared lane} \end{cases} \quad (115)$$

$$g_{q,2-6} = \begin{cases} \frac{3600N_6 + V_6(1 - P_{2-6})Cg_2}{S_6g_2 - V_6P_{2-6}C}, & \text{Exclusive RT lane} \\ \frac{3600(N_4 + N_5 + N_6) + (V_4 + V_5 + V_6)(1 - P_{2-6})Cg_2}{(S_{4-5} + S_6)g_2 - (V_4 + V_5 + V_6)P_{2-6}C}, & \text{Shared lane} \end{cases} \quad (116)$$

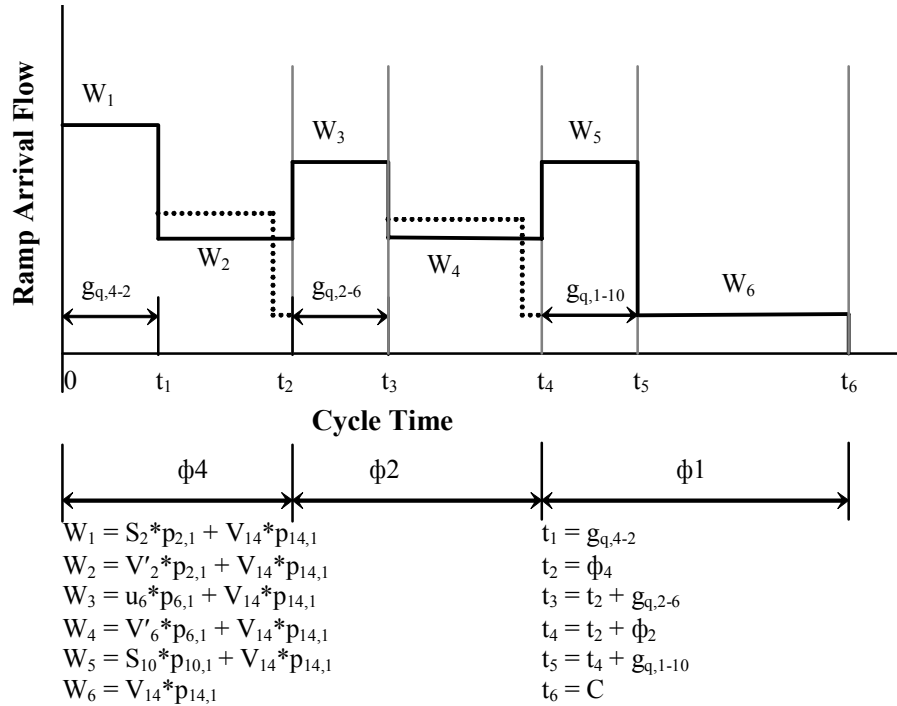


**FIGURE 35 Ramp arrival flow profile with right-turn control: three-phase.**

Figure 36 shows the profile with right-turn control and four-phase, and the related parameters,  $g_{q,4-2}$ ,  $g_{q,6-10}$ ,  $g_{q,2-6}$ ,  $u_6$ ,  $u_{10}$ ,  $V'_2$ , and  $V'_{10}$ , have been defined previously.

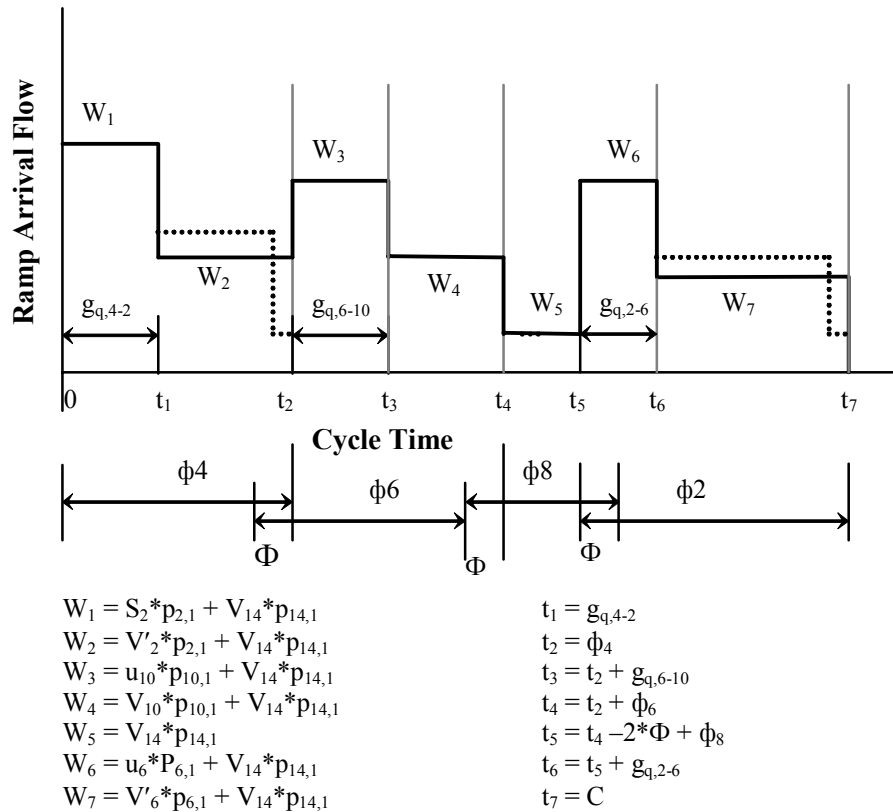


**FIGURE 36 Ramp arrival flow profile with right-turn control: four-phase.**

### MODELING RAMP QUEUE SPILLBACK

At the diamond interchange, the traffic released from the diamond signal may experience impedance from ramp queues once queue spillback occurs. In the previous section on modeling diamond interchange operations, the impeded discharging flow rate and the residual queues that resulted from ramp queue impedance need to be

determined. This section documents the modeling process of ramp queue spillback and how these variables are obtained.

When there is sufficient storage between the ramp meter and the diamond signal to store the vehicle queues, the diamond interchange signal can discharge the vehicles according to the traffic flow profiles depicted in Figure 33 through Figure 36 without incurring any impedance. However, when the storage space is filled with queued vehicles due to either limited spacing or simply over-saturation, the ramp queues would impede traffic flows discharged from the diamond signals, resulting in reduced capacity and increased delay for the affected traffic movements. Previous studies on modeling queue spillback at signalized intersections used two general approaches. One approach is to reduce the saturation flow rate (95, 96). For example, Messer and Bonneson (95) proposed using a simple factor to adjust the saturation flow rate based on the queue length of the downstream link. The other approach is to reduce the effective green time (97), considering the queue block effect as equivalent to the loss of effective green time. Both approaches proved to be appropriate in reaching similar modeling results.

Since the ramp operations and ramp queues are modeled on a second-by-second basis, it is possible to have a detailed modeling of the impact of spillback on diamond interchange operations. The following discussions describe the proposed modeling methodology, which follows the approach of adjusting discharge flows.

The basic principle used to model vehicle discharge from the diamond signal with potential queue spillback is that the vehicle would discharge at a flow rate that is governed by a minimum of three flows: the actual demand flow, the saturation flow, and the spillback and blocking flow. Because not all the traffic discharged from the diamond interchange will arrive at the ramp (some will go to the frontage road), there are two steps involved in deriving the number of vehicles impeded and the residual queues for the diamond movements that feed the ramp. The first step is to calculate the number of impeded vehicles in terms of the ramp arrival flow rate. The second step is then to convert the ramp vehicles to the diamond feeding movement vehicles.



Equation 117 shows the calculation of the ramp arrival flow rate at time  $t$ , which constitutes a portion of the flows from the diamond movements:

$$V_r(t) = \text{Min}[V_{Wr}(t), V_{Mr}(t), V_{Br}(t)] \quad (117)$$

In Equation 117,  $V_{Wr}(t)$  is the unimpeded demand flow when there is no queue spillback to the diamond signal so that vehicles can discharge freely from the signal according to traffic flow profiles described in Figure 33 through Figure 36.  $V_{Mr}(t)$  is the maximum possible flow rate that can be discharged from the diamond signal that would arrive at the ramp meter.  $V_{Br}(t)$  is the portion of flow that would arrive at the ramp meter when the diamond signal is discharging at saturation flow rates during a particular phase.  $V_{Br}(t)$  varies depending on the diamond phasing scheme, and its values are determined based on Table 6.

**TABLE 6 Determination of  $V_{Mr}(t)$  values**

Phasing Scheme	Phase Sequence (Ramp 1/Ramp 2)	Time and Maximum Flows	
		No Right-Turn Control	With Right-Turn Control
Three-Phase	$\phi 4/\phi 8$	$t_2, W_1$	$t_2, W_1$
	$\phi 2/\phi 6$	$t_3, W_3$	$t_4, W_3$
	$\phi 1/\phi 5$	$t_5, W_4$	$t_6, W_5$
Four-Phase	$\phi 4/\phi 8$	$t_2, W_1$	$t_2, W_1$
	$\phi 6/\phi 2$	$t_5 - \phi 2, W_3$	$t_7 - \phi 2, W_3$
	$\phi 8, 2/\phi 4, 6$	$t_5, W_5$	$t_7, W_6$

Note: Refer to Figure 33 through Figure 36 for referencing  $t_j, W_j$ .

As an example for ramp 1 with three-phase and no right-turn control (refer to Figure 33), the phasing sequence is  $\phi 4, \phi 2, \phi 1$ .  $W_1$  is the ramp arrival flow when  $M2$

discharges at its saturation flow rate. This flow can last to the point at  $t_2$  as long as there is sufficient demand.  $W_3$  is the ramp arrival flow when M6 and M14 discharge at their saturation flow rates, and it can last to the point at  $t_3$ .  $W_4$  is the ramp arrival flow when M10 of  $\phi I$  discharges at its saturation flow rate, and it can last to the point at  $t_5$ .

$V_{Br}(t)$  is the flow that would result in queue spillback at ramp  $r$  to block the diamond signal, which can be determined based on Equation 118:

$$V_{Br}(t) = 3600[Q_{Rr} - q_{Rr}(t-1)] + M_r(t) \quad (118)$$

The ramp queue storage space,  $Q_{Rr}$ , is expressed in an integer number and is assumed to be constant, although it may actually change depending on the ramp metering rate and the vehicle moving speed. Chapter V includes discussions on this assumption and how it should be counted when calibrating and validating the model based on microscopic simulation. In order to ensure enough accuracy, the queue length,  $q_{Rr}$ , needs to carry a significant number of digits because the analysis is on a 1-second basis. Equation 118 also implies that even with the queue storage filled up at time  $t$ , the ramp would still receive vehicle arrivals at the same rate as the metering rate,  $M_r(t)$ .

The above modeling approach to the blocking flow rate does not take into consideration the time lag for the current ramp-metering rate to take place at the diamond interchange location. The time lag is a result of a backward-moving shockwave due to changes in ramp-metering rates between metering intervals. For example, during the queue flush mode,  $M_r(t)$  reaches the highest metering rate, i.e., the saturation flow rate at the ramp. However, this ramp discharging flow rate could only take effect some time later when the backward shockwave reaches the diamond signal.

In general, the shockwave effect should not significantly impact the modeling results in this research. With queue flush operation, the advanced queue detector could be placed at such a location that the ramp queue would never reach the diamond signal

and cause blocking to the signal. When queue flush is not used, the shockwave effect would not be so obvious because dramatic changes in metering rates between metering intervals are not expected in real operations. Due to the complexity of accurately determining the shockwave speed (e.g., the ramp does not have a uniform arrival flow due to the diamond signal) and the insignificant impact on the modeling results, the modeling process used in this research does not specifically address the shockwave effect.

Given the demand profile and the discharge profile at the ramp, any vehicles that cannot be discharged freely are considered residual queues for the current cycle. These residual queues are recorded and will be used to calculate the traffic demand for the following cycle. They are also used to calculate delays, as discussed earlier in this chapter, where both the initial queue and the residual queue are taken into consideration.

Calculations of the residual queues are performed for each diamond movement that feeds the ramp, once the number of residual queues in terms of the ramp traffic is obtained with the procedures described. The ramp residual queues are distributed among all ramp-feeding movements based on the  $p_{m,r}$  values of the current cycle. Depending on the type of phasing scheme and whether the arterial right-turn movement is controlled by the signal, the distribution of the residual queues among all the movements is different. The following procedure illustrates when the diamond operates at three-phase and the arterial right-turn movement is not controlled by the signal.

During the current cycle  $j$ , the traffic demands feeding  $RI$  from the four feeding movements ( $M2$ ,  $M6$ ,  $M10$ , and  $M14$ ) are given by Equation 119 through Equation 122:

$$V_{2-1}^j = p_{2,1}^j V_2^j \quad (119)$$

$$V_{10-1}^j = p_{10,1}^j V_{10}^j \quad (120)$$

$$V_{6-1}^j = p_{6,1}^j V_6^j \quad (121)$$

$$V_{14-1}^j = p_{14,1}^j V_{14}^j \quad (122)$$

The phasing sequence at the diamond signal is  $\phi 4$ ,  $\phi 2$ ,  $\phi 1$ . The residual ramp queues are recorded as  $N_{\phi 4}^j$ ,  $N_{\phi 2}^j$ ,  $N_{\phi 1}^j$ , respectively, during each phase. Note that the arterial right-turn movement ( $M6$ ) and the U-turn traffic ( $M14$ ) are free movements and are assumed to arrive at the ramp uniformly. Therefore,  $N_{\phi 4}^j$  is contributed by three movements:  $M2$ ,  $M6$ , and  $M14$ ;  $N_{\phi 2}^j$  is contributed by two movements:  $M6$  and  $M14$ ; and  $N_{\phi 1}^j$  is contributed by three movements:  $M10$ ,  $M6$ , and  $M14$ .

The residual queue for  $M2$ ,  $NR_2^j$  is then:

$$NR_2^j = \frac{\left( \frac{V_{2-1}^j}{V_{2-1}^j + V_{6-1}^j + V_{14-1}^j} N_{\phi 4}^j \right)}{p_{2,1}^j} \quad (123)$$

The residual queue for  $M10$ ,  $NR_{10}^j$ , is determined by:

$$NR_{10}^j = \frac{\left( \frac{V_{10-1}^j}{V_{6-1}^j + V_{10-1}^j + V_{14-1}^j} N_{\phi 1}^j \right)}{p_{10,1}^j} \quad (124)$$

The residual queue for  $M6$ ,  $NR_6^j$ , is determined by:

$$NR_6^j = \frac{\left( \frac{V_{6-1}^j}{V_{2-1}^j + V_{6-1}^j + V_{14-1}^j} N_{\phi 4}^j \right)}{p_{6,1}^j} + \frac{\left( \frac{V_{6-1}^j}{V_{6-1}^j + V_{14-1}^j} N_{\phi 2}^j \right)}{p_{6,1}^j} + \frac{\left( \frac{V_{6-1}^j}{V_{6-1}^j + V_{10-1}^j + V_{14-1}^j} N_{\phi 1}^j \right)}{p_{6,1}^j} \quad (125)$$

The residual queue for  $M14$ ,  $NR_{14}^j$ , is determined by:

$$NR_{14}^j = \frac{\left( \frac{V_{14-1}^j}{V_{2-1}^j + V_{6-1}^j + V_{14-1}^j} N_{\phi 4}^j \right)}{p_{14,1}^j} + \frac{\left( \frac{V_{14-1}^j}{V_{6-1}^j + V_{14-1}^j} N_{\phi 2}^j \right)}{p_{14,1}^j} + \frac{\left( \frac{V_{14-1}^j}{V_{6-1}^j + V_{10-1}^j + V_{14-1}^j} N_{\phi 1}^j \right)}{p_{14,1}^j} \quad (126)$$

The queues distributed in this way have the underlying assumption that once the ramp queue blocks the diamond signal, the entire feeding movement will be blocked, including that traffic heading for the frontage road. However, spillback has no impact on those diamond movements that do not feed the on-ramps, such as the right-turn and left-turn movements on the frontage road, and the arterial through movements. The modeled situation is equivalent to the case when no blocking to the cross-street traffic is allowed, i.e., no interchange lockup would occur.

When the arterial right-turn movement is controlled by the signal, the distribution of the residual queues would be slightly different with the equations described below. The residual queue for  $M2$ ,  $NR_2^j$ , is determined by:

$$NR_2^j = \frac{\left( \frac{V_{2-1}^j}{V_{2-1}^j + V_{14-1}^j} N_{\phi 4}^j \right)}{p_{2,1}^j} \quad (127)$$

The residual queue for  $M10$ ,  $NR_{10}^j$ , is determined by:

$$NR_{10}^j = \frac{\left( \frac{V_{10-1}^j}{V_{10-1}^j + V_{14-1}^j} N_{\phi 1}^j \right)}{p_{10,1}^j} \quad (128)$$

The residual queue for *M6*,  $NR_6^j$ , is determined by:

$$NR_6^j = \frac{\left( \frac{V_{6-1}^j}{V_{6-1}^j + V_{14-1}^j} N_{\phi 2}^j \right)}{p_{6,1}^j} \quad (129)$$

The residual queue for *M14*,  $NR_{14}^j$ , is determined by:

$$NR_{14}^j = \frac{\left( \frac{V_{14-1}^j}{V_{2-1}^j + V_{14-1}^j} N_{\phi 4}^j \right)}{p_{14,1}^j} + \frac{\left( \frac{V_{14-1}^j}{V_{6-1}^j + V_{14-1}^j} N_{\phi 2}^j \right)}{p_{14,1}^j} + \frac{\left( \frac{V_{14-1}^j}{V_{10-1}^j + V_{14-1}^j} N_{\phi 1}^j \right)}{p_{14,1}^j} \quad (130)$$

## SUMMARY

Major modeling methodologies were developed and documented in this chapter for IDIRMS. The cumulative arrival and departure method was the basis for estimating performance measures at different traffic facilities within an IDIRMS. A non-linear programming model was developed for estimating the OD matrix, which is a major system input for analyzing IDIRMS. The OD estimation model can be solved using the *Solver* function included in Excel. Enhanced methodologies were developed for analyzing diamond interchange performance, with a special consideration of the impact of ramp-metering queue spillback. Modeling of queue spillback was only considered blocking on the ramp-feeding movements from the diamond interchange. Blocking on the cross-street traffic movements and interchange lockup were not considered but identified as potential future research topics. The ramp-metering threshold was investigated from the gap-acceptance theory, and the modeling process provided a

starting point for further research on the issues related to the ramp-metering threshold. Modeling methodologies were also developed for freeway and ramp-metering operations. Ramp traffic arrival profiles were established based on the diamond interchange signal timing and traffic flow, which are essential elements for providing reliable estimates of ramp performances. The two-capacity phenomenon was specifically considered in modeling freeway operations with ramp metering.

## **CHAPTER IV**

### **DEVELOPMENT OF THE DRIVE SOFTWARE**

This chapter documents the development of DRIVE (Diamond Interchange Ramp Metering Integration Via Evaluation), a computer software that implemented the modeling methodologies documented in Chapter III. DRIVE was designed to perform simulation and analysis for an IDIRMS, including performance measures at the diamond interchange, freeway ramp meters, and freeway mainlines. DRIVE is characterized as a mesoscopic simulation and analysis model. It models the traffic flow at the macroscopic level, but the stochastic variation in traffic demands was taken into consideration in a multi-cycle analysis process. Mesoscopic models have the advantage of the faster computing speed that macroscopic models possess while still considering the stochastic traffic flows as microscopic simulation models do. The main features and the modeling process of DRIVE were documented. A sample case study was also presented to illustrate its applications and modeling capabilities.

### **SOFTWARE FEATURES**

DRIVE is characterized as a mesoscopic simulation and analysis model, written using the VisualBasic programming language in Excel. VisualBasic in Excel has the advantages of both the traditional VisualBasic programming language features and Excel spreadsheet functions. Excel also served as the simple user interface for processing input and output information. The modeling methodologies documented in Chapter III serve as the primary theoretical basis for DRIVE. The current version of DRIVE was designed to perform analysis for a duration of 100 diamond signal cycles, considering stochastic traffic flow variations over the entire analysis period. The modeling features in DRIVE present significant enhancements over deterministic models such as PASSER III and HCM. Table 7 summarizes the major input and output parameters and variables for DRIVE.



**TABLE 7 Input/output information for DRIVE**

Input/Output	Input Data and Performance Measures	
<i>Input</i>	Traffic Demand	OD Traffic Demand Matrix
	Geometry and Traffic Flow	<i>Diamond</i> : Internal storage space, lane configuration, diamond spacing, arterial speed <i>On-Ramp/Frontage Road</i> : Ramp queue storage, queue block storage, ramp-metering rates, queue flush rate <i>Freeway</i> : Free-flow capacity and its standard deviation, queue-discharge capacity and its standard deviation, freeway breakdown factor
	Signal Timing	Cycle length, phasing scheme, lost time, metering interval
	Other	Right-turn control type, meter flush mode, signal control type, fixed or stochastic demand option, random number seed
<i>Output</i>	Diamond Interchange	Total delay, average delay, maximum queue, 95-percentile queue, average queue, residual queue
	Ramp	Throughput, maximum queue, 95-percentile queue, average queue, total delay, average delay, number of queue flush, time duration of queue flush, ramp-meter attainability, % time ramp queue spillback, % time queue blockage
	Freeway	Throughput, total delay, average delay
	Summary Profiles	For every time step: Queue length on both freeway mainline and on-ramp, ramp-metering rates, freeway mainline and on-ramp throughputs

The required data inputs mainly include those required for analyzing individual traffic facilities within an IDIRMS. However, the analysis considers the interrelationships among these system components in an integrated fashion and provides performance measures based on a comprehensive modeling process. In addition to the direct summary output for those specified performance measures, DRIVE also creates ASCII data files, detailing the second-by-second queue length and traffic flow rate at each traffic facility. These ASCII files can later be imported into standard software packages such as Excel for plotting various traffic flow profiles.

## MODULES AND FLOW CHART

The DRIVE software consists of several modeling and computational modules, which are depicted in Figure 37. The modeling workflow chart is shown in Figure 38.

### FLOW GENERATION

Generation of stochastic traffic flow demands in DRIVE consisted of two components: the freeway mainline demands (i.e., random flows with means of  $v_{1,1}$ ,  $v_{2,2}$ ) and the surface street demands (i.e., all other OD flows). The Poisson distribution has been widely used for generating random traffic flows in studying traffic issues. Figure 39 shows the probability density functions with different  $\lambda$  values, the average number of arrivals during time interval  $t$ . As can be observed in Figure 39, when  $\lambda$  is greater than 10, the Poisson distribution can be approximated by a Normal distribution. Therefore, in DRIVE, the Poisson distribution was used for generating the traffic demands for the surface street OD flows, while a Normal distribution was used to generate freeway mainline demands.

It should be noted that the random flows were generated once every cycle for the surface street demands, consistent with the previous assumption that the traffic demands within a particular cycle are uniform. For the freeway demands, however, the flows were generated once every second in order to adequately model the ramp-metering algorithm and freeway operations.

The length of the interval to use for random variable generation has a significant impact on the variations in flows generated. The variation has to be in a reasonable range for more realistic modeling of traffic operations. If the variation is too high, the analysis tends to predict worse performance measures. On the other hand, if the variation is not high enough, the analysis tends to predict better performance measures.

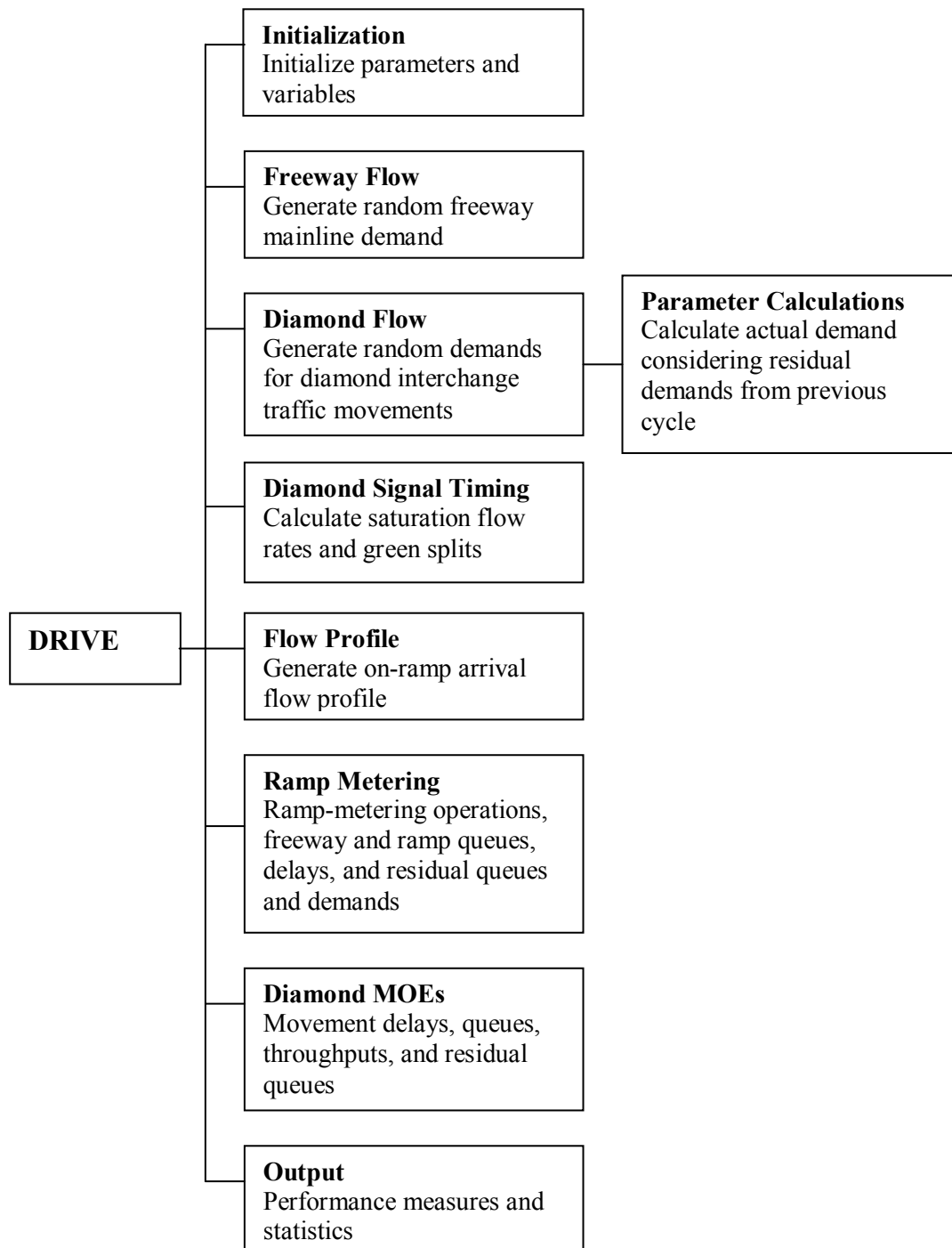


**FIGURE 37 DRIVE modules and functions.**

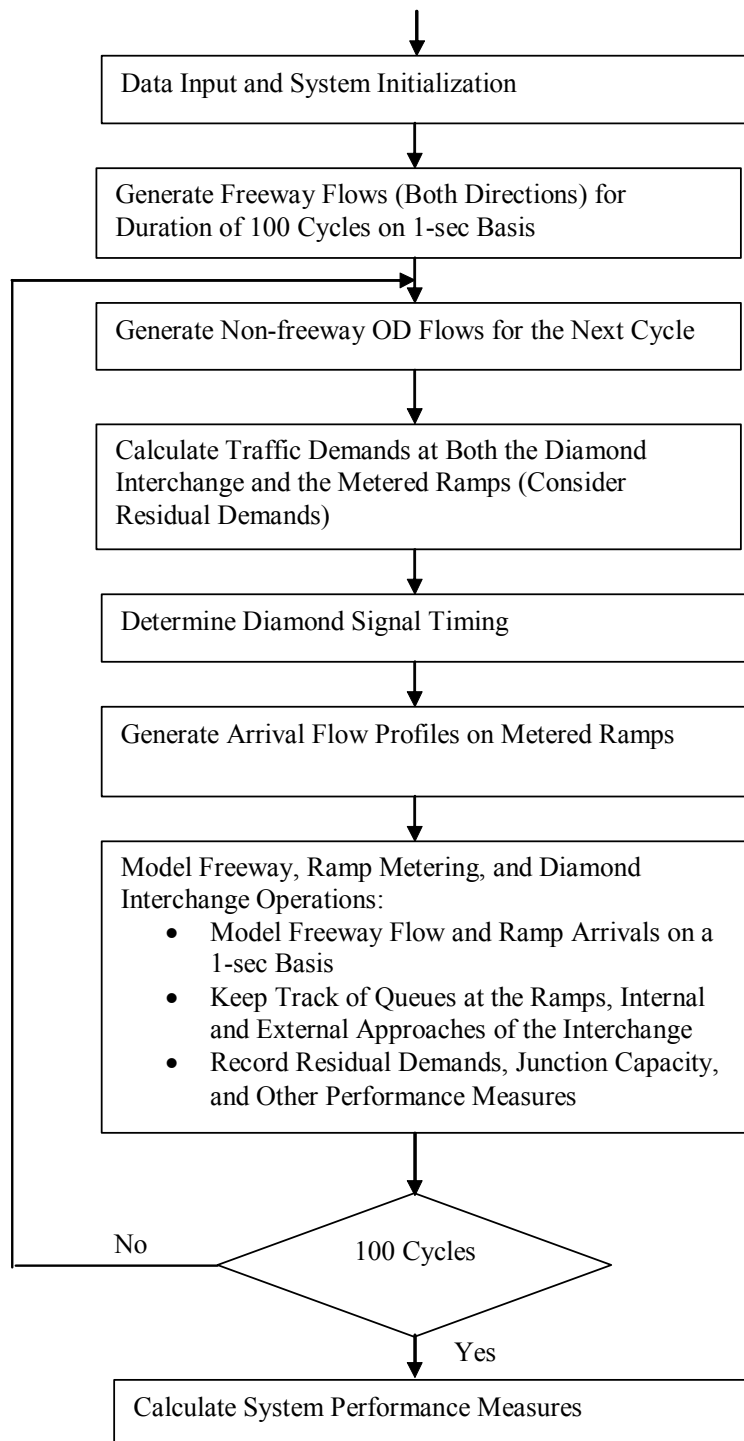


**FIGURE 38 DRIVE workflow chart.**

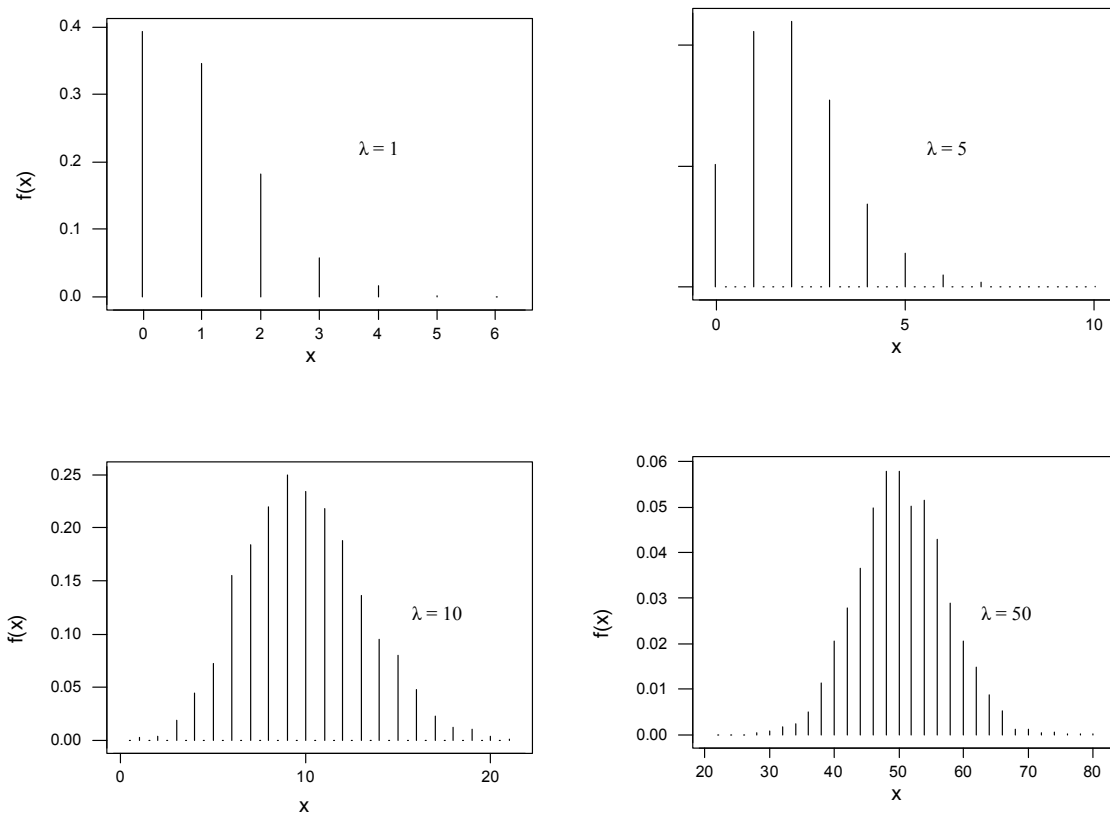
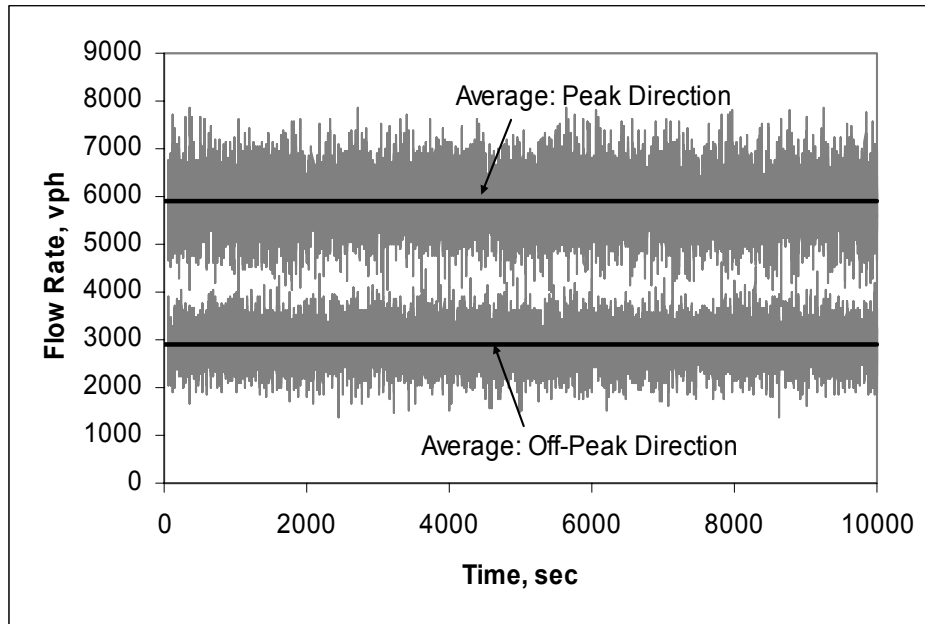


**FIGURE 39 Probability density functions for Poisson distribution with different  $\lambda$ .**

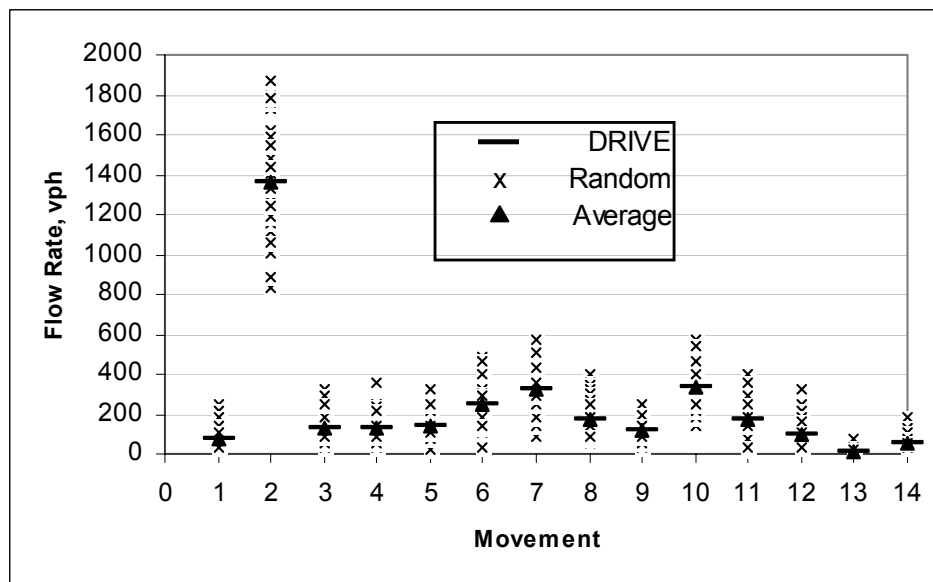
For surface street demand flows, which were generated once every cycle, the cycle length of the diamond interchange was used as the time interval. However, for freeway mainline demands, which were generated once every 1 second, the average arrivals during a 1-minute interval were used in order to produce a reasonable flow profile. The flow rate for each 1-second interval actually represents the flow for a 1-minute moving average. The mean for the Normal distribution is  $V_F/60$ , and the standard deviation is  $\text{sqrt}(V_F/60)$ .

Figure 40 illustrates the freeway mainline demand profile generated in DRIVE. The variations and the average demands on both freeway mainline directions are shown. Figure 41 illustrates the demand profiles summarized by the 14 traffic movements at the diamond interchange. Intuitively, the average demands based on the random variable generations matched the average input demands closely. Details on the flow generation

with statistical testing results will be documented in Chapter V when model calibration and validation are discussed.



**FIGURE 40 Freeway mainline random demands.**



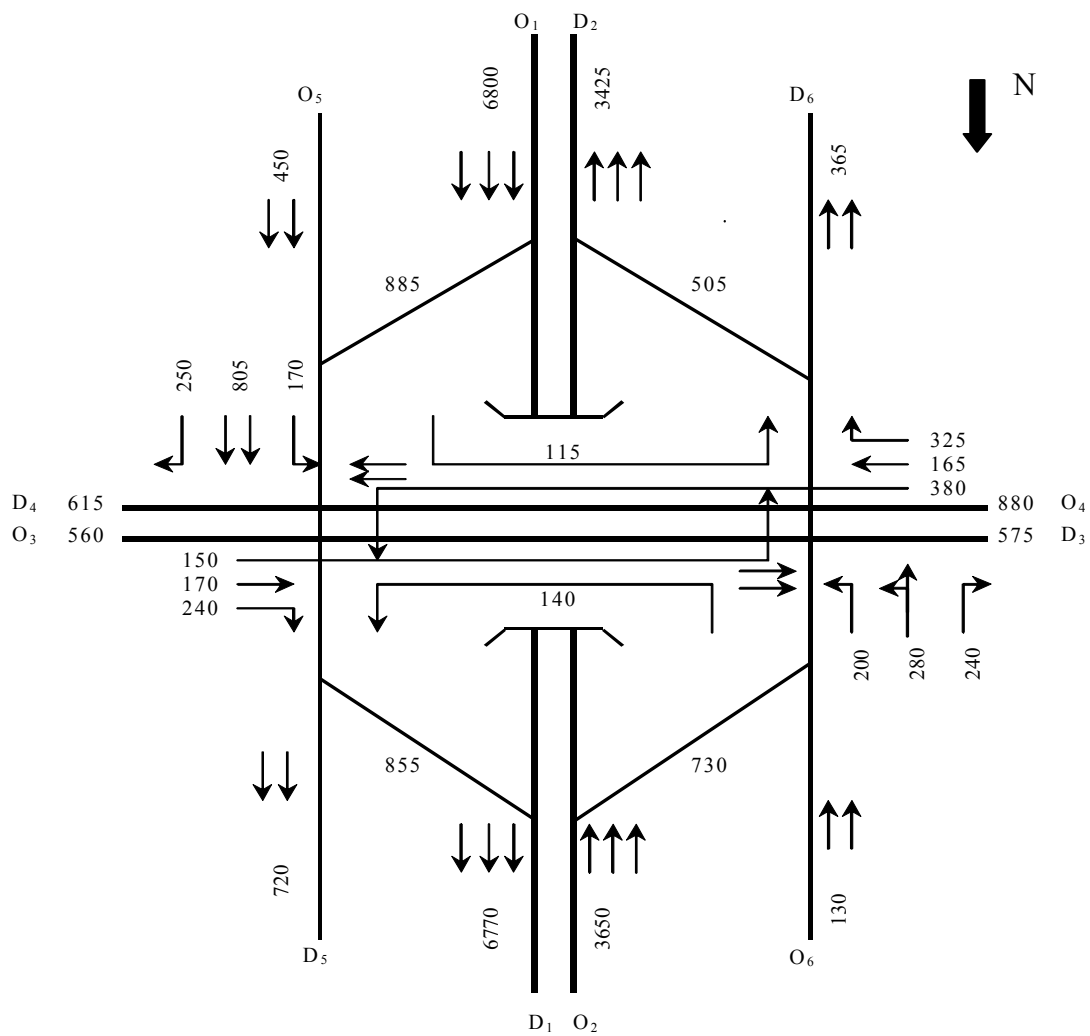
**FIGURE 41 Diamond interchange traffic movement random demands.**

## A SAMPLE CASE ANALYSIS

This section illustrates the applications of DRIVE in performing analysis for a sample network. Figure 42 shows the network configuration, the link traffic volume counts during the a.m. peak period, and the estimated OD matrix. The network data are based on the Mayfield Road/SH 360 interchange located in Arlington, Texas. The same network and traffic demand data are also used later in the model validation section. The Mayfield Road/SH 360 interchange is one of the interchanges along the SH 360 corridor. A ramp-metering system consisting of five diamond interchanges is in operation along the corridor. Ramp meters are installed only for the northbound direction (*R1*) at the subject interchange. They are in operation during the a.m. peak period between 6:00 a.m. and 9:00 a.m. For illustration purposes, ramp metering is assumed to exist on both ramps.

The diamond interchange signal is currently operating with three-phase, but it is not coordinated with the other signals on Mayfield Road. Ramp metering is operating as local traffic responsive; however, only one ramp-metering rate is being used, which is 900 vph, the maximum metering rate for a typical single-lane ramp meter. An excessive queue detector is located near the end of the on-ramp, and it is used for triggering the queue flush. To flush the ramp queue as a means of preventing spillback to the surface street is the policy adopted in many states (22).

As Figure 42 indicates, the average ramp demand is 855 vph during the peak hour. Due to stochastic traffic demand fluctuation, the ramp traffic demands exceed the 900 vph metering capacity during a portion of the peak period; therefore, queue flushes were occasionally observed in the field. The off-peak direction ramp (*R2*) has a relatively low demand, and the occurrence of queue spillback is unlikely. As for the diamond interchange itself, there is sufficient capacity to handle the traffic demands at the diamond interchange signal. Because the ramp meter is operating with the queue flush option, no queue spillback would occur.



O/D	D1	D2	D3	D4	D5	D6	Total
O1	5916	0	136	204	476	68	6800
O2	0	2920	219	183	110	219	3650
O3	207	129	168	0	34	22	560
O4	334	282	0	167	53	44	880
O5	284	41	32	45	45	5	450
O6	29	53	19	16	4	9	130
Total	6770	3425	575	615	720	365	12470

**FIGURE 42** Traffic demand data for the sample case analysis.



Table 8 lists the input parameters and variables for performing the sample analysis using DRIVE. The input parameters are grouped based on the three sub-systems: diamond interchange, ramps, and mainlines. Table 9 lists the major performance measures from DRIVE, which are also grouped based on the three sub-systems.

**TABLE 8 Input parameters for sample calculations**

Sub-system	Input Parameters	Values	
Diamond Interchange	Cycle Length $C$ , sec:	100	
	Phasing:	4	
	Spacing, ft:	300	
	Travel Time $TT$ , sec:	13	
	Overlap $\Phi$ , sec:	11	
	Left-Turn Storage $Q_{Mm}$ , cars:	Left: 20, Right: 20	
	Right-Turn Control:	No	
Ramps		R1 (NB)	R2 (SB)
	Ramp Storage, cars:	20	15
	Block Distance, cars:	50	30
	Metering Threshold, vph:	4000	4000
	Min. Metering Rate $M_{r,min}$ , vph:	900	900
	Max. Metering Rate $M_{r,max}$ , vph:	450	450
	Metering Interval $a$ , sec:	20	20
Queue Flush Option:	Yes	Yes	
	Queue Flush Flow, vph:	2000	2000
Freeway Mainlines		F <sub>1</sub> (NB)	F <sub>2</sub> (SB)
	Free-Flow Capacity $c_{Fr}$ , vph:	7040	7040
	F.F. Standard Deviation $\sigma_{Fr}$ , vph:	110	110
	Queue-Discharge Capacity $c_{Qr}$ , vph:	6700	6700
	Q.D. Standard Deviation $\sigma_{Qr}$ , vph:	50	50
	Breakdown Factor $\eta$ :	1.3	1.3

**TABLE 9 Output performance measures for the sample calculations**

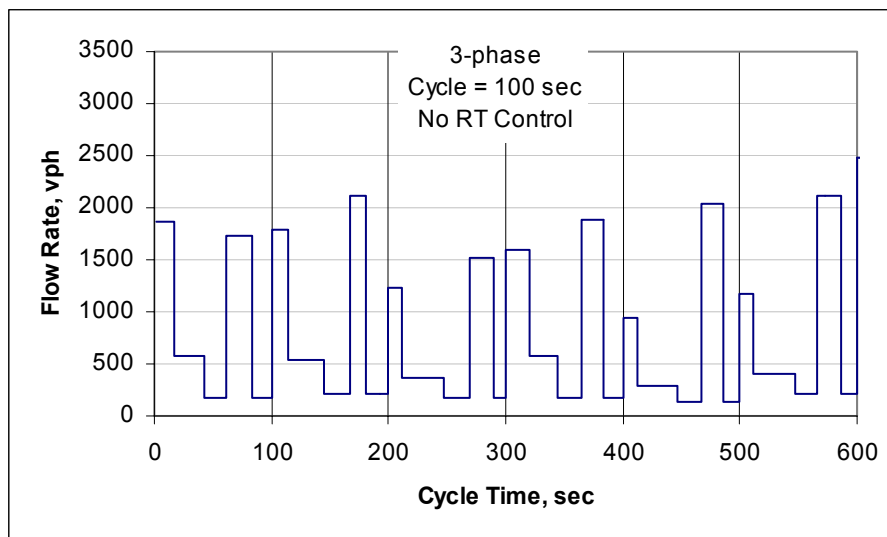
Sub-system	Performance Measures	Values	
Diamond Interchange		<u>By Movement</u> <i>M1, M2, M3, M4_5, M6, M7, M8, M9, M10_11, M12, M4, M10, M13, M14</i>	
	Average Delay $d_m$ , sec	20.6, 24.5, 22.1, 40.4, 43.8, 30.9, 33.0, 34.5, 31.8, 35.4, 0.7, 3.3, 0.0, 0.0	
	Maximum Queue $q_{Mm}$ , veh:	6.2, 22.9, 8.7, 15.3, 12.7, 9.5, 11.7, 10.3, 17.7, 11.1, 3.2, 9.0, 0.0, 0.0	
	95% Queue, veh:	5.0, 18.6, 6.2, 12.7, 9.3, 7.3, 10.3, 8.8, 15.5, 10.3, 2.1, 5.9, 0.0, 0.0	
	50% Queue, veh:	2.5, 13.6, 4.3, 7.6, 5.9, 3.7, 5.9, 5.1, 11.1, 6.6, 0.0, 3.1, 0.0, 0.0	
	Residual Queue $N_m$ , veh:	0, 0, 0, 0, 0, 0, 0, 0, 0, 0, 0, 0, 0, 0, 0	
Ramps		R1 (NB)	R2 (SB)
	Throughput $U_r$ , vph:	852	508
	Maximum Queue $q_{Mr}$ , veh:	24	6
	95% Queue, veh:	22	5
	50% Queue, veh:	18	2
	Average Delay $d_{Rr}$ , sec/veh:	55.8	10.5
	Queue Flush Rate, flush/hr:	14	0
	Metering Attainability, %:	78%	100%
Ramp Queue Spillback, %:	2.8%	0%	
Diamond Interchange Block, %:	0%	0%	
Freeway Mainlines		F1 (NB)	F2 (SB)
	Throughput $U_{Fr}$ , vph	6714	3431
	Average Delay $d_{Fr}$ , sec/veh	45.3	1.5

DRIVE produces a complete set of performance measures regarding different components of the IDIRMS. Some of the most useful information from DRIVE is related to the ramp performance on queue flush and queue spillback, which can be used to judge whether problems exist for the system operations and whether ICS are necessary to control queue spillback. Both the system throughput and delay measures can be used to evaluate ramp-metering policies such as trade-offs between queue flush and no queue flush. Besides the numerical output results shown in Table 9, DRIVE also

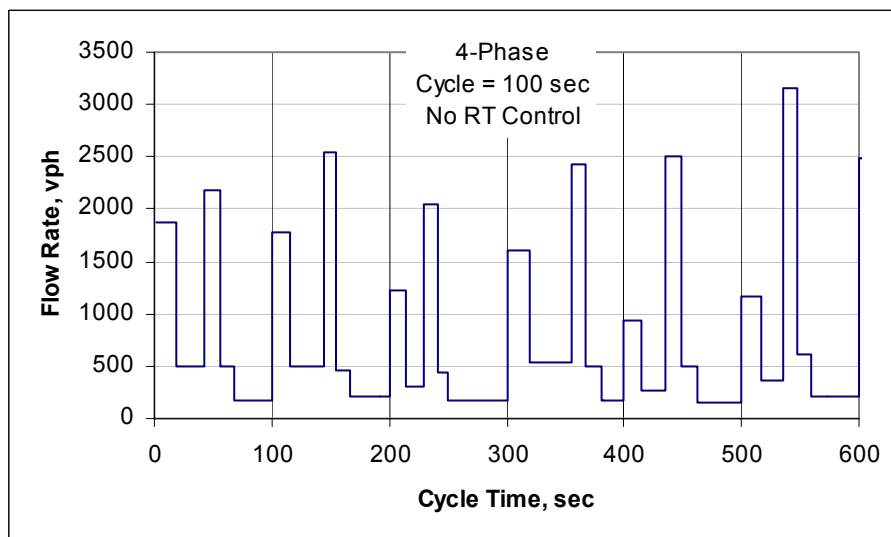
creates detailed data sets in ASCII format, which can be used for plotting various traffic flow profiles. Figure 43 and Figure 44 illustrate the ramp traffic arrival flow profiles (only the first six cycles are shown). Figure 43 shows the profiles with three-phase and four-phase operations when the arterial right-turn movement is not controlled, while Figure 44 shows when the arterial right-turn is controlled by the signal. From these figures, the stochastic variation in the traffic flows can also be seen.

Figure 45 illustrates the simulated ramp-metering rate based on the ramp-metering algorithm described in Chapter III, with the data given in the sample calculation. As shown in the figure, ramp metering remained in normal operation until about 1400 seconds after simulation started. It then fluctuated between queue flush, as indicated by the highest rate at 2000 vph and the minimum rate at 450 vph. Figure 46 illustrates the ramp queues at any instant during simulation. As can be seen, the ramp always had vehicle queues before queue flush started. Once queue flush started, the ramp queues varied between zero and the queue storage spaces of 20. Occasional queues exceeding the storage space 20 were observed because the ramp arrival rate (e.g., high platoon) exceeded the queue flush rate.

Figure 47 illustrates the simulated freeway capacity values as described in Chapter III. As can be seen, the freeway has stochastically varied capacity values. The average values of the capacity also indicate that the freeway operated at the higher free-flow capacity before queue flush started. Once queue flush started, the freeway experienced breakdown, and its capacity dropped to the lower queue-discharge capacity. The freeway never recovered from breakdown.

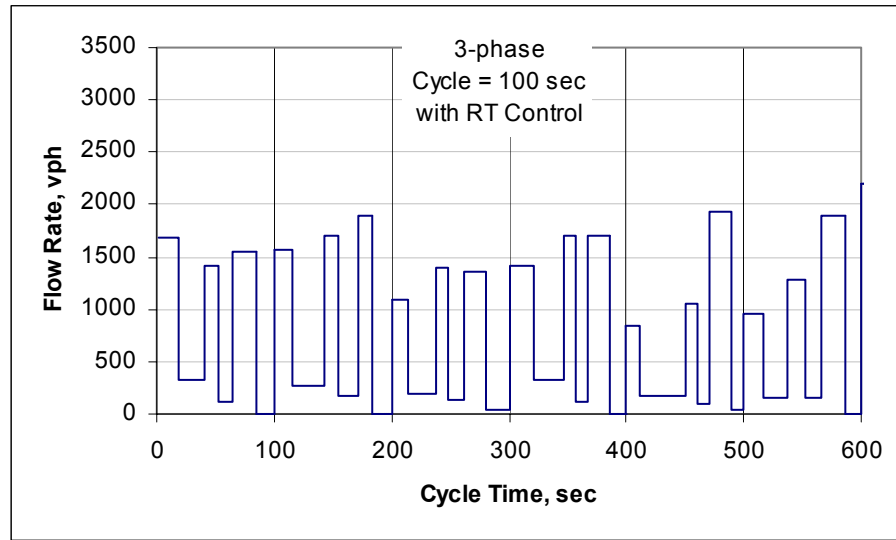


(a) With three-phase

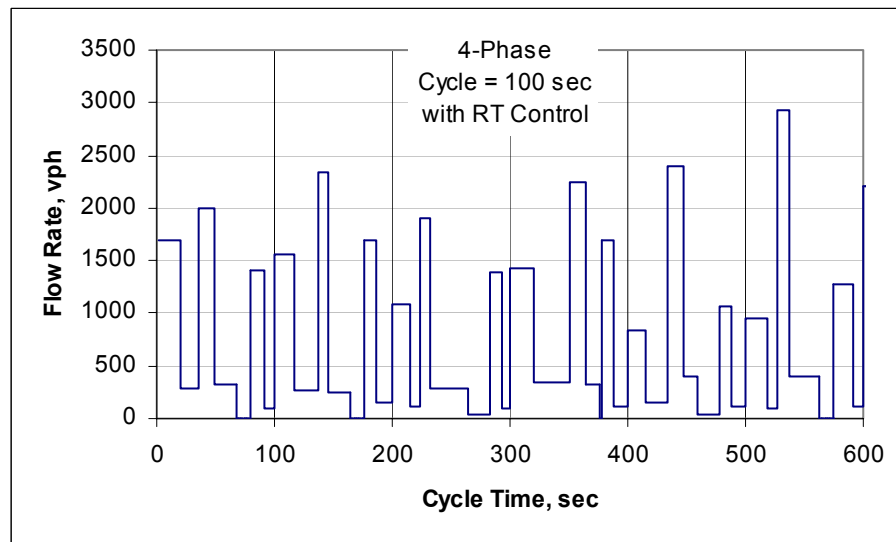


(b) With four-phase

**FIGURE 43 Ramp arrival flow profiles without arterial right-turn control.**



(a) With three-phase



(b) With four-phase

**FIGURE 44 Ramp arrival flow profiles with arterial right-turn control.**

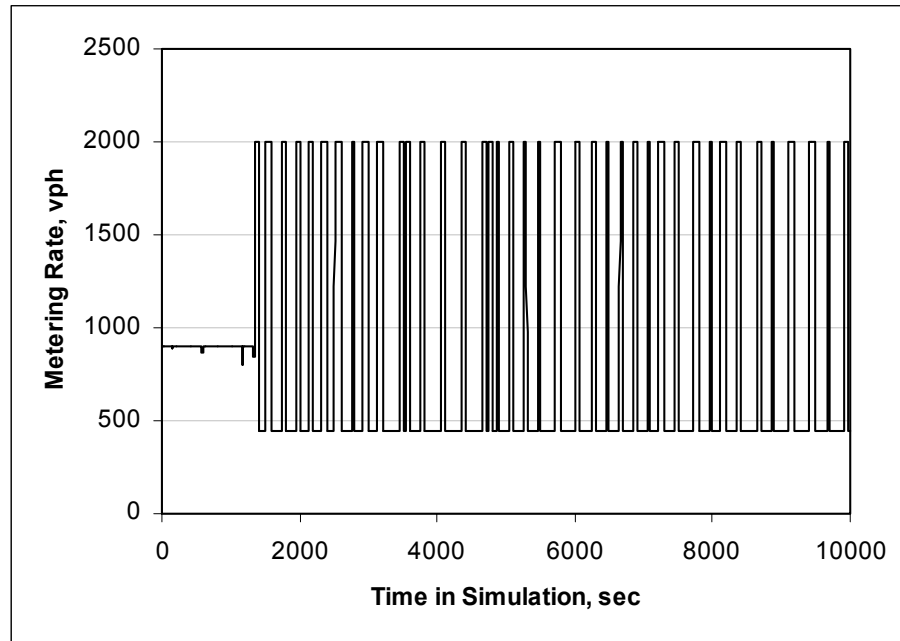


**FIGURE 45 Simulated ramp-metering rates.**

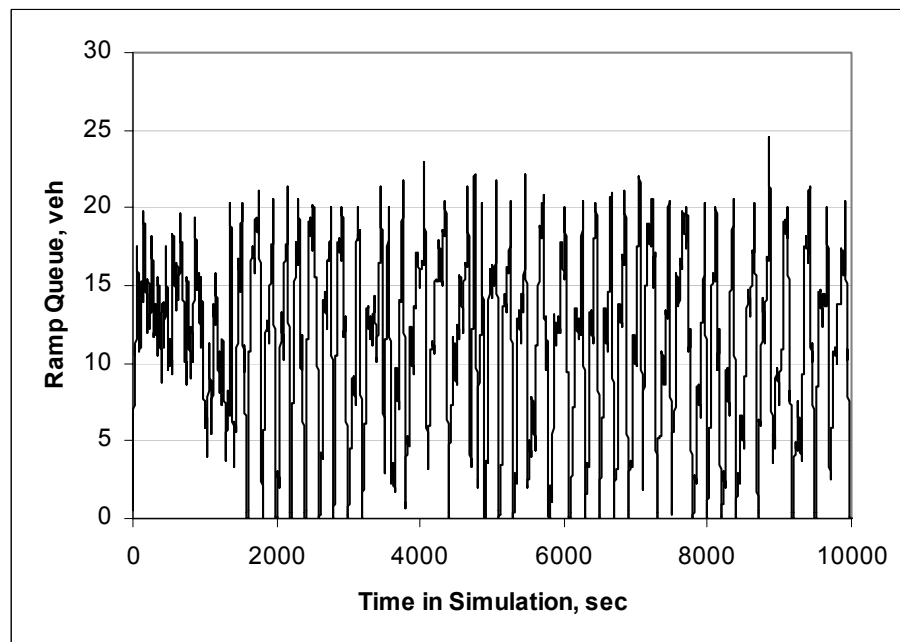


**FIGURE 46 Simulated ramp queues.**

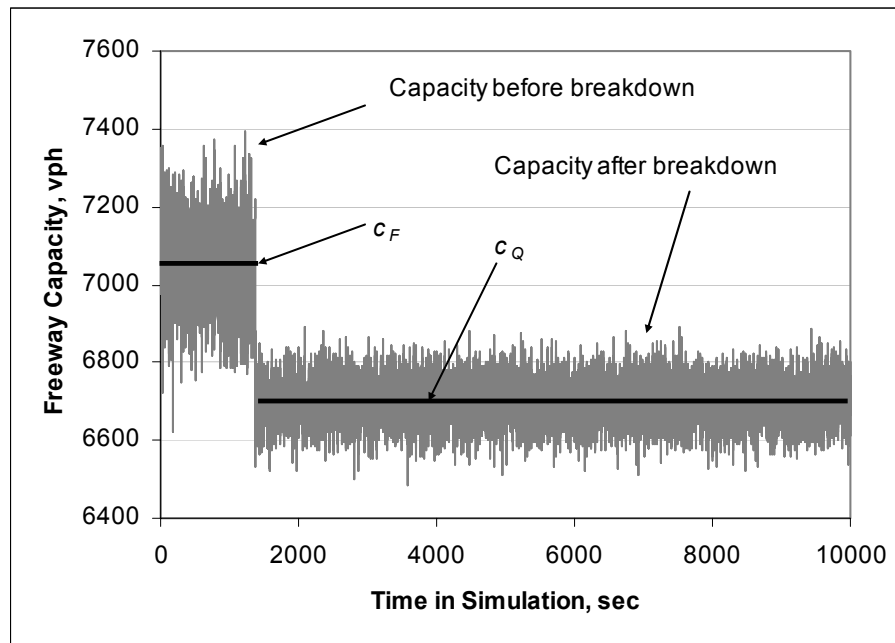


**FIGURE 47 Simulated freeway capacities for the case analysis.**

## SUMMARY

The development of DRIVE and the main features and functions of DRIVE were documented in this chapter. DRIVE is characterized as a mesoscopic simulation and analysis model for analyzing IDIRMS. It takes the advantages of both macroscopic models and microscopic models with fast computing speed and with consideration of stochastic traffic flows.

DRIVE is the first analysis tool yet developed to analyze freeway, ramp, and diamond interchange operations in an integrated manner. The current version of the model was developed based on the type of diamond interchange and phasing schemes typically seen in Texas. Modeling other types of interchange and signal control would require modification of the model structure.

Although the current version of DRIVE can be used to assess system performance with independent signal control at the diamond interchange and the ramp

meter, it does not yet have the capability to simulate the adaptive system required to achieve integrated control strategies for the diamond interchange signal and the ramp-metering signal. However, DRIVE provides an analysis tool for investigating and better understanding the system characteristics and operations of an IDIRMS.



## **CHAPTER V**

### **DRIVE MODEL CALIBRATION AND VALIDATION**

This chapter documents the process for calibration and validation of the DRIVE software. Model calibration is the process of modifying the model input parameters to produce output results that match a set of observed performance measures based on certain specified criteria. Model validation is used to test the model on another independent data set to see whether the model produces valid results.

In this study, field data were limited to some basic information, including traffic volumes and geometric data. Therefore, the model calibration and validation were carried out based on the VISSIM traffic simulation model. A VISSIM study was established based on the field-collected traffic volumes and geometry data. In practice, microscopic simulation models should also be calibrated based on field observations. Due to lack of comprehensive field data, the majority of the parameters in VISSIM were based on the model default values. However, adjustments were made on some of the parameters in order to yield a reasonable modeling situation. Based on the calibrated parameter settings in VISSIM, some emerging model parameters were then derived and used as inputs for the DRIVE software. Validation of DRIVE was then carried out by comparing the results between DRIVE and VISSIM. For diamond interchange operations, special considerations were given to validate diamond operations in the case of over-saturation and queue spillback.

#### **VISSIM MODEL DEVELOPMENT AND CALIBRATION**

A VISSIM model was established based on the traffic flow and geometric information at the Mayfield/SH 360 interchange location as presented in Figure 42 but with the following modifications:

- Since no information was available on the percentage of trucks in the traffic volumes, all the vehicles were coded as passenger cars.

- Ramp metering was coded for both directions to obtain one additional data point for the ramp. Traffic-activated ramp metering with a fixed metering rate was coded which was consistent with the current field operations.

Once the VISSIM network was established, a basic calibration process was conducted to ensure the coding accuracy and adequate representation of the general traffic flow characteristics. Specific issues addressed in the basic calibration process include the following:

- The traffic volumes obtained from simulation were checked to match the traffic counts from the field.
- The maximum ramp-metering throughput was checked to match the metering capacity (e.g., 900 vph).
- The two-capacity phenomenon on the freeway mainlines was well reflected.

One of the common mistakes in using simulation models is to have the traffic demands coded wrong, which would result in incorrect performance measures. One way to check such errors is to compare the output flows from simulation to the input demands. It is important to realize that the output from simulation may not necessarily reflect the true traffic demand, especially if a bottleneck in the network exists that filters the downstream demands. One strategy to avoid demand filtering is to code the entry links of the network with sufficient length. Modification of link geometry and signal control may be necessary measures to resolve bottleneck occurrences, such as increasing the number of lanes or eliminating signal control.

In VISSIM, there is no special signal control logic designed for ramp metering. Simply treating a ramp-meter signal as a regular traffic signal would not yield the correct metering rate. For example, the shorter ramp-metering cycle does not always guarantee every vehicle will stop at the signal. In this research, a ramp-metering control algorithm was specially developed using VAP in VISSIM. VAP is similar to an

advanced programming language and allows users to develop special signal control routines. One critical element in coding the ramp-metering control is to have a demand detector coded at the metering signal, similar to the demand detector used in the field. The ramp-metering signal would remain in red unless there is a demand call at the demand detector. Only in such a way does it ensure that all the vehicles stop at the metering signal and a flow of one car per metering cycle is achieved.

### **THE TWO-CAPACITY PHENOMENON IN VISSIM**

As discussed previously in Chapter II, the two-capacity phenomenon is one of the most critical aspects in modeling ramp-metering and freeway operations. It is the two-capacity phenomenon that signifies the importance and purpose of ramp-metering applications; therefore, any simulation model, when used for studying ramp-metering issues, should have the capability of producing the two-capacity phenomenon.

While microscopic simulation models have been widely used in evaluating ramp-metering algorithms, no literature has been found to document whether the simulation model used reflected this freeway operational feature. In fact, most microscopic simulation models were developed based on established car-following theories, and by default these car-following models do not necessarily yield the two-capacity phenomenon.

An investigation was conducted to see whether VISSIM, the selected simulation model for validating DRIVE and evaluating IDIRMS, can actually produce the two-capacity phenomenon. It was found that only with careful selection of the model parameters can the two-capacity phenomenon be produced in VISSIM. The following summarizes the specific model coding requirements in order to achieve the two-capacity phenomenon. It is noted, however, that these modifications only applied to VISSIM Version 3.60. With further development and enhancement, later versions of the software may better simulate the operations. The required modeling coding elements are:

- Code the freeway links as *urban motorized road* instead of freeway link.
- Use the Wiedemann-74 car-following model instead of the Wiedemann-99 model.
- Code the merging section no more than 400 feet.
- Create an adequate traffic demand profile such as that shown in Figure 48.

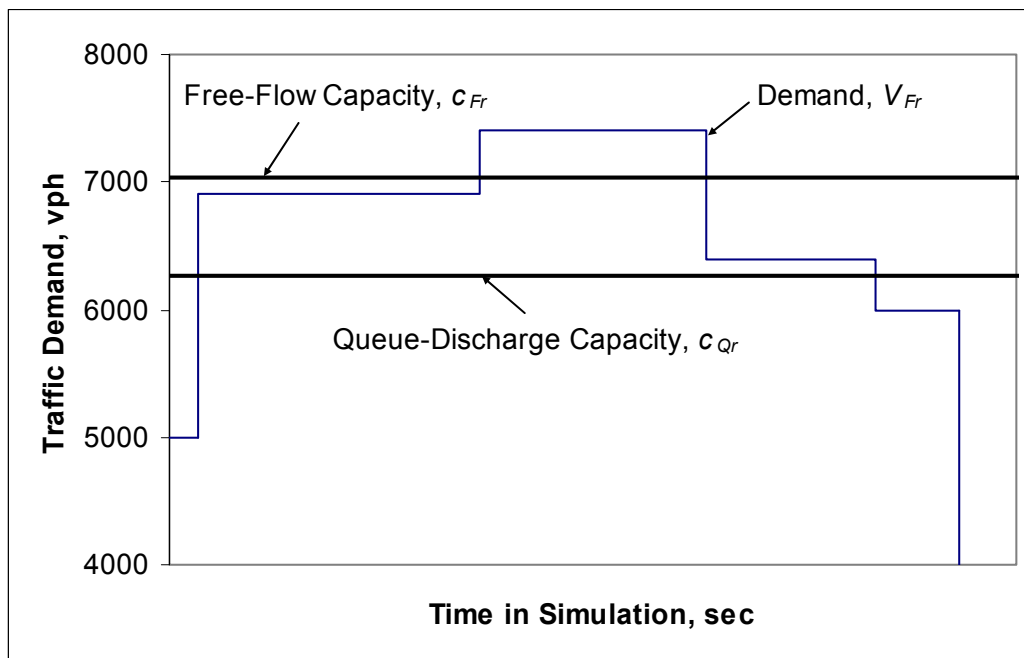


**FIGURE 48** Traffic demand profile for achieving the two-capacity phenomenon.

In Figure 48, the free-flow capacity and the queue-discharge capacity of the freeway bottleneck were assumed to be known as shown (they need to be measured and estimated from VISSIM). The traffic demand profile is created to ensure freeway breakdown occurrences by having a period of demand exceeding the free-flow capacity. On the other hand, a reasonable period of free-flow condition should also exist with sufficient demand so that the free-flow capacity can be estimated. While the queue-discharge capacity can normally be obtained over a prolonged period, the free-flow capacity is more difficult to obtain because breakdown could easily occur when the

demand is close to the capacity. Strictly speaking, estimating the free-flow capacity based on the throughput flows would always result in under-estimation because the freeway demand has to be below the free-flow capacity to maintain the free-flow condition. At the demand level close to the capacity, the free-flow condition could only last for a short period before breakdown occurs due to the stochastic nature of traffic flow. Of course, to achieve the above demand profile and a good estimate of the free-flow capacity, it would require several trial-and-error experimental runs.

Figure 49 illustrates the flow-occupancy plot obtained from VISSIM based on 20-second intervals. The data were collected at a detector location near the end of the merge lane. Again, it is important to emphasize that such flow-occupancy data should be collected downstream of the ramp where the flows would represent the total freeway mainline and ramp flows. Data collected upstream of the on-ramp would not reflect the true freeway capacity because a portion of the capacity is consumed by the ramp traffic (51). This figure was produced when the ramp metering was not on. As can be seen, the plot closely resembles the field data shown in Figure 9, where the two flow regimes can be clearly identified.

Figure 50 and Figure 51 are the time series flow-speed plots with a 20-second interval and 5-minute interval, respectively. Freeway breakdown and free-flow conditions can also be recognized from these figures. For this particular simulation run (seed = 100), the free-flow capacity was estimated at 7190 vph, and the queue-discharge capacity was estimated at 6320 based on the two time periods shown in Figure 50. Note from the two figures that much higher flow rates can be observed with the shorter 20-second time intervals than with the 5-minute time intervals. Under free-flow conditions, the average speed on the freeway is about 60 mph. Under breakdown conditions, the average speed is slightly above 30 mph. Figure 52 illustrates the time series flow-speed plots from different simulation runs based on different random seeds. The figure clearly indicates the stochastic nature of freeway breakdown and its capacity values, i.e., even with similar average traffic demand levels, freeway breakdown could occur under different conditions with different capacity flows.

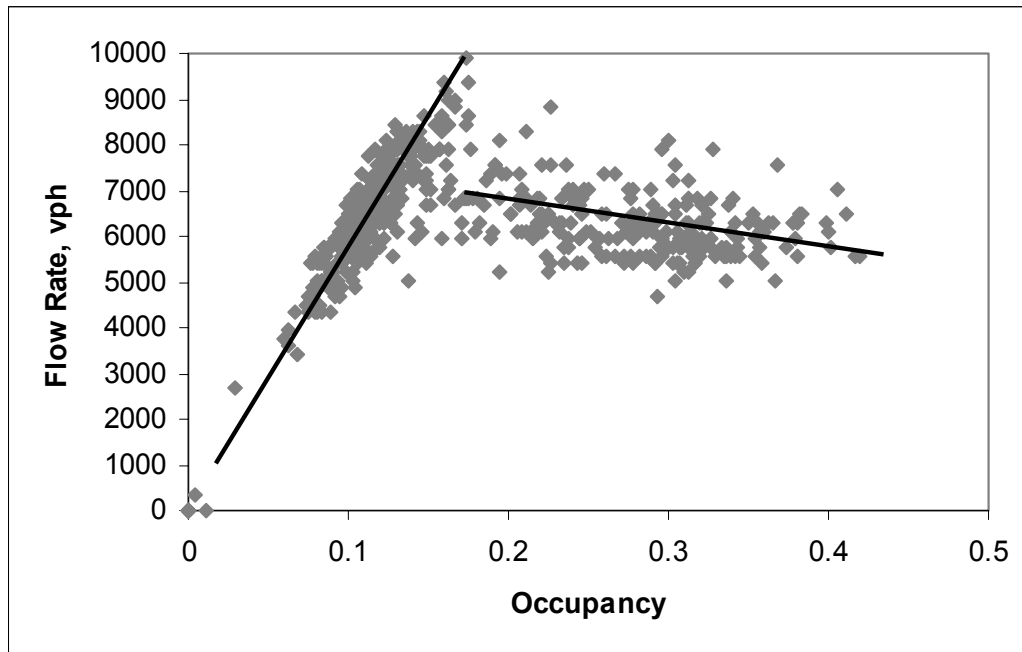


FIGURE 49 Flow-occupancy diagram from VISSIM.

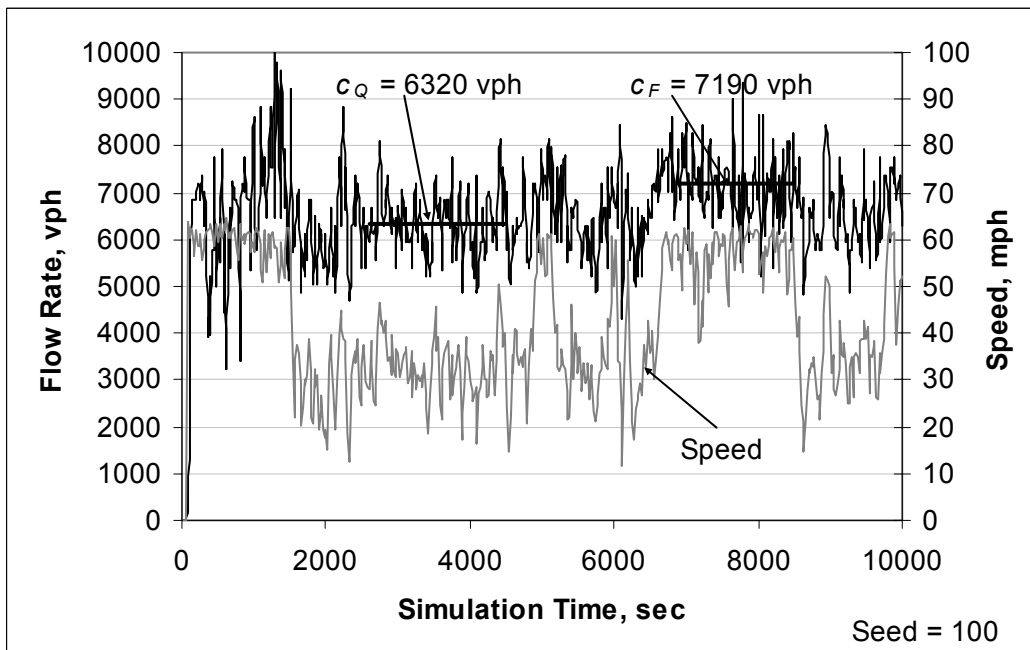


FIGURE 50 Speed-flow diagram from VISSIM with 20-second intervals.

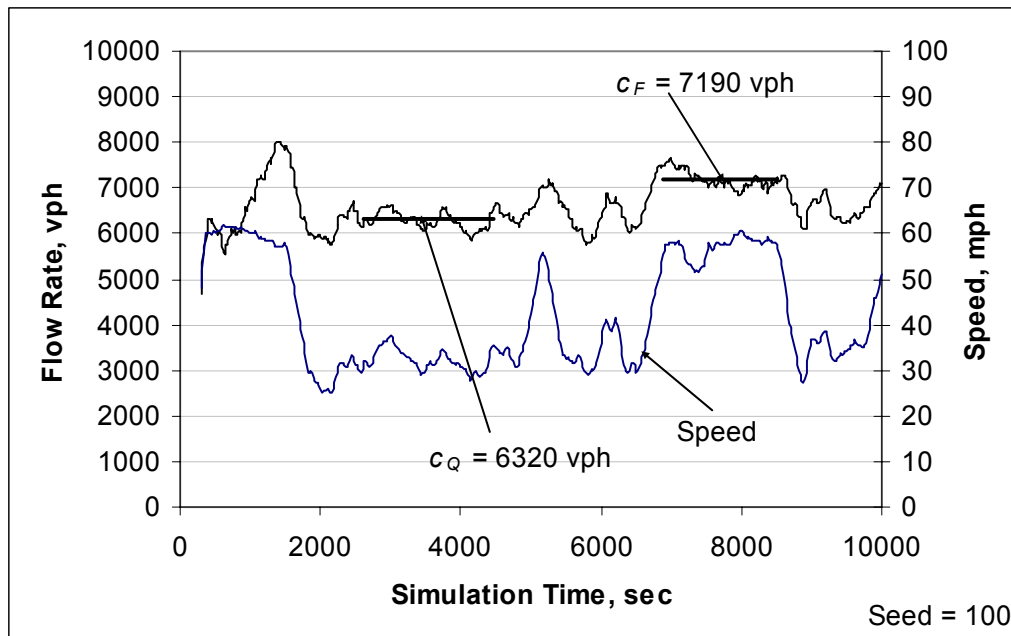


FIGURE 51 Speed-flow diagram from VISSIM with 5-minute intervals.

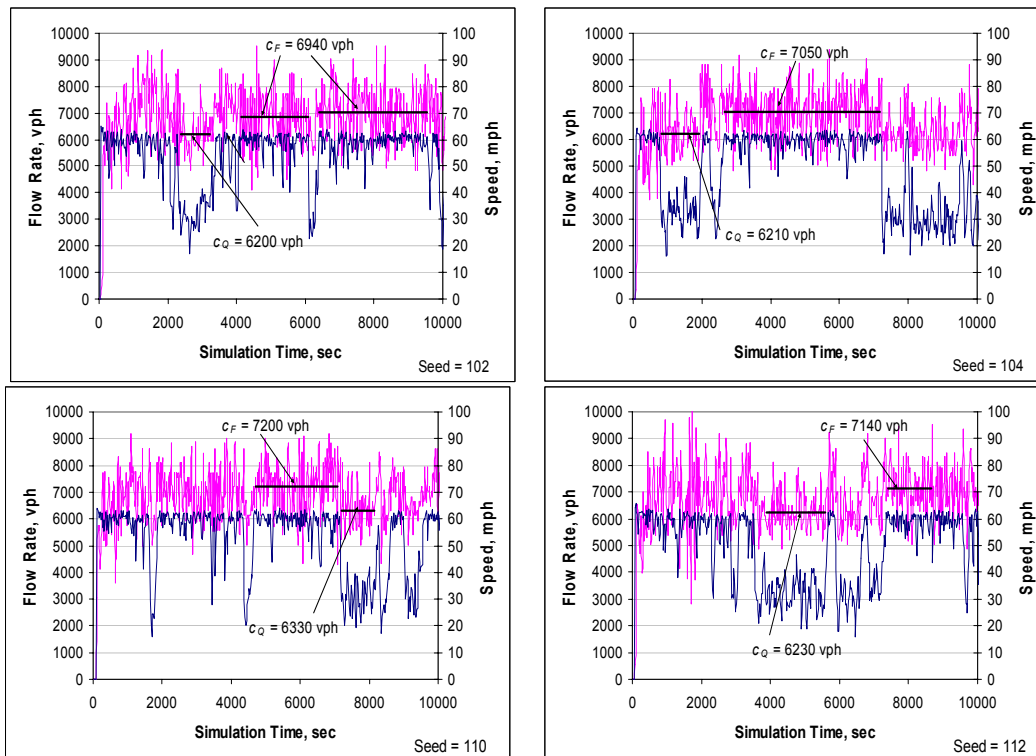
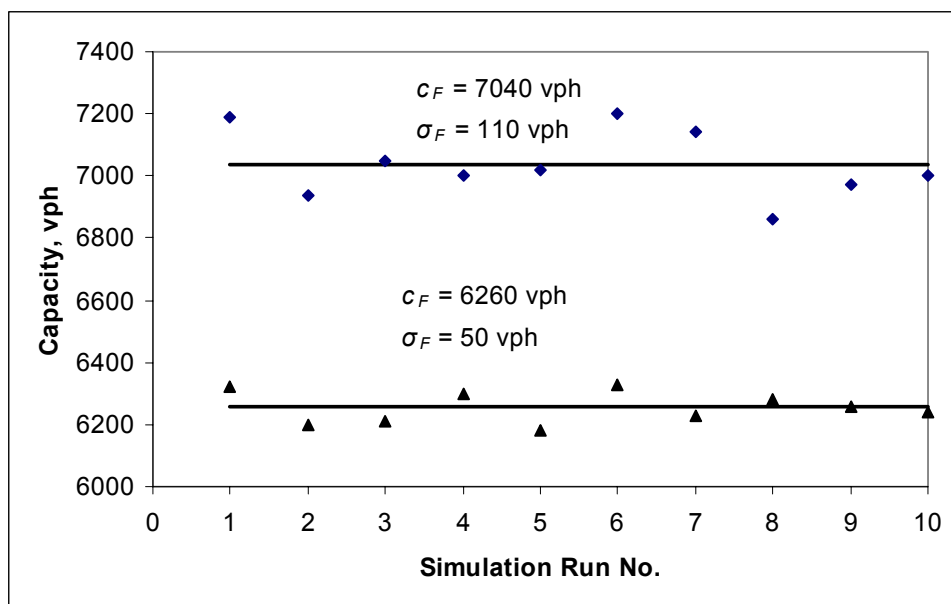


FIGURE 52 Speed-flow diagrams from different VISSIM runs.

Figure 53 illustrates the estimated capacity values from 10 different simulation runs with different random seeds. The average free-flow capacity is estimated at 7040 vph with a standard deviation of 110 vph, and the queue-discharge capacity is estimated at 6500 vph with a standard deviation of 55 vph. The variation in the queue-discharge capacity under breakdown conditions is smaller than that under the free-flow conditions, which confirms the findings from previous studies as discussed in Chapter II.



**FIGURE 53 Capacity values from 10 VISSIM runs.**

The simulation results presented above indicate that the two-capacity phenomenon is adequately reflected when ramp metering is not turned on in VISSIM. However, traffic flow characteristics were found to be different when ramp metering was turned on. Figure 54 through Figure 56 illustrate the flow-speed diagrams from three simulation runs with the same random seed but with different ramp controls. Figure 54 shows the diagram when ramp metering is not turned on; Figure 55 shows the diagram when ramp metering is on but without queue flush; and Figure 56 shows the diagram when the ramp metering is on but with queue flush.



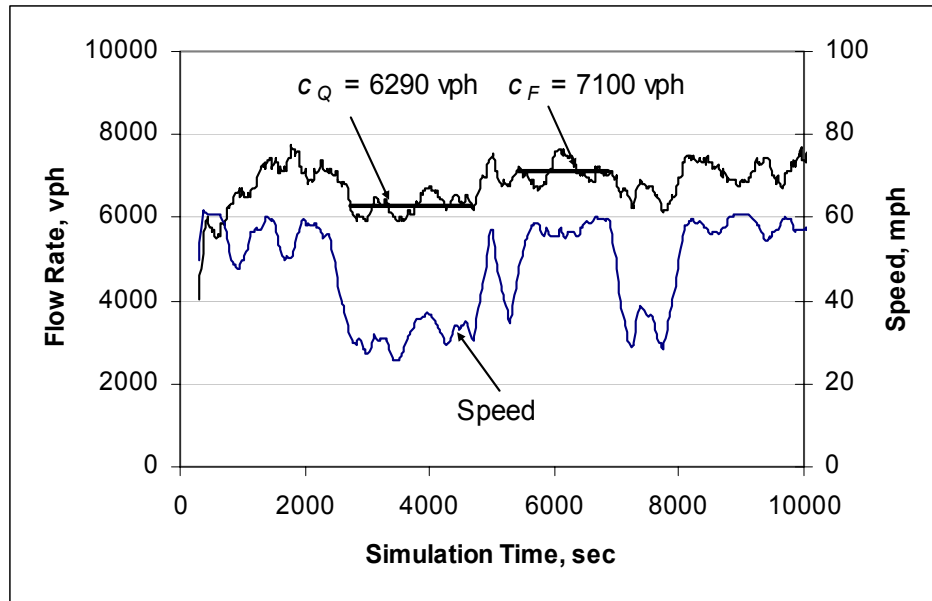


**FIGURE 54** Flow-speed diagram from VISSIM without ramp metering.

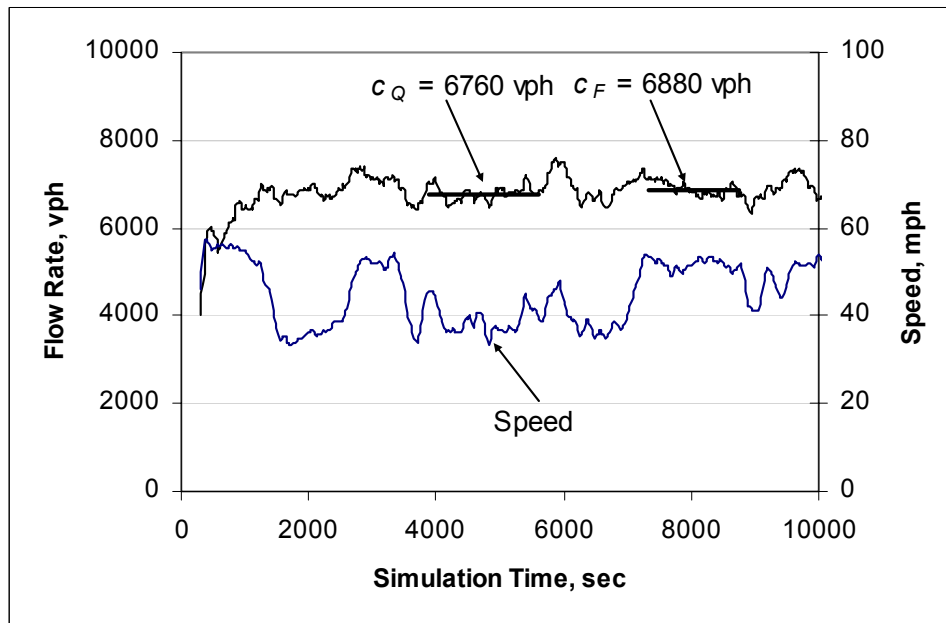


**FIGURE 55** Flow-speed diagram from VISSIM with ramp metering and no queue flush.

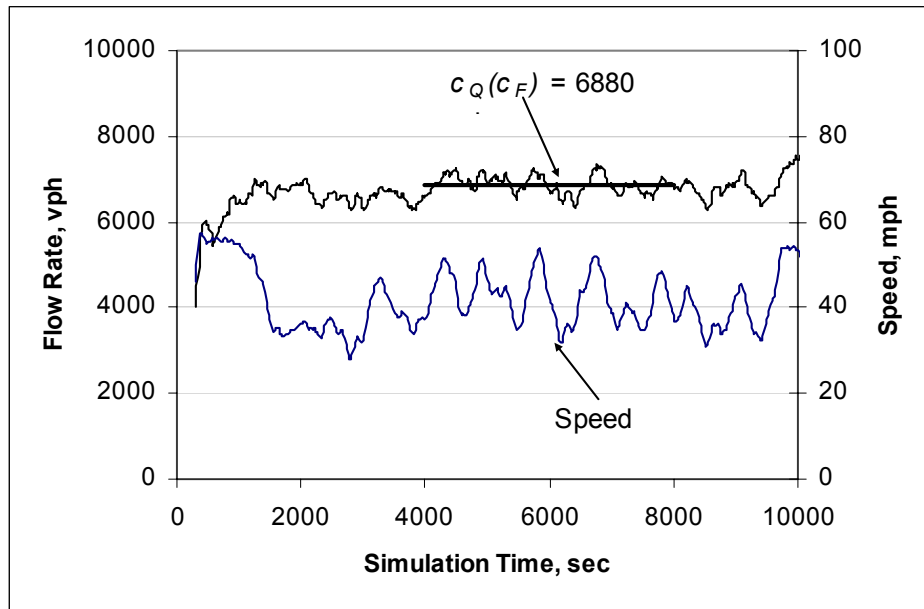


**FIGURE 56 Flow-speed diagram from VISSIM with ramp metering and queue flush.**

Figure 54 through Figure 56 reveal some interesting features. In general, higher capacity flows are associated with higher speeds in all the ramp control cases. However, the difference between the free-flow capacity and the queue discharge capacity is more significant when ramp metering is not on. For example, the free-flow capacity without ramp metering is about 7100 vph, while its queue-discharge capacity is about 6290 vph. With ramp metering and no queue flush, the two capacities are about 6880 vph and 6760 vph, respectively. The drop in free-flow capacity with ramp metering reflects the impact of ramp traffic (i.e., the ramp metering equivalency factor as discussed in Chapter II). Furthermore, with ramp metering and queue flush, it is no longer easy to differentiate the two capacity regimes (see Figure 56). For the model calibration and validation to be presented in the following sections, the queue-discharge capacity was estimated at 6700 vph from simulation and was used in DRIVE to reflect the effect of ramp-metering operations.

Figure 56 also indicates that the freeway at the merge location seems to frequently transition between breakdown (lower speed) and free-flow (higher speed), which was observed in VISSIM as a persistent shockwave movement. The average throughput flow under this traffic condition could be seen as approximately 6880 vph. Similar observations can also be found for the speeds. With ramp metering, the speeds under free-flow conditions are lower than those without ramp metering. This is due to the ramp traffic accelerating to its desired speed after entering the freeway from the ramp meter. On the other hand, with ramp metering the speeds under breakdown conditions are higher than those without ramp metering. This suggests that ramp metering does show some effectiveness in minimizing the capacity drop after breakdown, which confirms the findings by Zhang and Levinson (98) based on field studies, i.e., ramp metering can generally produce higher freeway throughputs under breakdown conditions than without ramp metering.

While the results based on simulation indicate frequent transitions between breakdown and recovery, it is not confirmed whether field operations would support this finding. In observing field operations, freeway recovery from breakdown seems much slower than what has been shown in simulation. The point to make here is that the calibration and validation of DRIVE will be based on VISSIM. DRIVE should have the flexibility of adjusting its various model parameters to match the VISSIM results. However, when discrepancies exist between the two models, it is not suggested which model is more accurate than the other, but rather further validation based on field studies is recommended. For example, the modeling of freeway operations, especially the breakdown phenomenon in VISSIM, should be further validated based on field data.

### **CALIBRATION AND VALIDATION FOR DRIVE**

The calibration of the DRIVE model mainly focused on comparing the random flows generated from DRIVE and VISSIM to ensure consistent traffic demand profiles between the two models. This requires that both models produce identical mean traffic demand values, but it also demands equal variance because the level of variation in traffic flows has a significant impact on the modeling results. The common parameters

in both models were kept consistent between the two models. Validation of the model was based on comparing various performance measures from the two models.

Table 10 lists the traffic demands from DRIVE and VISSIM for the 14 diamond interchange turning movements and the two freeway on-ramps. also includes the  $t$ -test results on comparing means and the  $F$ -test results on comparing the variances. The turning movement demands were based on the average of 100 simulated signal cycles. Because DRIVE generates and models freeway flows in a very different way than VISSIM does, it is not necessary to compare the flow profiles from both models as long as the average demands are identical in both models. Figure 40 in Chapter IV has demonstrated that DRIVE generated random freeway demands that have mean values well matched with the input demands.

As the results in Table 10 indicate, both VISSIM and DRIVE produced mean flows that are statistically identical to the true means. The majority of the movements also have equal variances except for  $M1$ ,  $M7$ , and  $M8$ . The two on-ramp flows also have equal means and variances, which ensures that the two models will produce ramp performance measures based on identical traffic flows.

The following results are presented to illustrate whether DRIVE yielded valid performance measures compared to VISSIM. For model validation, average delay was selected as the primary performance measure for comparison because the delays in both models are measured in identical manners. Queue length would be another candidate performance measure for comparison; however, the queues from both models are not identically measured. VISSIM reports the backup queues in distance measured from a specified location, while DRIVE reports the queues in terms of number of vehicles in a queue. Although the distance queue could be translated into the number of vehicles knowing the average space that a vehicle occupies, discrepancies would still exist in the queue lengths from both models. First, the ramp queue is not at a standstill state in VISSIM, and the space occupied by the vehicles varies depending on the ramp-metering rate. For example, a higher metering rate would result in longer spaces between

vehicles. Second, VISSIM reports the maximum backup queue, while DRIVE reports the number of vehicles in the queue. The maximum backup queue takes into account the shockwave effect, which is usually larger than the number of vehicles in the queue.

**TABLE 10 Traffic demands from DRIVE and VISSIM and statistical test results**

Movement	True Mean	VISSIM			DRIVE			P-value (F-test) <sup>2</sup>
		Mean	S.D.	P-value (t-test) <sup>1</sup>	Mean	S.D.	P-value (t-test) <sup>1</sup>	
M1	168	163	81	0.52√	159	68	0.19√	0.04
M2	805	799	165	0.71√	804	194	0.95√	0.05√
M3	249	249	99	0.98√	269	113	0.09√	0.09√
M4	151	152	78	0.94√	152	72	0.90√	0.19√
M4_5	319	308	104	0.28√	334	100	0.14√	0.36√
M6	241	245	86	0.66√	235	88	0.53√	0.40√
M7	198	187	72	0.12√	194	88	0.68√	0.02
M8	281	282	96	0.96√	286	116	0.66√	0.03
M9	238	233	91	0.55√	233	94	0.62√	0.35√
M10	387	391	139	0.78√	409	120	0.07√	0.07√
M10_11	554	551	152	0.85√	575	145	0.15√	0.33√
M12	326	316	107	0.34√	333	106	0.53√	0.46√
M13	113	103	63	0.13√	109	60	0.52√	0.35√
M14	142	154	72	0.09√	138	78	0.57√	0.21√
R1	854	878	200	0.24√	864	181	0.60√	0.19√
R2	504	488	131	0.23√	525	142	0.15√	0.22√

**Note:** (1). t-test is to test the mean against the true mean; (2). F-test is to test equal variance between VISSIM and DRIVE; (3). Movements with √ marked indicate the null hypothesis on either equal mean or equal variance is accepted at the 95% confidence level.

It should be noted that the cumulative arrival and departure method as applied in DRIVE for delay calculations does not capture the delays associated with vehicle deceleration and acceleration. However, the delays reported from VISSIM and other microscopic simulation models would include such delay components. Therefore, VISSIM would always report a minimum delay when ramp metering is in operation where all the vehicles would have to stop. On the other hand, freeway mainline traffic would also incur such deceleration and acceleration delays resulting from normal car-following and driving behavior.

To make it consistent between the delays reported by both DRIVE and VISSIM models, such minimum delays were estimated in VISSIM and then added to the delays from DRIVE. In estimating the minimum delay due to ramp metering, a very low ramp demand was coded to make sure that the delays reported from VISSIM were primarily due to ramp metering and not due to traffic congestion. This minimum delay was estimated to be about 7.0 sec/veh. Because the minimum delays for the freeway mainline traffic are related to traffic flow levels, they were estimated by using the same freeway mainline demands but with the ramp demands eliminated. In this way, the delays were primarily related to the normal car-following behavior at that freeway demand level while no delays related to breakdown were involved. For the northbound (peak) direction, the minimum delay was estimated to be at about 6.0 sec/veh, while for the southbound (off-peak) direction, the minimum delay was estimated to be about 1.5 sec/veh.

### **Under-saturated Conditions**

Considered as part of the model calibration process, the existing under-saturated conditions (i.e., no existence of ramp queue spillback) were analyzed using PASSER III, VISSIM, and DRIVE. Efforts were made to calibrate both VISSIM and DRIVE to match PASSER III results for the diamond interchange movements. Figure 57 and Figure 58 show the average delay results from the three models for the surface street traffic movements with the three-phase and four-phase schemes.

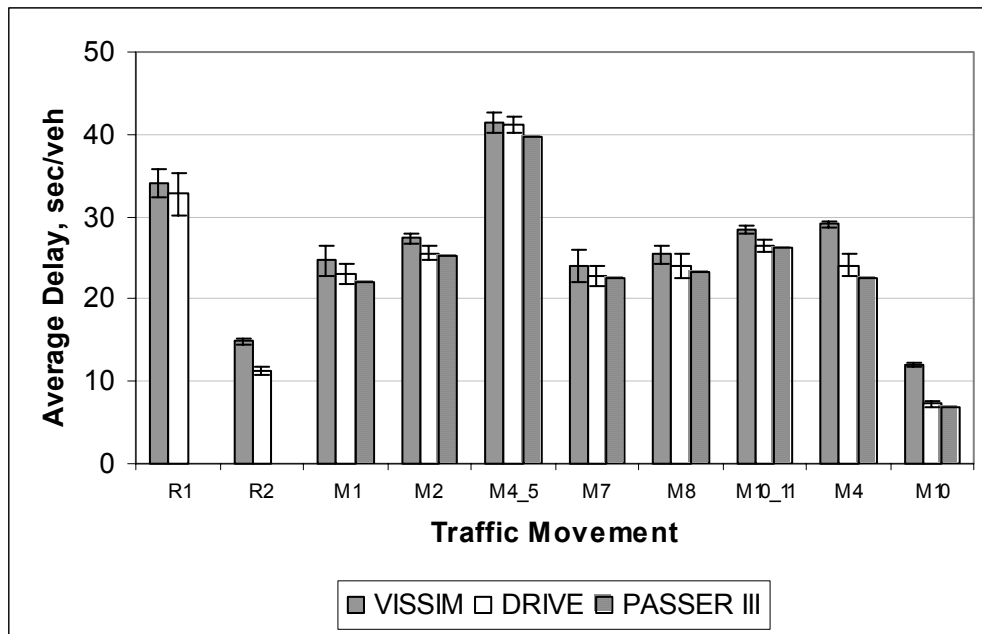


**FIGURE 57 Delays with three-phase and under-saturated conditions.**

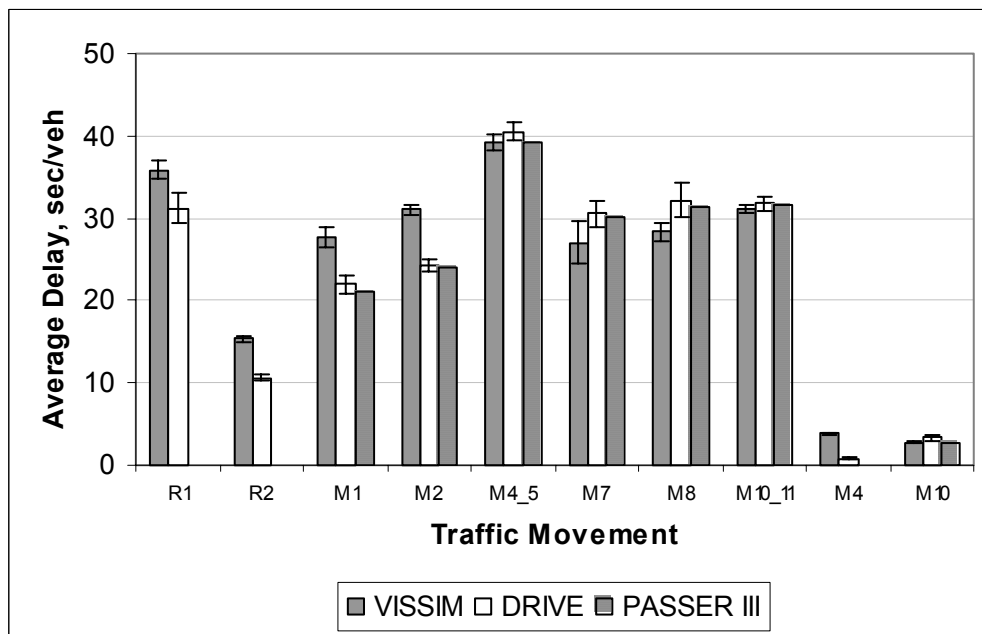


**FIGURE 58 Delays with four-phase and under-saturated conditions.**

Table 11 has the detailed results along with the t-statistical results. The ramp meters were set with a queue flush option. Only those movements being affected by the ramp meters are listed. Delays for *M4\_5* and *M10\_11* occurred on the external arterial approaches associated with *M4*, *M5*, *M10*, and *M11*. The results for both VISSIM and DRIVE were based on the average of 10 simulation runs, with a total simulation time of 100 cycles (10,000 seconds in this case for a cycle length of 100 seconds) in each run. The standard deviations from VISSIM and DRIVE runs are also shown in the figures.

Conducting multiple runs using any simulation model is a necessary step in order to provide reliable estimates and conduct statistical comparisons (99). Generally, the existence of higher variations would require a higher number of simulation runs in order to achieve the desired precision in the estimates. Modeling over-saturated traffic facilities has always been a challenge due to the high variability of its results. For the purpose of conducting statistical tests and adequate computing time, 100-cycle simulation with 10 replications is considered reasonable in this study.

A general observation of the results shown in Figure 57, Figure 58, and Table 11 is that both DRIVE and VISSIM produced delay estimates that matched well with those from PASSER III. Even though the null hypothesis on statistically identical means was rejected for the majority of the traffic movements, the delay difference between DRIVE and VISSIM was generally less than 5 seconds, which may be considered an acceptable level from a practical point of view. Statistically different results were mainly due to the small variances in the delays from each individual run.



**TABLE 11 Validation results for under-saturated conditions**

Movement	P-III	DRIVE		VISSIM		Error (1) - (2)	t-statistic	Accept Null Hypothesis?
	Mean	Mean (1)	s.d.	Mean (2)	s.d.			
	Three-Phase							
R1	NA	44.7	10.2	55.3	19.1	-1.3	1.55	Y
R2	NA	11.3	0.4	14.8	0.3	-3.6	22.06	N
M1	22.1	23.0	1.1	25.3	1.8	-1.6	3.32	N
M2	25.2	25.6	0.8	28.2	2.3	-1.8	3.45	N
M4_5	39.7	41.2	1.0	41.7	1.8	-0.2	0.78	Y
M7	22.5	22.8	1.2	23.5	1.8	-1.1	1.04	Y
M8	23.4	24.0	1.5	25.6	1.2	-1.4	2.63	N
M10_11	26.3	26.4	0.7	28.3	0.7	-2.0	6.01	N
M4	22.5	24.1	1.4	28.9	0.2	-4.9	10.99	N
M10	6.8	7.2	0.3	12.4	1.0	-4.8	15.40	N
	Four-Phase							
R1	NA	42.2	8.4	51.2	11.6	-4.7	1.99	Y
R2	NA	10.6	0.3	15.5	0.5	-4.7	26.84	N
M1	21	21.9	1.1	27.4	1.8	-5.8	8.36	N
M2	24	24.4	0.7	31.2	1.0	-6.7	17.27	N
M4_5	39.2	40.5	1.0	39.7	1.0	1.3	-1.92	Y
M7	30.1	30.5	1.6	26.1	1.2	3.5	-7.02	N
M8	31.3	32.2	2.2	28.6	0.7	3.8	-5.07	N
M10_11	31.6	31.8	0.8	31.3	0.8	0.7	-1.39	Y
M4	0	0.8	0.2	3.8	0.1	-3.0	54.88	N
M10	2.6	3.4	0.4	3.2	0.7	0.6	-0.49	Y

Note: (1) P-III: PASSER III; (2) Null Hypothesis: Means are equal; (3) Rejection Region:  $t_{0.025,18} = 2.101$

Figure 59 and Figure 60 compare the freeway mainline delays between DRIVE and VISSIM for the under-saturated cases when ramp metering was operating with queue flush. As can be seen, the freeway mainline delays were primarily in the peak (northbound) direction. The off-peak (southbound) direction only exhibited a minimal level of delay. The freeway delays showed significantly high variations among different simulation runs. Even though DRIVE seemed to have produced higher delays than VISSIM, the t-statistical tests indicate that both models yielded identical average delay values at the 95 percent confidence level as indicated by the *P*-values greater than 0.05. Although the delays in the off-peak direction showed statistically different results as indicated by the *P*-values less than 0.05, the delays were low and the difference is still acceptable from a practical point of view. The higher delays and variations in the freeway mainline as reported by DRIVE were probably contributed by the modeling process of freeway operations. As pointed out earlier, VISSIM results seemed to have shown much faster recovery from breakdown than what has been observed in the field.

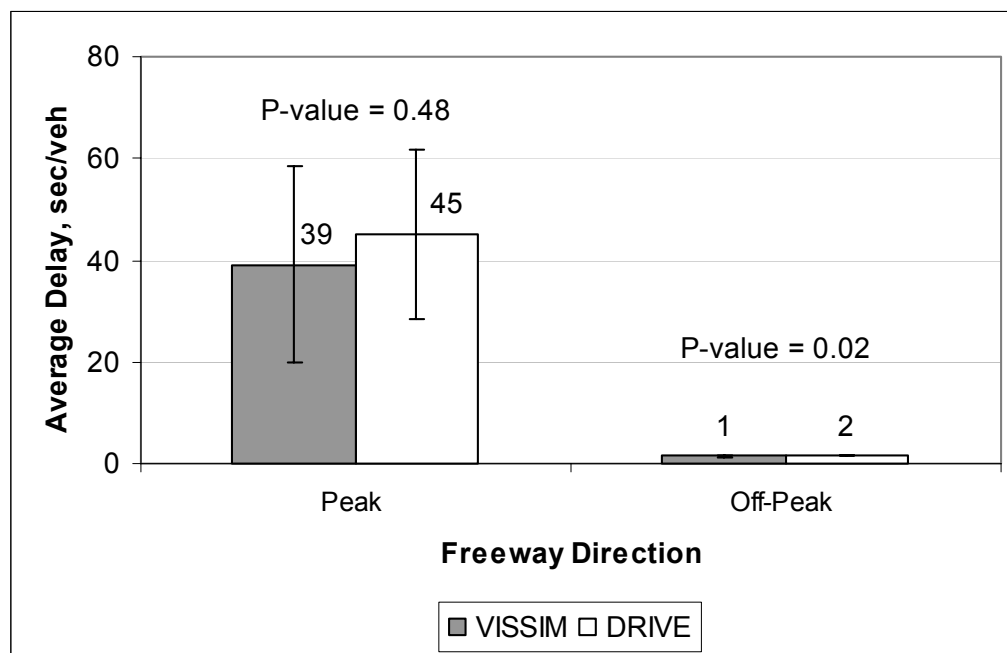


**FIGURE 59** Freeway mainline delays with three-phase: under-saturated conditions (with queue flush).

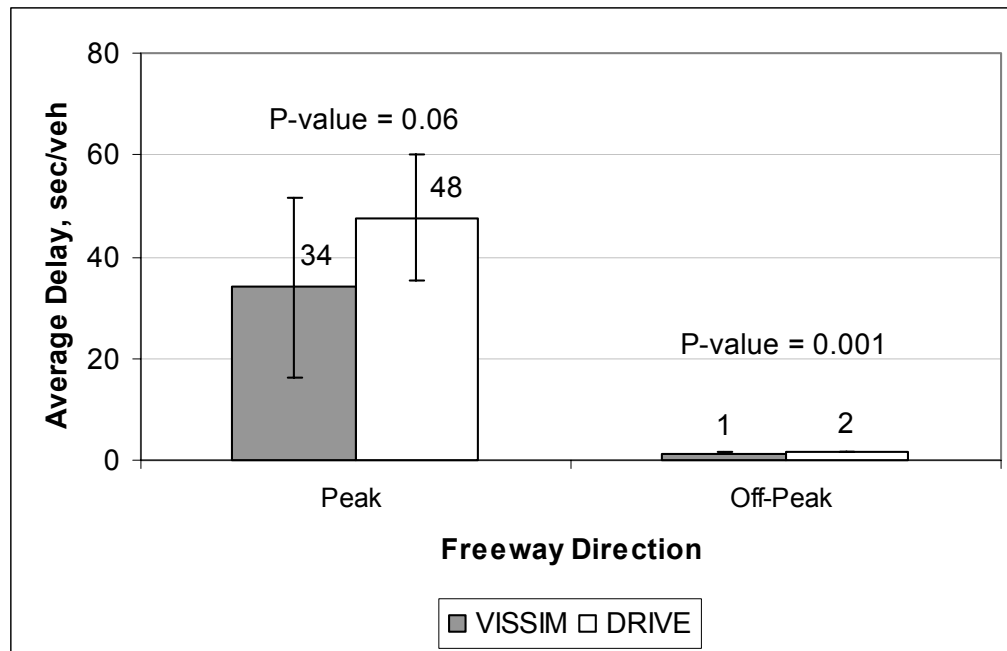


**FIGURE 60 Freeway mainline delays with four-phase: under-saturated conditions (with queue flush).**

### Over-saturated Conditions

Over-saturated conditions were created by increasing 10 percent of the traffic demands at the diamond interchange and freeway on-ramps from the under-saturated conditions presented previously. Ramp-metering operations were also set without queue flush to increase the queue spillback occurrences. PASSER III was no longer applicable to the over-saturated conditions; therefore, comparisons were made only between DRIVE and VISSIM. Similarly, Figure 61 and Figure 62 illustrate the delay results for the surface street traffic movements, and Table 12 includes the t-statistical results.

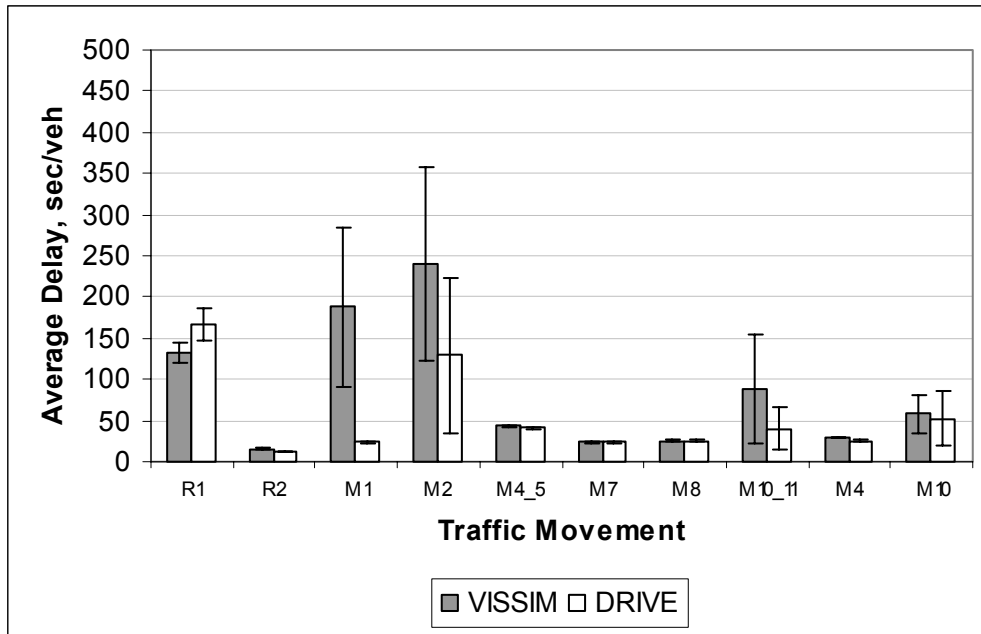


**FIGURE 61 Delays with three-phase and over-saturated conditions.**

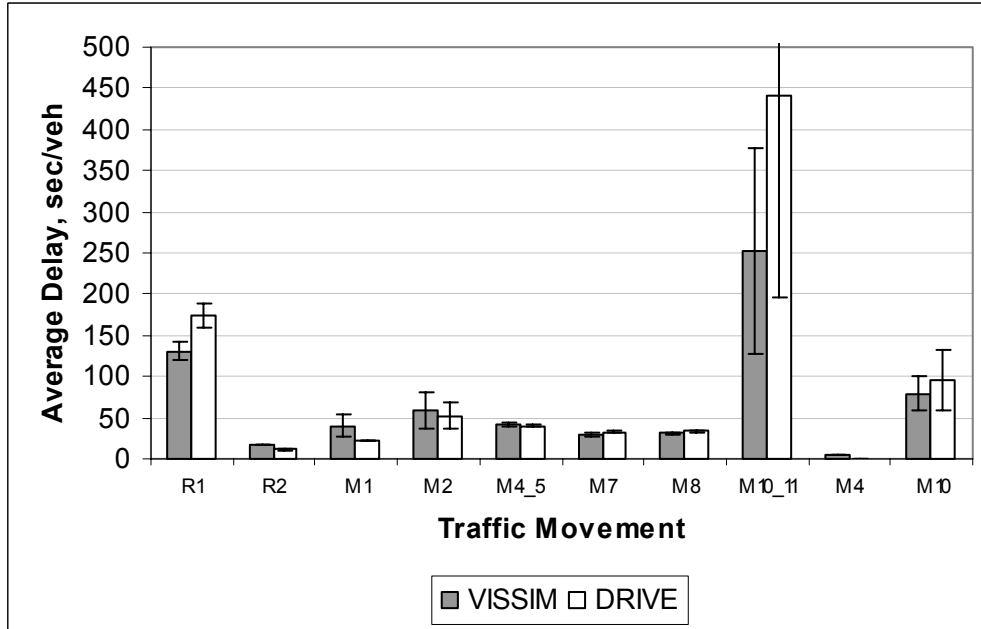


**FIGURE 62 Delays with four-phase and over-saturated conditions.**

**TABLE 12 Validation results for over-saturated conditions**

Movement	P-III	DRIVE		VISSIM		Error (1) - (2)	t-statistic	Accept Null Hypothesis?
	Mean	Mean (1)	s.d.	Mean (2)	s.d.			
Three-Phase								
R1	NA	166.0	19.9	131.9	11.6	34.1	-4.68	N
R2	NA	11.5	0.5	15.9	0.4	-4.4	23.72	N
M1	21	23.7	1.0	188.2	97.1	-164.5	5.36	N
M2	24	128.9	95.1	240.5	117.4	-111.6	2.34	N
M4_5	39.2	40.6	1.5	43.1	1.9	-2.5	3.31	N
M7	30.1	24.3	1.1	23.8	1.5	0.5	-0.91	Y
M8	31.3	25.3	0.9	25.0	1.1	0.3	-0.62	Y
M10_11	31.6	40.0	26.2	88.1	66.0	-48.1	2.14	N
M4	0	25.6	2.0	29.0	0.3	-3.4	5.37	N
M10	2.6	52.1	32.5	57.9	23.5	-5.8	0.45	Y
Four-Phase								
R1	NA	173.4	15.1	131.1	10.4	42.3	-7.31	N
R2	NA	11.2	0.4	17.1	0.6	-5.9	26.79	N
M1	21	22.3	1.0	40.2	13.1	-17.9	4.32	N
M2	24	52.6	16.1	58.9	22.5	-6.3	0.72	Y
M4_5	39.2	39.6	1.4	42.0	2.2	-2.4	2.91	N
M7	30.1	32.1	1.5	30.1	2.4	2.0	-2.31	N
M8	31.3	33.6	1.2	30.9	2.1	2.7	-3.50	N
M10_11	31.6	441.7	244.6	252.1	125.8	189.6	-2.18	N
M4	0	0.8	0.2	3.9	0.1	-3.1	47.31	N
M10	2.6	95.3	37.4	78.7	20.7	16.6	-1.23	Y

Note: (1) P-III: PASSER III; (2) Null Hypothesis: Means are equal; (3) Rejection Region:  $t_{0.025,18} = 2.101$

Some traffic movements, especially those feeding *R1* (e.g., *M1*, *M2*, and *M10*) experienced significant delay increases. The delay increases were contributed by ramp queue spillback to the diamond interchange. Both DRIVE and VISSIM also revealed significantly higher variances in the delays for these traffic movements. *R2* remained under-saturated, and, therefore, those traffic movements feeding *R2* were not significantly affected. Under three-phase operation, the delays for *M1* were also quite different from DRIVE and VISSIM, which was due to the so-called short-lane and blocking effect. In the field, *M1* (the frontage road left-turn movement) was served by a left-turn pocket, where queue spillback from *M2* would cause blocking to the *M1* traffic and significantly increase the delays. Microscopic simulation models such as VISSIM can easily simulate such a short-lane effect. However, like other deterministic analytical models, DRIVE was not designed to model the short-lane effect, i.e., a short-lane pocket was basically treated as an exclusive lane. Modeling of the short-lane effect involves complicated mathematical procedures (100), which is still one of the shortcomings for most deterministic analytical models such as the HCM and PASSER III.

Another interesting observation from the delays under the queue spillback condition is that three-phase and four-phase resulted in a different pattern of how the delays were increased for the related movements. Both DRIVE and VISSIM indicated that with three-phase, the delays increased more on the frontage road movements (e.g., *M1* and *M2*), while with four-phase, the delays increased more on the arterial left-turn movement (*M10* and *M10\_11*). Note that the delays on *M10* were capped at a level that was related to the left-turn storage space. Once the storage space was used up, the delays occurred on the external arterial street approach (i.e., *M10\_11*). The implication is that the two phasing schemes do exhibit different impacts on the arterial and frontage road movements once queue spillback occurs. Three-phase seems to favor the arterial movement, while four-phase seems to favor the frontage road movement. This operational feature is further verified later in the dissertation.

The statistical testing results in Table 12 still indicate significantly different results for most of the movements between VISSIM and DRIVE. The higher variations during over-saturated conditions are directly associated with the nature of traffic flow, and calibrating a traffic model during over-saturated conditions has always been a challenging task. While DRIVE does have its limitations in modeling the short-lane effect, VISSIM, like any other simulation models, also has limitations in modeling over-saturated conditions. A common problem found for most simulation models is modeling the driver's lane selection process. In reality, drivers tend to select the correct lane to travel in much in advance. Even when a driver may have entered a wrong lane, he/she would normally try to merge into the correct lane without having to block the following vehicles. In simulation, however, vehicles tried to get into the correct lane based on the availability of the gap. During over-saturated conditions, it is typical for a vehicle not being able to find a gap to merge into the correct lane to block the following vehicles. This situation was observed in VISSIM at two particular locations: the over-saturated ramp location and the over-saturated arterial street approach. For example, when the on-ramp and the frontage road were filled up with traffic queues, some traffic destined for the freeway entered the right-side lane and caused blocking to the traffic destined for the frontage road. Vehicle blocking was also observed on the arterial street approaches, where *M10* (the arterial left-turn traffic) vehicles blocked the *M11* (the arterial through) vehicles. In many cases, simulation models tend to overestimate such blocking effects compared to those observed in field operations. Due to the reasons discussed above, model validation during over-saturated conditions is probably only a qualitative perspective.

Figure 63 and Figure 64 are the delays for the freeway mainlines for the over-saturated conditions without ramp-metering queue flush. Again, significantly high variations can be observed for the peak direction freeway mainline. While DRIVE seemed to have yielded lower delays than VISSIM, the statistical test results showed that both models actually yielded statistically identical delay estimates based on the 95 percent confidence level, indicated by the *P*-values greater than 0.05 in both figures.

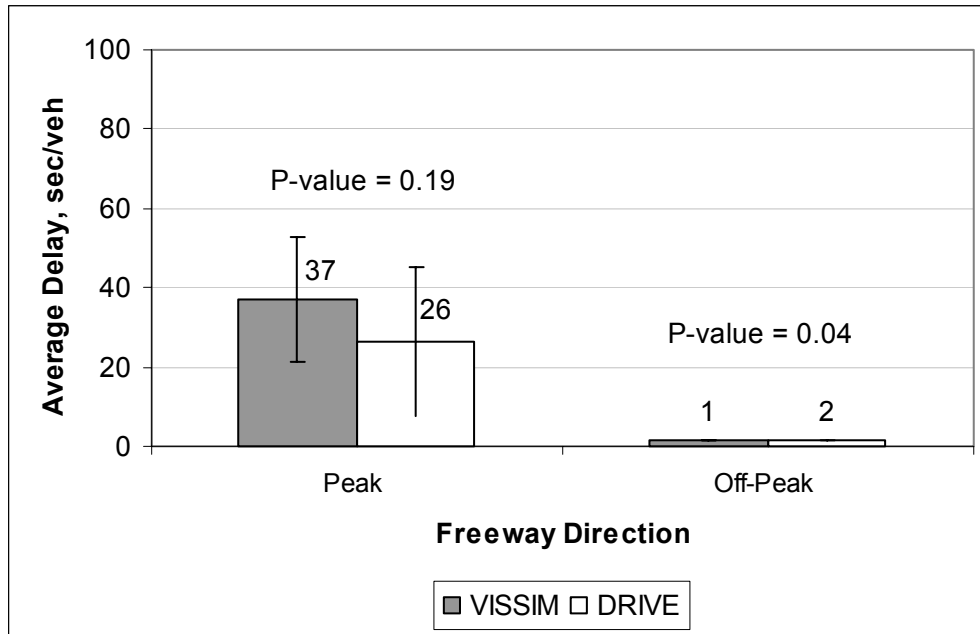


**FIGURE 63** Freeway mainline delays with three-phase: over-saturated conditions (no queue flush).

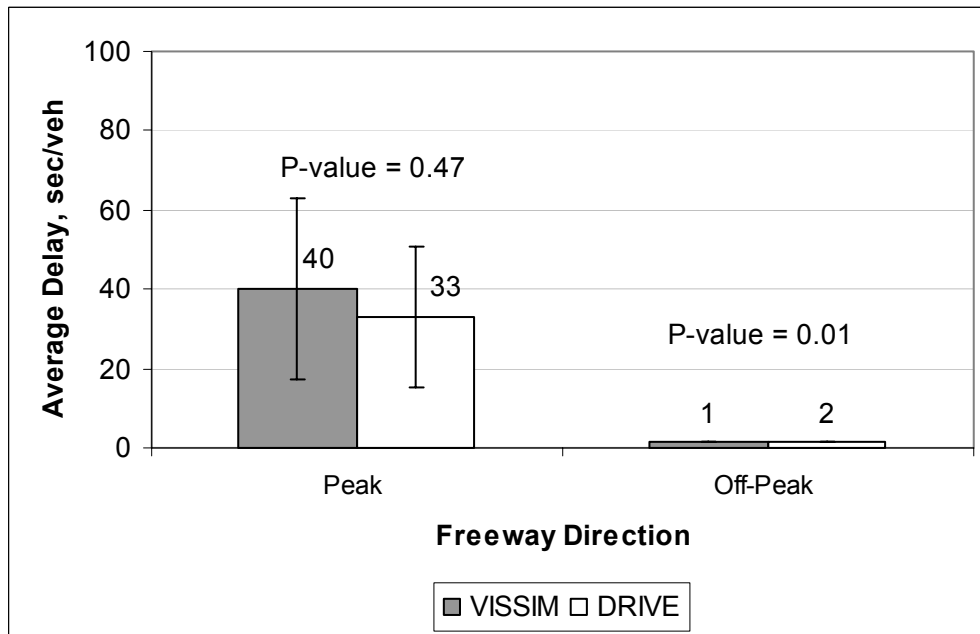


**FIGURE 64** Freeway mainline delays with four-phase: over-saturated conditions (no queue flush).



## **SUMMARY**

Calibration and validation of the DRIVE model were conducted against the VISSIM microscopic simulation model. Selecting VISSIM for model calibration and validation was mainly due to two reasons. The first was that no sufficient field data were available. VISSIM could provide adequate and sufficient information for model calibration and validation purposes, especially where data for statistical results were required. The second was that VISSIM is a well-calibrated simulation model, and it has been widely used in studying transportation problems.

A basic calibration of the VISSIM model was conducted on the modeling capabilities of the two-capacity phenomenon for freeway operations. The stochastic traffic demands generated from DRIVE were compared with those from VISSIM to ensure identical flow patterns in terms of equal means and variances. Both DRIVE and VISSIM were also calibrated against PASSER III for under-saturated conditions (with queue flush), which would reflect normal driving conditions in the United States. Validation of DRIVE was then carried out for the over-saturated conditions (without queue flush) where ramp queue spillback to the diamond interchange occurred. Delay was used as the primary performance measures for the model calibration and validation process.

It was found that with careful selection of the model parameters, VISSIM was able to produce the two-capacity phenomenon that resembled field data. The results confirmed the findings from previous studies that the freeway would have a lower queue-discharge capacity under breakdown than the free-flow capacity. Freeway breakdown and its associated traffic flows are stochastic in nature. The variations in the free-flow capacity are higher than that in the queue-discharge capacity. It was also found that the difference between the two capacities depended on the type of ramp control. The difference between the two capacities tends to reduce with ramp metering on, suggesting that ramp metering may be effective in minimizing the impact from breakdown. However, VISSIM seems to have shown much faster recovery from

breakdown than what has been observed in the field; therefore, the modeling of freeway breakdown warrants further field validation.

Regarding the results for the freeway mainlines, both DRIVE and VISSIM yielded statistically identical delay measures during both under-saturated (with queue flush) and over-saturated (without queue flush) ramp conditions. In the results for the surface street traffic movements, both DRIVE and VISSIM yielded delay results that matched well with PASSER III for under-saturated conditions without queue spillback. For over-saturated conditions with queue spillback, the difference between DRIVE and VISSIM was more significant, which could be caused by model limitations in both models. One specific case is the modeling of the short-lane effect and lane blocking. Nevertheless, for the one case studied, both DRIVE and VISSIM revealed a consistent trend in how the delays increase on the ramp-feeding traffic movements with the two types of diamond phasing schemes. Three-phase seems to favor the arterial left-turn traffic, while four-phase seems to favor the frontage road movement. As a result, validation of DRIVE for over-saturated conditions should probably be stated from a qualitative perspective.

## CHAPTER VI

### ANALYSES OF SYSTEM OPERATIONAL CHARACTERISTICS

One of the major objectives of this research is to develop operational strategies for better managing an IDIRMS. Development of operational strategies must be based on a good understanding of the system and its operational characteristics. The DRIVE software documented in Chapter IV provides an analysis tool for investigating such system operational characteristics. This chapter contains the analysis results using DRIVE from various system operational perspectives. Through investigating the system characteristics, it is desired to provide some theoretical bases for development and justification of implementing ICS. Specifically, the analyses in this chapter attempt to address the following questions related to IDIRMS:

- What effect does the random variation of traffic demand have on the ramp queues?
- What effect does the type of ramp-metering operations have on freeway operations (e.g., fixed metering versus responsive metering, queue flush versus no queue flush)?
- What effect does the type of phasing scheme at the diamond interchange have on system performance?
- What effect does a change of phase split and cycle length have on the ramp queues?
- What effect does the control on the arterial right-turn movement have on ramp-metering performance?
- What effect does the ramp flow split have on the ramp queues?

The results presented in this chapter were all produced from DRIVE based on similar traffic demand and network geometry data used in Chapters IV and V (see Figure 42 for the traffic demand data and Table 8 for the basic model parameters). Any modifications from this basic data set will be noted. All the results were based on 10

replications with different random seeds in DRIVE wherever statistical tests were required for presenting the results. The 95 percent confidence level was the criterion used in accepting or rejecting the null hypothesis while performing the statistical tests.

### **EFFECT OF RANDOM FLOW VARIATION**

For under-saturated ramp conditions, large ramp queues are mainly contributed by the random variation of the traffic demands at the diamond interchange and the ramps. Figure 65 and Figure 66 show the cumulative arrival and departure curves for four continuous simulation cycles with a fixed demand and a random demand, respectively.

As can be seen, if the ramp traffic released from the diamond interchange can be cleared every cycle (i.e., under-saturated condition every cycle), the ramp queues would only be contributed by the platoon arrivals. It is the random flow variation that results in over-saturation during certain cycles, where significantly longer queues might result. As indicated in Figure 66, the ramp experienced over-capacity between 100 seconds and 300 seconds in simulation (i.e., the second and third simulation cycle), and the queue length was significantly larger than that shown in Figure 65. Therefore, to minimize the ramp queues and potential queue spillback, signal-control strategies might be implemented at the diamond interchange to reduce the variations of the flows arriving at the ramp meter.

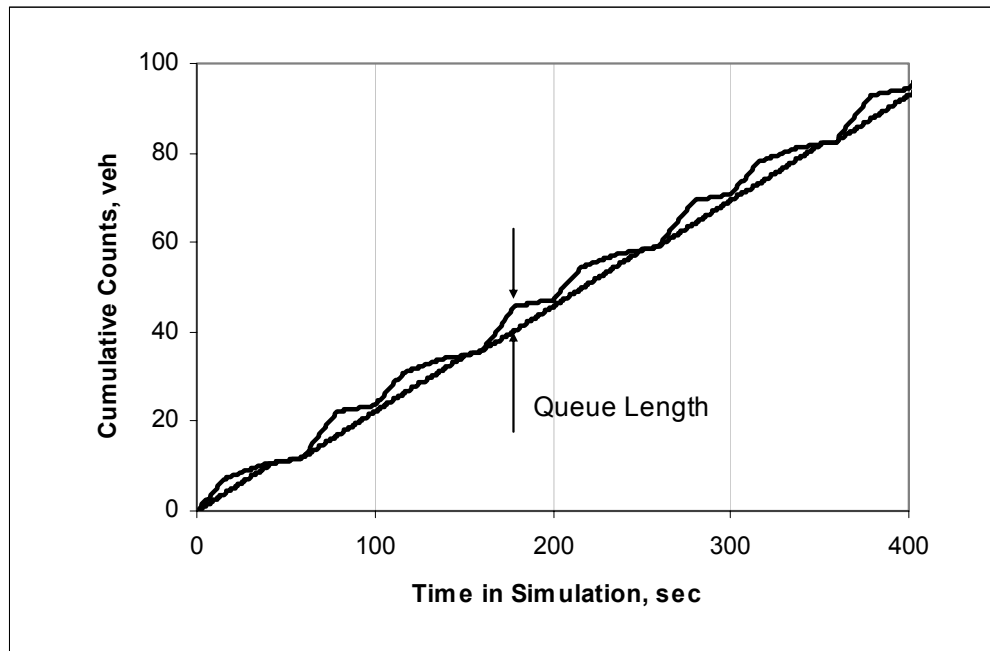


**FIGURE 65** Ramp arrival and departure flows with a fixed demand.



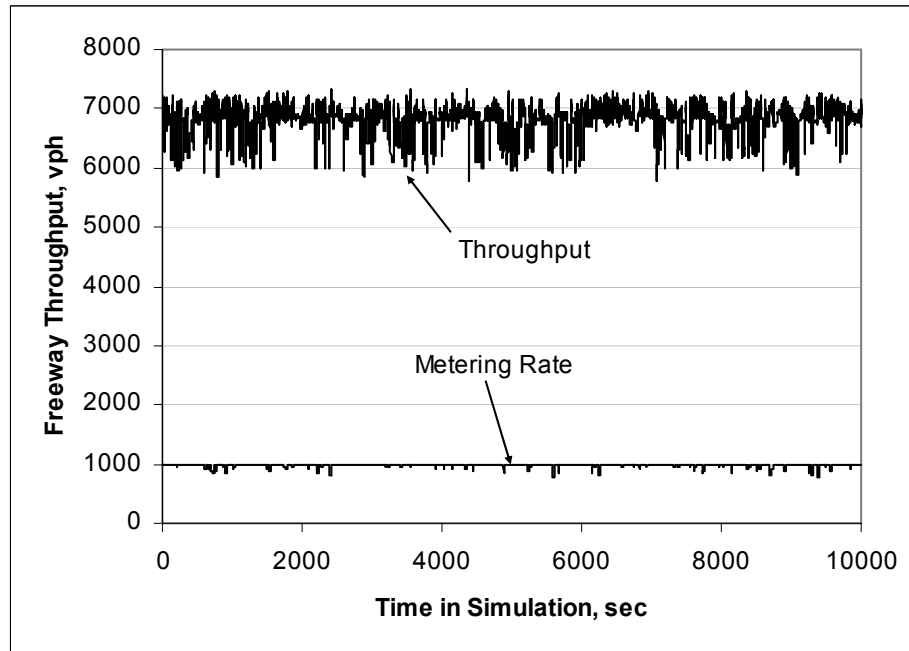
**FIGURE 66** Ramp arrival and departure flows with a stochastic demand.

## **EFFECT OF RAMP-METERING OPERATION**

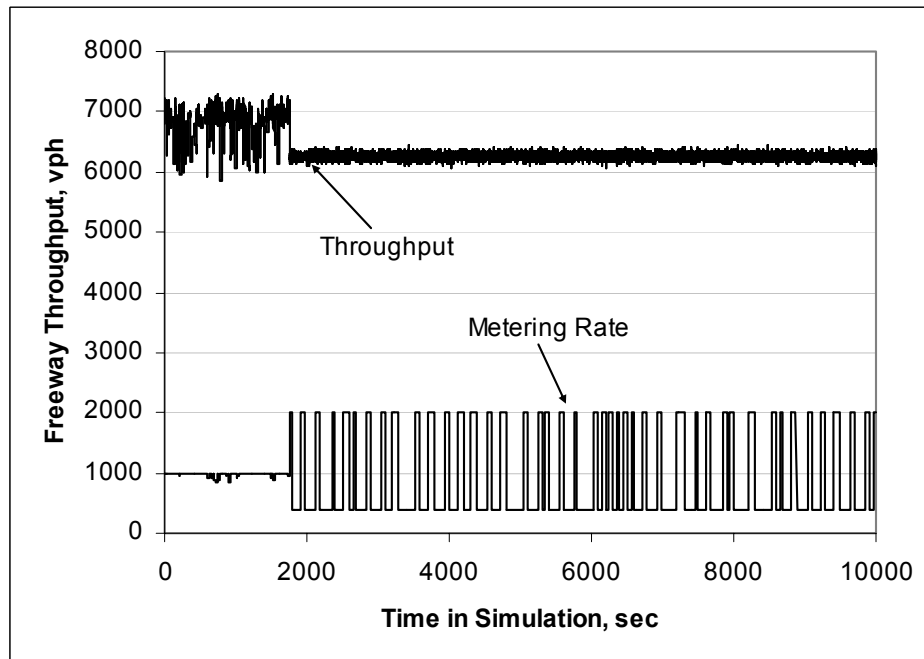
An investigation was conducted using DRIVE of how the ramp-metering operation and its policies (e.g., responsive versus fixed metering rates, metering with queue flush versus without queue flush) might affect freeway operations. Using the same random seed, three types of ramp-metering operations were analyzed: traffic-responsive metering without queue flush, traffic-responsive metering with queue flush, and fixed metering without queue flush. The ramp-metering rates for traffic-responsive operations ranged between 400 vph and 1000 vph, and the ramp-metering rate for fixed metering was 900 vph. The queue-discharge capacity of 6260 vph (about a 11 percent drop from the free-flow capacity) was used for easy identification of the impact of freeway breakdown on system performance.

Figure 67 shows the freeway throughput flows with a traffic-responsive ramp-metering operation and without queue flush. Figure 68 illustrates the freeway throughput flows with a traffic-responsive ramp-metering operation and with queue flush. In both figures, the random throughput flows and the ramp metering rates during the entire simulation (10,000 seconds) are shown.

Figure 67 indicates that with a traffic-responsive ramp-metering operation without queue flush, the freeway maintained higher throughput flows and did not experience breakdown. With queue flush, however, breakdown occurred on the freeway about 1800 seconds into the simulation, resulting in reduced throughput flows (see Figure 68). Once queue flush started, the ramp metering rates jumped between the minimum rate, 400 vph, and the maximum rate, 1000 vph.



**FIGURE 67** Freeway throughput flows from DRIVE with traffic-responsive metering and no queue flush.



**FIGURE 68** Freeway throughput flows from DRIVE with traffic-responsive metering and queue flush.

Figure 69 illustrates the freeway throughput flows from DRIVE with a fixed ramp-metering operation and without queue flush. As shown in Figure 69, freeway breakdown occurred with fixed metering operation even though queue flush was not permitted.

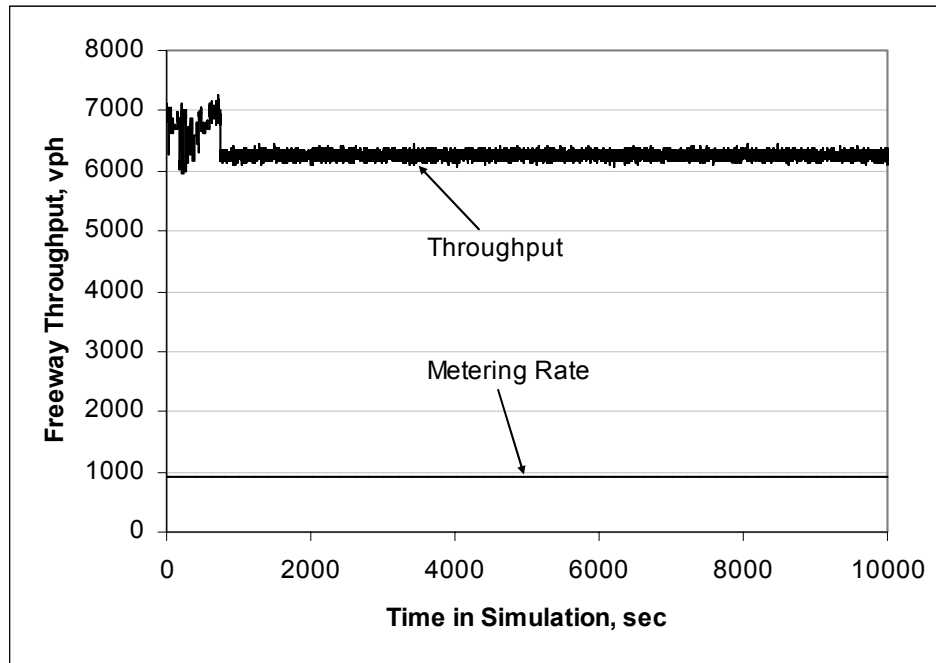


**FIGURE 69 Freeway throughput flows from DRIVE with fixed metering and no queue flush.**

The above analysis results indicated that ramp-metering operations with queue flush increased the likelihood of freeway breakdown, and the freeway never recovered once breakdown occurred for the case demonstrated. Traffic-responsive ramp metering provided the flexibility of adjusting ramp metering rate and showed more effective in preventing freeway breakdown, compared to fixed-metering operation. Therefore, a conclusion might be reached based on the analyzed case that keeping ramp metering in operation for as long as possible is a preferred operating strategy over metering with queue flush. Further more, traffic-responsive ramp metering, when properly designed, is more effective than fixed metering in preventing freeway breakdown.



## EFFECT OF DIAMOND PHASING SCHEME

One potential strategy that could be used to achieve better system operations would be selecting an appropriate diamond phasing scheme, either three-phase or four-phase, as addressed in this study. As shown in Figure 70 and Figure 71, three-phase and four-phase signal operations result in different ramp arrival patterns. As shown in these figures, the two signal-controlled ramp-feeding movements ( $M2$  and  $M10$ ) are served in different sequences. With the three-phase scheme,  $M10$  is served before  $M2$  and after a low ramp flow period of  $\phi2$ . The sequence for serving  $M10$  and  $M2$  is the opposite with the four-phase scheme, i.e.,  $M2$  is served before  $M10$  and after a low ramp flow period of  $\phi2$ . Therefore,  $M2$  would be more likely to experience ramp queue spillback with the three-phase scheme than with the four-phase scheme, a finding suggested in the previous chapter, i.e., the three-phase scheme favors the arterial left-turn movement ( $M10$ ), while the four-phase scheme favors the frontage road movement ( $M2$ ) when ramp queue spillback conditions exist. This operational feature is further verified based on the analysis results from DRIVE as presented next.

In analyzing the effect of the diamond phasing scheme, the first case investigated was ramp queues during under-saturated conditions, i.e., no queue spillback from the ramp meters. Using a 100-second cycle length, the queue lengths (both the average queue, i.e., the 50-percentile queue, and the 95-percentile queue) on  $RI$  were recorded from each analysis run with both three-phase and four-phase schemes. Because DRIVE generated the exact same traffic flow patterns when the same random seed was used under the cases of three-phase and four-phase, the paired  $t$ -test was conducted to compare the mean values. Figure 72 shows the results along with the  $P$ -values from the paired  $t$ -test.

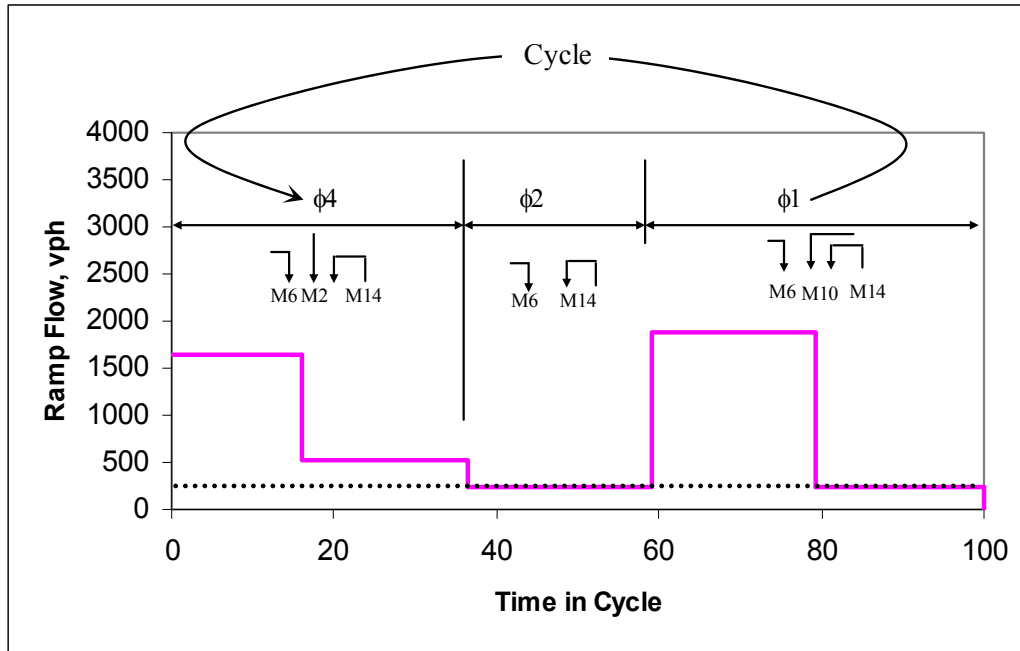


**FIGURE 70 Ramp flow profile with the three-phase scheme.**

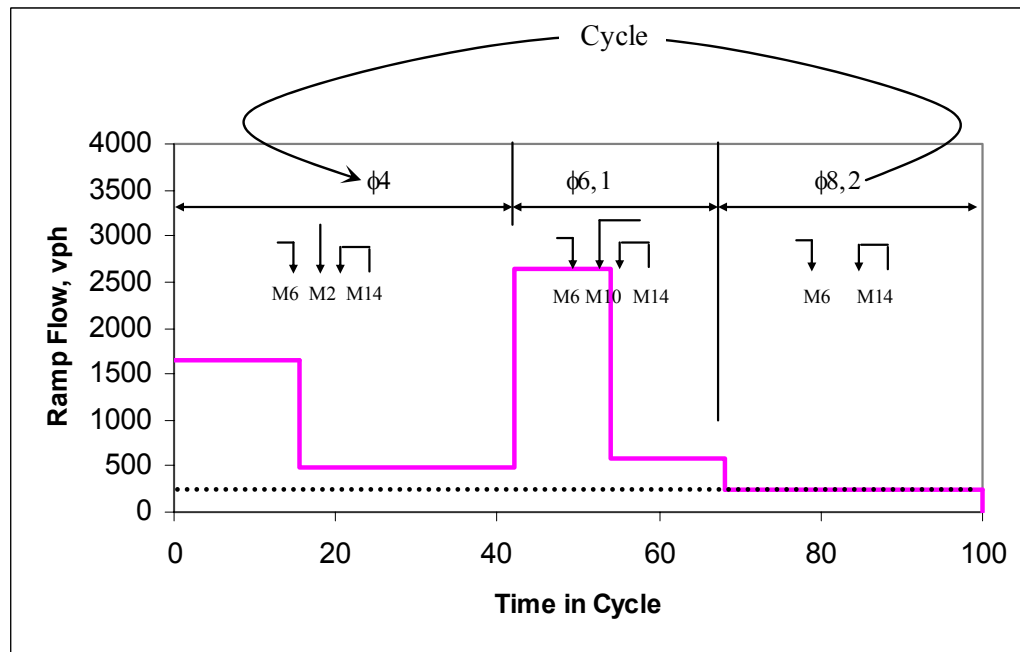


**FIGURE 71 Ramp flow profile with the four-phase scheme.**

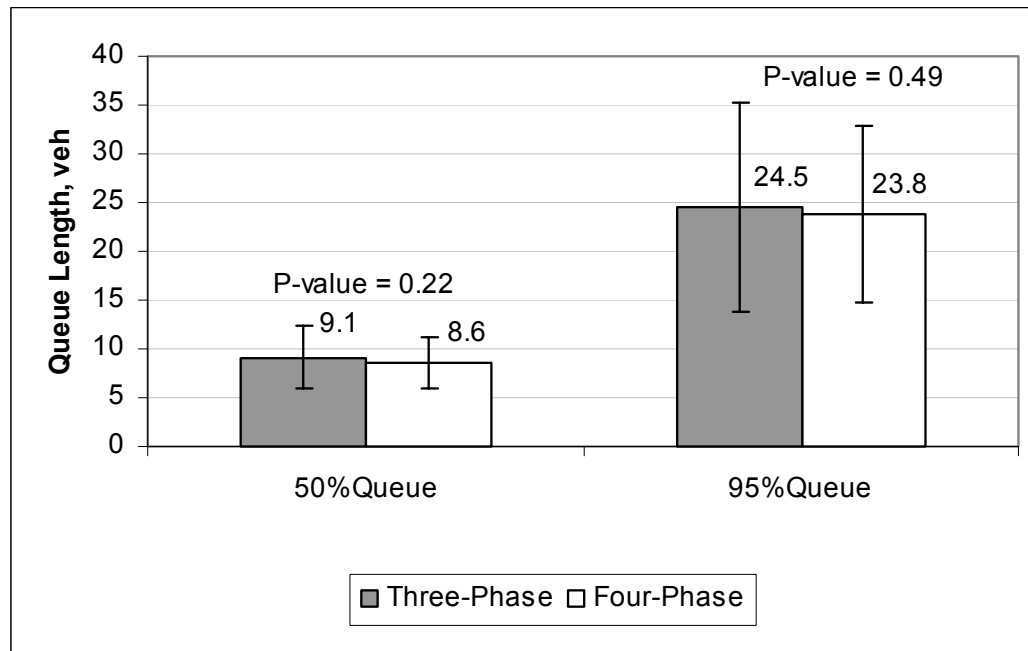


**FIGURE 72 Ramp queue length results with three-phase and four-phase schemes.**

As can be seen from Figure 72, although the four-phase scheme resulted in slightly lower queues than the three-phase scheme, no statistically significant difference was found between the queues with three-phase and four-phase schemes, as indicated by the  $P$ -values greater than the acceptable criterion 0.05. The slight difference reflects the stochastic nature of traffic flows, not the phasing schemes.

The effect of the diamond phasing scheme was further investigated for the over-saturated conditions, where ramp queue spillback occurred. The investigation in this case focused on how queue spillback would affect the diamond interchange movements. Figure 73 and Figure 74 illustrate how traffic demand evolved when the ramp queue to allowed to spill back to the diamond interchange, with the three-phase scheme and the four-phase scheme, respectively. Only the traffic movements being affected by the  $R/I$  queues are illustrated. For simplicity and demonstration purposes, a constant traffic demand was assumed for the entire analysis period, i.e., no demand variations existed among cycles.

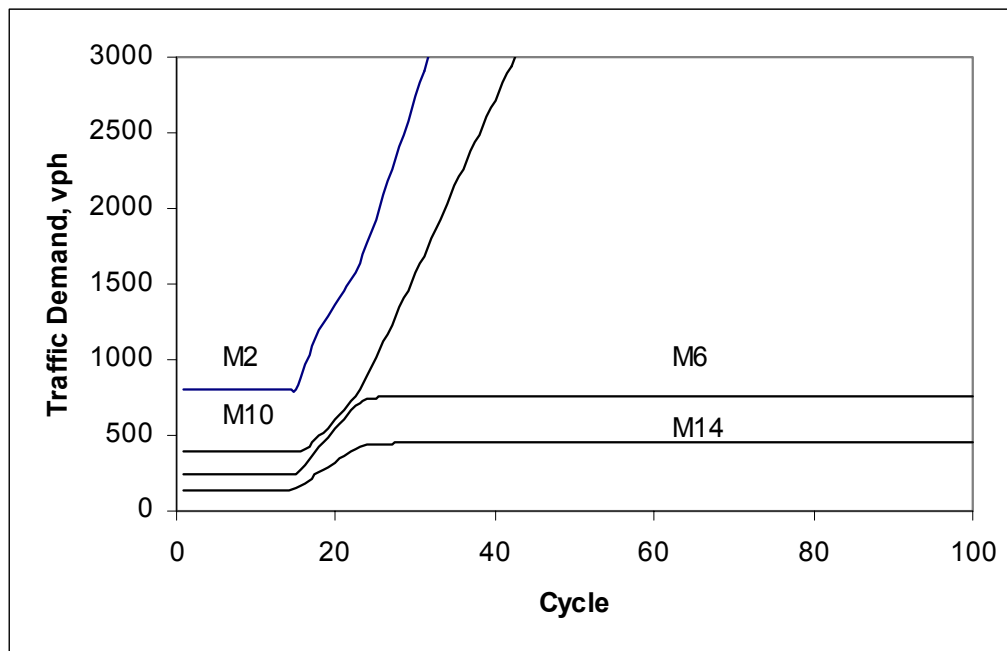


**FIGURE 73** Traffic demands evolution during over-saturated ramp conditions: three-phase.

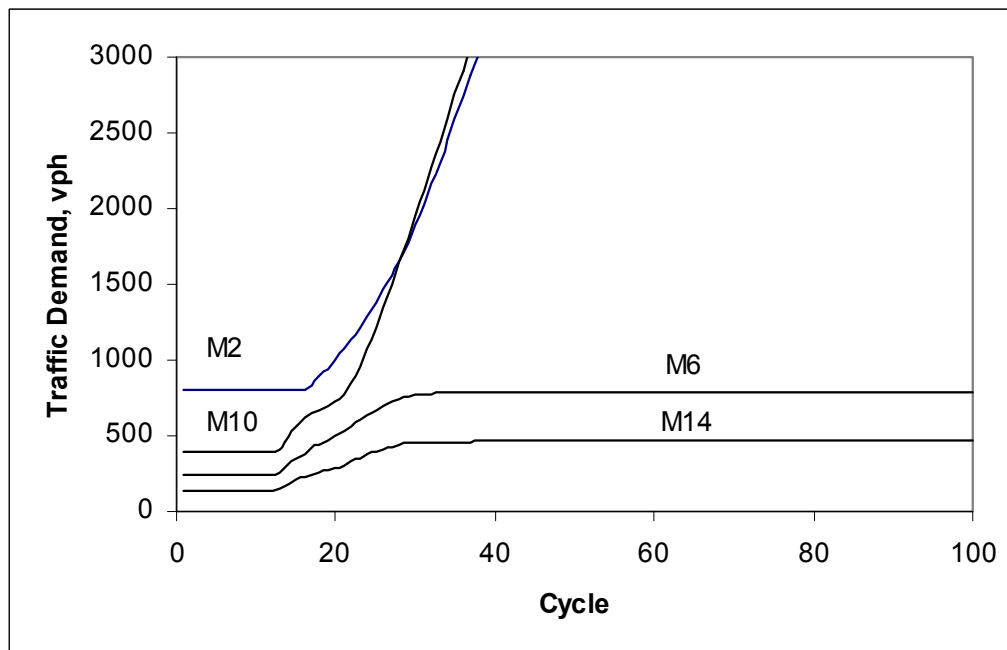


**FIGURE 74** Traffic demands evolution during over-saturated ramp conditions: four-phase.

In Figure 73 and Figure 74, each line represents the traffic demand in vehicles per hour in each cycle of a simulation of 100 signal cycles. The level horizontal lines at the beginning of the analysis indicate that the ramp queue had not reached the diamond interchange yet; therefore, no queue spillback occurred and no residual demand resulted. Once the ramp queue reached the diamond interchange, queue spillback blocked the traffic movements that feed *RI*, and residual demands resulted. Such residual demands were shifted to the following cycles, resulting in a continued increase in traffic demands in the following cycles.

Figure 75 and Figure 76 illustrate the impact of queue spillback on diamond interchange operations from the perspective of ramp-metering residual queues. Ramp-metering residual queues in each cycle are the number of vehicles that were kept at the diamond interchange due to spillback and that were supposed to be released from the diamond interchange and enter the ramp (refer to  $NR_m^j$  in Equation 123 through Equation 126).

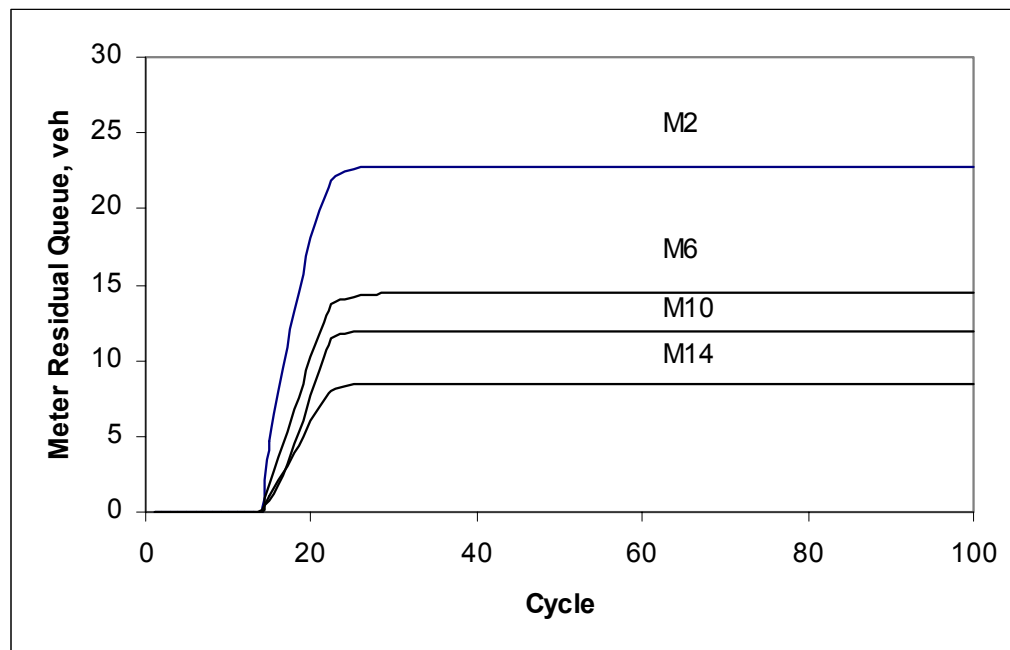


**FIGURE 75 Residual queues from ramp spillback: three-phase.**

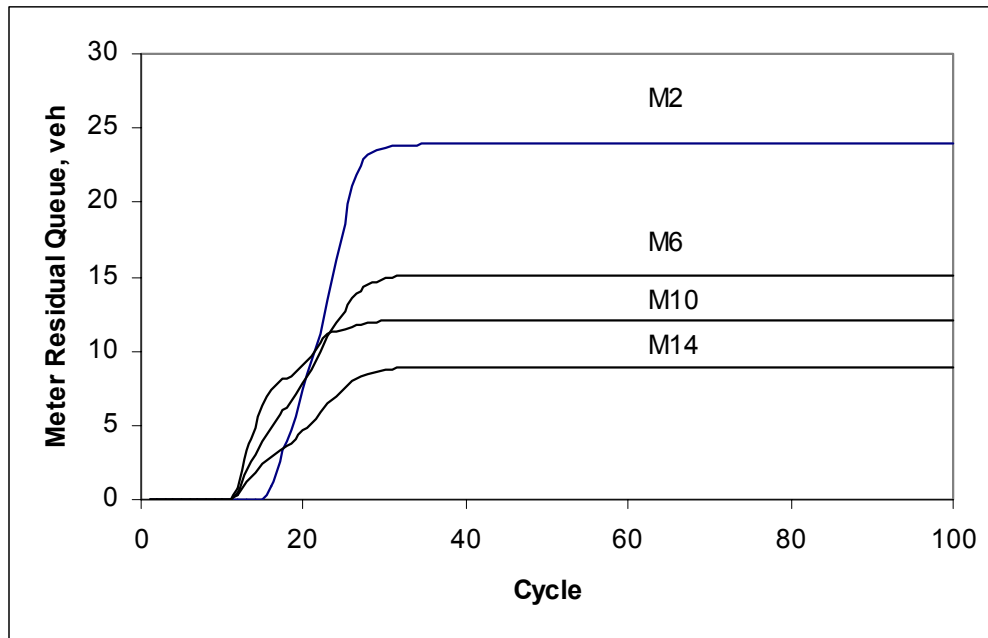


**FIGURE 76 Residual queues from ramp spillback: four-phase.**

By comparing the profiles for the three-phase and four-phase schemes as shown in the above figures, it can be seen that the demand increased faster for *M10* under the four-phase scheme (see Figure 73 and Figure 74). As a result, the residual queue also started later for *M2* with the four-phase scheme (see Figure 75 and Figure 76). With the three-phase scheme, all four movements started to experience queue spillback around the 16<sup>th</sup> cycle in the analysis. However, with the four-phase scheme, *M6*, *M10*, and *M14* started to experience queue spillback around the 13<sup>th</sup> cycle in the analysis, but *M2* only started to experience queue spillback around the 17<sup>th</sup> cycle. This phenomenon confirmed the author's earlier assumption with the particular case analyzed that four-phase scheme seemed to benefit the frontage road movement (*M2*), while three-phase scheme seemed to benefit the arterial movement (*M10*). From the above figures, an equilibrium condition was also observed as indicated by no further increases in the demands and queues for *M6* and *M14*. This equilibrium state may be directly related to the modeling process of queue spillback used in DRIVE. A further explanation of this equilibrium state is given below.

It is noted that *M6* and *M14* are non-signal-controlled free movements, and they arrive at the ramp uniformly. The capacities for these two movements were assumed to be equal to their saturation flow rates. As documented in Chapter III on the modeling of an over-saturated traffic movement at a diamond interchange, the residual queues for a particular ramp-feeding movement are composed of two parts: one is due to demand exceeding its signal capacity, and the other is due to ramp-metering queue spillback. The equilibrium state is when  $\phi_4$  and  $\phi_1$  are fully saturated, i.e., the total number of vehicles that are discharged from the diamond interchange and arrive at the ramp becomes constant every cycle. Therefore, the portion of the residual queues due to ramp-metering spillback also becomes constant. When distributing these residual queues among all the ramp-feeding movements, each movement gets its portion of the residual queues that also becomes constant. This residual queue plus the queue due to signal capacity overflow are transferred to the next cycle as the new demand. For the case analyzed, these new demands for *M6* and *M14* never exceeded their signal capacities (i.e., saturation flow rates); therefore, only the residual queue due to ramp-metering spillback was transferred to the next cycle, causing both the demands and the queues to become constant for *M6* and *M14* once the equilibrium state was reached. For the other two signal-controlled feeding movements, they experienced both signal over-capacity and meter queue spillback; therefore, the queues and the demands kept increasing.

In summary, three-phase and four-phase do not exhibit significant differences in the ramp queues during under-saturated conditions. However, based on the particular case studied, they do seem to have different impacts during over-saturated conditions when spillback occurs. Three-phase seems to benefit the arterial left-turn movement, and four-phase seems to benefit the frontage road phase movement.

#### **EFFECT OF CONTROLLED ARTERIAL RIGHT-TURN**

To effectively control the vehicles entering the ramps, the arterial right-turn movement may be placed under control of the diamond traffic signal. With signal control applied to the arterial right-turn movement, the traffic arrival patterns at the ramps will be

changed (see Figure 35 and Figure 36), which may result in different ramp performances. Similarly, the ramp queue lengths were obtained from DRIVE simulation runs for the cases where the arterial right-turn movement was controlled and not controlled by the diamond traffic signal. Both the average queue length and the 95-percentile queue lengths were compared as shown in Figure 77.

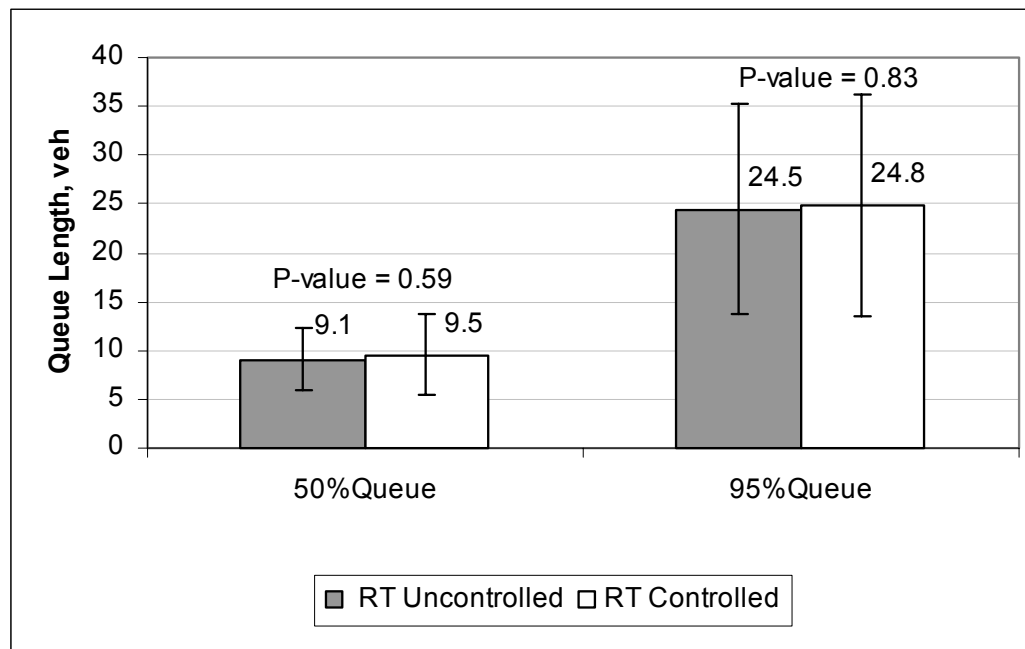


**FIGURE 77 Queue length results with and without arterial right-turn movement control.**

Although queues were slightly higher when the arterial right-turn movements were controlled by the traffic signal, the difference was not statistically significant (as indicated by the high  $P$ -values). As a result from the particular data set analyzed, whether or not the arterial right-turn movement is controlled by the signal does not seem to affect the ramp queues significantly. In fact, signal-controlled arterial right-turn traffic actually created more non-uniform ramp arrivals, which might have contributed to the slight increase in ramp queue lengths. However, the particular data set did not have a significant arterial right-turn traffic flow; therefore, the impact on ramp queues



due to signal control of the right-turn movement was not significant. When the arterial right-turn traffic becomes the major ramp-feeding movement, providing signal control to the right-turn movement might be essential to minimize spillback and provide equity service to all the traffic movements.

### **EFFECT OF PHASE SPLIT**

Another means of controlling vehicle entry to the metered ramps is by adjusting the phase splits at the diamond interchange. The effect of adjusting the phase split on the ramp queues was investigated. However, the objective of controlling ramp queues may not be achieved by simply reducing the phase splits. For a movement that is over-saturated (i.e., the demand exceeds its capacity), reducing the green time for that movement would also reduce the number of vehicle entries to the ramp, thus reducing the ramp demand and queue. However, for a movement that is under-saturated (i.e., the demand is less than its capacity), reducing the green time for that movement would actually increase the size of its platoon and, therefore, increase the cyclic queues.

The relationship between phase split,  $g_i$ , and the saturated green portion,  $g_{q,i-m}$  is demonstrated in Equation 131 and Figure 78. The size of the platoon is directly associated with  $g_{q,i-m}$  because  $g_{q,i-m}$  measures the time duration of vehicle discharge at the saturation flow rate.

As can be seen from Figure 78, with the increase of green split, the saturated green portion,  $g_{q,i-m}$ , increases during over-saturated conditions but decreases during under-saturated conditions. Such an operational feature was further validated using DRIVE and is presented next.

$$g_{q,i-m} = \text{Min} \left[ \frac{V_m(C - g_i)}{S_m - V_m}, g_i \right] = \text{Min} \left[ \frac{V_m C (1 - \frac{g_i}{C})}{S_m - V_m}, g_i \right] \quad (131)$$

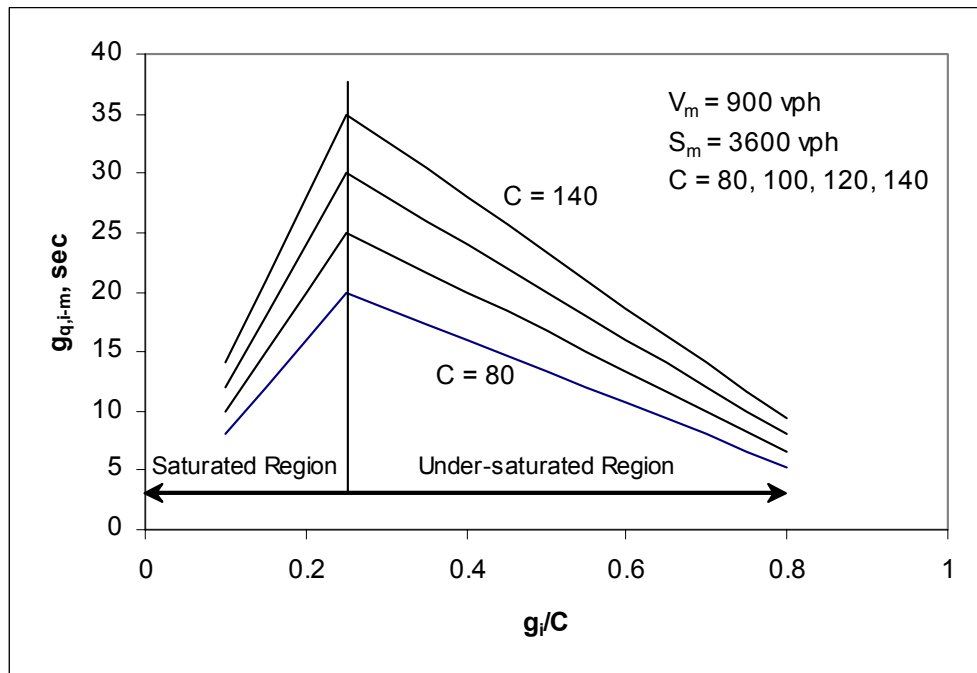


**FIGURE 78 Relationship between green splits and saturated portion of green.**

Using DRIVE, the effect of adjusting phase splits on ramp queue length was analyzed. Figure 79 illustrates the ramp queues for the cases with and without split adjustment. For the case with phase split adjustment, the ramp-feeding movement phase ( $\phi 1$  for  $M10$ ) was increased by 5 seconds (also 5 percent) from the normal phase splits, while the arterial phase ( $\phi 2$ ) was reduced by 5 seconds. It can be seen that while the queue lengths under both cases do not show significant difference from a practical point of view, the paired t-test results revealed statistically different queue length results. This is because the queue lengths were consistently lower with split adjustment than those without split adjustment. This analysis confirmed the conclusion that for under-saturated traffic movements at the diamond signal, increasing their phase splits would actually result in smaller ramp queues.

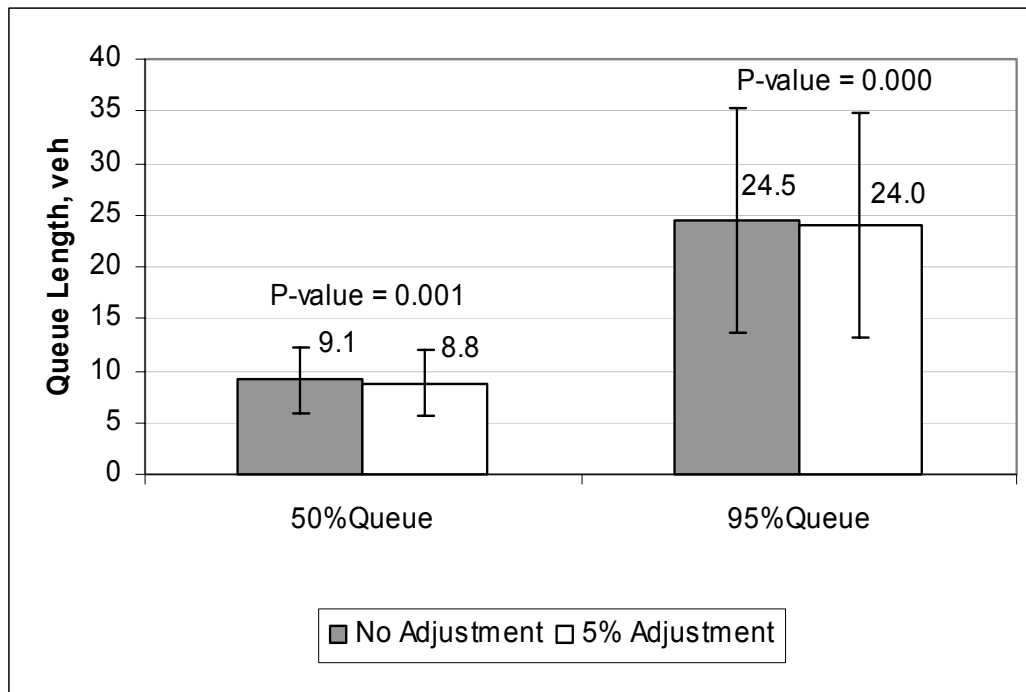
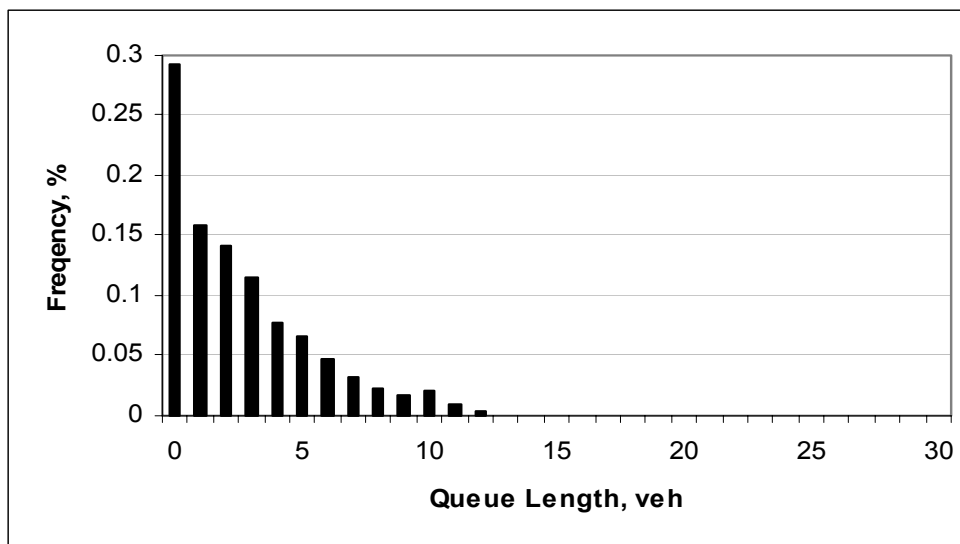


**FIGURE 79** Queue lengths with/without phase split adjustment.

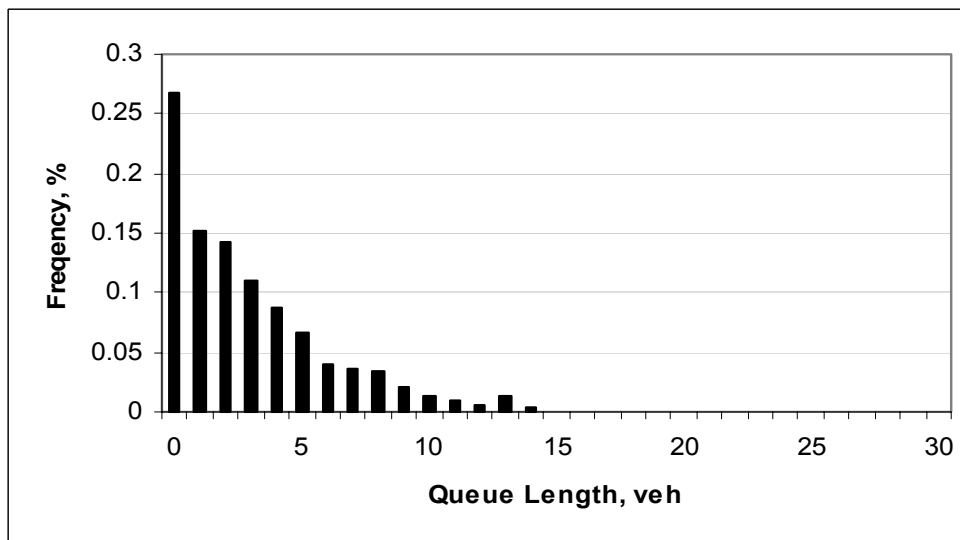
### EFFECT OF CYCLE LENGTH

Another potential strategy that could be used to minimize ramp queues in an IDIRMS would be changing the cycle length at the diamond interchange to. The effect of cycle length on ramp queues was investigated using DRIVE. The first case was to examine the ramp queue distribution in histogram forms with different cycle lengths. Figure 80 and Figure 81 compare the histograms of the queue length distributions with the two types of phasing schemes and two cycle lengths.

As can be seen, the median queues increase with longer cycle length; however, the shapes of the histograms are similar between three-phase and four-phase. The distribution resembles an exponential distribution with the shorter 60-second cycle length, while the distribution tends to resemble a normal distribution with the longer 120-second cycle, except for the high percentage of zero queues.

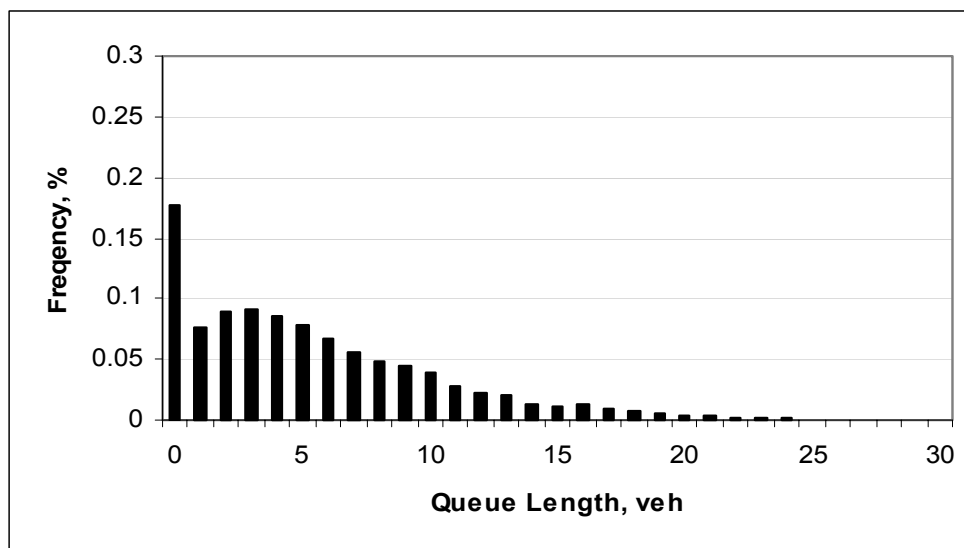


(a) With three-phase

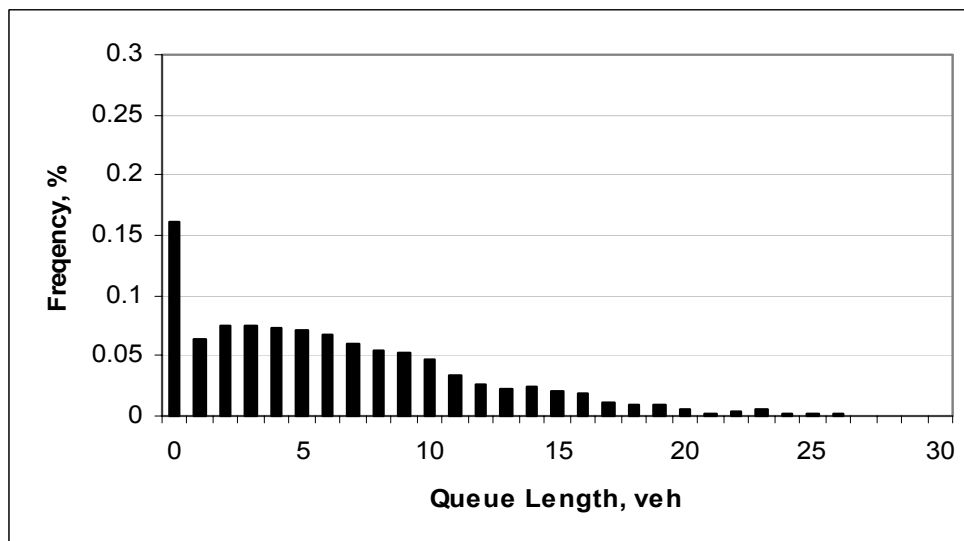


(b) With four-phase

**FIGURE 80 Queue length distribution histograms: 60-second cycle.**



(a) With three-phase



(b) With four-phase

**FIGURE 81 Queue length distribution histograms: 120-second cycle.**

Figure 82 illustrates the estimated cumulative density functions (CDF) for the ramp queue distributions with different cycle lengths. These CDF curves provide percentile queue length values that were counted over time. For example, with a cycle length of 60 seconds, the 80<sup>th</sup> percentile queue length is about three vehicles, i.e., the ramp queue length is less than three vehicles during 80 percent of the entire analysis

period. It can be seen that with the increase of cycle length, the maximum ramp queue length per cycle increases. This finding implies that under certain traffic conditions, such as a low ramp demand level, the ramp queues may be effectively contained by simply using a shorter cycle length at the diamond interchange without having to get into more sophisticated operation and control systems. In practice, however, there are limitations on how short the cycle length can be, either due to minimum phase constraints or capacity concerns at the diamond interchange.

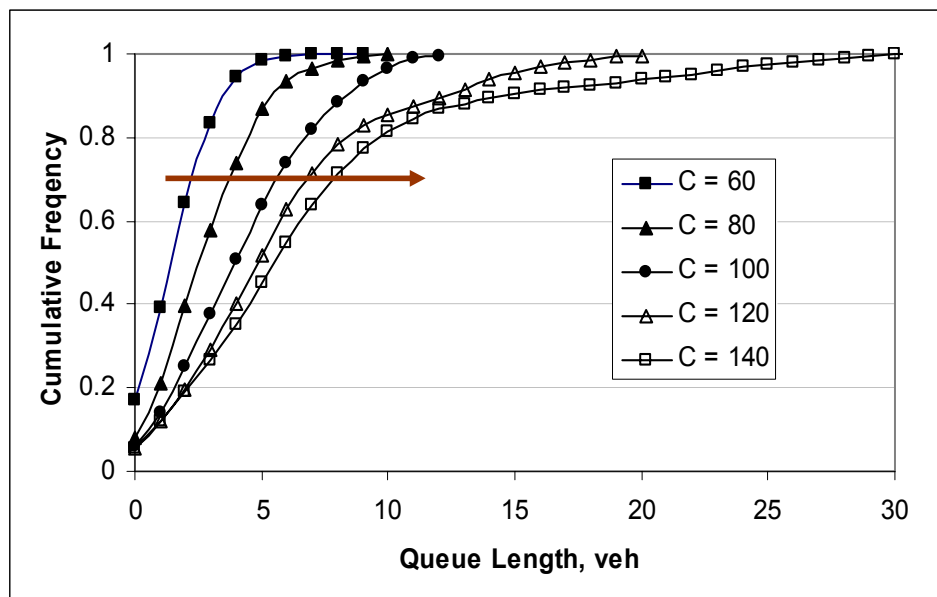


**FIGURE 82 Effect of cycle length on ramp queue length.**

### **EFFECT OF RAMP FLOW SPLIT**

Ramp flow split refers to the distribution of the traffic between the frontage road and the on-ramp. It is measured by the proportion of the on-ramp traffic over the total traffic released from the diamond interchange that heads for the ramp and the frontage road destinations. To investigate what the effect of ramp volume split has on ramp queues, the ramp demand was kept at the same level of 855 vph, while a range of flow split was generated randomly. The average ramp queue length was then obtained from DRIVE.

It should point out that the average queue length for each volume split case was based on one simulation run. Because the OD demands were generated randomly to obtain a specific volume split, each volume split case would only represent one out of many possible traffic flow patterns. For example, for the same ramp volume split of 0.30 (or 30%) at  $RI$ , there could be many combinations of the ramp-feeding movement volume,  $V_m$ , and the proportion of each movement going to  $RI$ ,  $p_{m,l}$ . Therefore, the results presented next would only be based on limited data points.

Figure 83 shows the average queue length (50-percentile) with respect to the ramp flow split. The regression model is also displayed along with the data points to illustrate the trend of data relationship.

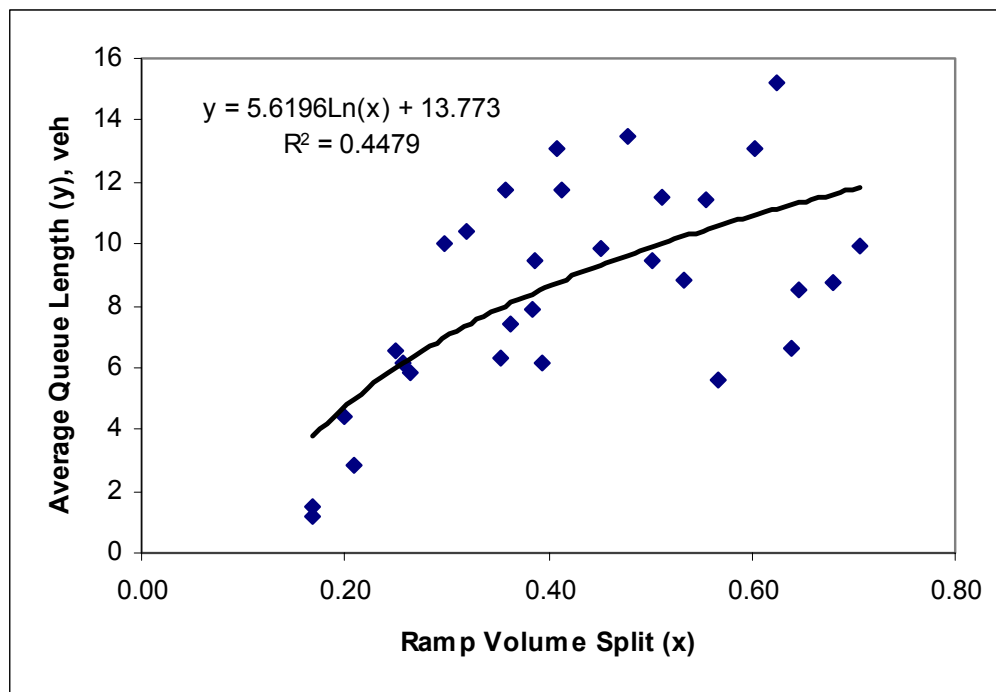


**FIGURE 83 Effect of ramp flow split on ramp queue length.**

As can be seen, the ramp queue length seems to be non-linearly related to the ramp flow split. The queue increases while the ramp flow split increases. The scattered data points could be explained by the high random variation due to many other factors

not being considered in the relationship between queue length and ramp flow split. There seem to be other factors that need to be taken into account in developing a better regression model, such as the turning movement volume distribution and the volume split for each individual feeding movement.

## **SUMMARY**

Traffic operational characteristics for the IDIRMS were analyzed using DRIVE from various perspectives for the purpose of gaining a better understanding of the system and providing justifications of pursuing integrated operations between diamond interchange and ramp metering operations. The analyses focused on the impact of ramp-metering operations, random variation in traffic demand, diamond signal timing (i.e., cycle, phasing, and split), arterial right-turn movement control, and ramp flow split. The analyses were conducted by examining both over-saturated and under-saturated cases.

Traffic-responsive ramp-metering operations with a varied metering rate proved to be more effective in maximizing freeway throughput flows and preventing freeway breakdown. Ramp metering with queue flush could result in earlier freeway breakdown; thus, this strategy is not a preferred operational strategy. Random variation in traffic demand has shown to be the primary contributor to large ramp queues. Therefore, ICS should be sought to prevent or delay the onset of ramp queue flush and smooth the ramp demand through better management of an IDIRMS, particularly through signal control strategies at the diamond interchange.

For the case of an under-saturated diamond interchange, no significant difference was found in the system performance between three-phase and four-phase operations and whether the arterial right-turn movement is signal controlled or not. The ramp queue length seems to be non-linearly related to the ramp flow split, indicating an increase in the ramp queue length with the increase of the ramp flow split. Ramp metering performance is directly affected by the length of the ramp storage. Longer ramp storage improves ramp-metering performance by reducing queue spillback and its related queue flush time. The analyses also proved that by increasing the phase split for



the ramp-feeding movement, the ramp queues may actually be reduced due to reduction in the size of platoons. To achieve control of ramp demand through split adjustment would only be possible when the ramp-feeding movement becomes over-saturated. The ramp queues were found to increase with the increase of diamond cycle length. The ramp queue length distributions do not follow normal distributions due to a significant number of zero queues.

For over-saturated ramp conditions where queue spillback existed, the type of phasing scheme exhibited different operational impacts on the diamond interchange operation. The four-phase scheme seemed to benefit the frontage road phase movement, while the three-phase scheme seemed to benefit the arterial left-turn movement.

Development and evaluation of viable ICS are addressed in the next chapter.

## **CHAPTER VII**

### **DEVELOPMENT AND EVALUATION OF INTEGRATED CONTROL STRATEGIES (ICS)**

The processes of developing and evaluating ICS for an IDIRMS are documented in this chapter. ICS for an IDIRMS were developed focusing on the strategies dealing with recurring freeway congestion. The primary system operational objective is to maintain ramp metering in operation as a means of preventing freeway breakdown, which would require minimizing ramp queues and spillback occurrences. The ICS were implemented and evaluated using the VISSIM microscopic simulation model. The VISSIM simulation model was used to capture the details and dynamics of the operations. Microscopic simulation models such as VISSIM also provide users with the capability of developing signal control logics that resemble actual signal controller operations. Evaluations of the effectiveness of ICS were conducted based on three generally defined demand scenarios as characterized by the ramp conditions. Finally, the proposed system architecture and the detailed system functional diagrams were also developed at the conceptual level to guide future field implementation of the ICS.

#### **RESOURCE MANAGEMENT PHILOSOPHY**

One of the key elements for a successful development and implementation of ICS is to achieve better management of the available resources in IDIRMS under various traffic flow conditions. The ICS should be designed to respond to specific traffic conditions such as recurring and non-recurring traffic congestion. The ICS should be applicable in real-time traffic operations, where the outcome can usually only be measured but not well predicted. The key to a successful operational strategy relies on identifying all the critical elements and determining which elements can be managed and controlled. Operational strategies should address a broader range of impacts on the entire transportation system.

The resources within an IDIRMS include three major facilities: the freeway mainlines, the ramp meters, and the diamond interchange. The properties of each

facility that needs to be managed include the capacities, throughput flows, and queue storage spaces. In general, we have little or no control of the freeway mainline demands. However, we can manage the freeway mainlines to maintain free-flow conditions without breakdown using ramp metering so that the freeway would produce the maximum throughput flows. Both field operations and previous analyses indicate that ramp queue flush is one of the major causes of freeway breakdown. Flushing the ramp queue results in a sudden increase in freeway demands due to platoon vehicles entering the freeway, which increases the likelihood of freeway breakdown. Therefore, an effective approach to prevent freeway breakdown is to maintain ramp metering in operation without queue flush. However, ramp metering implies restricted ramp entry, thus increasing the likelihood of ramp queue spillback into the diamond interchange signal.

Queue spillback into the diamond interchange can cause blockage to other traffic movements and result in unnecessary delays. While effective traffic-responsive ramp-metering operation is essential to reduce ramp queues, the best approach to controlling ramp queue spillback is probably through proactive signal control of the ramp-feeding traffic movements using the diamond interchange. Therefore, the best location for ramp demand control is at the diamond interchange.

Strategies to prevent queue spillback to the diamond interchange are then used to manage the demand and store the excessive queues outside the interchange, either on the arterial street approaches or on the frontage road approaches. However, the most advantageous queue storage locations must be determined based on the analyses of potential impacts and operational trade-offs. Storing the queues on the arterial street approaches seems to be a preferred alternative because excessive queues on the frontage road approach may present a more severe threat to the traffic system operations than storing queues on the arterial street. Queue spillback to the frontage road approach and perhaps extension to the freeway mainline may interfere with mainline operations, which would result in reduced freeway throughput (101, 102). Excessive queues on the frontage road approach would also cause blockage to the left-turn and right-turn

movements. On the other hand, queues on the arterial approaches must also be limited because excessive queues on the arterial approaches may interfere with other signalized intersections along the arterial.

Because the available queue storage spaces on both the frontage road and the arterial locations have limits, the objective of the ICS is therefore to maximize the usage of these available queue storage spaces. When the last resort (i.e., all storage spaces) is used up, the excessive queues and demands may eventually need to be released, such as by terminating the ramp-metering operation. If ramp queue flush is then considered as a failure event, the ICS should delay its occurrence, but it may not be able to completely avoid it.

### **THE SYSTEM'S OPERATING OBJECTIVES**

As discussed in the previous section, ICS should be developed for achieving specific operating objectives. In this study, the focus was on minimizing system delay as the primary objective although many other aspects of the operations, such as safety and equity issues, may also play important roles in practice. From the point of view of managing the entire IDIRMS operation and considering the trade-offs, the following operating objectives were identified for IDIRMS in priority order:

1. maximize freeway mainline operations at free-flow conditions and minimize freeway breakdown;
2. minimize ramp queue flushes and maximize normal ramp-metering operation;
3. minimize ramp queue spillback into the diamond interchange signals;
4. control vehicle entries to the ramp meters through proactive signal control at the diamond interchange; and
5. store excessive demands and queues in the most advantageous locations so that all the queue storage spaces can be efficiently used without interfering with freeway mainline and adjacent arterial signal operations.

## **DEVELOPMENT OF ICS**

ICS were developed to achieve the operating objectives noted above. The ICS can be classified into three categories, with each category dealing with a specific traffic condition: (a) low-level integration, (b) non-recurring congestion, and (c) recurring congestion. Descriptions of the general strategies related to the low-level integration and non-recurring congestion are briefly discussed next, followed by details of the strategies related to recurring congestion.

### **Low-Level Integration**

The low-level integration strategies are simply those that could be achieved through efficient management of the available resources without having to acquire additional sophisticated detection and control equipment. Examples of such strategies may include adjusting the cycle length and splits at the diamond interchange, more efficient traffic-responsive ramp-metering design, and adequate location of the advance queue detector.

Adjustment to the diamond signal cycle length and splits may result in smaller cyclic queues that are manageable with available resources. Adjustment to ramp-metering operations may involve changing the maximum and minimum metering rates to allow more flexibility for the ramp-metering flows to best utilize the freeway capacities. One alternative to increasing the metering rate is to allow multiple entry per green (also referred to as bulk metering) for a single-lane ramp meter. The location of the advance queue detectors should be set back as far as possible to maximize ramp queue storage space. For example, the advance queue detectors may be better located on the frontage road instead of the end of the on-ramp, as long as the ramp queues would not spill back to block the diamond interchange. These low-level integration strategies are primarily fine-tuning with existing resources and therefore may be treated as mitigation measures under low traffic demand conditions. The DRIVE model could be used to provide assessments of the traffic conditions and whether such operational strategies would provide satisfactory system performance measures.

### **Non-recurring Congestion**

Non-recurring congestion is also referred to as incident-related congestion, where dramatic change in traffic flow patterns may result. Non-recurring congestion often creates significant turbulence to normal traffic operations. Incidents can block freeway lanes, distract drivers, and thus significantly reduce freeway capacities. Incidents could also result in travel pattern changes due to traffic diversion from routine travel paths. The travel pattern change and traffic diversion will depend on the nature of an incident such as its location and its severity. The changes in traffic flow patterns would require special treatments of the diamond signal timing and ramp-metering operations.

Figure 84 and Figure 85 illustrate the two types of incident locations and the possible traffic diversions. For example, an incident occurring within the interchange (refer to Figure 84) may result in traffic diversion via the off-ramp, and the on-ramp demand would increase while the mainline demand at the ramp merge location would decrease. Strategies dealing with such an incident may involve increasing the ramp-metering rate or metering suspension, and increasing the green split for the frontage road/off-ramp approach (27). On the other hand, incidents occurring downstream of the on-ramp (refer to Figure 85) would result in reduced freeway capacity. While traffic may divert through the off-ramp and attempt to enter the freeway at the downstream on-ramp, the reduced downstream capacity may require restricted ramp entry. Therefore, the strategies dealing with such an incident may involve traffic control measures such as ramp closure. Ramp closure would result in traffic diversion to the downstream diamond interchange, where the potential impact on the downstream interchange should be further evaluated. This study does not go beyond the scope of an isolated diamond interchange location. Therefore, strategies dealing with major incident conditions are not further addressed in this study.

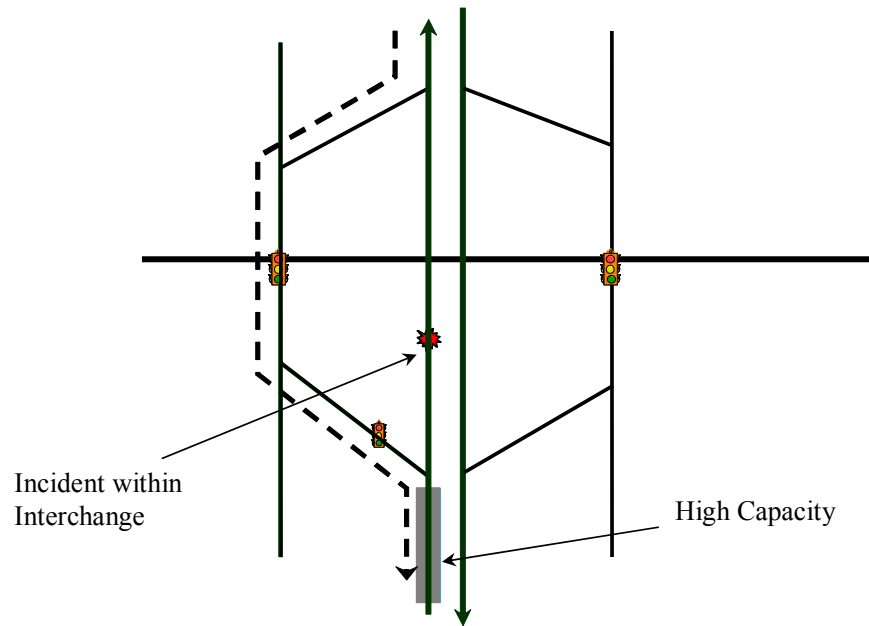


**FIGURE 84 Incident within interchange.**

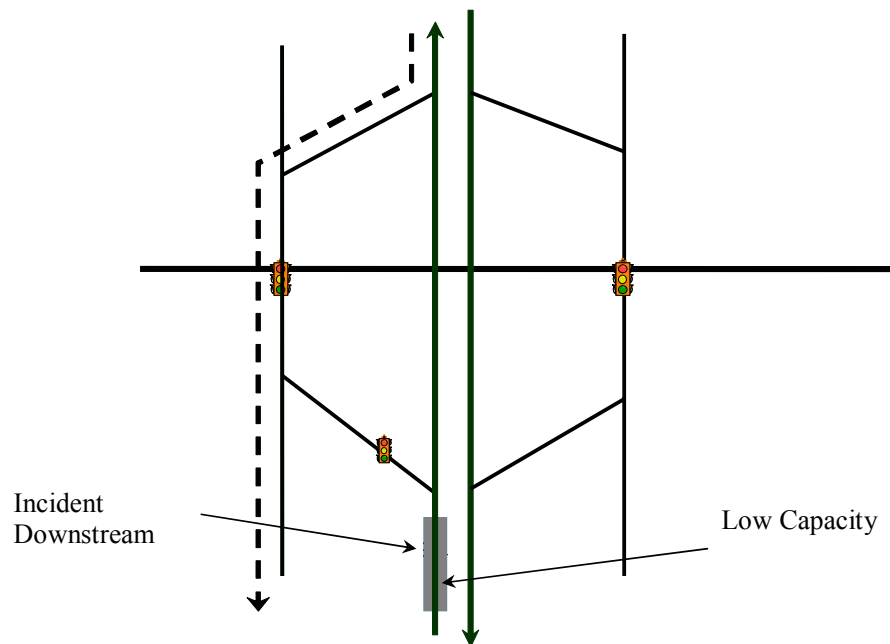


**FIGURE 85 Incident downstream of interchange.**

## **Recurring Congestion**

Recurring congestion refers to the situation where traffic demand exceeds capacity on a regular basis. Recurring congestion can be classified into short-term and long-term congestion, which are all subjectively defined. Short-term congestion may refer to the situation where over-saturation lasts only for a short period of time (e.g., a period of 15 minutes or a few signal cycles at the diamond). Long-term recurring congestion may refer to a situation where over-saturation may last for a prolonged period (e.g., at least 30 minutes or more). Both short-term and long-term congestion are encountered in daily operation and, therefore, are addressed in this research.

Under conditions of short-term congestion, queue spillback to the diamond interchange may or may not occur depending on how long the congestion period is and whether there are enough queue storage spaces between the ramp meter and the diamond interchange. Under long-term congestion, traffic demands exceed the ramp-metering capacity for a prolonged period, and queue spillback to the diamond interchange signal will most likely occur.

In either case, proactive control at the diamond interchange must be executed in order to prevent queue spillback occurrences. Such a proactive control could be achieved through adjustment of the diamond interchange signal timing. For example, in order to prevent queue spillback to the diamond interchange, the traffic movements feeding the ramp may be restricted entry to the downstream frontage road and the ramp. Such a control measure could not be accomplished by some minor adjustments to the signal cycle length and splits. Special signal timing may be necessary to achieve restricted vehicle entry such as using all-red extensions or holding a particular signal phase. All-red extension implies displaying extended red signal indications as a means of stopping traffic going through the interchange. Such an operation, although it may serve the purpose of restricting vehicle flows, may not be a practical application. The ICS developed in this research are based on the principle of holding a particular signal phase to achieve the objective of restricted vehicle entry.



## ICS UNDER RECURRING CONGESTION

### A Demand Reduction Model for Spillback Control

Under recurring congestion, when ramp demand exceeds its metering capacity, ramp queues will grow steadily until spillback to the diamond interchange occurs. In order to prevent queue spillback, the traffic demand feeding the ramp must be reduced during the period of consideration, which has to be implemented through adjustment of signal operation at the diamond interchange. A demand reduction model is presented next to illustrate the basic principles. Demand reduction can be applied equally to all the feeding movements or to just one of the movements. When demand reduction is applied to more than one movement, an equal  $v/c$  approach as used in determining normal diamond signal timing is appropriate. When demand reduction is applied to only one movement, the exact amount of green split reduction can be calculated. The following presentation of the model uses on-ramp  $RI$  as an example.

The normal traffic demand at  $RI$  is shown in Equation 132. Note that the throughput  $u_m$  is used in the equation instead of the demand  $V_m$ .

$$R_1 = u_2 p_{2,1} + u_6 p_{6,1} + u_{10} p_{10,1} + u_{14} p_{14,1} \quad (132)$$

With this demand, the predicted ramp queue length is  $q_{RI}$ , which is  $\Delta q_{RI}$  longer than the queue storage space  $Q_{RI}$ .

$$\Delta q_{RI} = q_{RI} - Q_{RI} \quad (133)$$

The required hourly flow rate reduction to  $RI$ ,  $\Delta R_1$ , is obtained from:

$$\Delta R_1 = \frac{3600 \Delta q_{RI}}{C} \quad (134)$$

This amount of demand reduction can be applied to either *M2* or *M10* or both by reducing the phase splits associated with these two movements. The following example illustrates the demand reduction applied to both *M2* and *M10*, with consideration of achieving equal  $v/c$  ratios after the phase split adjustments.

$$u_2 p_{2,1} + u_{10} p_{10,1} - \Delta R_1 = u'_2 p_{2,1} + u'_{10} p_{10,1} \quad (135)$$

$u'_2$  and  $u'_{10}$ , the new demands after reduction, should be set equal to the capacity flows of *M2* and *M10* with the reduced green splits of  $g'_4$  and  $g'_{10}$ .

$$u'_2 = c_2 = \frac{g'_4}{C} S_2 \quad (136)$$

Demand reduction of *M10* can be achieved through adjusting either the left-turn phase ( $\phi_1$ ) or the external arterial phase ( $\phi_6$ ) as indicated in Equation 137:

$$u'_{10} = \text{Min}(c_{10}, c_{10-11} \frac{V_{10}}{V_{10} + V_{11}}) = \text{Min}(\frac{g'_1}{C} S_{10}, \frac{g'_6}{C} S_{10-11} \frac{V_{10}}{V_{10} + V_{11}}) \quad (137)$$

With different diamond signal phasing schemes, the demand reduction will be achieved differently. With the four-phase scheme, the throughputs for *M2* and *M10* can be reduced by reducing the phase splits of  $\phi_4$  and  $\phi_6$ . The extra time can then be allocated to  $\phi_2$  and  $\phi_8$ . Equation 138 through Equation 142 describe how the phase splits can be adjusted to achieve equal  $v/c$  ratios for *M2* and *M10*:

$$\frac{V_2}{c_2} = \frac{V_{10} + V_{11}}{c_{10-11}} \quad (138)$$

$$\frac{V_2 C}{g'_4 S_2} = \frac{(V_{10} + V_{11}) C}{g'_6 S_{10\_11}} \quad (139)$$

From Equation 134 through Equation 137:

$$\frac{g'_4 S_2}{C} p_{2,1} + \frac{g'_6 S_{10\_11} V_{10}}{C(V_{10} + V_{11})} p_{10,1} = (u_2 p_{2,1} + u_{10} p_{10,1}) - \frac{3600 \Delta q_{R1}}{C} \quad (140)$$

Solve Equation 139 and Equation 140 for  $g'_4$  and  $g'_6$ .

$$g'_4 = \frac{V_2 [C(u_2 p_{2,1} + u_{10} p_{10,1}) - 3600 \Delta q_{R1}]}{(V_2 p_{2,1} + V_{10} p_{10,1}) S_2} \quad (141)$$

$$g'_6 = \frac{(V_{10} + V_{11}) [C(u_2 p_{2,1} + u_{10} p_{10,1}) - 3600 \Delta q_{R1}]}{(V_2 p_{2,1} + V_{10} p_{10,1}) S_{10\_11}} \quad (142)$$

The extra green times  $[(g_4 - g'_4) + (g_6 - g'_6)]$  can be distributed to  $\phi_2$  and  $\phi_8$  to achieve equal  $v/c$  ratios for the associated traffic movements, or the time can be distributed to one of the phases, which is equivalent to holding that phase, a strategy with adaptive signal control that will be discussed later in this chapter.

With the three-phase scheme, there are two alternatives to control throughputs for  $M2$  and  $M10$ . One alternative is to only reduce throughput for  $M10$ , which can be achieved by reducing the green split for  $\phi_6$  as illustrated in Equation 143 through Equation 145:

$$u_{10} p_{10,1} - \Delta R_1 = u'_{10} p_{10,1} \quad (143)$$

$$u'_{10} = \frac{g'_6}{C} S_{10\_11} \frac{V_{10}}{V_{10} + V_{11}} \quad (144)$$

Solve Equation 143 and Equation 144 for  $g'_6$ :

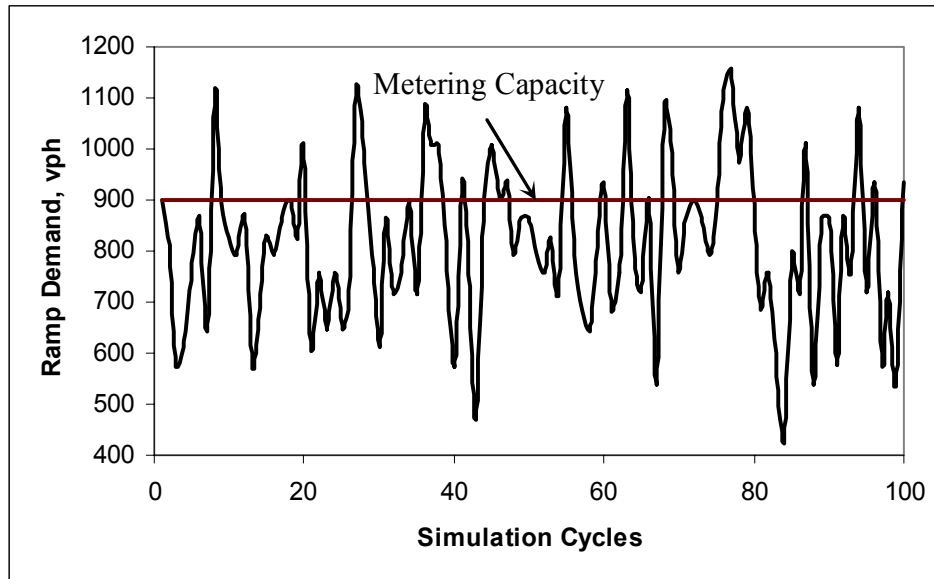
$$g'_6 = \frac{(u_{10} p_{10,1} - \frac{3600 \Delta q_{R1}}{C}) C (V_{10} + V_{11})}{S_{10\_11} V_{10} p_{10,1}} \quad (145)$$

Similarly, the green split for  $\phi_2$  can be reduced to reduce throughput for  $M4$  for controlling demand for  $R2$ . The extra green times,  $(g_6 - g'_6)$  and  $(g_2 - g'_2)$ , can be distributed only to the internal phases ( $\phi_1$  and  $\phi_5$ ), which is equivalent to holding the internal left-turn phases as a means of reducing flows to both ramps.

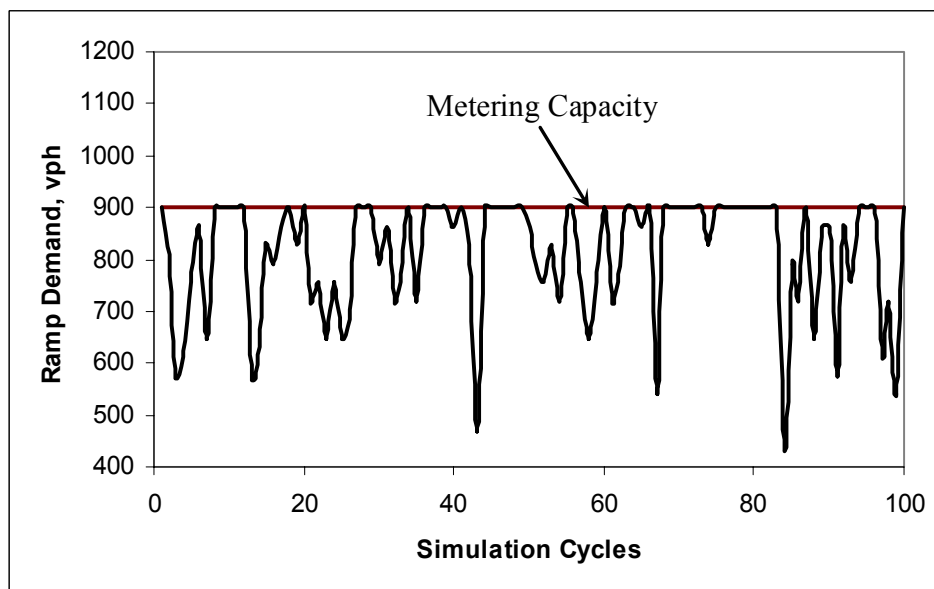
Another alternative to controlling demand with the three-phase scheme is to reduce phase splits for  $\phi_4$  and  $\phi_1$ . The extra time can then be reallocated to  $\phi_2$  and perhaps  $\phi_6$ , which is equivalent to holding  $\phi_2$  and  $\phi_6$ , another strategy that will be discussed later in the chapter.

Strategies of spillback control through proactive diamond signal timing are used to achieve smoothed ramp demand, as shown in Figure 86. Figure 86a shows the ramp demand profile when proactive control was not applied to the traffic from the diamond interchange, while Figure 86b shows the profile after proactive control was applied. In these cases, the ramp meter had a fixed metering capacity of 900 vph. As can be seen, even when the average ramp demand is less than the metering capacity, the stochastic traffic flow variation resulted in several cycles where the demand exceeded the metering capacity, which could potentially result in queue spillback. With proactive diamond signal control, the ramp demand never exceeded its metering capacity during the entire analysis period, while the same ramp-metering throughput was maintained. Of course, the figures here illustrate the best scenario that could be achieved. In reality, to achieve such perfect demand control would require accurate demand detection and

quick signal operation response, which has been a challenging task facing traffic engineers and researchers.



(a) Uncontrolled Ramp Demand



(b) Smoothed Ramp Demand

**FIGURE 86** Smoothed ramp demand profile through diamond control.

### **Basic System Requirements for Adaptive Control**

To prevent ramp queue spillback, the diamond interchange signal must be able to sense any ramp queue buildup and respond with adequate signal control. Therefore, the diamond signal system must have adaptive control features, which would require additional detection, communication, and signal control devices. Such a system can be developed based on the existing functions and features of most traffic signal controllers currently used in Texas.

Figure 87 is a proposed detection design, where additional detectors need to be installed in addition to the detectors used for a standard diamond interchange control system and a traffic-responsive ramp-metering system. The additional detectors on the arterial street approaches and the freeway off-ramps serve the purpose of detecting excessive vehicle queues so that the system can respond to the traffic queues and prevent further spillback that would interfere with freeway mainline and adjacent signalized intersections.

There are two types of queue detectors on each external approach to the diamond interchange: the boundary queue detectors and the intermediate queue detectors. The boundary queue detectors set limits of allowable queue spillback at a particular location. Further queue spillback beyond these boundaries should be avoided since interference with other traffic facilities might occur, such as the adjacent traffic signals in the arterial or the freeway mainlines. Selecting these boundary detector locations should be based on analyses of site-specific characteristics. The intermediate queue detectors sense the potential queue buildup that results from the special signal operations during ICS applications, and they would serve the purpose of adjusting the phase splits to achieve balanced use of available queue storage spaces. The queue spillback/interface detectors on the frontage roads downstream of the diamond interchange signals are for the purpose of detecting ramp queue buildups and serve as interfaces between the ramp metering system and the diamond interchange system. Traffic flow data such as occupancy and volume could be measured using the queue

spillback/interface detectors, serving as the outputs from the diamond interchange and the inputs for the ramp metering.

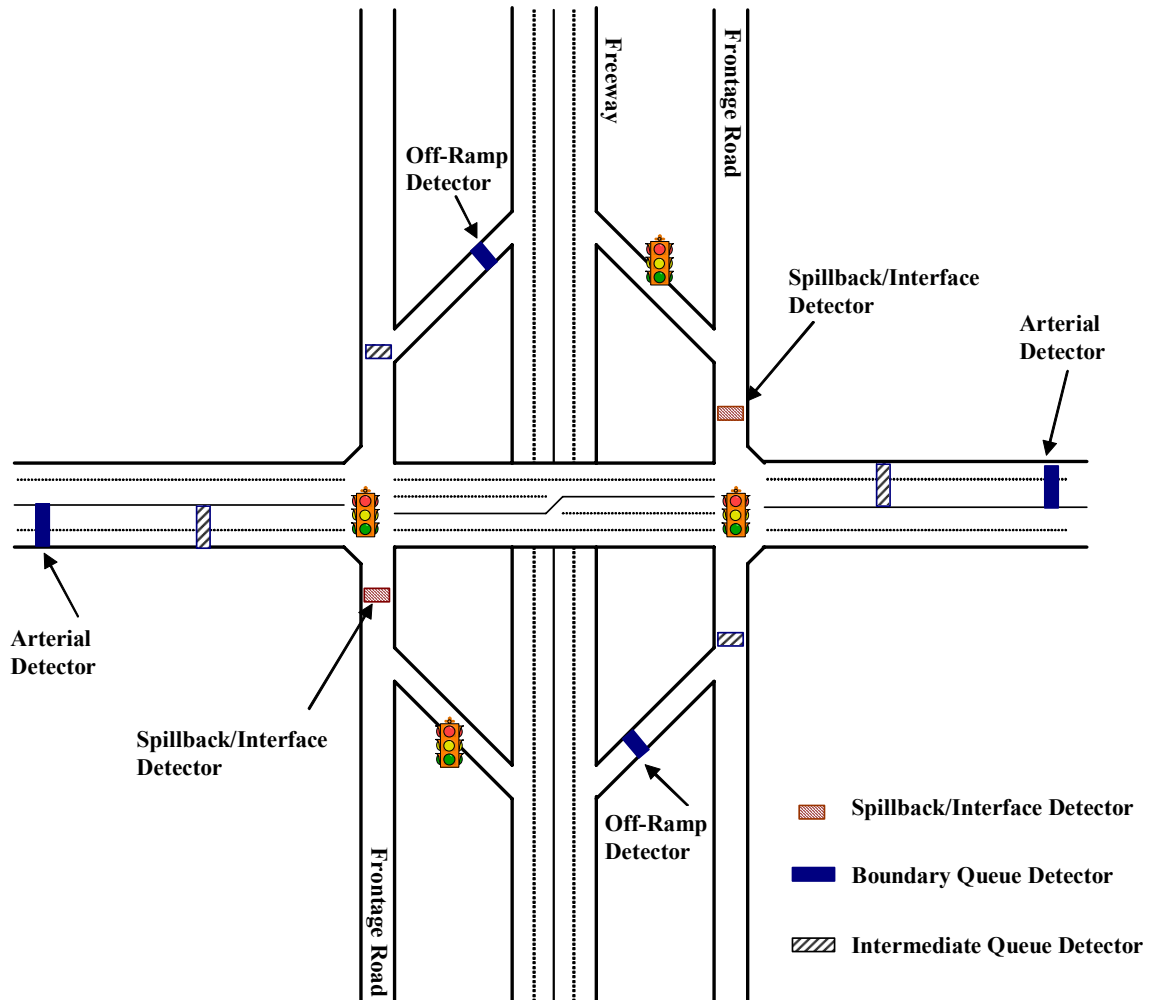


**FIGURE 87 Enhanced detection system and detector layouts.**

A brief description of the basic principles of ICS is presented next. The diamond interchange signal would remain in normal operation if none of the boundary queue detectors (i.e., arterial detectors, off-ramp detectors, and spillback detectors) detects traffic queues. However, minor phase splits may be adjusted based on the queue conditions at the intermediate queue detectors. The existence of a traffic queue is

typically determined based on a specified occupancy level from the detectors. The occupancy of a queue detector is usually sampled over specified time intervals (e.g., 20 seconds). A traffic queue is defined when the sampled occupancy exceeds a predefined threshold value (e.g., 60 percent). Whenever a ramp queue is detected by the queue spillback detector, the diamond signal quickly transitions to a particular signal phase to hold so that further vehicle entry to the ramp is controlled and queue spillback to the diamond interchange signal would be prevented. The diamond signal goes back to normal operation once the ramp queue is dissipated.

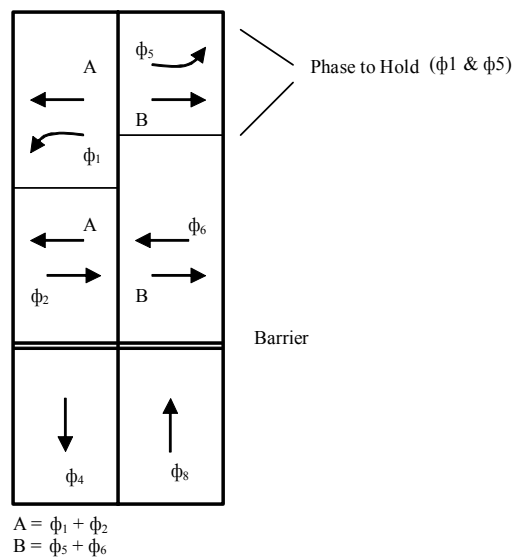
The location of the queue spillback detector should be some distance away from the diamond signal to avoid queue spillback occurring during the transition period between normal diamond signal operations and the special integrated control operations. The signal phase(s) to hold should be the one(s) that would restrict further release of vehicles from those traffic movements feeding the ramp (e.g., the through movement on the frontage road approach and the left-turn movement on the internal arterial street approach). The green splits after the phase hold may be designed to facilitate clearing excessive queues that resulted from the phase hold. The control strategies should be designed to result in the maximum usage of the available queue storage spaces on the external diamond interchange approaches. Ramp metering would remain in operation until all the queue storage spaces are filled up.

It should be pointed out that ICS do not consider switching between phasing schemes during the operations because it is uncommon to use two types of phasing schemes at the same diamond interchange location during different time periods of the day. One particular case to prevent phasing scheme switching is related to the special lane configuration for the internal movements. For example, a shared left/through lane may be used for the internal movements with the four-phase scheme. With the three-phase scheme, however, the left-turn lanes need to be exclusive lanes. Unless a dynamic lane assignment strategy is implemented, switching between three-phase and four-phase schemes may not be a viable option. The following discussions specifically address the conditions and the possible holding phases with three-phase and four-phase strategies.

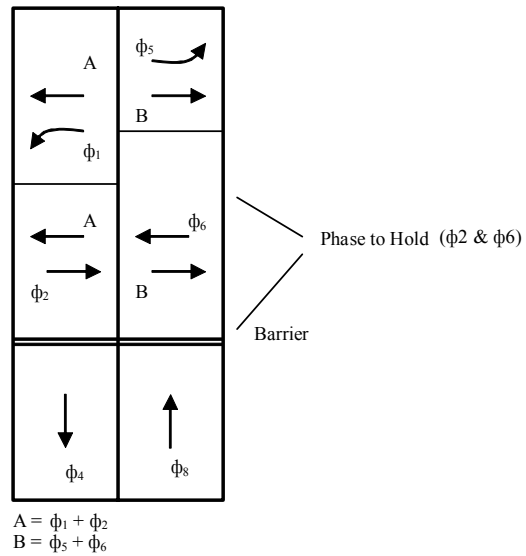


### Strategies with Three-Phase

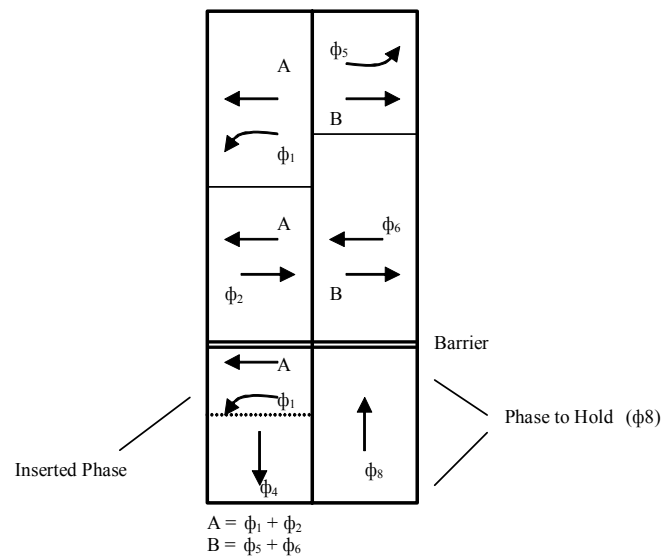
Figure 88 through Figure 90 illustrate the conditions and the proposed holding phases with three-phase operations. Figure 88 shows the holding phases being the internal left-turn phases ( $\phi_1$  and  $\phi_5$ ). By holding these phases, no further vehicle entries to the metered ramps would result (except for the uncontrolled arterial right-turn and U-turn traffic). Holding the internal left-turn phases would provide equal treatment to the two metered ramps; therefore, it would be suitable when the two ramps have similar traffic conditions. The disadvantage of holding the internal phases is that the arterial through traffic would be stopped and unnecessary delays to the traffic would occur.



**FIGURE 88 Hold internal phases with three-phase.**



**FIGURE 89 Hold arterial phases with three-phase.**



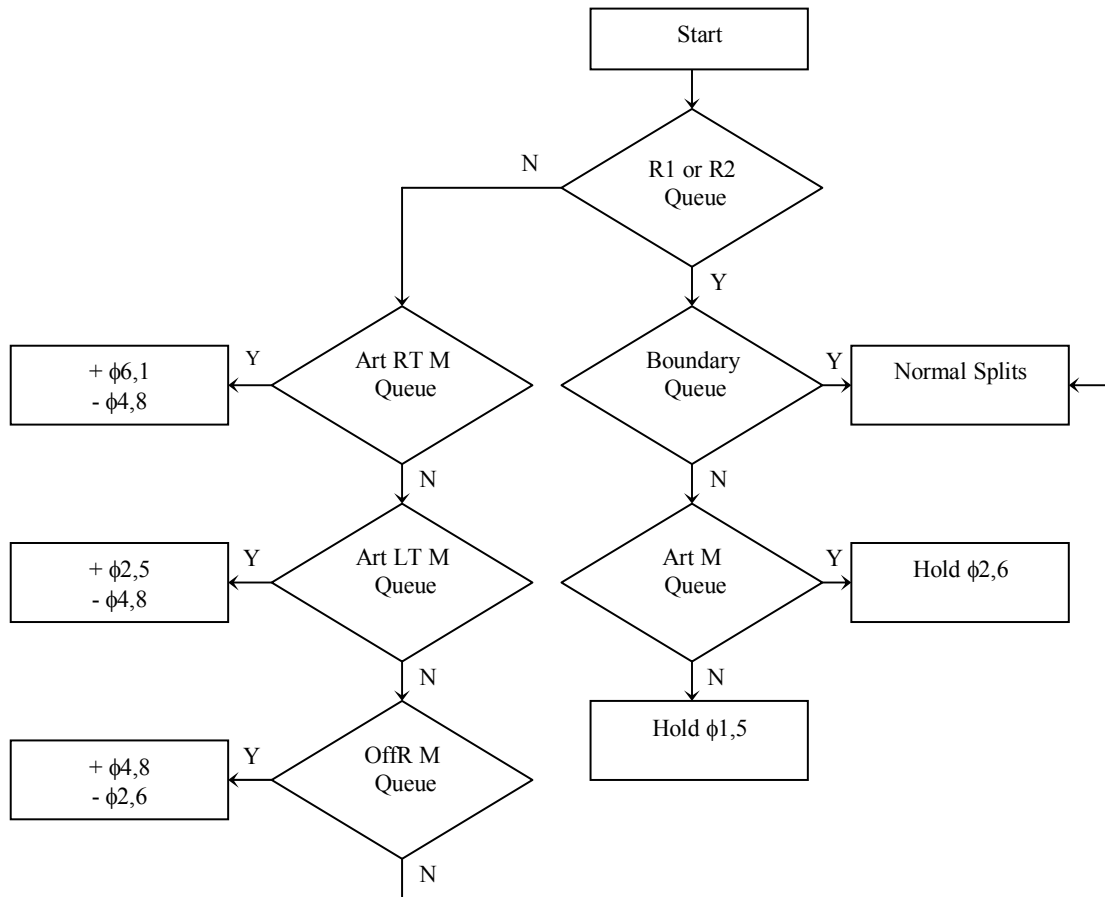
**FIGURE 90 Hold frontage road phase with three-phase and conditional service.**

Figure 89 shows the holding phases being the arterial through phases ( $\phi 2$  and  $\phi 6$ ). Although control of vehicle entry to the ramps would also be achieved by holding these phases, it has the potential of queue spillover within the internal left-turn lanes, which may cause lockup of the diamond interchange. However, the advantage of holding the arterial through phases is to allow arterial through traffic going through the interchange so that unnecessary delays to these vehicles can be avoided.

Figure 90 shows the holding phases being the frontage road phases with the diamond interchange operating with a special feature called conditional service. With conditional service, an additional arterial left-turn phase ( $\phi 1$  as shown in the figure) can be serviced while one of the frontage road phases is being serviced ( $\phi 8$  as shown in the illustrated case). The use of conditional service would result in unequal treatment to the two ramp meters. As shown in this case, holding the frontage road phase ( $\phi 8$ ) would restrict vehicle entries to the left-side ramp meter (*RI*).

The control algorithm for the diamond interchange signal that incorporates the above phase-holding strategies under the three-phase scheme is shown in Figure 91. The signal control logic illustrated in Figure 91 is described as follows. When there are no queues detected by the spillback queue detectors, the signal phases either receive the normal splits or the adjusted splits, depending on the intermediate queue detector information. For example, if the intermediate queue detector on the right-side arterial approach detects a queue, the phase splits for  $\phi 6$  and  $\phi 1$  need to be increased, while the phase splits for  $\phi 4$  and  $\phi 8$  need to be reduced. If none of the intermediate queue detectors detect a queue, the diamond signal will have the normal splits. The phases would also receive normal splits whenever the boundary queue detectors detect a queue, when the ramp-metering operations are suspended. When queues are detected on either metered ramps, the diamond signal would hold particular phases, either  $\phi 1$  and  $\phi 5$  or  $\phi 2$  and  $\phi 6$ , depending on the intermediate queue conditions on the arterial street. For example, if queues are detected by the intermediate queue detectors on the arterial

approaches, the diamond controller would hold  $\phi_2$  and  $\phi_6$ . Otherwise, the controller would hold  $\phi_1$  and  $\phi_5$ .



Note: R – On-Ramp; OffR – Off-Ramp; Art – Arterial; RT – Right Side; LT – Left Side; M – Intermediate  
+  $\phi$  – Increase Phase Split; -  $\phi$  – Reduce Phase Split (See Figure 3 for reference)

**FIGURE 91 ICS logic and flow chart with three-phase operation.**

The current algorithm does not incorporate operations with conditional service. The control algorithm was coded in VAP, which is used in VISSIM for evaluating the ICS. The complete VAP code for the algorithm is given in Appendix B.

### Strategies with Four-Phase

Figure 92 and Figure 93 show the conditions and the proposed holding phases when the diamond signals operate with four-phase. These figures illustrate the holding phases, either the right-side frontage road phase ( $\phi_8$ ) or the arterial through phase ( $\phi_2$ ) to control vehicle entry to the left-side ramp ( $R1$ ). Similarly,  $\phi_4$  and  $\phi_6$  are the holding phases if vehicle entry to the right-side ramp ( $R2$ ) needs to be controlled. The strategies illustrated in Figure 92 and Figure 93 would only achieve controlling vehicle entry to one of the ramps at a time. Under special circumstances, the holding phases can be the internal left-turn phases ( $\phi_1$  and  $\phi_5$ ) if vehicle entry to both ramps needs to be controlled. This is achieved through the use of dummy phases for the internal movements to cross the controller barriers under four-phase operation. For example, the Eagle EPAC300 controller defines a dummy  $\phi_9$  for the left-side internal movement phase, which is on the same side of the barrier as the arterial phase ( $\phi_2$ ) and the frontage road phase ( $\phi_4$ ).

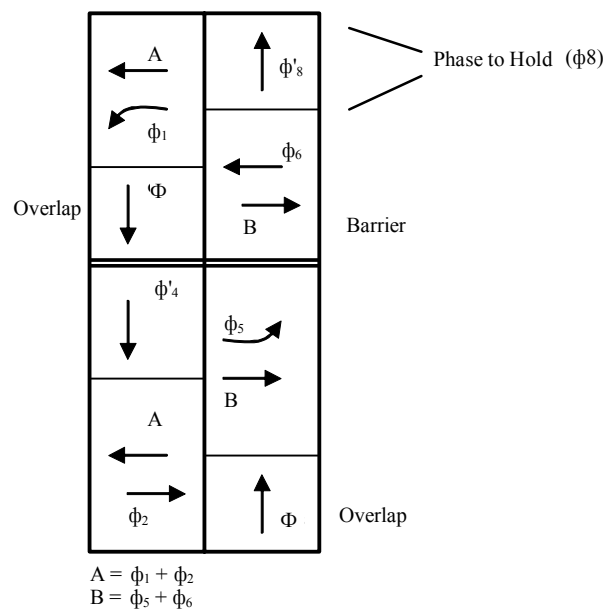


**FIGURE 92 Hold  $\phi_8$  to control left-side ramp entry with four-phase.**

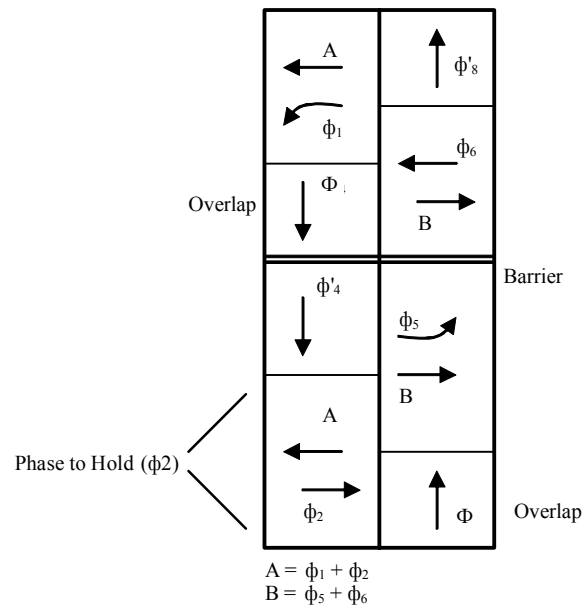
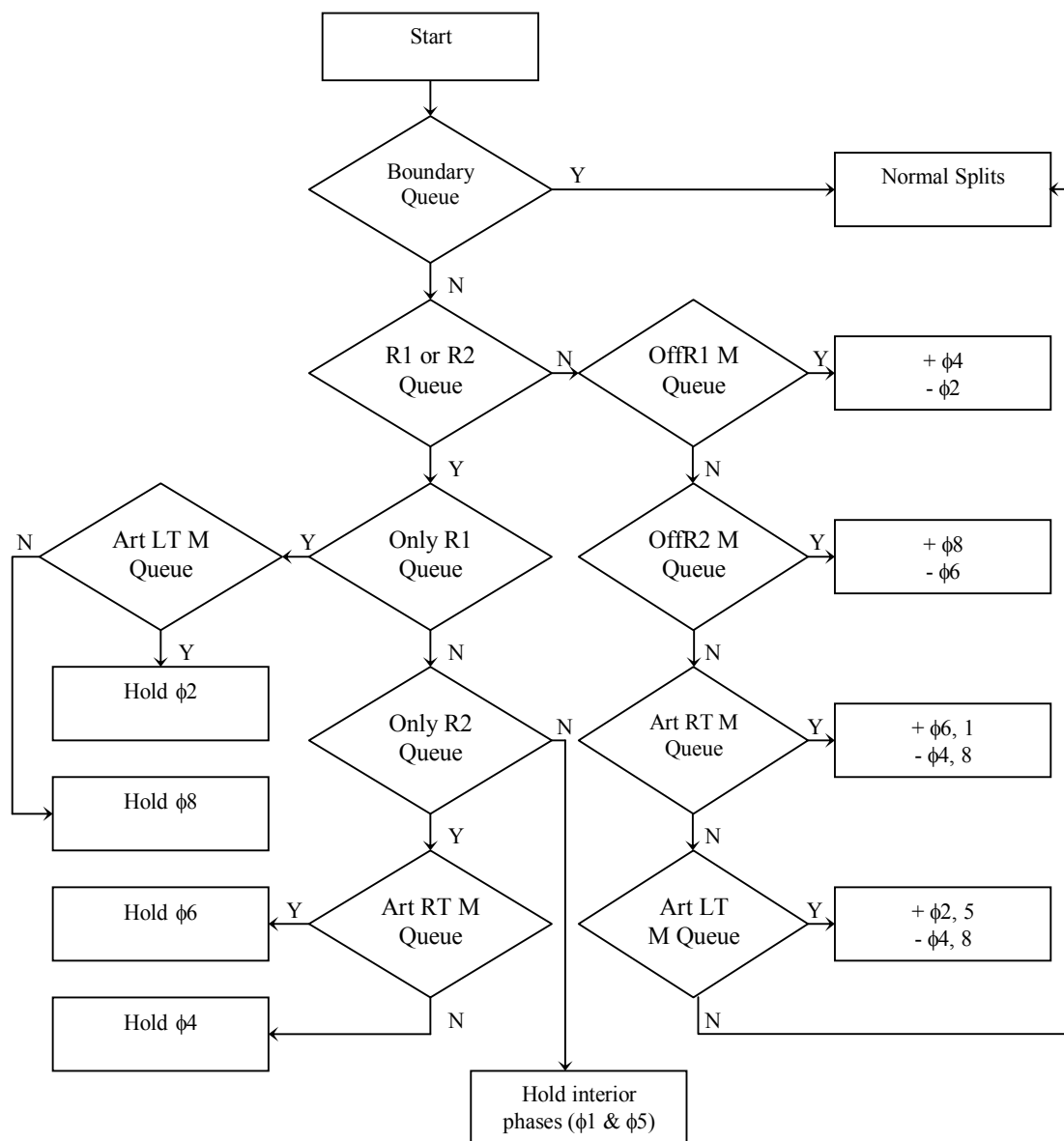


**FIGURE 93 Hold  $\phi_2$  to control left-side ramp entry with four-phase.**

Similarly, the control algorithm incorporating these phase-holding strategies under four-phase operation is depicted in Figure 94.

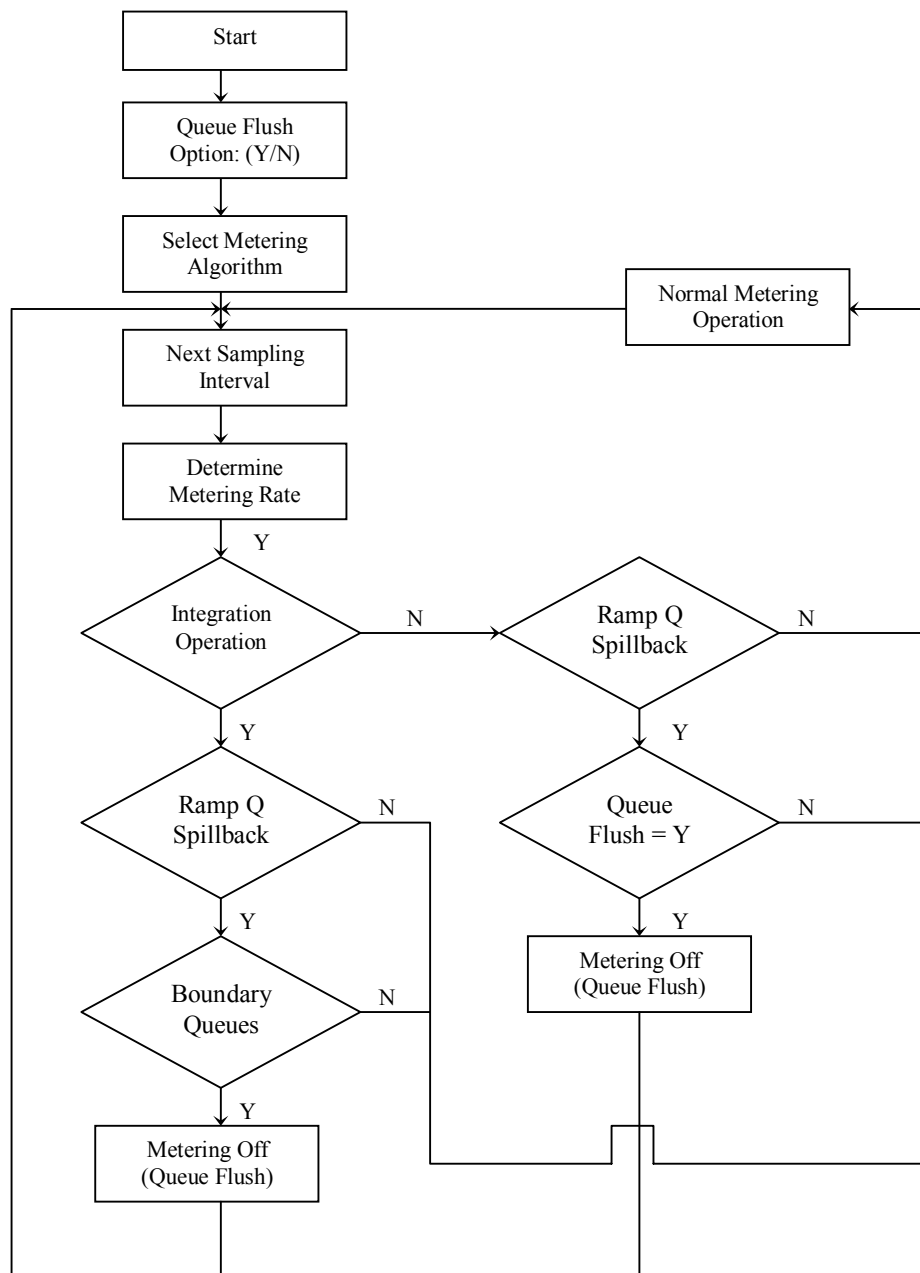
### **ICS's Ramp-Metering Component**

Figure 95 illustrates the component concerning the ramp-metering operations in ICS. Under the integrated operations, ramp-metering queue flush would occur only when a traffic queue exceeds one of the boundary detector locations.



Note: R – On-Ramp; OffR – Off-Ramp; Art – Arterial; RT – Right Side; LT – Left Side;  
 M – Intermediate; + φ – Increase Phase Split; - φ – Reduce Phase Split (See Figure 3 for reference)

**FIGURE 94 ICS logic and flow chart with four-phase operation.**



**FIGURE 95 Ramp-metering component in ICS.**

### **Other Considerations for IDIRMS Components**

The IDIRMS and its operations addressed in this research are considered first steps to explore a truly high level intelligent IDIRMS. Besides the vehicle detection system depicted in Figure 87, the IDIRMS would require additional communication and



traveler information systems. Dynamic message signs and advanced warning signs might be essential equipment for conveying necessary information to roadway users. Under integrated operation, the surface street vehicles will likely experience longer queues and delays due to implementation of phase holding in ICS. They would also likely experience unusual signal timing due to phase holding. Drivers should be informed of such timing changes to minimize their confusion and frustration. Examples of dynamic warning signs may include “Do not block intersection,” “Signal in special transition,” etc. The communication system should enable uninterrupted data exchange between the surface street signal system (diamond interchange signal), and the freeway and ramp-metering system. NTCIP-compliant (103) devices for field implementation are then critical to ensure data exchangeability between the two systems. With the advance of detection, communication, and information technologies, more accurate traffic flow data could be obtained and applied in real time to improve system performance, which would require development of more sophisticated control algorithms.

### **EVALUATION OF ICS UNDER RECURRING CONGESTION**

The ICS discussed earlier in this chapter for ramp queue spillback control under recurring congestion were evaluated using the VISSIM simulation model under three generally defined traffic demand scenarios as characterized by the ramp conditions: low, medium, and high. These general traffic demand scenarios are qualitatively described in Table 13.

Instead of using a fixed metering rate, the ALINEA traffic-responsive ramp-metering algorithm was coded in VISSIM using VAP; therefore, the ramp-metering capacities that were used to calculate the  $v/c$  ratios were only estimates based on the ALINEA algorithm. The following discussions describe the process of estimating the ramp-metering capacities based on ALINEA.

**TABLE 13 Traffic demand scenarios for ICS evaluation**

Demand Scenarios	Traffic Conditions	
	<i>R1</i> (Peak Direction)	<i>R2</i> (Off-Peak Direction)
Case I: Low	Demand is less than capacity but does experiences short-term over-capacity (e.g., several cycles).	Demand is less than capacity with no experience of short-term over-capacity.
Case II: Medium	Demand is slightly over the ramp's capacity and experiences relatively longer periods of over-capacity.	Demand is less than the ramp's capacity and may experience short-term over-capacity.
Case III: High	Demand exceeds capacity by a significant margin and the ramp experiences over-capacity during most of the analysis period.	Demand is near or above capacity and the ramp experiences a longer period of over-capacity.

The system operations were evaluated using VISSIM under the traffic demand scenarios described above for the cases with and without ICS. The same Mayfield/SH 360 interchange network was used but with modified traffic demands to reflect the three demand scenarios as described in Table 13. Table 14 describes the experimental design matrix, including a total of 16 traffic scenarios and simulation cases. Two sub-cases were included in the high demand scenario, with *case III-B* reflecting a more highly over-saturated condition for *R2* than that in *case III-A*. Table 15 provides more specific information about each scenario in terms of the  $v/c$  ratios and the percentage of cycles that demand exceeding metering capacity. It should be noted that over-capacity during a particular cycle does not necessarily result in queue spilling back to the diamond interchange, because the queue storage space between the ramp meter and the diamond interchange provides buffers to temporarily hold the vehicle queues. Detailed traffic volumes for the three demand scenarios are included in Appendix C.

**TABLE 14 Naming scheme of traffic scenarios and experimental runs**

Traffic Demands	Three-Phase		Four-Phase	
	<i>Without ICS</i>	<i>With ICS</i>	<i>Without ICS</i>	<i>With ICS</i>
<i>Low</i>	3PNL	3PYL	4PNL	4PYL
<i>Medium</i>	3PNM	3PYM	4PNM	4PYM
<i>High – A</i>	3PNHA	3PYHA	4PNHA	4PYHA
<i>High – B</i>	3PNHB	3PYHB	4PNHB	4PYHB

Note: *xP*-Diamond phasing; *N*-Without ICS; *Y*-With ICS; *L*-Low demand; *M*-Medium demand; *HA*-High demand, case A; *HB*-High demand, case B.

**TABLE 15 Quantitative description of the traffic demand scenarios**

Demand Scenarios	Ramp Conditions			
	<i>v/c</i> Ratio		% Cycles Demand Exceeding Capacity	
	<i>R1</i>	<i>R2</i>	<i>R1</i>	<i>R2</i>
Case I: Low	0.88	0.54	20	3
Case II: Medium	1.01	0.60	65	10
Case III: High	1.06	A: 0.63 B: 1.03	90	A: 20 B: 80

During the VISSIM simulation, the queue flush option was turned off so that the ramp-metering rate during each interval given by ALINEA would best represent the actual ramp capacity based on the freeway mainline conditions. The ramp-metering rates given by ALINEA during the entire course of simulation were recorded. *Cases II* and *III* (medium and high demand scenarios) have the same freeway mainline demands; therefore, the ramp-metering capacities for the two cases could be assumed to be the same. Simulation runs were conducted for *cases I* and *II* (low and medium demand

scenarios) with ten duplicate runs for each case. The ramp-metering capacity was then determined based on the average results from the 10 runs for each case. For example, for the low demand scenario, the ramp-metering capacity for *R1* was estimated at 828 vph with the standard deviation of 19 vph, and the capacity for *R2* was estimated at 878 with a standard deviation of 6 vph. For the medium and high demand scenarios, the metering capacity for *R1* was estimated at 753 vph with a standard deviation of 18 vph, while the metering capacity for *R2* was estimated at 832 vph with a standard deviation of 24 vph. For the high demand scenario of *case III-B*, the maximum metering rate in ALINEA for *R2* was modified from 900 vph to 515 vph, resulting in an estimated ramp-metering capacity of 510 vph, where the ramp meter basically operated at the highest rate most of the time during simulation due to the low freeway mainline demand for the off-peak direction. The modification of the metering rate resulted in *R2* being oversaturated, and more frequent queue spillback and queue flush occurred when ICS were not applied.

Each simulation run lasted 12,000 seconds; however, the system performance measures were only reported between 600 seconds and 12,000 seconds in simulation. The initial 600 seconds were considered a system warm-up time. At 10,600 seconds into simulation, no further vehicle entry to the network was coded; therefore, the time after 10,600 was to clear the remaining traffic in the network. Again, ten multiple simulation runs were conducted using different random seeds with each traffic demand scenario. Three major performance measures were used for the evaluation, including vehicle delays, the percent time that the ramp meter was in queue flush mode, and the ramp-meter queue flush rate defined by the number of queue flushes per hour. The performance measures of queue flush time and queue flush rate have been used in practice to indicate the quality of ramp-metering operations (32). Ramp queue flush is perhaps one of the primary causes of freeway breakdown; therefore, the performance measures related to queue flush may be good indicators for evaluating the effectiveness of ICS.

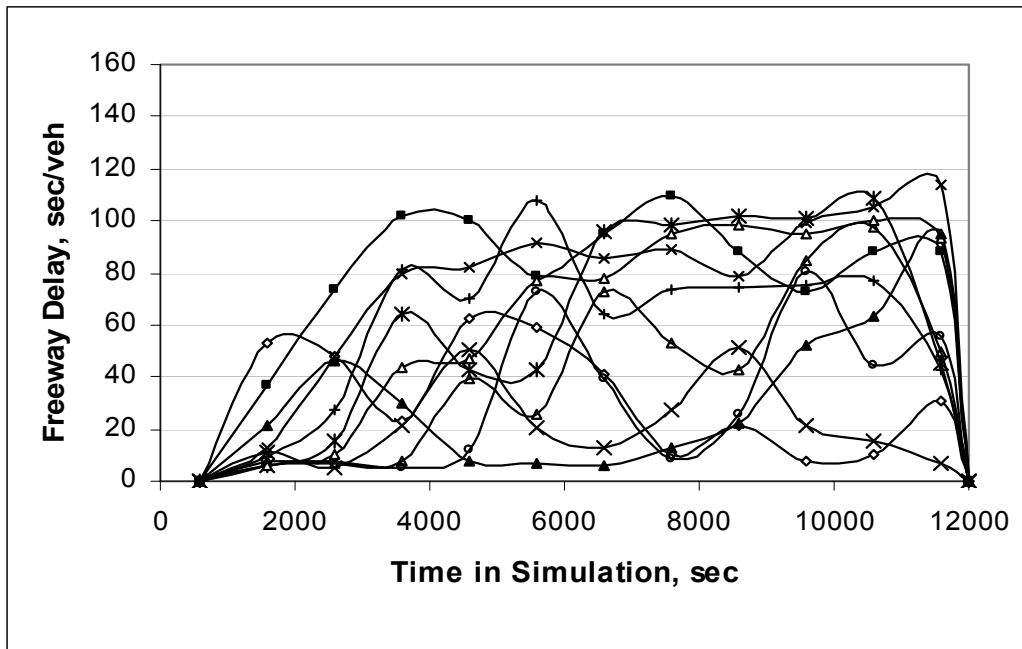
### **Freeway Mainline Delays and Variations**

Because the major purpose of implementing ICS is to minimize ramp queue flush and therefore to prevent freeway breakdown, it is expected that the significant savings in freeway mainline delays would offset the delay increases on the surface street traffic. As discussed in Chapter II, the freeway has unique operating characteristics. When the freeway operates in free-flow conditions (i.e., without breakdown), only minimal delays occur. Delays increase significantly once the freeway breaks down.

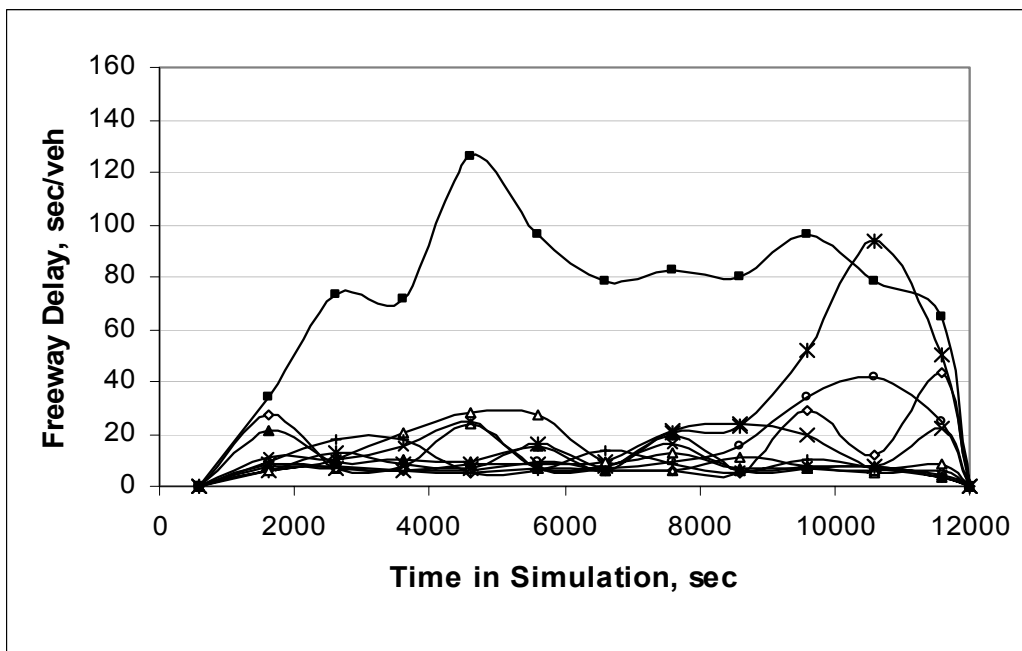
Figure 96 and Figure 97 demonstrate that freeway mainline delays can vary significantly between simulation runs due to the stochastic nature of traffic flow and the freeway operating characteristics. In Figure 96, the delays on the freeway mainline (the northbound peak direction) during simulation are plotted for each of the 10 runs for the case of the medium demand scenario and three-phase operation.

It can be seen that the freeway experienced more severe breakdowns and higher delays without ICS. However, significant variations in when breakdown occurred and how severe the breakdown was as indicated by the delay values can be observed between each simulation run. Similarly, Figure 97 shows the results for the high demand scenario. As can be seen from both figures, for the medium demand scenario, freeway breakdown was prevented in most of the simulation runs except for one case with ICS. As for the high demand scenario, although ICS still showed effectiveness in delaying the onset of breakdown, breakdown could not be completely avoided.

It is noted that in Figure 96 and Figure 97, as well as in other figures to be presented next, the freeway traffic delay started and ended with zeros. This is due to the system warm-up period and clearance period. The system clearance period is to allow the remaining traffic in the system to clear; therefore, the areas under the curves would reflect the total delays experienced by all the traffic entering the system.

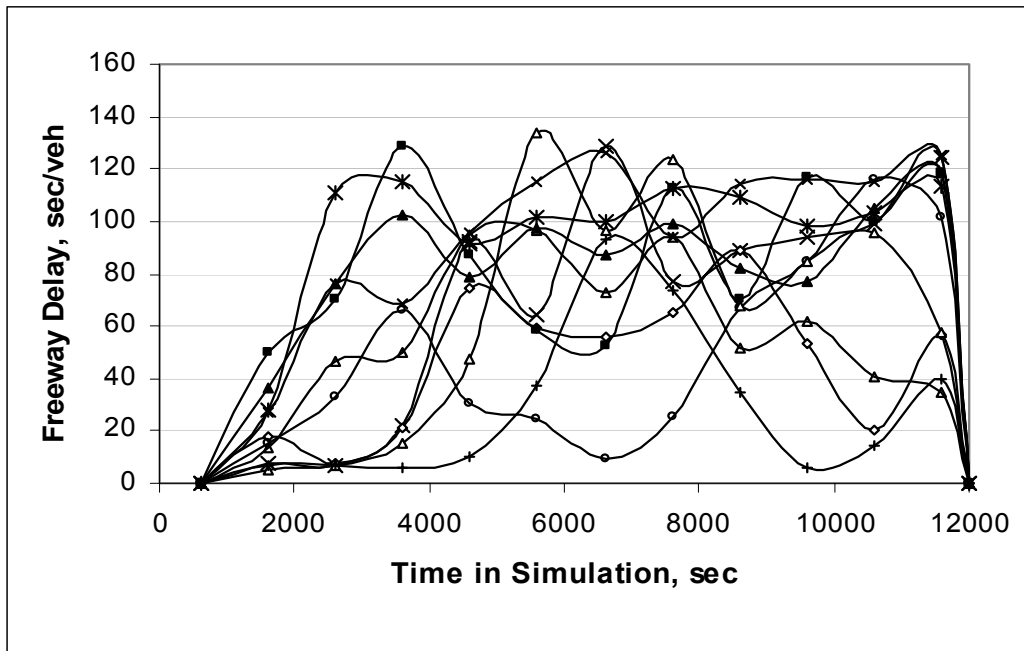


(a) Without ICS

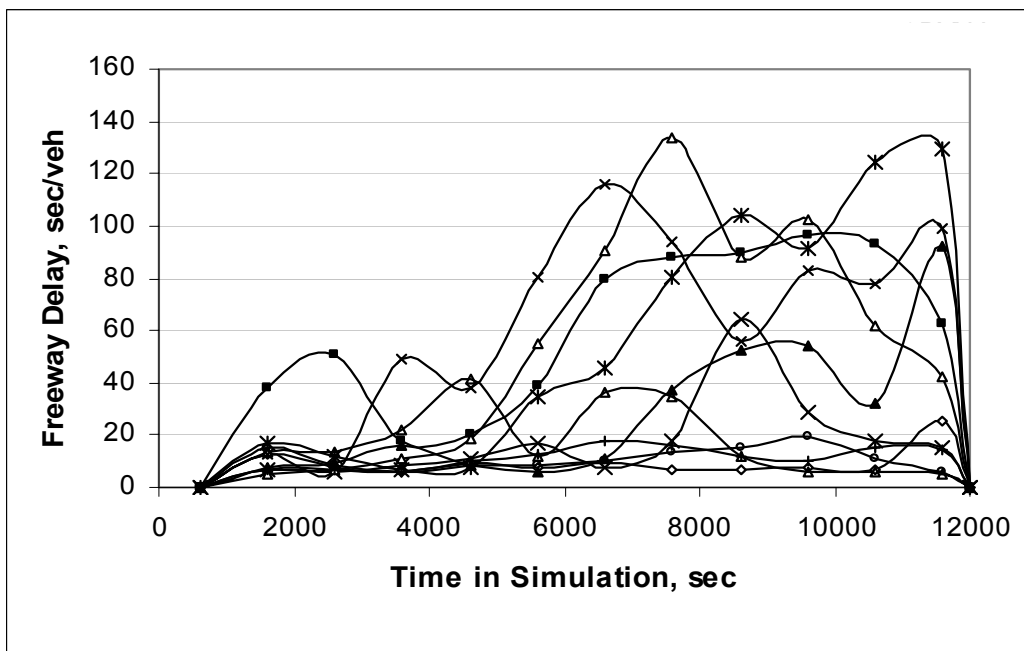


(b) With ICS

**FIGURE 96 Freeway mainline delays and variations: medium demand.**



(a) Without ICS



(b) With ICS

**FIGURE 97 Freeway mainline delays and variations: high demand.**

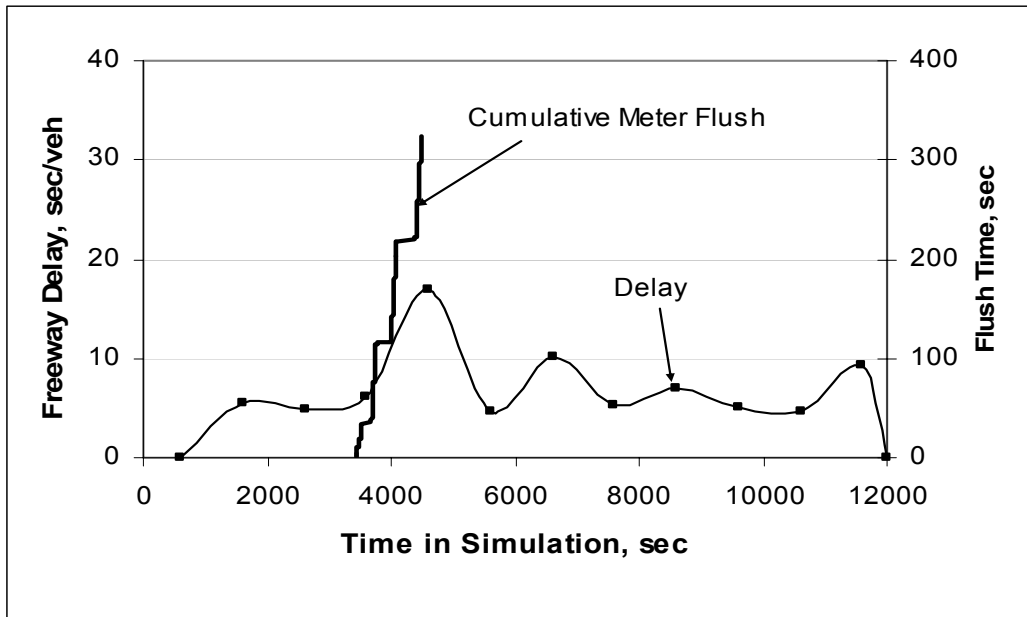
## Ramp Performance

The effectiveness of ICS was evaluated from the perspective of ramp-metering performance. More specifically, the two performance measures of percent queue flush time and queue flush rate were compared.

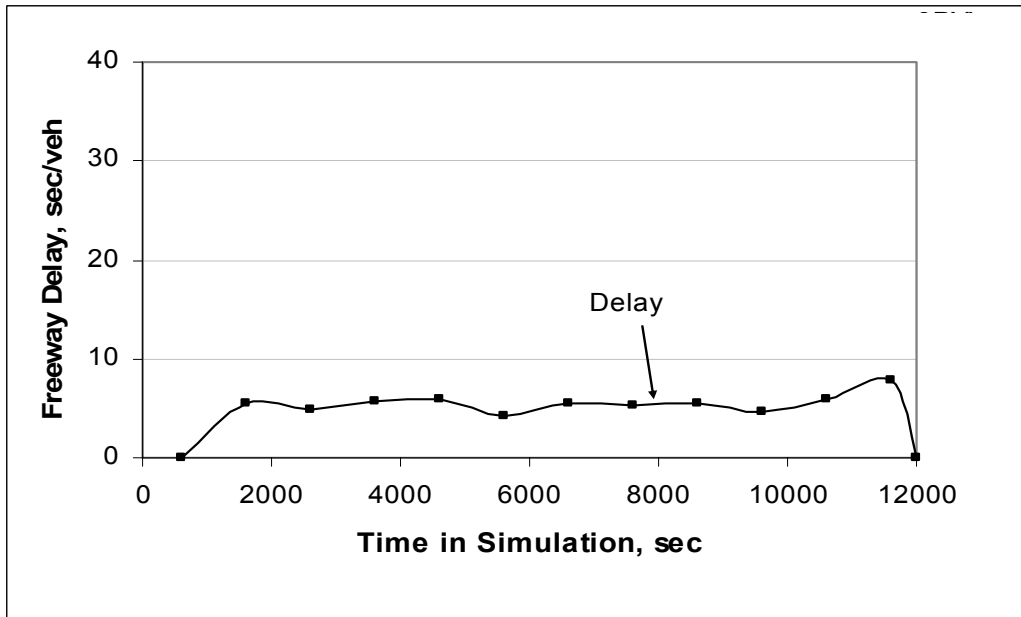
It is believed that frequent ramp queue flush increases the likelihood of freeway breakdown. Figure 98 through Figure 100 illustrate the relationship between freeway mainline delays and ramp-meter queue flush based on the VISSIM simulations for the three traffic demand scenarios. The curve for queue flush is represented in the form of cumulative queue flush time, where the horizontal segment indicates the period when the ramp meter was in normal operation without queue flush. Each figure includes two parts: (a) the delay profiles without ICS and (b) the profiles with ICS. The two cases in *a* and *b* were based on identical random seeds; therefore, they had identical traffic demand profiles in both cases.

As can be seen, the freeway mainline breakdown as indicated by the significant increase in the delays directly corresponds to the queue flush operation. In each of the traffic demand scenarios, the onset of queue flush, the total queue flush time, and the number of queue flushes (represented by the number of horizontal segments in the cumulative queue flush curve) were all improved with ICS. For example, ICS did not result in any queue flush under the low demand scenario. Under the medium demand and high demand scenarios, the onset of queue flush was delayed by a significant margin; therefore, the onset of freeway breakdown was also delayed. Another interesting observation is that the freeway delay was capped at approximately 120 sec/veh once breakdown occurred and persisted, suggesting that keeping ramp metering in operation may no longer be effective in reducing freeway delays.



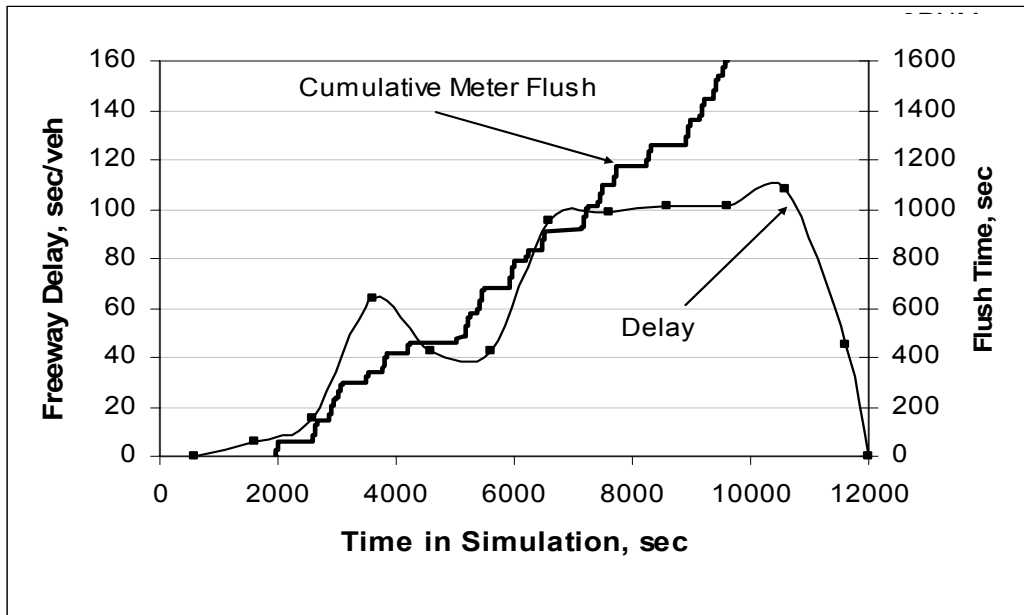


(a) Without ICS

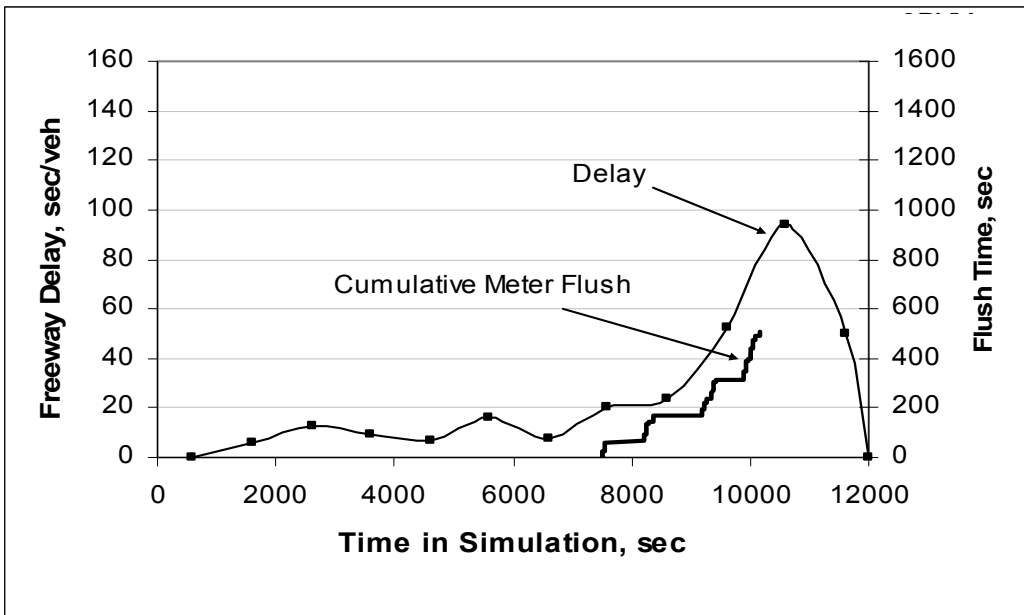


(b) With ICS

**FIGURE 98 Relationship between freeway breakdown and queue flush: low demand.**

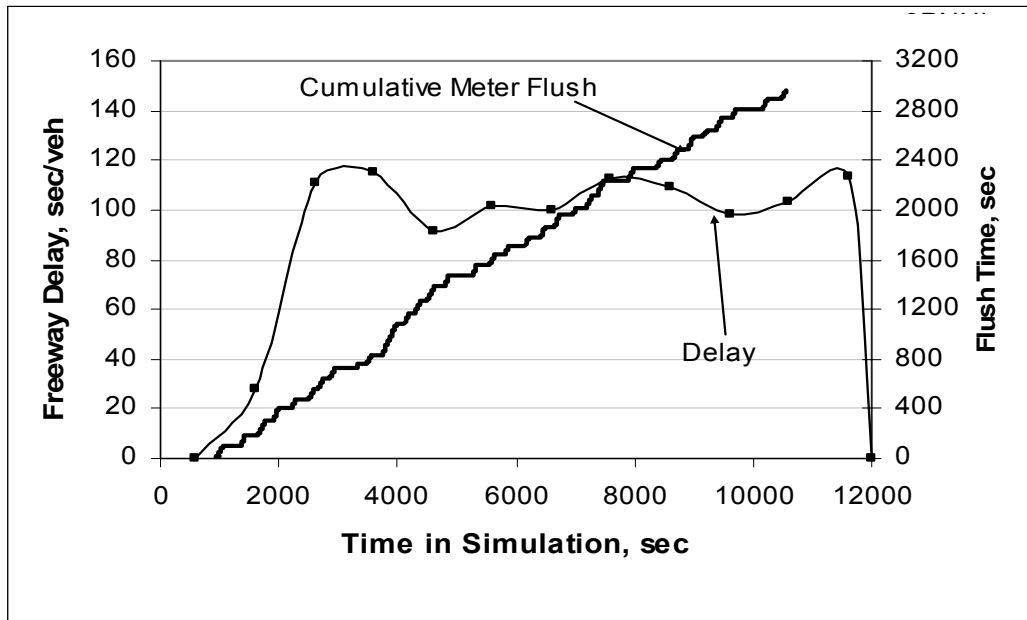


(a) Without ICS

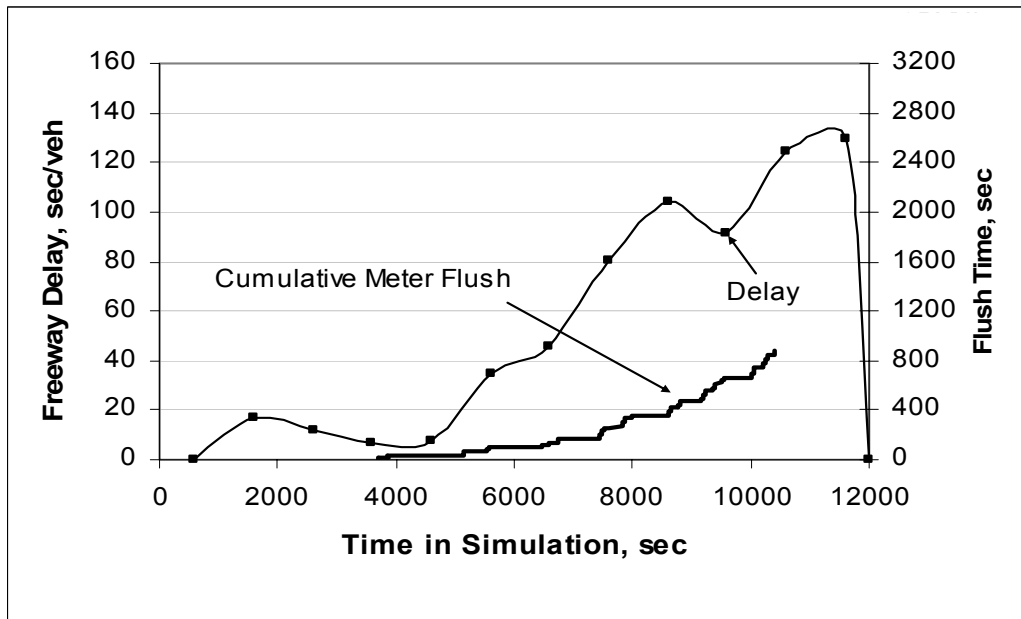


(b) With ICS

**FIGURE 99 Relationship between freeway breakdown and queue flush: medium demand.**



(a) With ICS

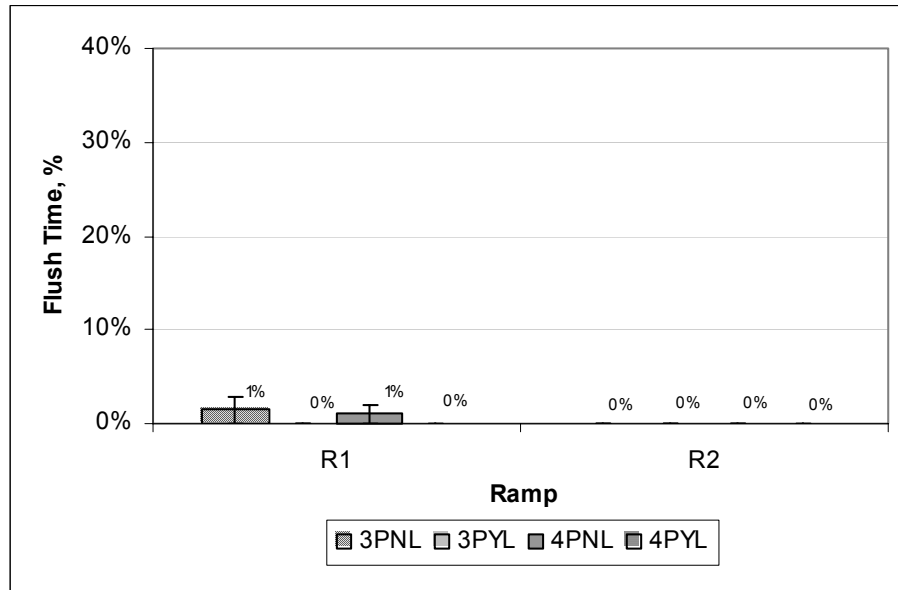


(b) Without ICS

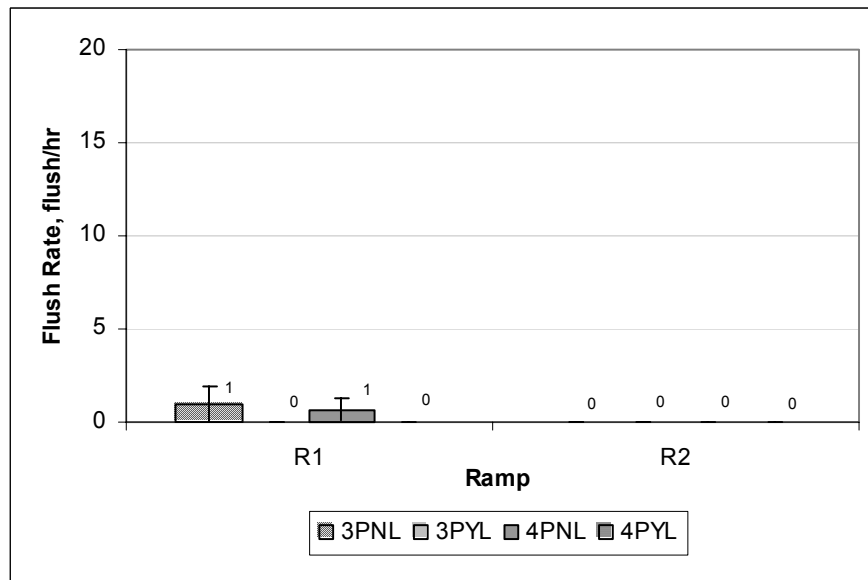
**FIGURE 100 Relationship between freeway breakdown and queue flush: high demand.**

Figure 101 and Figure 102 compare the percent queue flush time and queue flush rate under the low demand scenario. Table 16 provides detailed statistical test

results on the two performance measures expressed in the gross queue flush time and number of queue flushes. Again, it is noted that no transition period was specifically modeled between queue flushes.



**FIGURE 101 Percent queue flush time: low demand.**



**FIGURE 102 Queue flush rate: low demand.**

**TABLE 16 t-statistical tests comparing ramp performances: low demand.**

Ramp	Performance Measures	Three-Phase					
		Without ICS		With ICS		t-statistic	Reject Null Hypothesis?
		Mean	S.D.	Mean	S.D.		
R1	Flush Time, sec	143.8	149.2	0.0	0.0	3.05	Y
	No. Flushes	2.6	2.8	0.0	0.0	2.85	Y
R2	Flush Time, sec	0.0	0.0	0.0	0.0	NA	NA
	No. Flushes	0.0	0.0	0.0	0.0	NA	NA
Four-Phase							
R1	Flush Time, sec	102.7	97.0	0.0	0.0	3.35	Y
	No. Flushes	1.9	1.7	0.0	0.0	3.61	Y
R2	Flush Time, sec	0.0	0.0	0.0	0.0	NA	NA
	No. Flushes	0.0	0.0	0.0	0.0	NA	NA

Note: (1) Null Hypothesis: Means are equal; (2) Rejection Region:  $t_{0,025,18} = 2.101$

The results in Figure 101, Figure 102, and Table 16 indicate that queue flush occurred rarely on both ramps under the low demand scenario even without ICS. ICS completely eliminated queue flushes in each of the 10 simulation runs. The statistical results indicate that the performance measures with ICS are statistically different from those without ICS.

Similarly, the ramp performance measures and statistical testing results for the medium demand scenario are shown in Figure 103, Figure 104, and Table 17. The results indicate that both the queue flush time and the number of queue flushes were significantly lower with ICS for *R1*. *R2* remained under-saturated with queue flush occurring in only 1 out the 10 simulation runs.

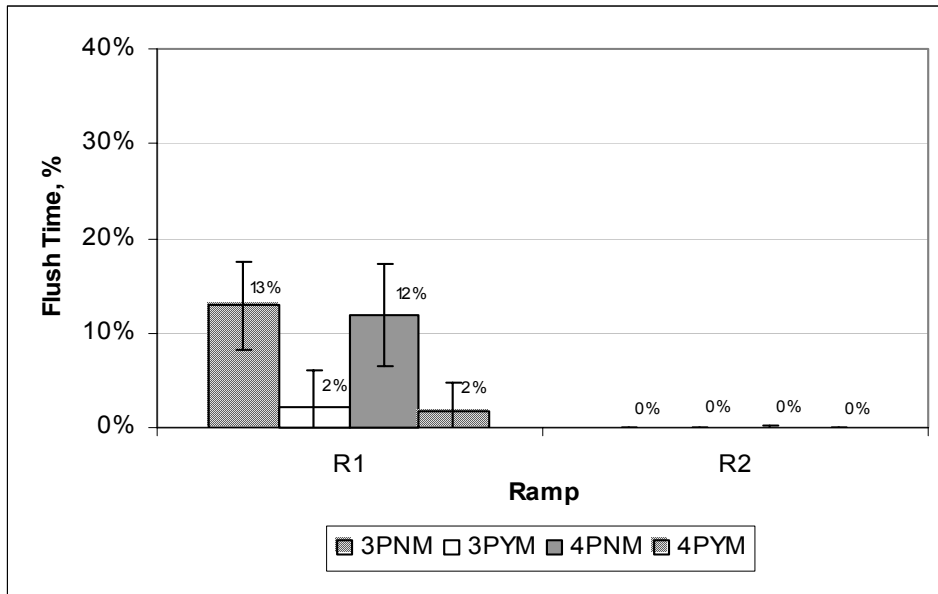


**FIGURE 103 Percent queue flush time: medium demand.**

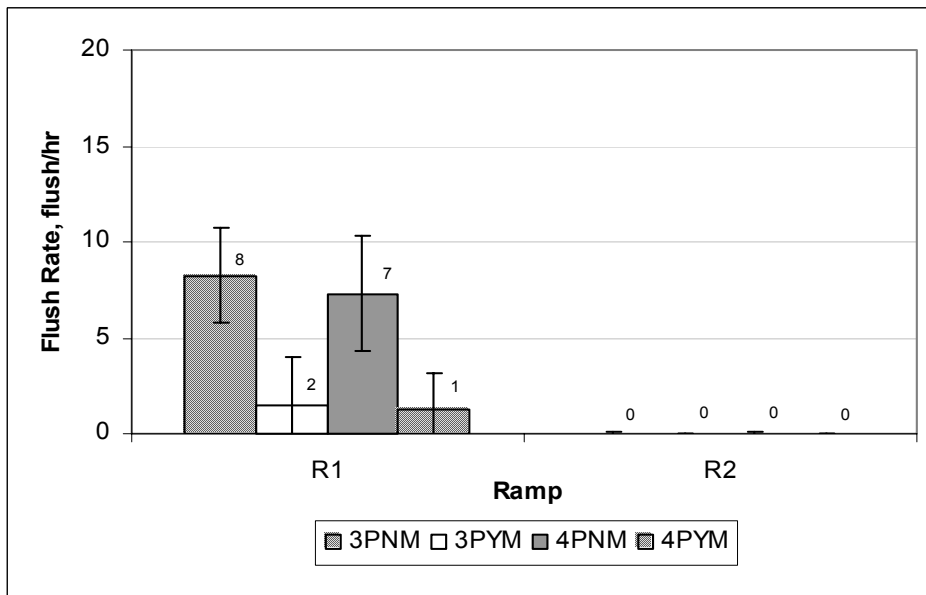


**FIGURE 104 Queue flush rate: medium demand.**

**TABLE 17 t-statistical tests comparing ramp performances: medium demand**

Ramp	Performance Measures	Three-Phase					
		Without ICS		With ICS		t-statistic	Reject Null Hypothesis?
		Mean	S.D.	Mean	S.D.		
R1	Flush Time, sec	1292.7	469.5	213.5	399.0	5.54	Y
	No. Flushes	22.9	6.9	4.2	6.8	6.11	Y
R2	Flush Time, sec	2.0	6.3	0.0	0.0	1.00	N
	No. Flushes	0.1	0.3	0.0	0.0	1.00	N
Four-Phase							
R1	Flush Time, sec	1184.1	535.0	183.5	300.2	5.16	Y
	No. Flushes	20.3	8.3	3.4	5.4	5.40	Y
R2	Flush Time, sec	6.2	19.6	0.0	0.0	1.00	N
	No. Flushes	0.1	0.3	0.0	0.0	1.00	N

Note: (1) Null Hypothesis: Means are equal; (2) Rejection Region:  $t_{0,025,18} = 2.101$

The ramp performance measures and statistical testing results for the high demand scenario (case A) are shown in Figure 105, Figure 106, and Table 18. Again, the results indicate that both the queue flush time and the number of queue flushes were significantly lower with ICS for *R1*. *R2* basically still remained under-saturated although the queue flush time increased slightly.

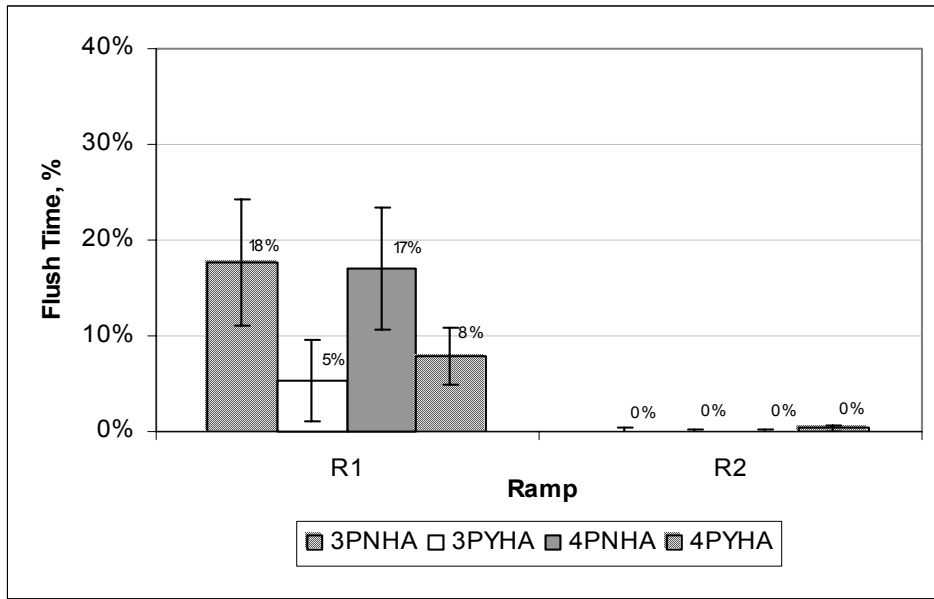


**FIGURE 105 Percent queue flush time: high demand (case A).**

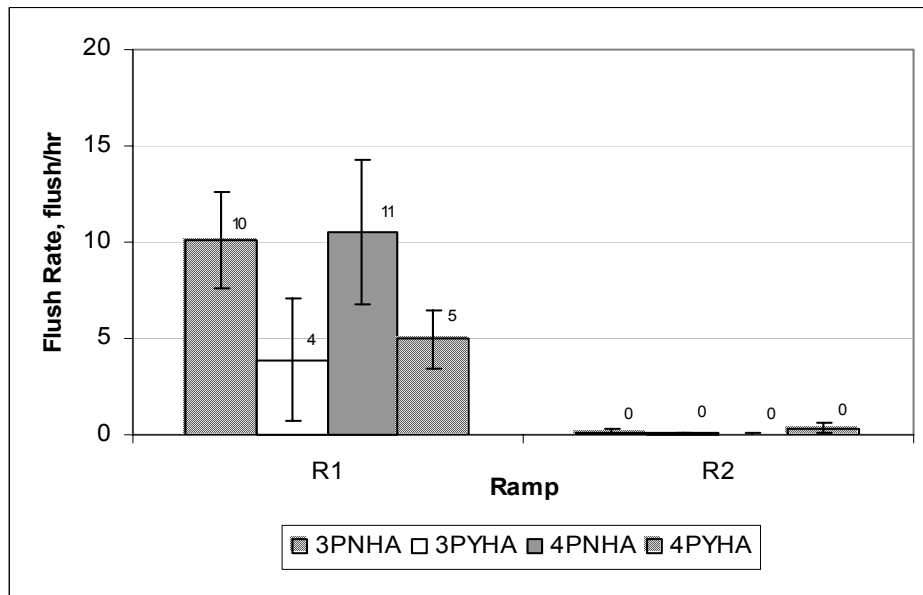


**FIGURE 106 Queue flush rate: high demand (case A).**



**TABLE 18 t-statistical tests comparing ramp performance:  
high demand (case A)**

Ramp	Performance Measures	Three-Phase					
		Without ICS		With ICS		t-statistic	Reject Null Hypothesis?
		Mean	S.D.	Mean	S.D.		
R1	Flush Time, sec	1773.8	659.7	528.8	423.0	5.02	Y
	No. Flushes	28.0	6.9	10.8	8.8	4.86	Y
R2	Flush Time, sec	10.1	31.9	7.6	19.3	0.21	N
	No. Flushes	0.2	0.6	0.2	0.4	0.00	N
Four-Phase							
R1	Flush Time, sec	1702.9	644.1	790.3	295.1	4.07	Y
	No. Flushes	29.2	10.4	13.8	4.2	4.36	Y
R2	Flush Time, sec	7.6	24.0	33.8	26.7	-2.31	Y
	No. Flushes	0.1	0.3	1.0	0.7	-3.86	Y

Note: (1) Null Hypothesis: Means are equal; (2) Rejection Region:  $t_{0.025,18} = 2.101$

The ramp performance measures and statistical testing results for the high demand scenario (case B) are shown in Figure 107, Figure 108, and Table 19. In this case, the maximum ramp-metering rate for R2 was changed from 900 vph to 515 vph, resulting in an over-saturated condition for R2. While similar results were shown for R1 where both the queue flush time and the number of queue flushes were significantly lower with ICS, there were basically no differences for R2 with and without ICS.

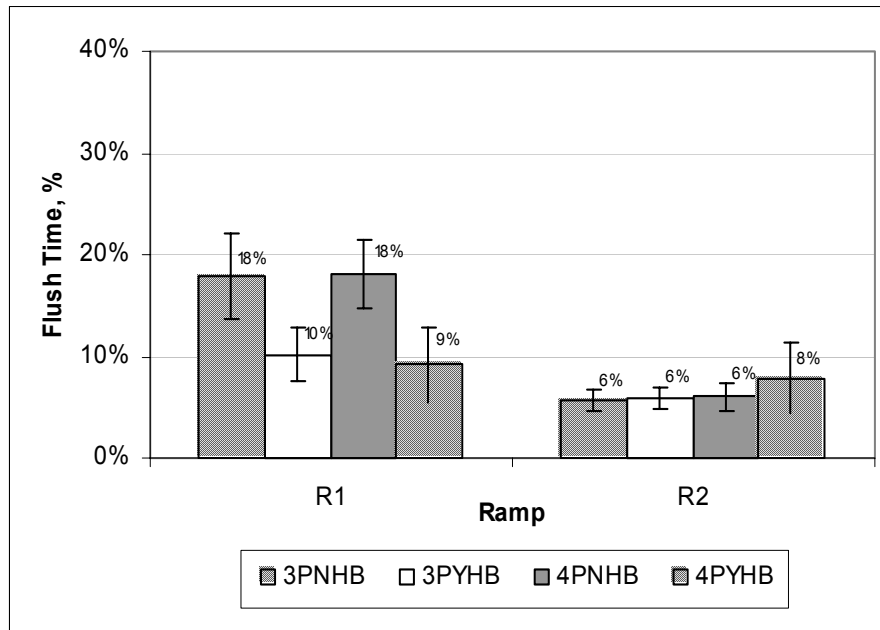


**FIGURE 107 Percent queue flush time: high demand (case B).**

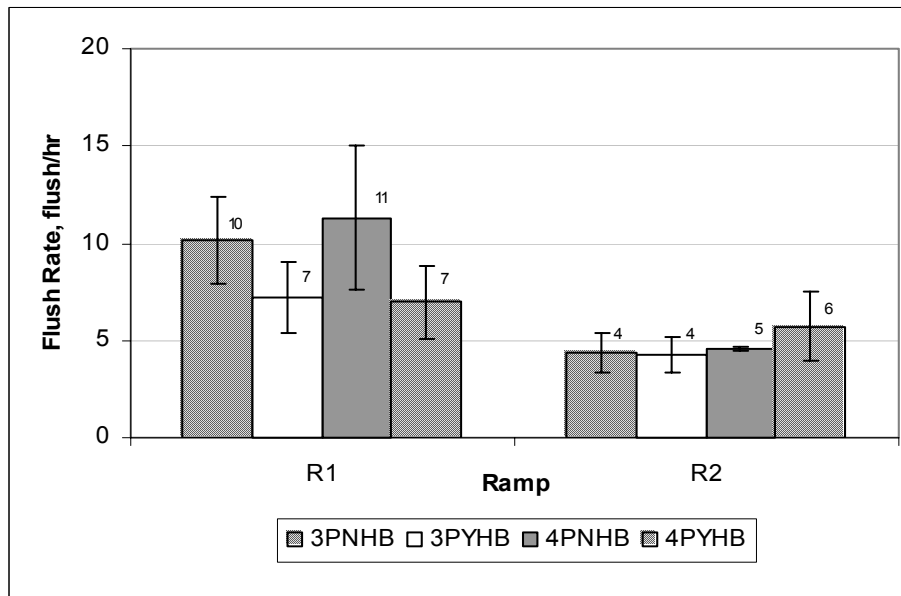


**FIGURE 108 Queue flush rate: high demand (case B).**

**TABLE 19 t-statistical tests comparing ramp performances: high demand (case B)**

Ramp	Performance Measures	Three-Phase					
		Without ICS		With ICS		t-statistic	Reject Null Hypothesis?
		Mean	S.D.	Mean	S.D.		
R1	Flush Time, sec	1794.5	416.9	1018.7	257.9	5.00	Y
	No. Flushes	28.3	6.2	20.0	5.1	3.28	Y
R2	Flush Time, sec	569.3	114.6	587.9	101.0	-0.39	N
	No. Flushes	12.1	2.8	11.8	2.5	0.25	N
Four-Phase							
R1	Flush Time, sec	1803.7	334.5	917.3	360.4	5.70	Y
	No. Flushes	31.4	5.7	19.4	5.2	4.90	Y
R2	Flush Time, sec	603.5	130.3	787.1	348.0	-1.56	N
	No. Flushes	12.6	1.7	15.8	4.9	-1.94	N

Note: (1) Null Hypothesis: Means are equal; (2) Rejection Region:  $t_{0,025,18} = 2.101$

In fact, an interesting phenomenon could be seen that a slightly higher queue flush time and higher number of queue flushes were observed for *R2* with ICS. By examining in detail the simulation process, it was found that the majority of the cases when the diamond signal was in a phase hold state were caused by the queues in *R1*, not *R2*. During the period of phase holding, long queues were generally observed on the right-side arterial approach ( $\phi_6$ ). The long queues caused blocking of the arterial right-turn movement (*M12*) which would otherwise arrive at *R2* freely without impedance. When the phase holding was disengaged, the dissipation of the long queues on the right-side arterial approach resulted in *M12* arriving at *R2* in large platoons. As a result, *R2* experienced longer queues and more frequent ramp queue flushes. This phenomenon suggests that during the over-saturated conditions at both ramps, one of the ramps

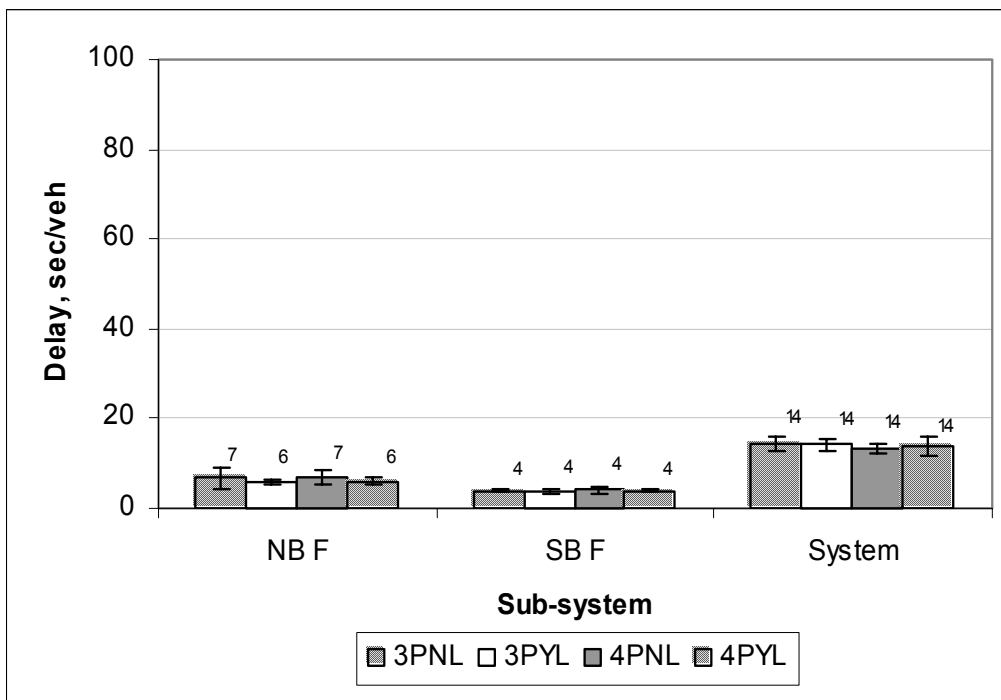
(usually the ramp with less congestion) may actually experience worse operations with ICS.

### **Vehicle Delays**

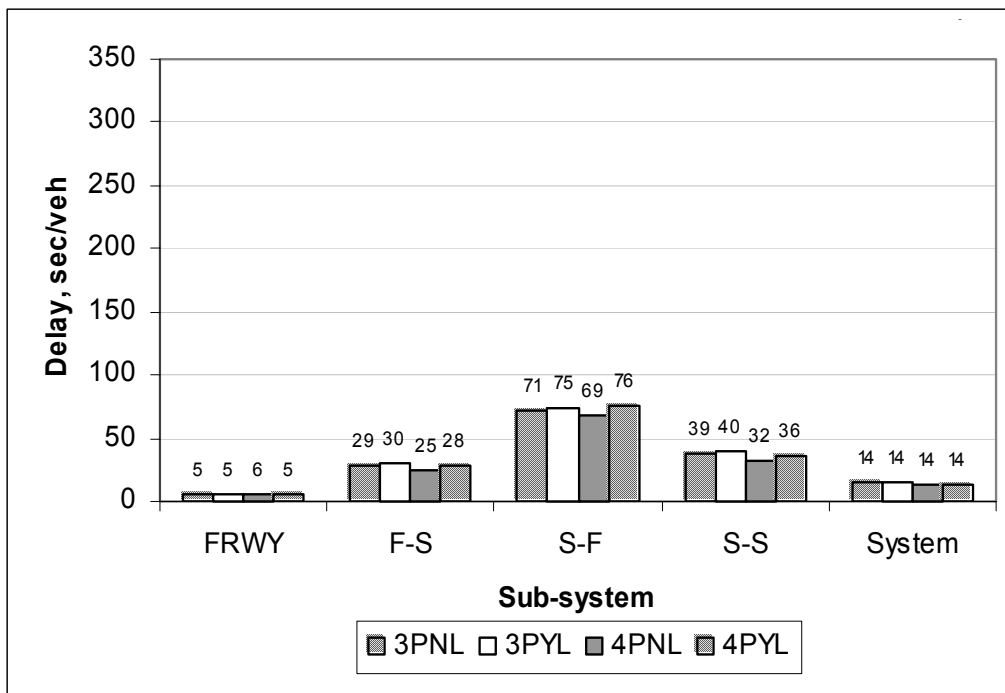
The effectiveness of ICS were also investigated based on the average delays of different system facilities. The average delays were summarized based on system-wide and sub-system levels. The following notations and their meanings were used in subsequent figures to denote the delays at different sub-system levels:

NBF – northbound freeway	SBF – southbound freeway
System – system wide	FRWY – freeway both directions
F-S – freeway to surface street	S-F – surface street to freeway
S-S – surface street to surface street	

Figure 109 shows the average delays at the system-wide and sub-system levels for the low demand scenario, and Table 20 has the detailed t-statistical test results. The t-statistical tests were conducted to compare only the freeway mainline delays and the system-wide delays for the cases with and without ICS. Minimizing freeway breakdown (also reducing freeway mainline delays) is one of the major objectives for developing ICS. The system-wide delay measures represent the system performances for the entire IDIRMS as a whole; therefore, system delay is a good indicator whether ICS would benefit the operations from the system's perspective, but not just for the freeway operations. The results indicate that no statistically different delays were found between the operations with and without ICS. Both ramps were under-saturated with rare queue flush occurrences. Even when occasional queue flush occurred, the freeway mainline was able to maintain free-flow conditions or was able to recover quickly from a short-term breakdown due to the relatively low mainline demand. As a result, ICS did not show a significant impact on either the freeway mainlines or the surface street traffic under the low demand scenario.



(a) Freeway and system delays



(b) Freeway, surface street, and system delays

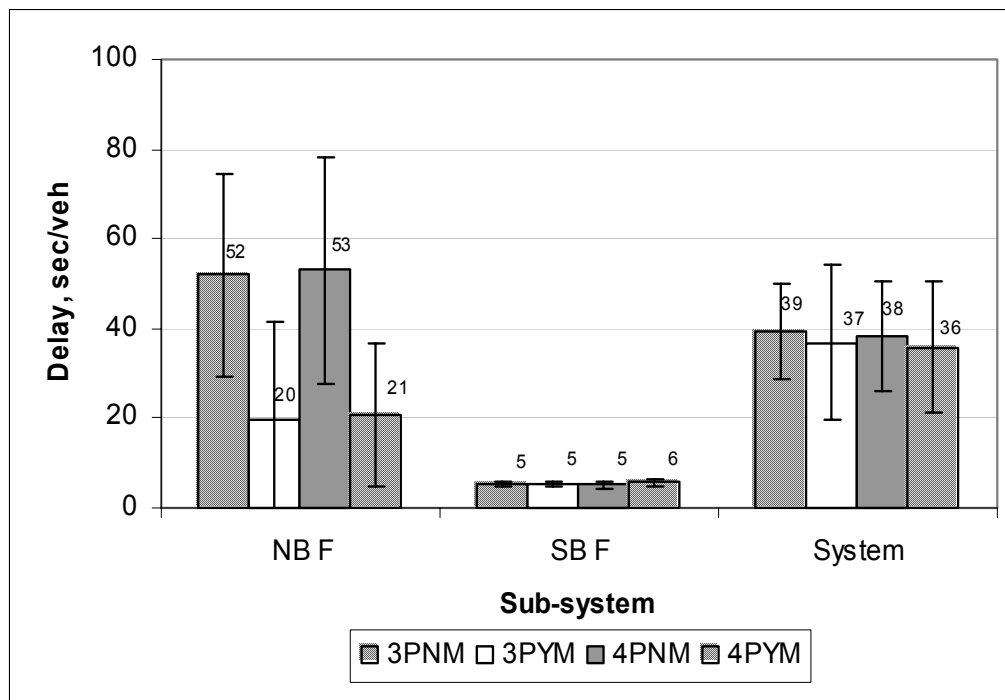
**FIGURE 109 Average vehicle delays with ALINEA metering: low demand.**

**TABLE 20 t-statistical tests for comparing delays: low demand**

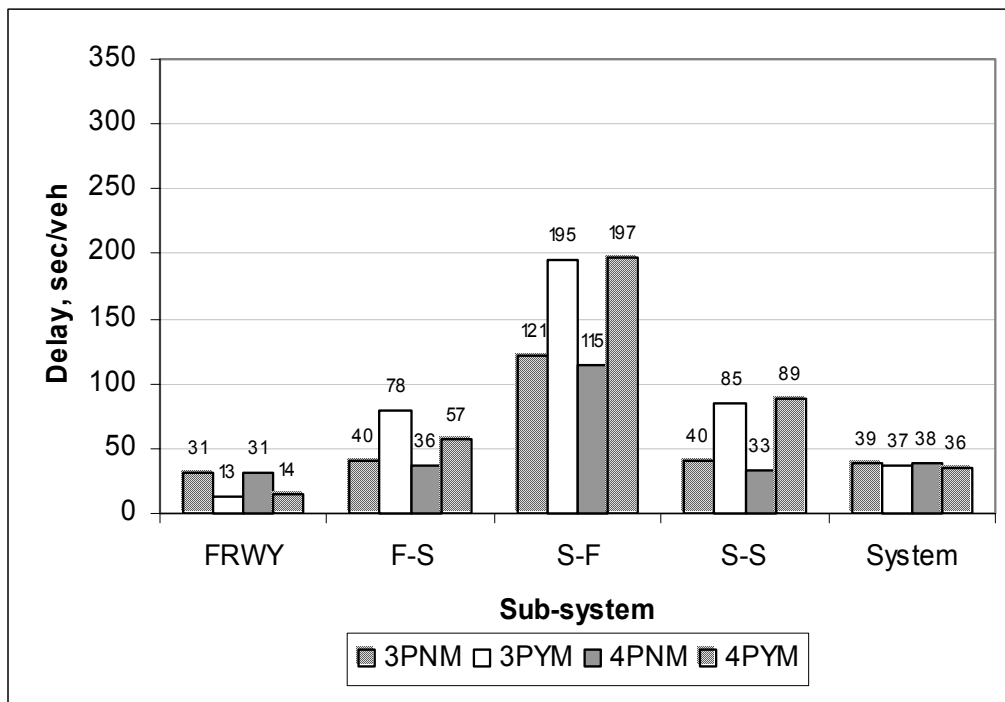
Sub-system	Three-Phase					
	Without ICS		With ICS		t-statistic	Reject Null Hypothesis?
	Mean	S.D.	Mean	S.D.		
NBF	6.7	2.3	5.9	0.7	1.06	N
SBF	3.9	0.4	3.8	0.5	0.63	N
System	14.3	1.5	14.2	1.4	0.07	N
Four-Phase						
NBF	6.8	1.7	5.9	0.9	1.54	N
SBF	4.0	0.6	3.9	0.4	0.66	N
System	13.5	1.0	14.1	2.1	-0.73	N

Note: (1) Null Hypothesis: Means are equal; (2) Rejection Region:  $t_{0.025,18} = 2.101$

Similarly, Figure 110 shows the average delays on system and sub-system levels for the medium demand scenario, and Table 21 has the detailed t-statistical results. The results indicate that significant delay savings were achieved with ICS for the northbound freeway mainline. The southbound freeway delays remained at the same low level due to the low traffic demand. Although the system-wide delays were reduced slightly with ICS, no statistical difference was found between the results with and without ICS. The significant delay savings on the northbound freeway mainline were diminished by the significant delay increases for the non-freeway traffic, such as the freeway-to-surface (F-S), surface-to-freeway (S-F), and surface-to-surface (S-S) traffic. Similar results could also be seen between three-phase and four-phase strategies.



(a) Freeway and system delays



(b) Freeway, surface street, and system delays

**FIGURE 110 Average vehicle delays with ALINEA metering: medium demand.**

**TABLE 21 t-statistical tests for comparing delays: medium demand**

Sub-system	Three-Phase					
	Without ICS		With ICS		t-statistic	Reject Null Hypothesis?
	Mean	S.D.	Mean	S.D.		
NBF	51.9	22.5	19.8	21.9	3.23	Y
SBF	5.4	0.4	5.1	0.5	1.40	N
System	39.2	10.8	36.8	17.3	0.39	N
Four-Phase						
NBF	53.0	25.3	20.7	15.7	3.42	Y
SBF	5.1	0.7	5.6	0.6	-1.65	N
System	38.4	12.3	35.8	14.5	0.44	N

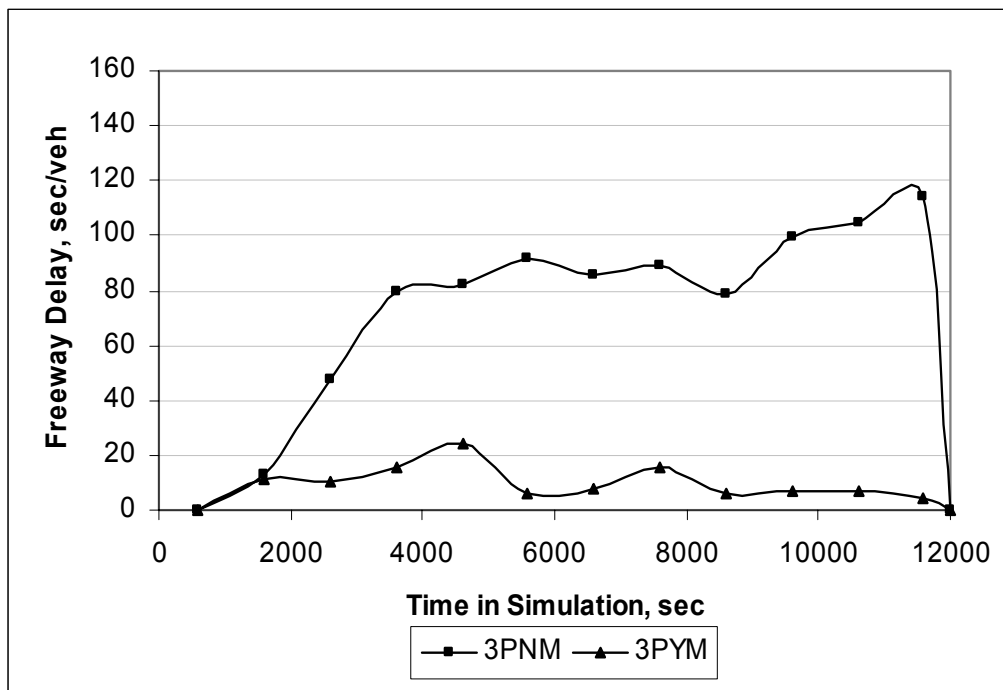
Note: (1) Null Hypothesis: Means are equal; (2) Rejection Region:  $t_{0.025,18} = 2.101$

It is noted that the results presented in Figure 110 and Table 21 represent the average of 10 simulation runs, and the stochastic traffic demand variations may have resulted in slightly lower- or higher-level traffic demands within the generally defined medium demand scenario.

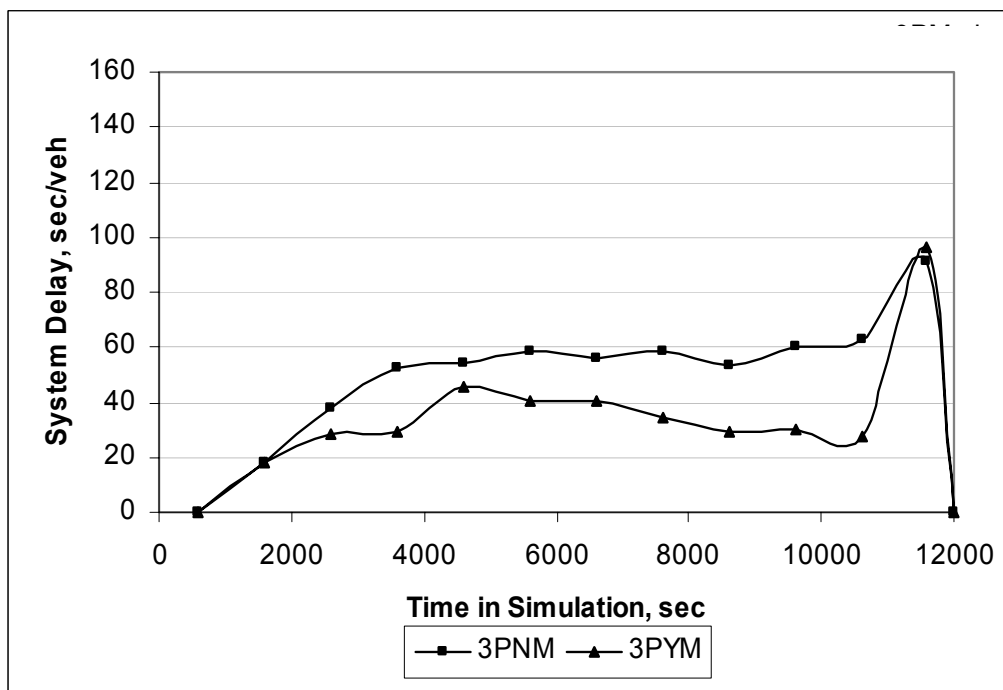
Figure 111 through Figure 113 illustrate three representative cases which may explain the results presented in Figure 110 and Table 21.

Case 1 (see Figure 111) represents a condition where freeway breakdown was completely eliminated with ICS operations. As a result, significant delay savings were achieved on the freeway mainline, and such savings outweighed the delay increases on the non-freeway traffic movements. As a result, the system delays also showed at a lower level with ICS in this case. ICS would be more effective when such a condition exists, i.e., the freeway breakdown could be completely eliminated with ICS.



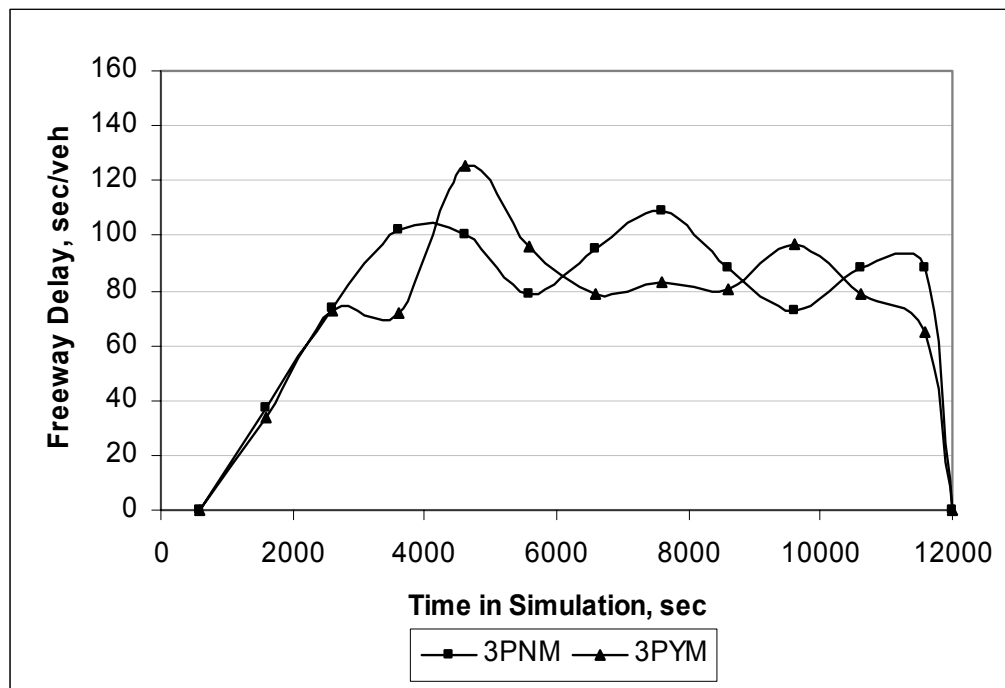


(a) Freeway Delay

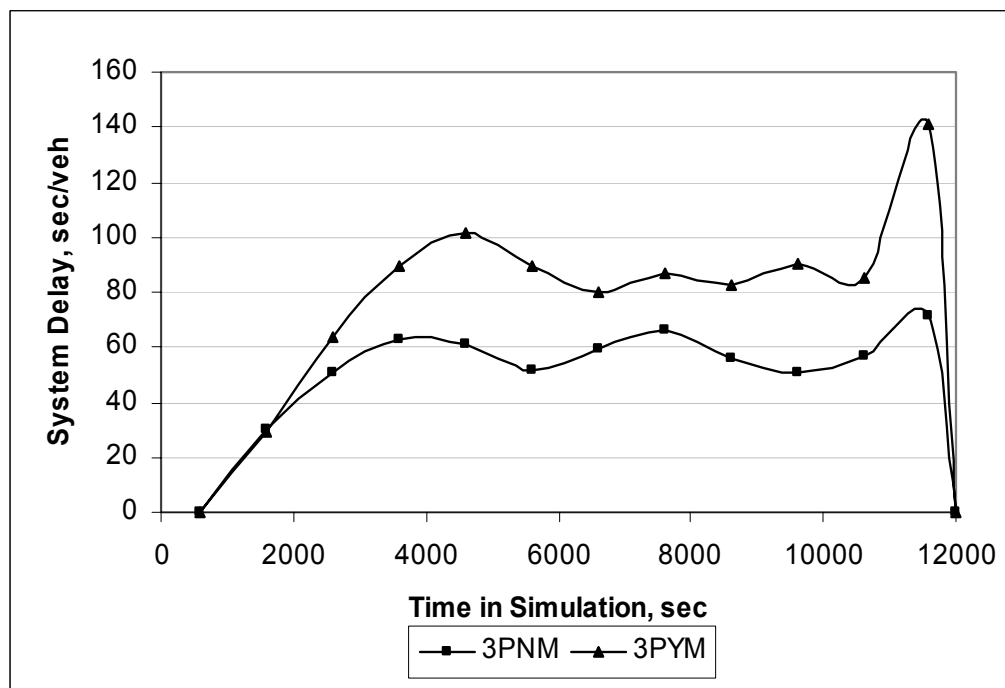


(b) System Delay

**FIGURE 111 No breakdown with ICS and reduced system delay (case 1).**

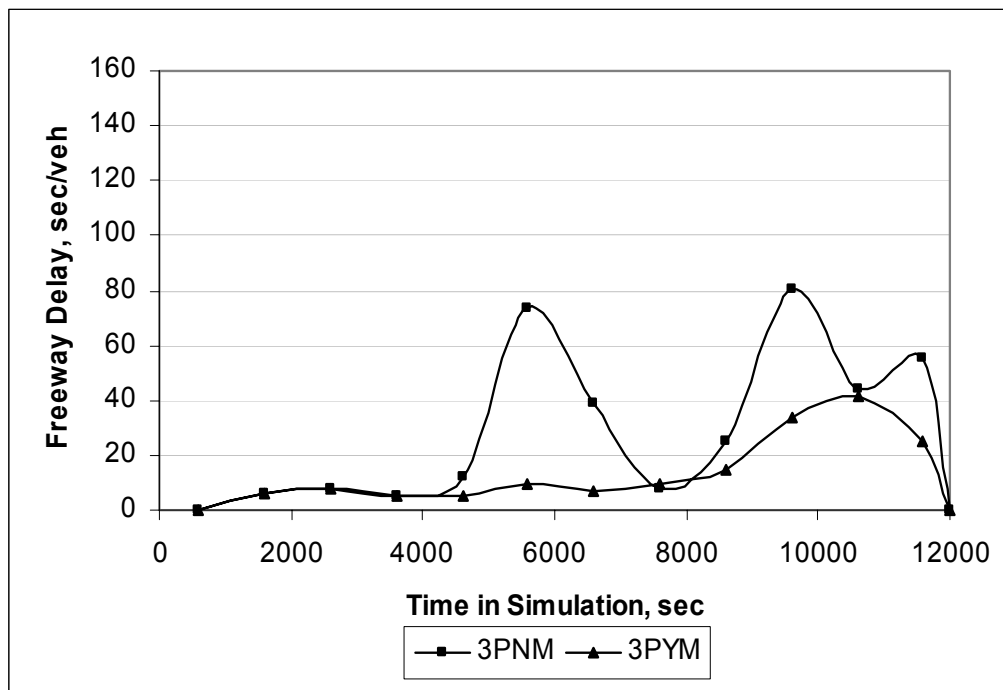


(a) Freeway Delay

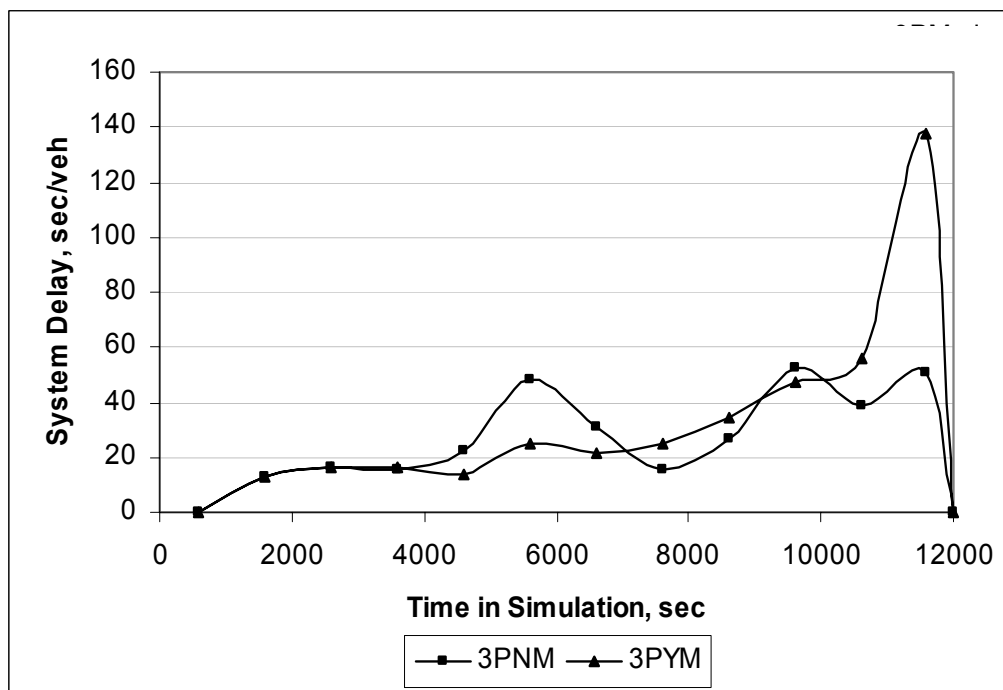


(b) System Delay

**FIGURE 112 With breakdown and increased system delay (case 2).**



(a) Freeway Delay



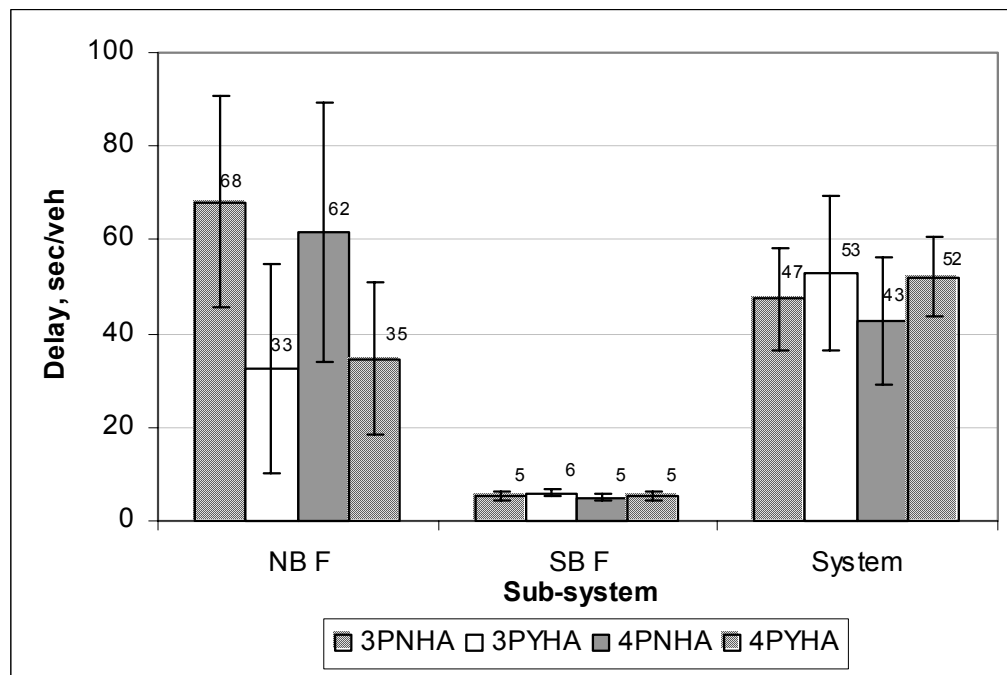
(b) System Delay

**FIGURE 113 Delayed breakdown and identical system delay (case 3).**

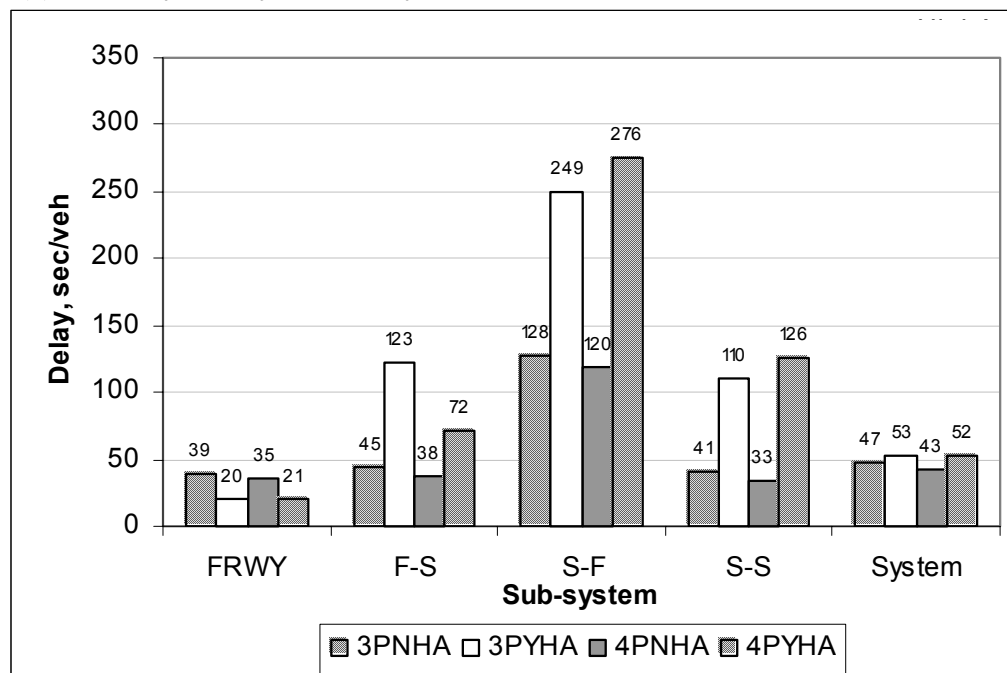
Case 2 (see Figure 112) represents a condition where freeway breakdown was not avoided with ICS because high traffic demand occurred at a much earlier stage. As a result, ICS did not result in delay savings on the freeway mainline, and the system-wide delays were actually increased with ICS due to significant delay increases on the non-freeway traffic movements. In such a case, ICS would not be effective but would rather be likely to increase the system-wide delays. This same conclusion will be seen under the high demand scenario where freeway breakdown cannot be eliminated with ICS operations.

Case 3 (see Figure 113) represents a condition where the onset of freeway breakdown was delayed with ICS, but breakdown occurred at a later stage. Freeway mainline traffic achieved some delay savings; however, the system delays remained at similar levels with and without ICS due to the delay increases on the non-freeway traffic movements. In such a case, ICS would be effective in delaying the onset of freeway congestion; therefore, the freeway traffic would receive priority service over the surface street traffic.

Figure 114 shows the average delays at the system and sub-system levels for the high demand scenario (case A), and Table 22 has the detailed t-statistical results. The results indicate that although the savings on the northbound freeway were significant with ICS, the system-wide delays somehow showed a slight increase. This was due to the significant increases in the delays for the non-freeway traffic. As pointed out earlier, freeway breakdown could not be completely eliminated with ICS when the traffic demands reached a high level. The delay savings on the freeway mainline traffic could not outweigh the delay increases on the non-freeway traffic. In such a case, only the freeway traffic would receive higher priority services, while non-freeway traffic would probably suffer from significantly higher delays.



(a) Freeway and system delays



(b) Freeway, surface street, and system delays

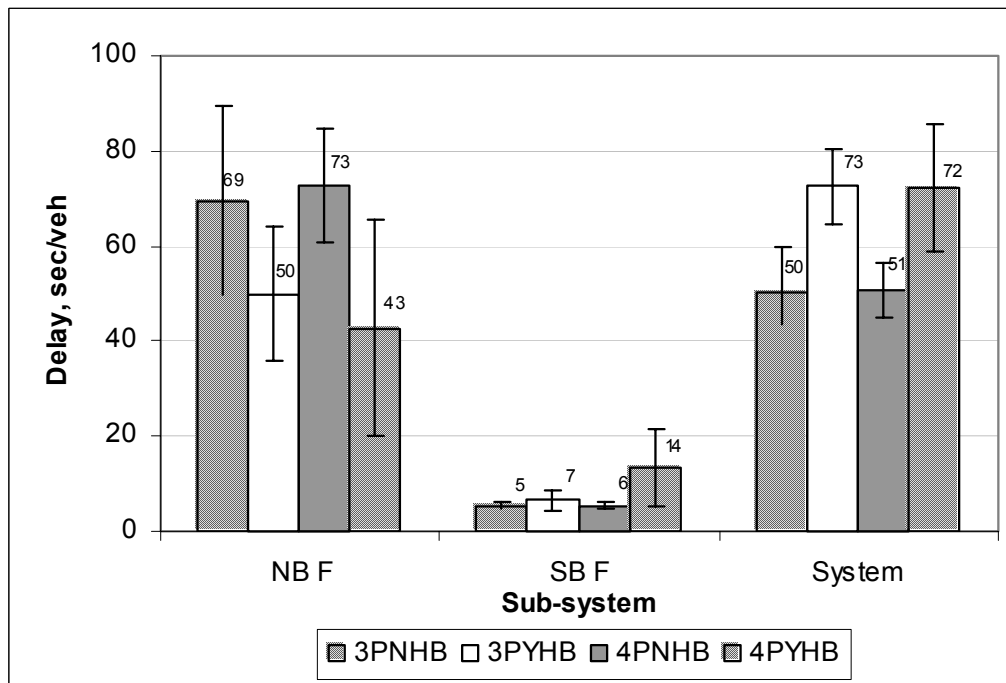
**FIGURE 114 Average vehicle delays with ALINEA: high demand (case A).**

**TABLE 22 t-statistical tests comparing delays: high demand (case A)**

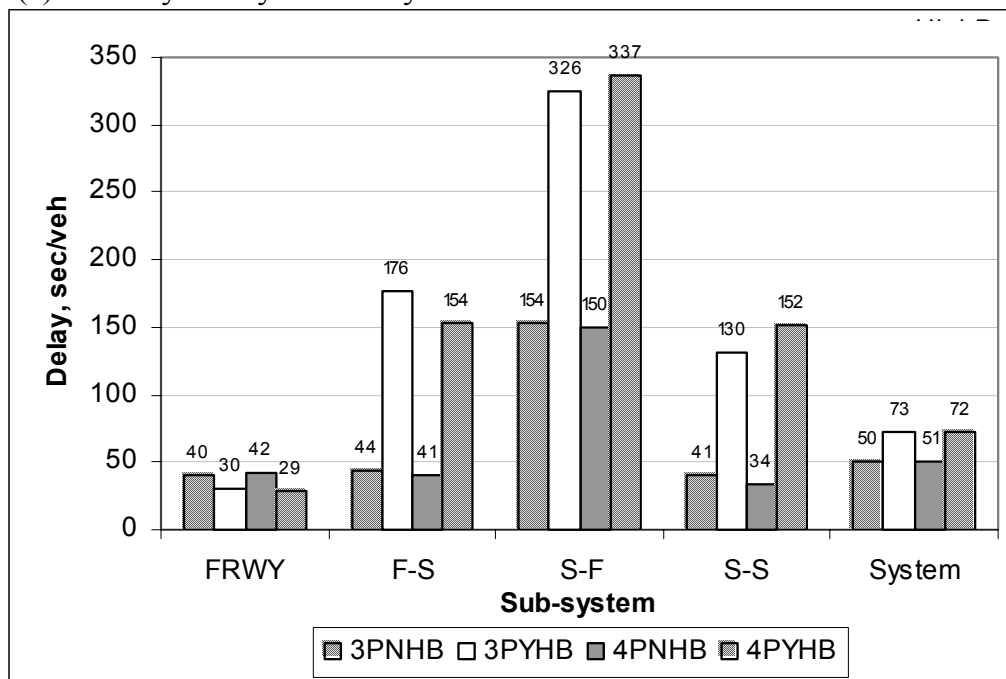
Sub-system	Three-Phase					
	Without ICS		With ICS		t-statistic	Reject Null Hypothesis?
	Mean	S.D.	Mean	S.D.		
NBF	68.1	22.6	32.5	22.4	3.54	Y
SBF	5.5	0.9	6.0	0.9	-1.45	N
System	47.4	11.0	52.8	16.5	-0.87	N
Four-Phase						
NBF	61.6	27.8	34.6	16.2	2.65	Y
SBF	5.1	0.7	5.4	0.9	-0.93	N
System	42.9	13.6	52.1	8.5	-1.82	N

Note: (1) Null Hypothesis: Means are equal; (2) Rejection Region:  $t_{0.025,18} = 2.101$

Figure 115 shows the average delays at the system and sub-system levels for the high demand scenario (case B), and Table 23 has the detailed t-statistical results. Similarly, the results indicate that the delays for the northbound freeway traffic were significantly lower with ICS. However, the system-wide delays were also significantly higher with ICS. Again, this was due to the significant increases in the delays for the non-freeway traffic. Interestingly, the southbound freeway traffic also experienced delay increases with ICS, a scenario explained previously. With ICS, the temporary phase-holding stage resulted in long queues in the arterial that blocked the right-turn movement which would otherwise arrive at the ramp without impedance. When this right-turn traffic was released as platoons, the ramp could not handle the long queues, causing more frequent queue flush and, therefore, increasing the likelihood of mainline breakdown. It is therefore concluded that ICS will not be effective under high demand scenarios in reducing system delays.



(a) Freeway and system delays



(b) Freeway, surface street, and system delays

**FIGURE 115 Average vehicle delays with ALINEA: high demand (case B).**

**TABLE 23 t-statistical tests comparing average delays: high demand (case B)**

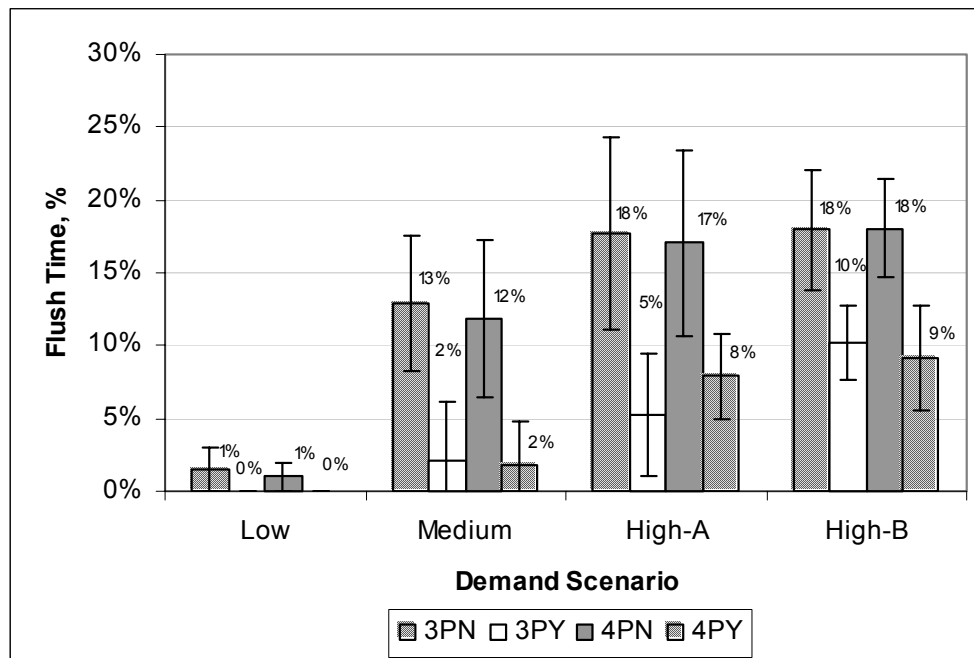
Sub-system	Three-Phase					
	Without ICS		With ICS		t-statistic	Reject Null Hypothesis?
	Mean	S.D.	Mean	S.D.		
NBF	69.5	19.9	50.0	14.0	2.53	Y
SBF	5.4	0.8	6.5	2.1	-1.60	N
System	50.2	9.5	72.5	7.9	-5.71	Y
Four-Phase						
NBF	72.8	12.1	42.8	22.9	3.66	Y
SBF	5.5	0.5	13.5	8.3	-3.06	Y
System	50.7	5.7	72.1	13.4	-4.66	Y

Note: (1) Null Hypothesis: Means are equal; (2) Rejection Region:  $t_{0.025,18} = 2.101$

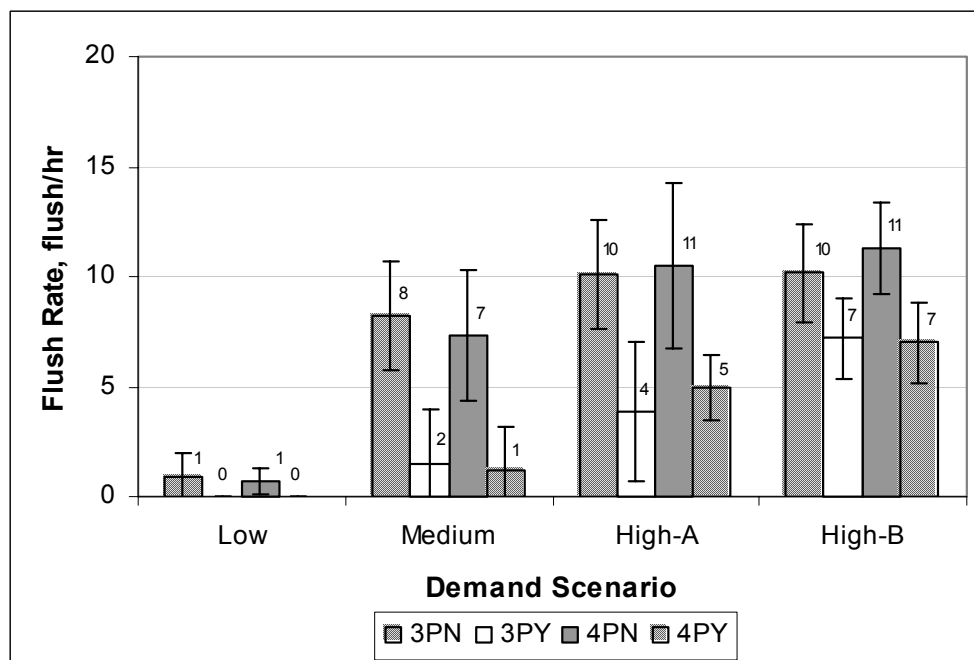
Figure 116 through Figure 121 present the performance measure results by traffic demand scenarios. Figure 116 illustrates the percent queue flush time for *R1* under different traffic demand scenarios, and Figure 117 illustrates the ramp-metering queue flush rate for *R1* under different traffic demand scenarios. In general, ICS significantly improved the ramp performance, as indicated by the lower queue flush time and the number of queue flushes. With the increasing demand level, both queue flush and queue flush rate increased. The most significant improvements could be seen under the medium demand scenario.

Figure 118 and Figure 119 illustrate similar ramp performance measures for *R2*. Significant impact on *R2* performance only emerged under the case of *High-B* (both *R1* and *R2* became over-saturated). As can be seen, worse performance measures were obtained with ICS, as explained early in this chapter. Both the queue flush time and the queue flush rate increased with ICS.





**FIGURE 116 Percent queue flush time by demand levels and control strategies: ramp 1.**



**FIGURE 117 Queue flush rates by demand levels and control strategies: ramp 1.**

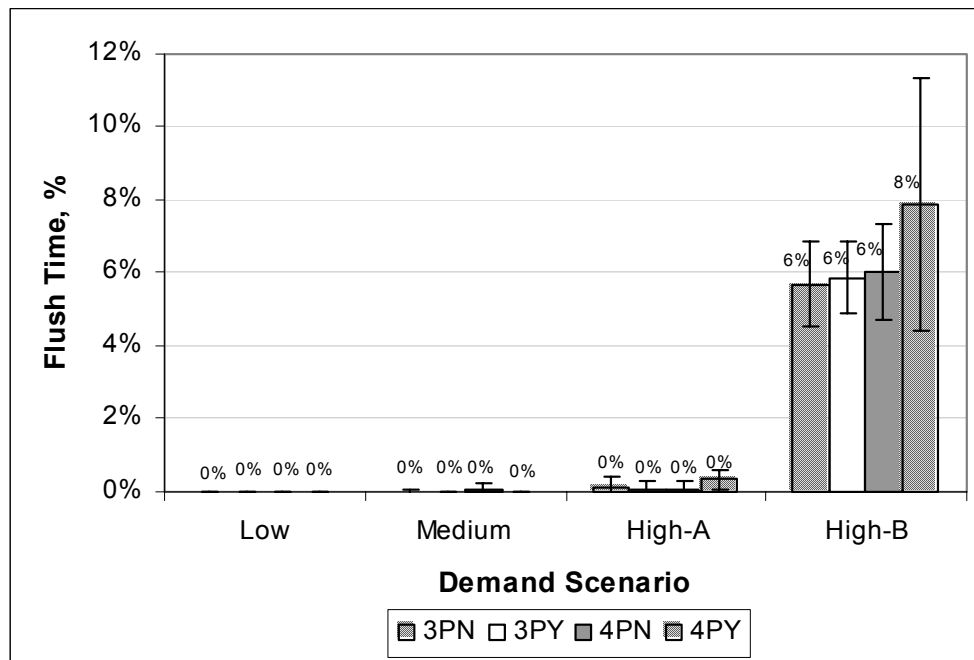


**FIGURE 118** Percent flush time by demand levels and control strategies: ramp 2.

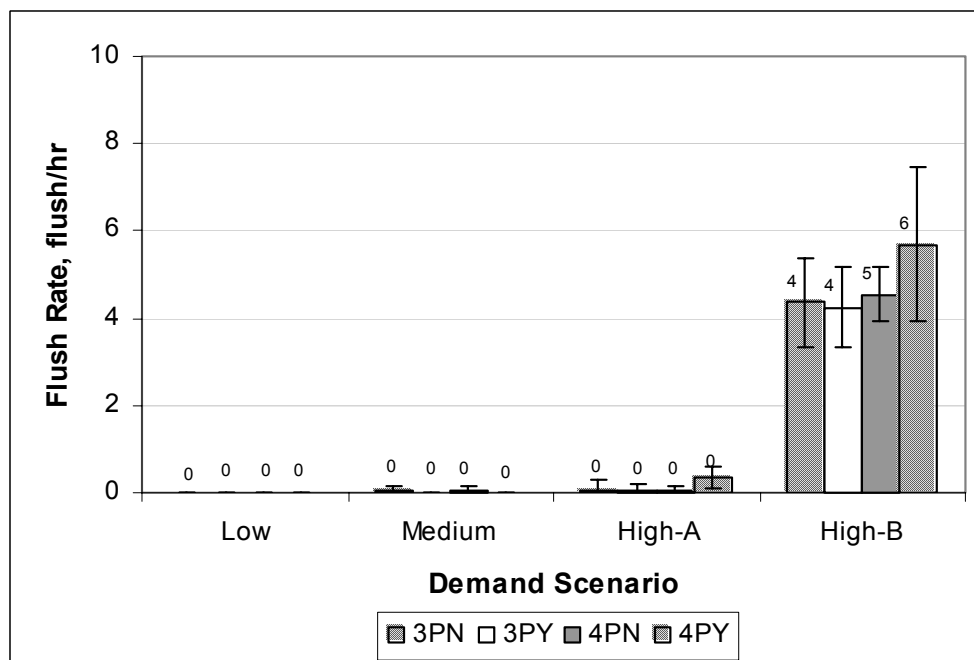


**FIGURE 119** Queue flush rates by demand levels and control strategies: ramp 2.

Figure 120 illustrates the delay results for the peak-direction (northbound) freeway mainline. In general, ICS resulted in delay savings for the freeway mainline traffic. The most significant delay savings can be seen for the medium demand and High-A demand scenarios. These delay savings were due to a significant reduction in ramp queue flush where freeway breakdowns were minimized. Under the low demand scenario, the delay savings with ICS was not significant. This is because ramp queue flush was minimal under the low demand scenario, and freeway breakdown hardly occurred even without ICS. For the High-B scenario, more frequent queue flush occurred due to over-saturation at *R2*. As a result, the freeway mainline experienced increased delays compared to the High-A scenario.

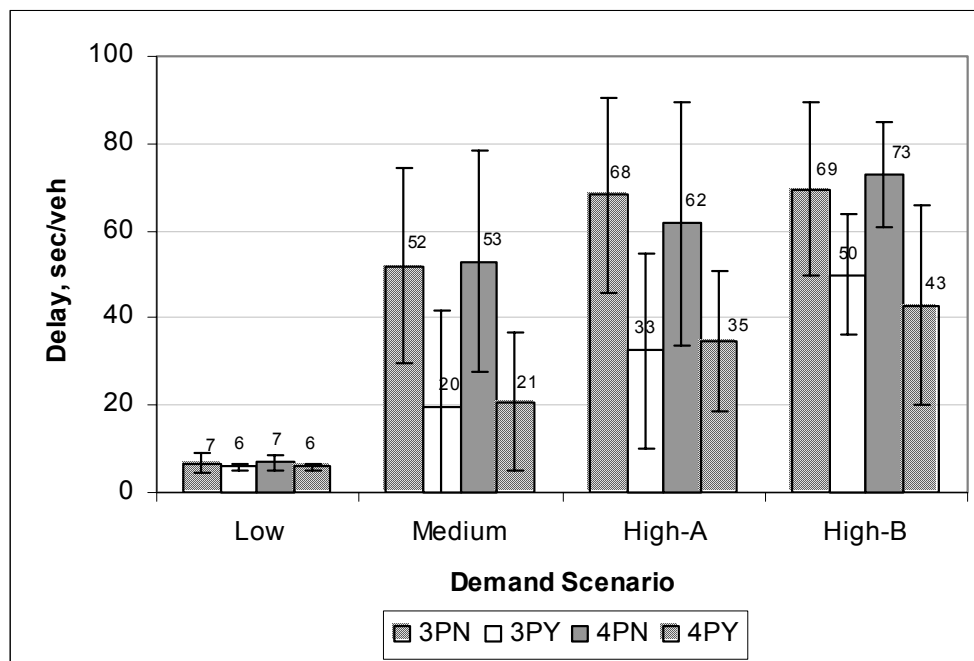


**FIGURE 120 Peak-direction freeway mainline delays by demand levels and control strategies.**

Figure 121 illustrates the system-wide delay measures by traffic demand scenarios. The system-wide delay is the weighted average of all the traffic in the system, including both freeway mainline traffic and the surface street traffic. As can be

seen, ICS only resulted in lower system delays under the medium demand scenario although the differences are not significant. Under both the High-A and High-B scenarios, the system delays were actually increased with ICS, especially for the High-B scenario. The increase in system delays reflected the situations where the surface street traffic experienced significant delay increases due to ICS. The delay increases for the surface traffic outweighed the delay savings in the freeway mainline. Under the low demand scenario, the system-wide delays are basically the same with and without ICS.

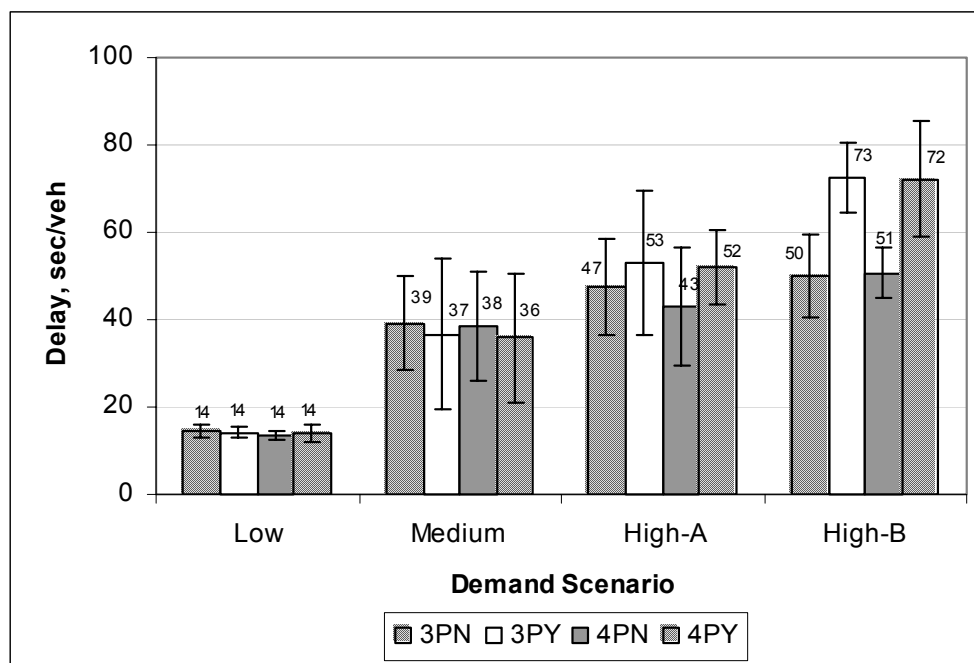


**FIGURE 121 System-wide delays by demand levels and control strategies.**

### Results with Fixed Metering

The results in the previous section indicate that ICS would be effective in reducing system-wide delays only when freeway breakdown could be avoided or minimized. Compared to fixed ramp metering, traffic-responsive ramp metering can actively respond to freeway congestion; therefore, it is more effective in preventing freeway breakdown. Due to the existence of high traffic demands at many ramp-metering locations, ramp metering is often set to operate at its maximum rate in order to

minimize ramp queue spillback, resembling a fixed metering operation. To illustrate whether ICS would still be effective if ramp metering would operate as fixed metering, this section presents some simulation results when fixed ramp metering was used.

Figure 122 and Figure 123 provide delay results similar to those presented in the previous section, except for the conditions when ramp metering was operating at a fixed rate rather than the varied rate. Only the mean values are shown in these figures. No statistical tests were conducted on these results.

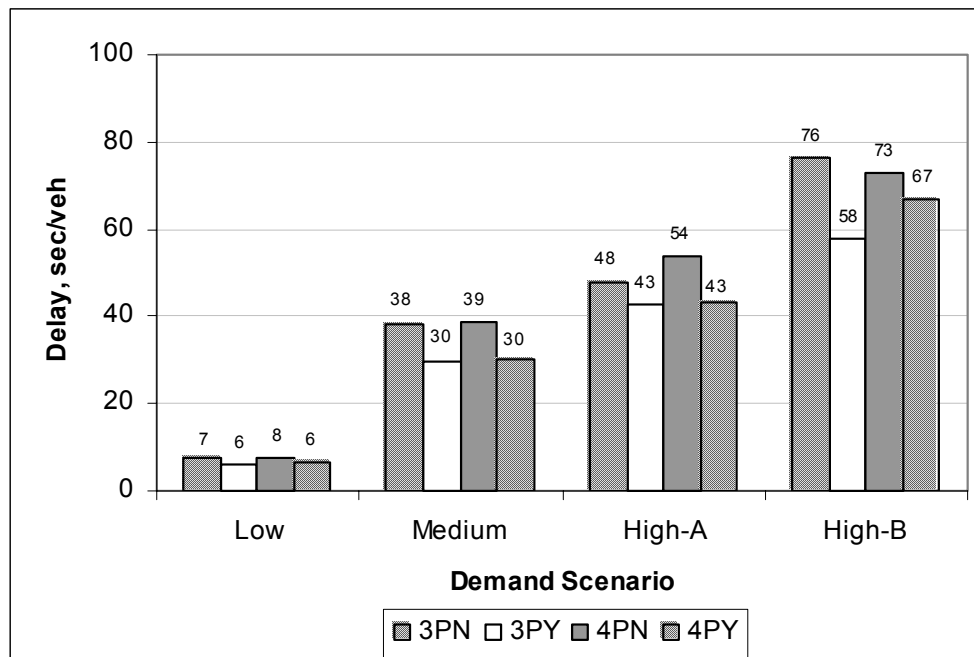


**FIGURE 122 Peak-direction freeway mainline delays by demand levels and control strategies with fixed metering.**

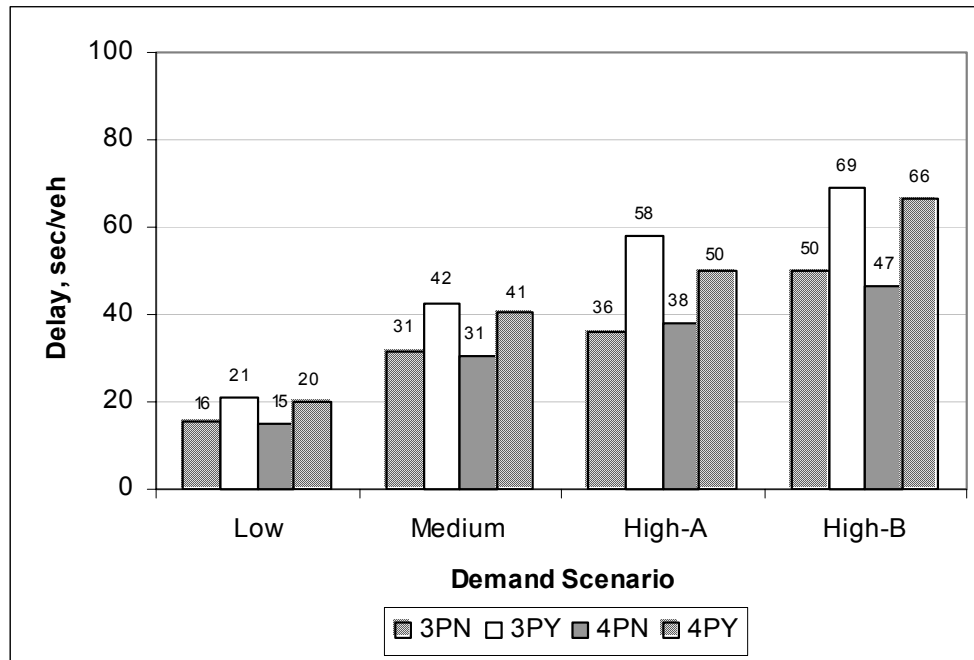


**FIGURE 123 System-wide delays by demand levels and control strategies with fixed metering.**

What can be noticed from the results is that the delay savings on the freeway mainline were no longer as significant as those when ALINEA traffic-responsive ramp metering was used. As a result, system delays were all higher with ICS for the three general traffic demand scenarios when fixed ramp metering was used. It is therefore concluded that traffic-responsive ramp metering has a significant advantage over fixed metering operations in preventing freeway breakdown and minimizing freeway delays.

### **A FRAMEWORK FOR IMPLEMENTING ICS**

In the previous sections of this chapter, the proposed ICS were documented and the additional detection system components for implementing ICS and its algorithm were tested in a simulation environment. This section documents the development of a framework for potential field implementation of ICS in an IDIRMS. The ICS algorithm and architecture are described in this section. Detailed functional diagrams for the algorithm are provided in Appendix D.

Figure 124 illustrates the proposed system architecture for an IDIRMS with the ICS algorithm. Figure 125 illustrates the data flow within the ICS algorithm. In addition to the standard vehicle detection and signal control elements at the ramp-metering sub-system and the diamond interchange sub-system, IDIRMS with ICS requires additional vehicle detection systems, namely the boundary queue detection, intermediate queue detection, and queue spillback detection. The required detector locations were illustrated previously in Figure 87.

The ICS algorithm consists of three major functions: the *Integration Need Assessor*, the *Strategy Selector*, and the *Strategy Implementer*. The Integration Need Assessor processes information from the various queue detectors and determines whether ICS is needed based on the queuing conditions. Once the queuing conditions warrant ICS, the Strategy Selector will determine what strategy [i.e., the candidate phase(s) to hold] should be implemented based on the conditions of the queues and the diamond control mode (i.e., phasing schemes). The Strategy Implementer will facilitate the transition from normal signal operation to integrated control or vice versa based on the current signal status and queuing conditions. The detailed functional descriptions of the ICS algorithm are provided in Appendix D.

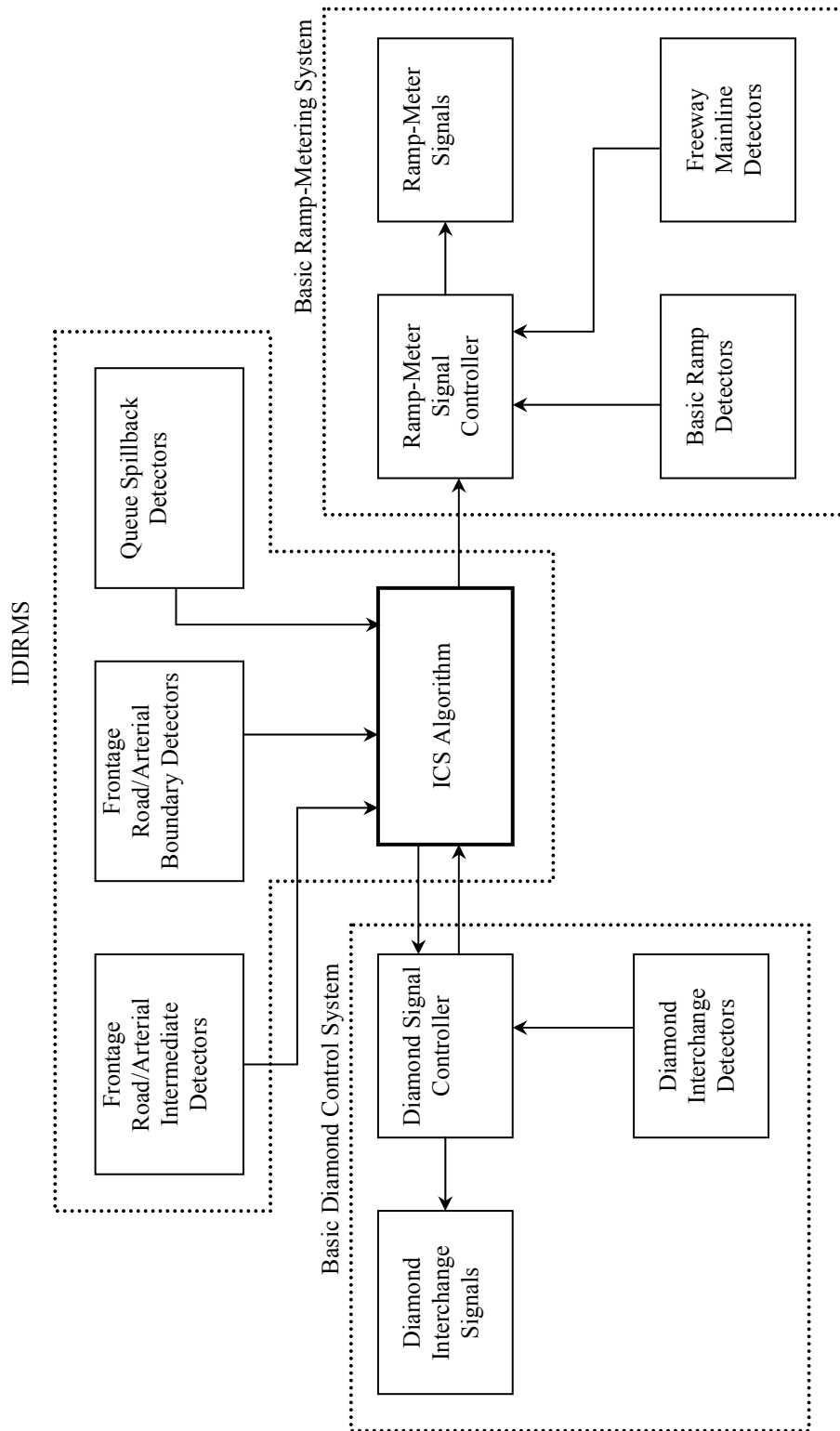


**FIGURE 124 IDIRMS architecture.**



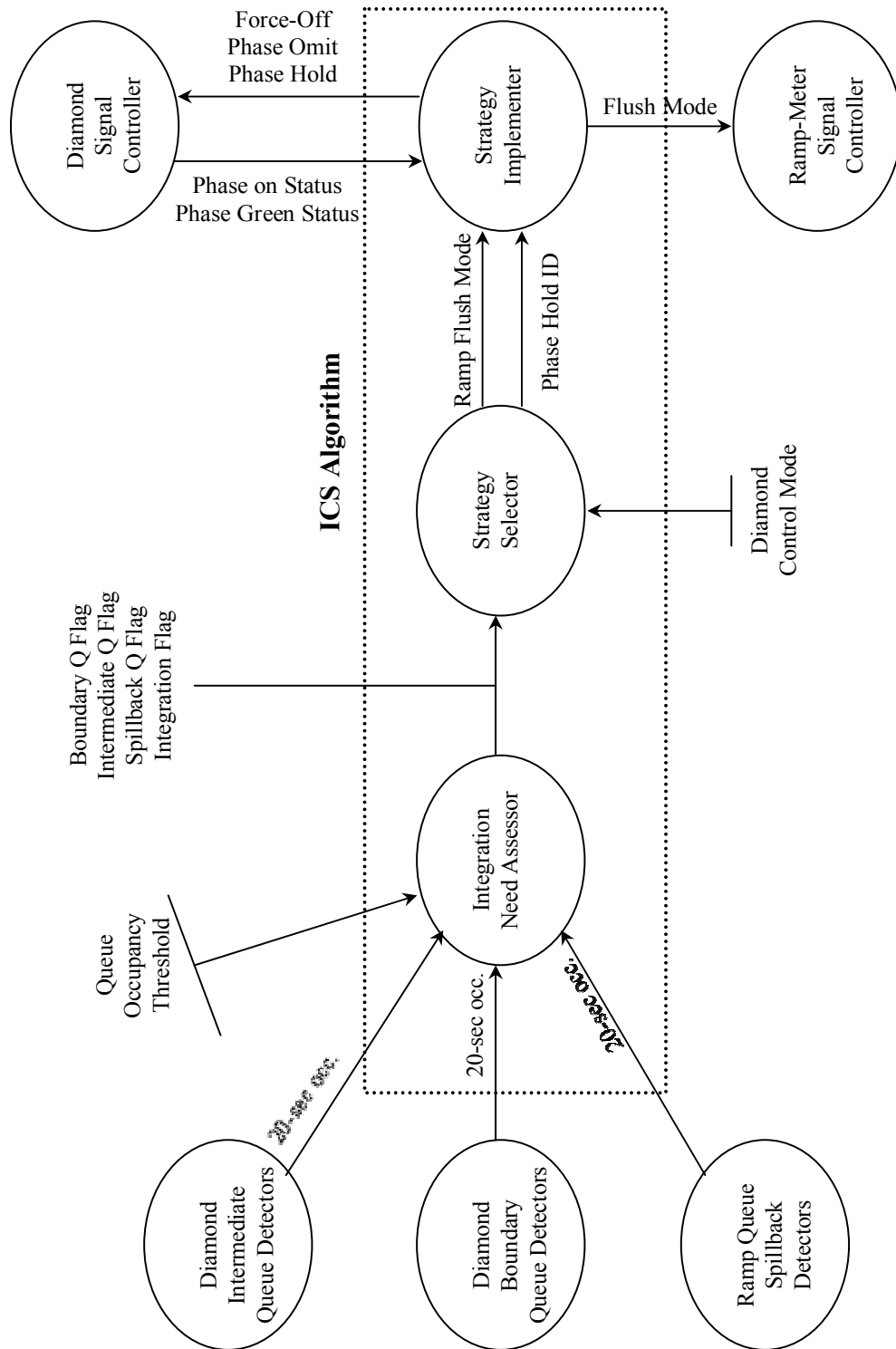


FIGURE 125 Diagram of data flow of the proposed ICS algorithm.

## SUMMARY

This chapter has documented the development and evaluation of ICS for managing an IDIRMS. ICS were developed with a focus on dealing with recurring congestion from daily traffic operations. Evaluations of the effectiveness of ICS were conducted using the VISSIM simulation model under three generally defined traffic demand scenarios: low, medium, and high. Detailed system architecture and ICS algorithm functional diagrams were also developed for potential field implementation.

One critical element of ICS is to have the ramp metering operate with traffic-responsive instead of fixed metering. Traffic-responsive ramp-metering algorithms, such as ALINEA, can actively respond to freeway congestion; thus, they are more effective in preventing freeway breakdown and achieving significant delay savings for the freeway traffic. Fixed metering, although it may still be effective in improving freeway operations under certain circumstances, is less effective in preventing freeway breakdown.

ICS proved to be effective only within a certain traffic demand level, e.g., the medium level as defined in this study. Under the low demand scenario, where both the freeway mainlines and the ramps have sufficient capacities, implementing ICS would not result in significant difference in the system performances. On the other hand, when the traffic demands are high for both the freeway mainlines and the ramps, ICS would only provide marginal benefits for the freeway mainline operations by delaying the onset of ramp queue flush and freeway breakdown. Once the traffic queues on the surface street exceed boundary limits and ramp queue flush starts, the delay savings on the freeway traffic will be significantly diminished. The non-freeway traffic would experience excessive delays and queues, which would normally outweigh the delay savings of the freeway traffic. ICS proved to be most effective under the generally defined medium demand scenario, where temporary phase hold would not result in overflow of the queue storage spaces and freeway breakdown can be effectively prevented or delayed. Although non-freeway traffic would still generally experience

increased delays, the delay savings on the freeway traffic would normally outweigh the delay increases on the non-freeway traffic.

ICS associated with three-phase and four-phase schemes yielded similar system performance measures although individual surface street traffic movements may experience different delay levels.

Finally, the system architecture for an IDIRMS with ICS indicates that the system can be developed based on the existing controller features and functions although additional detection and communication equipment will be needed.

## CHAPTER VIII

### SUMMARY AND CONCLUSIONS

#### SUMMARY OF MAJOR TASKS PERFORMED

This research aimed at developing integrated control strategies for better managing an integrated diamond interchange ramp-metering system. New methodologies were developed to provide enhanced modeling features for an IDIRMS. The research focused on the type of diamond interchange with U-turn lanes and one-way frontage roads typically seen in urban areas in the state of Texas and some other states. The signal phasing schemes included the two most commonly used phasing schemes: basic three-phase and TTI four-phase.

The primary principle of the modeling methodologies for vehicle queues and delays was based on the cumulative arrival and departure queue polygon method. Modeling of the diamond interchange and ramp-metering operations took into consideration the close interrelationship between the diamond signal and the ramp-metering signal. Ramp-metering operations and ramp performances were modeled considering the unique traffic flow profiles and the stochastic freeway flows. A gap-acceptance-based model was developed to provide a theoretical basis for establishing freeway mainline volume thresholds for ramp-metering applications. Diamond interchange operations were modeled considering the impact of queue spillback from the ramp meters. Modeling of freeway operations took into consideration the stochastic nature of freeway breakdown, and the two-capacity phenomenon was specifically considered in the modeling process.

A computer model named DRIVE was developed to implement the enhanced modeling methodologies. DRIVE is classified as a mesoscopic simulation and analysis model that can be used to perform system analysis for IDIRMS over multiple cycles and with consideration of stochastic traffic demands. Mesoscopic models have the advantages of both microscopic and macroscopic models in terms of fast computing speed and consideration of stochastic traffic demand variations. DRIVE was validated

against the VISSIM microscopic simulation model. System operational characteristics were investigated using DRIVE to gain a better understanding of the IDIRMS operations.

ICS were developed for an IDIRMS, and a proof-of-concept evaluation was conducted using VISSIM under three generally defined traffic demand scenarios: low, medium, and high, as characterized by the volume-to-capacity ratios at the ramps. Finally, a framework for implementing the ICS was developed, where detailed data flow and functional diagrams were provided. Major findings and conclusions reached in this research are documented in the next section.

## **MAJOR FINDINGS AND CONCLUSIONS**

### **System Operational Features and Characteristics**

Using the DRIVE software developed in this research, the system operational features and characteristics were investigated based on one field case. Major findings from this case analysis are summarized below:

- For the case of an under-saturated diamond interchange, no significant difference was found in the system performance measures between three-phase and four-phase operations, and whether the arterial right-turn movement was signal controlled or not. Stochastic variation in the traffic demands was a major contributing factor for the ramp queues. The ramp queue length seemed to be non-linearly related to the proportion of the ramp volume split. With the same ramp demand level, the queue length seemed to increase with the increase of the ramp volume split.
- For over-saturated ramp conditions where queue spillback existed, the type of phasing scheme exhibited different operational impacts on the diamond interchange operation. The four-phase scheme seemed to benefit the frontage road phase movement, while the three-phase scheme seemed to benefit the arterial left-turn movement. Traffic-responsive ramp-metering operations with varied metering rates were more effective in maximizing freeway throughput flows and preventing

freeway breakdown. Ramp metering with queue flush could result in earlier freeway breakdown; thus, it is not a preferred operational strategy. Ramp-metering operations should avoid or delay the onset of ramp queue flush, which would require development of ICS for managing an IDIRMS.

- To achieve control of ramp demand through split adjustment would only be possible when the ramp-feeding movement becomes over-saturated. The analyses demonstrated that when a ramp-feeding movement was under capacity at the diamond signal, increasing its phase split actually resulted in smaller ramp queues due to a reduction in the size of platoons.
- The ramp queues were found to increase with the increase of diamond cycle length. The ramp queue length distributions do not follow normal distributions due to a significant number of zero queues.

### **Model Calibration and Validation**

Calibration and validation of the DRIVE model were conducted based on the results of VISSIM microscopic simulation model. Specific findings and conclusions regarding the calibration and validation processes are summarized below:

- The two-capacity phenomenon of freeway operations is one of the key features for evaluating the effectiveness of ramp-metering operations. It was found that with careful selection of the model parameters, VISSIM is able to produce the two-capacity phenomenon that compared well with field data collected in this research. However, VISSIM seems to have shown much faster recovery from breakdown than what has been observed in the field; therefore, the modeling of freeway breakdown warrants further field study and validation.
- Results from VISSIM also confirmed the findings from previous studies that freeways have a lower queue-discharge capacity under breakdown than the free-flow capacity. Freeway breakdown and its associated traffic flows are stochastic in nature. The variations in the free-flow capacity are higher than the variations in the

queue-discharge capacity. It was also found that the difference between the two capacities depends on the type of ramp control. The difference between the two capacities tends to decrease with ramp metering on, suggesting that ramp metering may be effective in minimizing the impact of breakdown.

- For the results for the freeway mainlines, both DRIVE and VISSIM yielded statistically identical delay measures during both under-saturated (with queue flush) and over-saturated (without queue flush) ramp conditions.
- For the results for the surface street traffic movements, both DRIVE and VISSIM yielded delay results that matched well with PASSER III for under-saturated conditions without queue spillback. For over-saturated conditions with queue spillback, the difference between DRIVE and VISSIM was more significant, which the limitations in both models could have contributed to. One specific case was the modeling of the short-lane effect and lane blocking. Nevertheless, with the specific case analyzed, both DRIVE and VISSIM revealed a consistent trend in how the delays increased on the ramp-feeding traffic movements with the two types of diamond phasing schemes. Three-phase seemed to benefit the arterial left-turn traffic, while four-phase seemed to benefit the frontage road movement. As a result, validation of DRIVE for over-saturated conditions should probably be stated from a qualitative perspective.

### **ICS Development and Evaluation**

Various ICS were developed in this research for the purpose of achieving better system performance measures. The ICS addressed in this research were considered as first steps to further explore a truly intelligent IDIRMS. Evaluations of ICS were carried out using VISSIM with one particular interchange location and with three generally defined traffic demand scenarios. Major findings and conclusions are summarized below:

- ICS proved to be effective only within a specified traffic demand level, e.g., the medium level as defined in this study. Under the low demand scenario where both

the freeway mainlines and the ramps have sufficient capacities, implementing ICS would not result in a significant difference in the system performances. On the other hand, when the traffic demands are high for both the freeway mainlines and the ramps, ICS would only provide marginal benefits for the freeway mainline operations by delaying the onset of ramp queue flush and freeway breakdown. Once the traffic queues on the surface street exceed boundary limits and ramp queue flush starts, the delay savings on the freeway traffic will be significantly diminished. The non-freeway traffic would experience excessive delays and queues, which would normally outweigh the delay savings to the freeway traffic.

- One critical element for achieving the expected effectiveness with ICS is to have the ramp meter operate with traffic-responsive instead of fixed metering. Traffic-responsive ramp-metering algorithms, such as ALINEA, can actively respond to freeway congestion; thus, they are more effective in preventing freeway breakdown and achieving significant delay savings for the freeway traffic. Fixed metering, although it may still be effective in improving freeway operations under certain circumstances, is less effective in preventing freeway breakdown.
- ICS associated with three-phase and four-phase schemes yielded similar system performance measures although individual surface street traffic movements may experience different delay levels.
- The proposed system architecture for an IDIRMS with ICS indicated that the system can be developed based on the existing controller features and functions although additional detection and communication equipment will be necessary.

### **Future Research**

Several research areas identified for further research are summarized below:

- Field studies of the freeway operational features related to breakdown are needed to verify the modeling accuracy for both the DRIVE model and other microscopic simulation models. There seems to be a lack of literature to address this operational



feature of using microscopic simulation models. For example, why was the Wiedemann-74 model able to replicate the two-capacity phenomenon but the improved Wiedemann-99 was not?

- The preliminary findings of system operational features drawn from the one case analysis should be further validated based on more case studies, requiring a broader range of network configuration and traffic flow scenarios.
- Other potential enhancements to the DRIVE model include the modeling of advanced adaptive signal control features, modeling of potential interchange lockup, and interference between the freeway mainline and off-ramp queue spillback.
- The modeling methodologies developed in this research should address more generalized surface street signalized intersections since those might be encountered often in other countries and states.
- Field implementation and testing of the proposed ICS are necessary steps to evaluate their viability and effectiveness in managing the operations of an IDIRMS in real time. More sophisticated control algorithms could be developed with the advance of detection, communication, and information technologies where more accurate traffic flow and system status data could be obtained in real time.

## REFERENCES

1. Garber, N.J., and M.D. Fontaine. *Guidelines for Preliminary Selection of the Optimum Interchange Type for a Specific Location*. Report FHWA/VTRC 99-R15. Federal Highway Administration, Washington, D.C., 1999.
2. Kim, Y., and C.J. Messer. *Traffic Signal Timing Models for Oversaturated Signalized Interchanges*. Report 1148-2. Texas Transportation Institute, College Station, Texas, 1992.
3. Tian, Z. Implementation and Operational Guidelines on Coordinated Ramp Metering Systems. In *Compendium: Papers on Advanced Surface Transportation Systems, 2002*. Report SWUTC/02/473700-00003-4. Texas Transportation Institute, College Station, Texas, 2002, pp. 200-231.
4. Messer, C.J., and D.J. Berry. Effects of Design Alternatives on Quality of Service at Signalized Diamond Interchanges. In *Transportation Research Record 538*, Transportation Research Board, National Research Council, Washington, D.C., 1975, pp. 20-31.
5. Messer, C.J., D.B. Fambro, and S.H. Richards. Optimization of Pretimed Signalized Diamond Interchanges. In *Transportation Research Record 644*, Transportation Research Board, National Research Council, Washington, D.C., 1977, pp. 78-84.
6. Pooran, F., and R. Sumner. *Coordinated Operation of Ramp Metering and Adjacent Traffic Signal Control Systems*. Report FHWA-RD-95-130. Federal Highway Administration, Washington D.C., 1996.
7. *VISSIM 3.60 User Manual*. PTV, Stumpfstraße 1, D-76131 Karlsruhe, Germany, 2002.
8. Venglar, S.P., and P.J. Koonce. *PASSER III-98 Application and User's Guide*. Texas Transportation Institute, College Station, Texas, 1999.
9. Messer, C.J., D.B. Fambro, and S.H. Richards. Optimization of Pretimed Signalized Diamond Interchanges. In *Transportation Research Record 644*, Transportation Research Board, National Research Council, Washington, D.C., 1977, pp. 78-84.
10. Intersection Control Software, TS-2 Version 50.1. Naztec, Inc., Sugarland, Texas, 2001.

11. *EPAC300 Actuated Controller Unit Product Manual*. Eagle Traffic Control Systems, Austin, 1997.
12. Webster, F.V. *Traffic Signal Settings*. Road Research Technical Paper 39. Her Majesty's Stationery Office, London, 1958.
13. Webster, F.V., and B.M. Cobbe. *Traffic Signals*. Her Majesty's Stationery Office, London, 1966.
14. *Highway Capacity Manual 2000*. Transportation Research Board, National Research Council, Washington, D.C., 2000.
15. McShane, W.R., R.P. Roess, and E.S. Prassas. *Traffic Engineering*, 2<sup>nd</sup> ed. Prentice-Hall, Englewood Cliffs, New Jersey, 1998.
16. Lawson, T.W., D.J. Lovell, and C.F. Daganzo. Using Input-Output Diagram to Determine Spatial and Temporal Extents of a Queue Upstream of a Bottleneck. In *Transportation Research Record 1572*, Transportation Research Board, National Research Council, Washington, D.C., 1997, pp. 140-147.
17. Wagner, F.A., D.L. Gerlough, and F.C. Barnes. *NCHRP Report 73: Improved Criteria for Traffic Signal Systems on Urban Arterials*. Transportation Research Board, National Research Council, Washington, D.C., 1969.
18. Wagner, F.A., F.C. Barnes, and D.L. Gerlough. *NCHRP Report 124: Improved Criteria for Traffic Signal Systems in Urban Networks*. Transportation Research Board, National Research Council, Washington, D.C., 1971.
19. Park, B., C.J. Messer, and T. Urbanik. Enhanced Genetic Algorithm for Signal-Timing Optimization of Oversaturated Intersections. In *Transportation Research Record 1727*, TRANSPORTATION RESEARCH BOARD, National Research Council, Washington, D.C., 2000, pp. 32-41.
20. Kovvali, V.G., C.J. Messer, N.A. Chaudhary, and C-L Chu. Program for Optimizing Diamond Interchanges in Oversaturated Conditions. In *Transportation Research Record 1811*, TRANSPORTATION RESEARCH BOARD, National Research Council, Washington, D.C., 2002, pp. 166-176.
21. Bogenberger, K., and A.D. May. *Advanced Coordinated Traffic Responsive Ramp Metering Strategies*. Report UCB-ITS-PWP-99-19. University of California, Berkeley, 1999.
22. Piotrowicz, G. *Ramp Metering Status in North America, 1995 Update*. Report DOT-T-95-17. FHWA, Washington, D.C., 1995.

23. Kenis, E., and R. Tegenbos. *Centrico: Ramp Metering Synthesis*. <http://www.centrico.net/documents/RAMP%20METERING%20SYNTHESIS.pdf>, 2001.
24. Jacobson, L.N., K.C. Henry, and O. Mehyar. Real-Time Metering Algorithm for Centralized Control. In *Transportation Research Record 1232*, Transportation Research Board, National Research Council, Washington, D.C., 1989, pp. 17-26.
25. Lipp, L.E., L.J. Corcoran, and G.A. Hickman. Benefits of Central Computer Control for Denver Ramp-metering System. In *Transportation Research Record 1320*, Transportation Research Board, National Research Council, Washington, D.C., 1991, pp. 3-6.
26. Gettman, D., L. Head, and P. Mirchandani. *RHODES-ITMS Corridor Control Project*. Report FHWA-AZ99-462. The University of Arizona, Tucson, 1999.
27. Tian, Z., K. Balke, R. Engelbrecht, and L. Rilett. Integrated Control Strategies for Surface Street and Freeway Systems. In *Transportation Research Record 1811*, Transportation Research Board, National Research Council, Washington, D.C., 2002, pp. 92-99.
28. Paesani, G.F., J. Kerr, P. Perovich, and F.E. Khosravi. System Wide Adaptive Ramp Metering in Southern California. ITS America 7<sup>th</sup> Annual Meeting, Washington, D.C., 1997.
29. McNally, M.G., J.E. Moore, and C.A. MacCarley. *Documentation of the Irvine Integrated Corridor Freeway Ramp Metering and Arterial Adaptive Control Field Operational Test*. Report UCB-ITS-PRR-2001-2. California PATH Program, Institute of Transportation Studies, University of California at Berkeley, Berkeley, 2001.
30. *Integrated Corridor Traffic Management-Final Evaluation Report*. Booz Allen Hamilton, <http://ntl.bts.gov/data/9xb011.pdf>, 2000.
31. MacCarley, C.A., S.P. Mattingly, M.G. McNally, J.E. Moore, and D.B. Mezger. Lessons Learned from the Irvine Integrated Freeway Ramp Metering/Arterial Adaptive Signal Control Field Operational Test. In *Transportation Research Board 80<sup>th</sup> Annual Meeting Compendium of Papers CD-ROM*, Washington, D.C., 2001.
32. Messer, C.J. *Advanced Freeway System Ramp Metering Strategies for Texas*. Report 1232-23. Texas Transportation Institute, College Station, Texas, 1993.
33. Papageorgiou, M., H. Hadj-Salem, and J. Blosseville. ALINEA: A Local Feedback Control Law for On-Ramp Metering. In *Transportation Research Record 1320*,

- Transportation Research Board, National Research Council, Washington, D.C., 1991, pp. 58-64.
34. Papageorgiou, M., and E. Smaragdis. A Series of New Local Ramp Metering Strategies. In *Transportation Research Board 82<sup>nd</sup> Annual Meeting Compendium of Papers CD-ROM*, Washington, D.C., 2003.
  35. Oh, H., and V.P. Sisiopiku. A Modified ALINEA Ramp Metering Model. In *Transportation Research Board 81<sup>st</sup> Annual Meeting Compendium of Papers CD-ROM*, Washington, D.C., 2002.
  36. Papageorgiou, M., and A. Kotsialos. Freeway Ramp Metering: An Overview. In *Proceedings of the 3<sup>rd</sup> IEEE International Conference on Intelligent Transportation Systems*, IEEE, Dearborn, Michigan, 2000, pp. 228-239.
  37. Papageorgiou, M., H. Hadj-Salem, and F. Middleham. ALINEA Local Ramp Metering: Summary of Field Results. In *Transportation Research Record 1603*, TRANSPORTATION RESEARCH BOARD, National Research Council, Washington, D.C., 1997, pp. 90-98.
  38. Newell, G.G. *Applications of Queuing Theory*, 2<sup>nd</sup> ed. Chapman & Hall, London, 1982.
  39. Pinnell, C., D.R. Drew, W.R. McCasland, and J.A. Wattleworth. *Evaluation of Entrance Ramp Control on a Six-Mile Freeway Section*. Texas Transportation Institute, College Station, Texas, 1966.
  40. May, A.D. *Traffic Flow Fundamentals*. Prentice Hall, Englewood Cliffs, New Jersey, 1990.
  41. Gartner, N. Microscopic Analysis of Traffic Flow Patterns for Minimizing Delay on Signal-Controlled Links. In *Highway Research Record 445*, Highway Research Board, Washington, D.C., 1973, pp. 12-23.
  42. Imada, T., and A.D. May. *FREQ8PE-A Freeway Corridor Simulation and Ramp Metering Optimization Model*. Report UCB-ITS-RR-85-10. California PATH Program, Institute of Transportation Studies, University of California at Berkeley, Berkeley, 1985.
  43. *FREQ10, Version 10, Release 3.0*. California PATH Program, Institute of Transportation Studies, University of California at Berkeley, Berkeley, 2002.

44. Messmer, A. *NETANET, A Simulation Program for Motorway Networks*. Dynamic Systems and Simulation Laboratory, Technical University of Crete, Chania, Greece, 2000.
45. Gettman, D. A Multi-objective Integrated Large-Scale Optimized Ramp Metering Control System for Freeway/Surface-Street Traffic Management. Ph.D. dissertation. The University of Arizona, Tucson, 1998.
46. Papageorgiou, M., J.M. Blosselville, and H. Hadj-Salem. Macroscopic Modeling of Traffic Flow on the Boulevard Peripherique in Paris. *Transportation Research*, Part B, Vol. 23B, No. 1, 1989, pp. 29-47.
47. Zhang, H., and S. Ritchie. An Integrated Traffic Responsive Ramp Control Strategy via Nonlinear State Feedback. In *Transportation Research Board 74<sup>th</sup> Annual Meeting Compendium of Papers*, Washington, D.C., 1995, pp. 11-13.
48. Payne, H. Models of Freeway Traffic and Control. In *Mathematical Models of Public Systems*, La Jolla, California: Simulation Councils, Inc., 1971, pp. 51-61.
49. Payne, H. FREFLO: A Macroscopic Simulation Model of Freeway Traffic. In *Transportation Research Record 722*, Transportation Research Board, National Research Council, Washington, D.C., 1979, pp. 68-77.
50. Hurdle, V.F., and B. Son. Shock Wave and Cumulative Arrival and Departure Models. In *Transportation Research Record 1776*, Transportation Research Board, National Research Council, Washington, D.C., 2001, pp. 159-166.
51. Hall, F.L., and K. Agyemang-Duah. Freeway Capacity Drop and Definition of Capacity. In *Transportation Research Record 1320*, Transportation Research Board, National Research Council, Washington, D.C., 1991, pp. 91-98.
52. Banks, J.H. The Two-Capacity Phenomenon: Some Theoretical Issues. In *Transportation Research Record 1320*, Transportation Research Board, National Research Council, Washington, D.C., 1991, pp. 234-241.
53. Daganzo, C.F. *Fundamentals of Transportation and Traffic Operations*. Elsevier Science Inc., New York, pp. 133-135, 1997.
54. Persaud, B., S. Yagar, D. Tsui, and H. Look. Breakdown-Related Capacity for Freeway with Ramp Metering. In *Transportation Research Record 1748*, Transportation Research Board, National Research Council, Washington, D.C., 2001, pp. 110-115.

55. Nita Rajcoomar, Traffic Analyst, Ministry of Transportation, Ontario, Canada, Personal Communication, April, 2003.
56. Cassidy, M.J., and R.L. Bertini. Some Traffic Features at Freeway Bottlenecks. *Transportation Research*, Part B, Vol. 33, 1999, pp. 25-42.
57. Persaud, B., S. Yagar, and R. Brownlee. Exploration of the Breakdown Phenomenon in Freeway Traffic. In *Transportation Research Record 1634*, Transportation Research Board, National Research Council, Washington, D.C., 1998, pp. 64-69.
58. Lorenz, M.R., and L. Elefteriadou. Defining Freeway Capacity as a Function of the Breakdown Probability. In *Transportation Research Record 1776*, Transportation Research Board, National Research Council, Washington, D.C., 2001, pp. 43-51.
59. Zhang, L., and D. Levinson. Some Properties of Flows at Freeway Bottlenecks. In *Transportation Research Board 83<sup>rd</sup> Annual Meeting Compendium of Papers CD-ROM*, Washington D.C., 2004.
60. Twin Cities Ramp Meter Evaluation. Cambridge Systematics, Inc. <http://www.dot.state.mn.us/rampmeterstudy/pdf/finalreport/tc.pdf>, February, 2001.
61. *A Study of Ramp Meters in Atlanta, Georgia*. Unpublished Report. Office of Traffic Operations, Georgia Department of Transportation, Atlanta, Georgia, 1997.
62. Kang, S., and D. Gillen. *Assessing the Benefits and Costs of Intelligent Transportation Systems: Ramp Meters*. Report UCB-ITS-PRR-99-19. California PATH Program, Institute of Transportation Studies, University of California at Berkeley, Berkeley, 1999.
63. Banks, J.H. Two-Capacity Phenomenon at Freeway Bottlenecks: A Basis for Ramp Metering? In *Transportation Research Record 1320*, Transportation Research Board, National Research Council, Washington, D.C., 1991, pp. 83-89.
64. Ringert, J., and T. Urbanik. Study of Freeway Bottlenecks in Texas. In *Transportation Research Record 1398*, Transportation Research Board, National Research Council, Washington, D.C., 1994, pp. 31-41.
65. Elefteriadou, L., R.P. Roess, and W.R. McShane. Probabilistic Nature of Breakdown at Freeway Merge Junctions. In *Transportation Research Record 1484*, Transportation Research Board, National Research Council, Washington, D.C., 1995, pp. 80-89.

66. Chin, C-S. An Integrated Freeway Corridor Control with Signals, Ramp Meterings, and Route Guidance. Ph.D. dissertation. University of Maryland, College Park, 1993.
67. Papageorgiou, M. An Integrated Control Approach for Traffic Corridors. *Transportation Research*, Part C, Vol. 3, No. 1, 1995, pp. 19-30.
68. Wu, J., and G.L. Chang. An Integrated Optimal Control and Algorithm for Commuting Corridors. *International Transactions in Operational Research*, Vol. 6, 1999, pp. 39-55.
69. Yang, H., and S. Yagar. Some Developments in Traffic Control of Freeway-Arterial Corridor Systems. *Transportation Systems: Theory and Application of Advanced Technology*, Vol. 1, 1995, pp. 293-298.
70. Van Aerde, M., and S. Yagar. Dynamic Integrated Freeway/Traffic Signal Networks: Problems and Proposed Solutions. *Transportation Research*, Part A, Vol. 22A, No. 6, 1988, pp. 445-453.
71. Gordon, R.L. Algorithm for Controlling Spillback from Ramp Meters. In *Transportation Research Record 1554*, Transportation Research Board, National Research Council, Washington, D.C., 1996, pp. 162-171.
72. Chaudhary, N.A., and C.J. Messer. Freeway On-Ramp Design Criteria for Ramp Meters with Excessive Queue Detectors. In *Transportation Research Board 81<sup>st</sup> Annual Meeting Compendium of Papers CD-ROM*, Washington D.C., 2002.
73. Han, B., and R.A. Reiss. Coordinating Ramp Meter Operation with Upstream Intersection Traffic Signal. In *Transportation Research Record 1446*, Transportation Research Board, National Research Council, Washington, D.C., 1994, pp. 44-47.
74. Yuan, L.S., and J.B. Kreer. Adjustment of Freeway Ramp Metering Rates to Balance Entrance Ramp Queues. In *Transportation Research*, Vol. 5, 1969, pp.127-133.
75. Head, L., and P. Mirchandani. *RHODES-ITMS*. Report AZ-SP-9701. Arizona Department of Transportation, Phoenix, 1997.
76. Venglar, S.P., and T. Urbanik. *Real-Time, Multimodal Traffic-Adaptive Diamond Interchange Control System: Laboratory Demonstration*. Report TTI/ITS RCE-95/01. Texas Transportation Institute, College Station, Texas, 1995.



77. Hasan, M., M. Jha, and M. Ben-Akiva. Evaluation of Ramp Control Algorithms Using Microscopic Traffic Simulation. *Transportation Research, Part C*, Vol. 10, No. 3, 2002, pp. 229-256.
78. Chu, L., H.X. Liu, W. Recker, and H.M. Zhang. Development of a Simulation Laboratory for Evaluating Ramp Metering Algorithms. In *Transportation Research Board 81<sup>st</sup> Annual Meeting Compendium of Papers CD-ROM*, Washington, D.C., 2002.
79. Zhang, M., T. Kim, X. Nie, and W. Jin. *Evaluation of On-Ramp Control Algorithms*. Report UCB-ITS-PRR-2001-36. California PATH Program, Institute of Transportation Studies, University of California at Berkeley, Berkeley, 2001.
80. Paramics Modeler, Version 3.0 Users Guide. Quadstone, Ltd., Windsor, United Kingdom, 2000.
81. *CORSIM User Manual, Version 5.2*. Federal Highway Administration, Washington, D.C., 2002.
82. Van Aerde, M. INTEGRATION User's Guide-Volume I and II: Fundamental Model Features and Advanced Model Features. Department of Civil Engineering, Kingston, Ontario, Canada, 2000.
83. *Synchro User's Manual, Version 5.2*. Trafficware, Inc., Berkeley, California, 2003.
84. Ashok, K., and M. Ben-Akiva. Alternative Approaches for Real-Time Estimation and Prediction of Time-Dependent Origin-Destination Flows. In *Transportation Science*, Vol. 34, No. 1, 2000, pp. 21-36.
85. Ploss, G., and H. Keller. Dynamic Estimation of Origin and Destination Flows from Traffic Counts in Networks. In *Proceedings of International Conference on Transportation Systems Studies*, Tata McGraw-Hill, Delhi, India, 1986, pp. 211-221.
86. Dixon, M.P., and L.R. Rilett. Real-Time OD Estimation Using Automatic Vehicle Identification and Traffic Count Data. *Computer-Aided Civil and Infrastructure Engineering*, Vol. 17, Issue 1, 2002, pp 7-21.
87. Mountain, L.J., and P. Westwell. The Accuracy of Estimation of Turning Flows from Automatic Counts. In *Traffic Engineering and Control*, Vol. 24, No. 1, 1983, pp. 3-7.
88. Cowan, R.J. Useful Headway Models. In *Transportation Research*, Vol. 9, No. 6, 1975, pp. 371-375.

89. Sullivan, D.P., and R. Troutbeck. Use of Cowan's M3 headway distribution for modeling urban traffic flow. *Traffic Engineering & Control*, Vol. 35, No. 7/8, 1994, pp. 445-450.
90. Sullivan, D.P., and R. Troutbeck. *Review of Data Collection and Analysis to Produce Headways at a Series of Locations down a Roadway*. Physical Infrastructure Center Research Report 92-19, QUI, Brisbane, Australia, 1992.
91. Tanner, J.C. A Theoretical Analysis of Delays at an Uncontrolled Intersection. *Biometrika*, Vol. 49, 1968, pp. 163-170.
92. Park, E. *Critical Assessment of the Features of Two Ramp Metering Optimization Models*. Ph.D. dissertation. Texas A&M University, College Station, Texas, 1993.
93. Grossmann, M. Methods for Calculation and Judgment of Capacity and Traffic Quality at Intersections without Traffic Signals. Chair of Traffic Engineering, Vol. 9, Ruhr-University Bochum, Germany, 1994.
94. Wu, N., and Z. Tian. Determination of Probability of No Disruption and Freeway Volume Threshold for Ramp Metering Based on Gap Acceptance Theory. Submitted to *Journal of Transportation Research*, Part B, November 2003.
95. Messer, C.J., and J.A. Bonneson. *Capacity Analysis of Interchange Ramp Terminals*. Final Report. NCHRP #3-47, Transportation Research Board, Washington D.C., 1997.
96. Rouphail, N.M., and R.A. Akcelik. A Preliminary Model of Queue Interaction at Signalized Paired Intersections. In *Proc. 16<sup>th</sup> ARRB Conference*, Australian Road Research Board, Ltd., Vermont South, Victoria, Australia, 1998, pp. 325-345.
97. Prosser, N., and M. Dunne. A Procedure for Estimating Movement Capacities at Signalized Paired Intersections. In *Proceedings of the 2<sup>nd</sup> International Symposium on Highway Capacity*, Sydney, Australia, 1994, pp. 473-492.
98. Zhang, L., and D. Levinson. Ramp Metering and Capacity of Active Freeway Bottlenecks. In *83<sup>rd</sup> Annual Meeting Compendium of Papers CD-ROM*, Transportation Research Board, Washington, D.C., January 2004.
99. Tian, Z., T. Urbanik, R. Engelbrecht, and K. Balke. Variations on Capacity and Delay Estimates from Microscopic Simulation Models. In *Transportation Research Record 1802*, Transportation Research Board, National Research Council, Washington, D.C., 2002, pp. 23-31.

100. Tian, Z., N. Wu, and M. Vandahey. Capacity with Short Right-Turn Lane at Signalized Intersections. In *Transportation Research Board 81<sup>st</sup> Annual Meeting Compendium of Papers CD-ROM*, Washington, D.C., 2001.
101. Munoz, J.C., and C.F. Daganzo. The Bottleneck Mechanism of a Freeway Diverge. *Transportation Research*, Part A, Vol. 36A, No. 6, 2002, pp. 483-506.
102. Cassidy, M.J., S.B. Anani, and J.M. Haigwood. Study of Freeway Traffic Near an Off-Ramp. *Transportation Research*, Part A, Vol. 36, No. 6, 2002, pp. 563-572.
103. The NTCIP (National Transportation Communications for ITS Protocol) Guide. AASHTO, ITE, and NEMA. <http://www.ntcip.org/library/documents/pdf/9001v0302b.pdf>, October 2002.

## APPENDIX A

### GLOSSARY

#### PARAMETERS AND VARIABLES

$A_1, A_2, A_3$	= total area (also total delay in veh-sec) during specific portions of the cycle (see Figure 14)
$A(t)$	= cumulative vehicle arrivals at a facility during time interval $t$ , veh
$A_{Rr}(t)$	= cumulative vehicle arrivals at ramp $r$ during time interval $t$ , veh
$A_{Fr}(t)$	= cumulative vehicle arrivals in mainline freeway direction $r$ during time interval $t$ , veh
$B$	= platoon size of freeway on-ramp traffic, sec
$b$	= roadway segment in the flow conservation model (see Equation 35)
$C$	= cycle length, sec
$c$	= capacity for a traffic facility, vph
$c_{ramp}$	= capacity for freeway on-ramp, vph
$c_m$	= capacity for movement $m$ at a diamond interchange, vph
$c_m^j$	= unimpeded capacity of movement $m$ during cycle $j$ (see Equation 46)
$c_{Fr}(t)$	= freeway mainline capacity of direction $r$ during time interval $t$ , vph
$c_F$	= general notation for free-flow capacity, vph
$c_Q$	= general notation for queue-discharge capacity, vph
$c_{Fr}$	= free-flow capacity of direction $r$ , vph
$c_{Qr}$	= queue-discharge capacity of direction $r$ , vph
$D(t)$	= cumulative vehicle departures at a facility during time interval $t$ , veh
$D_{Rr}(t)$	= cumulative vehicle departures at ramp $r$ during time interval $t$ , veh
$D_{Fr}(t)$	= cumulative vehicle departures in freeway direction $r$ during time interval $t$ , veh

$d_{L-T}, d_{L-L}$	= average delays for the internal through and left-turn movements of the left-side diamond interchange, sec/veh
$d_{R-T}, d_{R-L}$	= average delays for the internal through and left-turn movements of the right-side diamond interchange, sec/veh
$F_r(t)$	= randomly generated freeway mainline demand of direction $r$ at time interval $t$ , vph
$F'_r(t)$	= capped freeway mainline arrival flow rate at the point of ramp merge location, vph
$F''_r(t)$	= average mainline arrival flow rate at time $t$ during a ramp-metering interval, vph
$\Delta F_r(t)$	= mainline residual demand at time interval $t$ , vph
$g_{q,i-m}$	= queue discharge portion of the green interval for signal phase $i$ and movement $m$ , sec
$g_i$	= effective green time for phase $i$ , sec
$g_{u,m}^j$	= portion of the green interval when movement $m$ can discharge freely without impedance, sec
$h$	= time headway within ramp traffic platoon, sec
$i$	= phase index, $i = 1, 2, 4, 5, 6, 8$
$j$	= general index for cycle, time interval, gap, etc.
$K_R$	= constant in ALINEA algorithm
$k$	= index for roadway segment
$l_i$	= lost time for phase $i$
$m$	= index for movement at the diamond interchange, $m = 1\sim 14$
$M_r(t)$	= ramp-metering rate at ramp $r$ during time interval $t$ , vph
$M_{r,k}(t)$	= ramp-metering rate at ramp $r$ of segment $k$ during time interval $t$ , vph
$M_{r,min}$	= minimum metering rate for ramp $r$ , vph
$M_{r,max}$	= maximum metering rate for ramp $r$ , vph

$M_o(t)$	= off-ramp traffic flow rate during time interval $t$ , vph
$M_{o,k}(t)$	= off-ramp traffic flow rate of segment $k$ during time interval $t$ , vph
$N_{L-T}(t)$	= number of vehicles in queue at time $t$ , veh
$N'_m$	= queue length for movement $m$ at the start of green of a particular cycle, veh
$N''_m$	= queue length at the time when ramp queue spills back and impedes the discharge of movement $m$ , veh
$NR^j_m$	= portion of the residual queue at the end of cycle $j$ due to ramp queue spillback, veh
$NC^j_m$	= portion of the residual queue at the end of cycle $j$ due to movement $m$ itself over its capacity, veh
$N_m$	= residual queue for movement $m$ from the previous cycle, veh
$N^j_m$	= residual queue for movement $m$ at the end of cycle $j$ , veh
$N^j_i$	= ramp residual queue at the end of phase $i$ during cycle $j$ , veh
$n_k(t)$	= number of vehicles in roadway segment $k$ at time $t$ , veh
$O(t)$	= throughput at a traffic facility during time interval $t$ , vph
$O_{Rr}(t)$	= throughput at ramp $r$ during time interval $t$ , vph
$O_{Fr}(t)$	= freeway mainline throughput of direction $r$ during time interval $t$ , vph
$Q_{M,m}$	= internal queue storage space for left-turn movement $m$ , veh
$O_{L-T}(t)$	= departure flow rate for the left-side interchange internal through movement at time $t$ , vph
$O_{L-L}(t)$	= arrival flow rate for the left-side interchange internal left-turn movement at time $t$ , vph
$O_{R-T}(t)$	= arrival flow rate for the right-side interchange internal through movement at time $t$ , vph
$O_{R-L}(t)$	= arrival flow rate for the right-side interchange internal left-turn movement at time $t$ , vph

$p_l$	= proportion of traffic in lane $l$ on freeway mainline
$p_{m,r}$	= proportion of traffic from movement $m$ to ramp $r$
$P_m$	= proportion of arrival during green for movement $m$
$P_{ND}$	= total probability of no disruption of freeway mainline
$P_{ND,a}$	= probability of no disruption of freeway mainline in case $a$
$P_{ND,b}$	= probability of no disruption of freeway mainline in case $b$
$P_{ND,c}$	= probability of no disruption of freeway mainline in case $c$
$q_{Mm}$	= maximum queue that would exist for movement $m$ (residual plus arrival) during the current cycle, veh
$q(t)$	= queue length at a traffic facility at time interval $t$ , veh
$q_{Fr}(t)$	= freeway mainline queue length of direction $r$ at time interval $t$ , veh
$q_{Rr}(t)$	= queue length at time interval $t$ and ramp $r$ , veh
$Q_{Mm}$	= internal queue storage space for left-turn movement $m$ , veh
$Q_{Rr}$	= queue storage space for ramp $r$ , veh
$r$	= index for freeway direction and metered on-ramp, $r = 1, 2$
$R_r$	= traffic demand at ramp $r$ , vph
$R_r(t)$	= traffic arrival rate at time interval $t$ at ramp $r$ , vph
$R_{off,r}$	= off-ramp $r$ traffic flow, vph
$r_m^j$	= effective red time for movement $m$ in cycle $j$ , sec
$r_i$	= effective red time for phase $i$ , sec
$S_m$	= saturation flow rate for movement $m$ , vph
$S_{Rr}$	= ramp queue flush rate at ramp $r$ , vph
$S_A, S_B$	= saturation flow rates for interchange internal through movements, vph
$S'_m$	= departure flow rate when impeded by the ramp queue, vph

$S_{I0\_11}$ ,	= saturation flow rate for the external arterial approach related to $M10\_11$ , vph
$T$	= analysis period, sec or hr
$\Delta T$	= length of time interval in the traffic flow model, sec
$TT_{2,1}$	= travel time from the right-side to the left-side interchange, sec
$TT_{1,2}$	= travel time from the left-side to the right-side interchange, sec
$TD_{Fr}$	= total freeway mainline delay of direction $r$ , veh-hr
$TD_{Rr}$	= total delay for ramp $r$ , veh-hr
$TD_{Tr}$	= total delay for freeway mainline and ramp of direction $r$ , veh-hr
$TD_{L-L}$	= total delay for left-side internal left-turn movement, veh-sec
$TD_{L-T}$	= total delay for left-side internal through movement, veh-sec
$TD_{R-L}$	= total delay for right-side internal left-turn movement, veh-sec
$TD_{R-T}$	= total delay for right-side internal through movement, veh-sec
$t_j$	= time interval in describing ramp arrival/departure flow profiles, sec
$u_m$	= throughput for movement $m$ , vph
$U_{L-T}(t)$	= arrival flow rate at time $t$ for left-side internal through movement, veh
$U_{L-L}(t)$	= arrival flow rate at time $t$ for left-side internal left-turn movement, veh
$U_{R-T}(t)$	= arrival flow rate at time $t$ for right-side internal through movement, veh
$U_{R-L}(t)$	= arrival flow rate at time $t$ for right-side internal left-turn movement, veh
$v_{o,d}$	= origin-destination demand from origin $o$ to destination $d$ , veh/hr
$v$	= flow rate in the flow conservation model (see Equation 35), veh/sec
$v_k(t)$	= flow rate at roadway segment $k$ at time $t$ , veh/sec
$VO_o$	= total demand for origin $o$ , vph
$VD_d$	= total demand for destination $d$ , vph



$V_{lj}$	= traffic flow rate in freeway lane $j$ , vph
$V_m$	= average traffic demand for movement $m$ , vph
$V_T$	= mainline volume threshold for ramp metering $m$ , vph
$V'_m$	= estimated average traffic demand for movement $m$ , vph
$V_{m-r}^j$	= traffic demand from movement $m$ to ramp $r$ during cycle $j$ , vph
$V_m^j$	= traffic demand for movement $m$ during cycle $j$ , vph
$V(t)$	= traffic demand at a facility, vph
$V_{Rr}(t)$	= portion of the discharging flow from the diamond signal that would arrive ramp $r$ during time interval $t$ , vph
$V_{Wr}(t)$	= unimpeded demand flow during time interval $t$ for ramp $r$ , vph
$V_{Mr}(t)$	= maximum portion of the discharging flow from the diamond interchange signal that would arrive at ramp $r$ during time interval $t$ , vph
$V_{Br}(t)$	= portion of the discharging flow that would result in queue spillback at ramp $r$ during time interval $t$ , vph
$V_F$	= freeway mainline demand, vph
$V_{Fr}$	= freeway mainline demand of direction $r$ , vph
$W_j$	= ramp arrival flow rate during time period $t_{j-1}$ and $t_j$ of a particular cycle, vph
$x_m$	= v/c ratio for movement $m$
$x_R$	= v/c ratio for freeway on-ramp
$x_{10\_11}$	= v/c ratio for external movement on the arterial related to $M10$ and $M11$
$y_m$	= ratio of demand to saturation flow rate for movement $m$
$\phi_i$	= phase duration for phase $i$ , sec
$\Phi$	= overlap phase duration in four-phase scheme, sec
$\sigma_{Fr}$	= standard deviation of free-flow capacity for mainline direction $r$ , veh

$\sigma_{Qr}$	= standard deviation of queue-discharge capacity for mainline direction $r$ , veh
$\gamma$	= flow cap factor, 1.2 (see Equation 92)
$\eta$	= breakdown factor, 1.2 ~ 1.5 (see Equation 95)
$\omega$	= ramp-metering equivalency factor, 1/1.83
$\alpha_{m,r}$	= lower limit for the proportion of movement $m$ traffic going to ramp $r$
$\beta_{m,r}$	= upper limit for the proportion of movement $m$ traffic going to ramp $r$
$\rho$	= density, veh/mile
$f_\rho$	= a calibration factor for density
$\pi_m$	= optimal (target) freeway mainline occupancy, %
$\pi(t)$	= occupancy level during time interval $t$ , %
$\mu$	= vehicle speed, mph
$\mu_{s,k}(t)$	= shockwave speed at segment $k$ and time $t$ , mph
$\tau^j$	= $j^{\text{th}}$ gap on lane 1 of freeway mainline, sec
$\tau_{c,l}$	= critical gap for traffic to merge into freeway lane $l$ , sec
$\tau_f$	= on-ramp traffic follow-up time, sec
$\varepsilon$	= proportion of free vehicles in a traffic stream
$\delta$	= minimum headway in a traffic stream, sec
$\lambda$	= average flow rate of a Poisson arrival process, veh/sec
$\theta$	= flow rate within non-bunched vehicles, veh/sec
$\Delta_k$	= length of roadway segment $k$ , mile

**ACRONYMS**

IDIRMS = integrated diamond interchange ramp-metering system

DRIVE = diamond interchange ramp metering integration via evaluation

ICS = integrated control strategies

Mm = movement *m*

Rr = ramp *r*

## APPENDIX B

### VAP CODE

#### B1. DIAMOND SIGNAL CONTROL

```

PROGRAM One;
/* This is the VAP code for Diamond Interchange Signal */

CONST

Integration = 1, /* 1 - Yes; 0 - No */
ControlType = 1, /* 1 - Fixed; 2 - Actuated; 3 - No Signal Control */
Phasing = 4, /* 3 - Basic 3-phase; 4 - TTI 4-phase */
Overlap = 11, /* overlap phase used for TTI-4-Phase, in sec */

OffRampR1Det = 10,
OffRampR2Det = 11,
QueueBlockR1Det = 20,
QueueBlockR2Det = 21,
ArtRightDet = 30,
ArtLeftDet = 40,
ArtRightDetMid = 50,
ArtLeftDetMid = 70,
OffRampR1DetMid = 60,
OffRampR2DetMid = 61,
QueueCountInterval = 20,
Queue_Threshold = 0.60;

ARRAY
tAmber[8] = [4,4,4,4,4,4,4,4],
FixPhaseSplit3[8] = [41,19,0,40,24,36,0,40], /*3-phase, 100 sec cycle */
FixPhaseSplit4[8] = [45,20,0,35,34,31,0,35], /*4-phase, 100 sec cycle */
CycleLength[1]= [100],

/*****
**** TTI 4- Phase Control Fixed ****
*****/

SUBROUTINE TTI4PhaseFix;

IF (Integration) THEN
  tAmber2 := tAmber[2];
  tAmber4 := tAmber[4];
  tAmber6 := tAmber[6];
  tAmber8 := tAmber[8];
  tAmber1 := tAmber[1];
  tAmber5 := tAmber[5];

  IF (OffRampR1QueueSpill) OR (OffRampR1QueueSpill) OR (ArtRightQueueSpill) OR
  (ArtLeftQueueSpill) THEN
    /* Any Queue spill on these locations would go back to normal timing */
    PhaseSplit2 := FixPhaseSplit4[2];
    PhaseSplit4 := FixPhaseSplit4[4];
    PhaseSplit6 := FixPhaseSplit4[6];
    PhaseSplit8 := FixPhaseSplit4[8];
    PhaseSplit1 := FixPhaseSplit4[1];
    PhaseSplit5 := FixPhaseSplit4[5];
  ELSE
    IF (BlockR1 = 0) AND (BlockR2 = 0) THEN
      IF (OffRampR1MidQueueSpill) THEN /*favor Left Frontage Road */
        PhaseSplit2 := FixPhaseSplit4[2] - CycleLength[1]*0.10;
        PhaseSplit4 := FixPhaseSplit4[4] + CycleLength[1]*0.10;
        PhaseSplit6 := FixPhaseSplit4[6];

```

```

PhaseSplit8 := FixPhaseSplit4[8];
PhaseSplit1 := FixPhaseSplit4[1];
PhaseSplit5 := FixPhaseSplit4[5];
ELSE
  IF (OffRampR2MidQueueSpill) THEN /*favor RT F.Road */
    PhaseSplit2 := FixPhaseSplit4[2];
    PhaseSplit4 := FixPhaseSplit4[4];
    PhaseSplit6 := FixPhaseSplit4[6] -
      CycleLength[1]*0.10;
    PhaseSplit8 := FixPhaseSplit4[8] +
      CycleLength[1]*0.10;
    PhaseSplit1 := FixPhaseSplit4[1];
    PhaseSplit5 := FixPhaseSplit4[5];
  ELSE
    IF (ArtRightMidQueueSpill) THEN /*favor artRT*/
      PhaseSplit2 := FixPhaseSplit4[2];
      PhaseSplit4 := FixPhaseSplit4[4] -
        CycleLength[1]*0.10;
      PhaseSplit6 := FixPhaseSplit4[6] +
        CycleLength[1]*0.10;
      PhaseSplit8 := FixPhaseSplit4[8] -
        CycleLength[1]*0.10;
      PhaseSplit1 := FixPhaseSplit4[1] +
        CycleLength[1]*0.10;
      PhaseSplit5 := FixPhaseSplit4[5];
    ELSE
      IF (ArtLeftMidQueueSpill) THEN /*ArtLT */
        PhaseSplit2 := FixPhaseSplit4[2] +
          CycleLength[1]*0.10;
        PhaseSplit4 := FixPhaseSplit4[4] -
          CycleLength[1]*0.10;
        PhaseSplit6 := FixPhaseSplit4[6];
        PhaseSplit8 := FixPhaseSplit4[8] -
          CycleLength[1]*0.10;
        PhaseSplit1 := FixPhaseSplit4[1];
        PhaseSplit5 := FixPhaseSplit4[5] +
          CycleLength[1]*0.10;
      ELSE /*Normal*/
        PhaseSplit2 := FixPhaseSplit4[2];
        PhaseSplit4 := FixPhaseSplit4[4];
        PhaseSplit6 := FixPhaseSplit4[6];
        PhaseSplit8 := FixPhaseSplit4[8];
        PhaseSplit1 := FixPhaseSplit4[1];
        PhaseSplit5 := FixPhaseSplit4[5];
      END;
    END;
  END;
END;

Else
  IF (BlockR1) AND (BlockR2 = 0) THEN
    Trace (variable(BlockR1));
    Trace (variable(BlockR2));
    Trace (variable(PhaseSplit8));

    IF (ArtLeftMidQueueSpill) THEN /*hold p.2 */
      PhaseSplit2 := 200;
      PhaseSplit4 := 12;
      PhaseSplit6 := Overlap;
      PhaseSplit8 := 12;
      PhaseSplit1 := 0;
      PhaseSplit5 := 0;
    ELSE /*hold p.8*/
      PhaseSplit2 := Overlap;
      PhaseSplit4 := 12;
      PhaseSplit6 := Overlap;
      PhaseSplit8 := 200;
    END;
  END;

```

```

PhaseSplit1 := 0;
PhaseSplit5 := 0;
END;
ELSE
  IF (BlockR1 = 0) AND (BlockR2) THEN
    IF (ArtRightMidQueueSpill) THEN /*hold p.6 */
      PhaseSplit2 := Overlap;
      PhaseSplit4 := 12;
      PhaseSplit6 := 200;
      PhaseSplit8 := 12;
      PhaseSplit1 := 0;
      PhaseSplit5 := 0;
    ELSE /*hold p.4*/
      PhaseSplit2 := Overlap;
      PhaseSplit4 := 200;
      PhaseSplit6 := Overlap;
      PhaseSplit8 := 12;
      PhaseSplit1 := 0;
      PhaseSplit5 := 0;
    END;
  ELSE /*both block, hold p.8*/
    PhaseSplit2 := Overlap;
    PhaseSplit4 := 12;
    PhaseSplit6 := Overlap;
    PhaseSplit8 := 200;
    PhaseSplit1 := 0;
    PhaseSplit5 := 0;
  END;
END;
END;
END;
ELSE
  PhaseSplit2 := FixPhaseSplit4[2];
  PhaseSplit4 := FixPhaseSplit4[4];
  PhaseSplit6 := FixPhaseSplit4[6];
  PhaseSplit8 := FixPhaseSplit4[8];
  PhaseSplit1 := FixPhaseSplit4[1];
  PhaseSplit5 := FixPhaseSplit4[5];
  tAmber2 := tAmber[2];
  tAmber4 := tAmber[4];
  tAmber6 := tAmber[6];
  tAmber8 := tAmber[8];
  tAmber1 := tAmber[1];
  tAmber5 := tAmber[5];
END;
IF t_green(2) THEN
  IF t_green(2) >= (Overlap - tAmber8) THEN
    sg_red(8); /* phase 8 green ends, red starts after yellow */
    Start(Phase8ClearTimer);
  END;
  IF t_green(2) >= (PhaseSplit2 - tAmber2) THEN
    sg_red(2);
    start(Phase2ClearTimer);
  END;
END;
IF t_green(4) THEN
  IF t_green(4) >= (PhaseSplit4 - Overlap - tAmber5) THEN
    IF t_green(5) then
      sg_red(5); /*phase 5 green ends, red starts after yellow */
      Start(Phase5ClearTimer);
    END;
  END;

```

```

        END;

        IF t_green(4) >= (PhaseSplit4 - tAmber4) THEN
            sg_red(4);
            Start(Phase4ClearTimer);
        END;
    END;

    IF t_green(6) THEN
        IF t_green(6) >= (Overlap - tAmber4) THEN
            sg_red(4);
            Start(Phase4ClearTimer);
        END;

        IF t_green(6) >= (PhaseSplit6 - tAmber6) THEN
            sg_red(6);
            start(Phase6ClearTimer);
        END;
    END;

    IF t_green(8) THEN
        IF t_green(8) >= (PhaseSplit8 - Overlap - tAmber1) THEN
            sg_red(1);
            Start(Phase1ClearTimer);
        END;

        IF t_green(8) >= (PhaseSplit8 - tAmber8) THEN
            sg_red(8);
            Start(Phase8ClearTimer);
        END;
    END;

    /*****
    /**** YELLOW TIMERS ****/
    /*****/

    IF (Phase8ClearTimer >= tAmber8) THEN
        sg_green(5);
        stop(Phase8ClearTimer);
        reset(Phase8ClearTimer);
    END;

    IF (Phase2ClearTimer >= tAmber2) THEN
        sg_green(4);
        stop(Phase2ClearTimer);
        reset(Phase2ClearTimer);
    END;
    IF (Phase4ClearTimer >= tAmber4) THEN
        sg_green(1);
        stop(Phase4ClearTimer);
        reset(Phase4ClearTimer);
    END;
    IF (Phase6ClearTimer >= tAmber6) THEN
        sg_green(8);
        stop(Phase6ClearTimer);
        reset(Phase6ClearTimer);
    END;

    IF (Phase1ClearTimer >= tAmber1) THEN
        sg_green(2);
        stop(Phase1ClearTimer);
        reset(Phase1ClearTimer);
    END;

    IF (Phase5ClearTimer >= tAmber5) THEN
        sg_green(6);
        stop(Phase5ClearTimer);

```

```

        reset(Phase5ClearTimer);
END.

/*****
/**** Basic 3- Phase Control Fixed ****
/****
SUBROUTINE Basic3PhaseFix;

IF (Integration) THEN
    /*Trace(variable(AvgOccup_BlockR1Det ));*/
    tAmber2 := tAmber[2];
    tAmber4 := tAmber[4];
    tAmber6 := tAmber[6];
    tAmber8 := tAmber[8];
    tAmber1 := tAmber[1];
    tAmber5 := tAmber[5];
    IF (BlockR1) OR (BlockR2) THEN
        IF (OffRampR1QueueSpill) OR (OffRampR2QueueSpill) OR (ArtRightQueueSpill)
            OR (ArtLeftQueueSpill) THEN

            /* Any Queue spill on these locations would run another timing */
            PhaseSplit2 := FixPhaseSplit3[2];
            PhaseSplit4 := FixPhaseSplit3[4];
            PhaseSplit6 := FixPhaseSplit3[6];
            PhaseSplit8 := FixPhaseSplit3[8];
            PhaseSplit1 := FixPhaseSplit3[1];
            PhaseSplit5 := FixPhaseSplit3[5];

        ELSE
            IF (ArtRightMidQueueSpill) OR (ArtLeftMidQueueSpill) THEN
                /* hold p.6 and p.2 */
                PhaseSplit2 := 100;
                PhaseSplit4 := 10;
                PhaseSplit6 := 100;
                PhaseSplit8 := 10;
                PhaseSplit1 := 200;
                PhaseSplit5 := 200;
            ELSE /*hold p. 1 and p.5 */
                PhaseSplit2 := 10;
                PhaseSplit4 := 10;
                PhaseSplit6 := 10;
                PhaseSplit8 := 10;
                PhaseSplit1 := 200;
                PhaseSplit5 := 200;
            END;

            Trace (variable(PhaseSplit1));
            Trace (variable(PhaseSplit2));
            Trace (variable(PhaseSplit4));
            Trace (variable(PhaseSplit5));
            Trace (variable(PhaseSplit6));
            Trace (variable(PhaseSplit8));
        END;
    ELSE
        IF (ArtRightMidQueueSpill) THEN
            PhaseSplit2 := FixPhaseSplit3[2];
            PhaseSplit4 := FixPhaseSplit3[4] - CycleLength[1]*0.10;
            PhaseSplit6 := FixPhaseSplit3[6] + CycleLength[1]*0.10;
            PhaseSplit8 := FixPhaseSplit3[8] - CycleLength[1]*0.10;
            PhaseSplit1 := FixPhaseSplit3[1] + CycleLength[1]*0.10;
            PhaseSplit5 := FixPhaseSplit3[5];
        ELSE
            IF (ArtLeftMidQueueSpill) THEN
                PhaseSplit2 := FixPhaseSplit3[2] + CycleLength[1]*0.10;
                PhaseSplit4 := FixPhaseSplit3[4] - CycleLength[1]*0.10;
                PhaseSplit6 := FixPhaseSplit3[6];
                PhaseSplit8 := FixPhaseSplit3[8] - CycleLength[1]*0.10;
                PhaseSplit1 := FixPhaseSplit3[1];
            END;
        END;
    END;
END.

```



```

PhaseSplit5 := FixPhaseSplit3[5] + CycleLength[1]*0.10;
ELSE
  IF (OffRampR1MidQueueSpill) OR (OffRampR2MidQueueSpill)
    THEN
      PhaseSplit2 := FixPhaseSplit3[2] -
        CycleLength[1]*0.10;
      PhaseSplit4 := FixPhaseSplit3[4] +
        CycleLength[1]*0.10;
      PhaseSplit6 := FixPhaseSplit3[6] -
        CycleLength[1]*0.10;
      PhaseSplit8 := FixPhaseSplit3[8] +
        CycleLength[1]*0.10;
      PhaseSplit1 := FixPhaseSplit3[1];
      PhaseSplit5 := FixPhaseSplit3[5];
    ELSE
      PhaseSplit2 := FixPhaseSplit3[2];
      PhaseSplit4 := FixPhaseSplit3[4];
      PhaseSplit6 := FixPhaseSplit3[6];
      PhaseSplit8 := FixPhaseSplit3[8];
      PhaseSplit1 := FixPhaseSplit3[1];
      PhaseSplit5 := FixPhaseSplit3[5];
    END;
  END;
END;
ELSE
  PhaseSplit2 := FixPhaseSplit3[2];
  PhaseSplit4 := FixPhaseSplit3[4];
  PhaseSplit6 := FixPhaseSplit3[6];
  PhaseSplit8 := FixPhaseSplit3[8];
  PhaseSplit1 := FixPhaseSplit3[1];
  PhaseSplit5 := FixPhaseSplit3[5];
  tAmber2 := tAmber[2];
  tAmber4 := tAmber[4];
  tAmber6 := tAmber[6];
  tAmber8 := tAmber[8];
  tAmber1 := tAmber[1];
  tAmber5 := tAmber[5];
END;
IF t_green(2) THEN
  IF t_green(2) >= (PhaseSplit2-tAmber2) THEN
    sg_red(2);
    start(Phase2ClearTimer);
  END;
END;
IF t_green(4) THEN
  IF t_green(4) >= (PhaseSplit4-tAmber4) THEN
    sg_red(4);
    Start(Phase4ClearTimer);
    sg_red(8);
    Start(Phase8ClearTimer);
  END;
END;
IF t_green(6) THEN
  IF t_green(6) >= (PhaseSplit6-tAmber6) THEN
    sg_red(6);
    start(Phase6ClearTimer);
  END;
END;
IF t_green(8) THEN
  IF t_green(8) >= (PhaseSplit8-tAmber8) THEN
    sg_red(8);
    Start(Phase8ClearTimer);
  END;
END;

```

```

        sg_red(4);
        Start(Phase4ClearTimer);
    END;
END;

IF t_green(1) THEN
    IF t_green(1) >= (PhaseSplit1-tAmber1) THEN
        sg_red(1);
        Start(Phase1ClearTimer);
        sg_red(5);
        Start(Phase5ClearTimer);
    END;
END;

IF t_green(5) THEN
    IF t_green(5) >= (PhaseSplit5-tAmber5) THEN
        sg_red(5);
        Start(Phase5ClearTimer);
        sg_red(1);
        Start(Phase1ClearTimer);
    END;
END;

/*****
/**** YELLOW TIMERS ****
/****
IF (Phase8ClearTimer >= tAmber8) THEN
    sg_green(6);
    sg_green(2);
    stop(Phase8ClearTimer);
    reset(Phase8ClearTimer);
END;
IF (Phase2ClearTimer >= tAmber2) THEN
    sg_green(1);
    stop(Phase2ClearTimer);
    reset(Phase2ClearTimer);
END;
IF (Phase4ClearTimer >= tAmber4) THEN
    sg_green(2);
    sg_green(6);
    stop(Phase4ClearTimer);
    reset(Phase4ClearTimer);
END;
IF (Phase6ClearTimer >= tAmber6) THEN
    sg_green(5);
    stop(Phase6ClearTimer);
    reset(Phase6ClearTimer);
END;

IF (Phase1ClearTimer >= tAmber1) THEN
    sg_green(4);
    sg_green(8);
    stop(Phase1ClearTimer);
    reset(Phase1ClearTimer);
END;

IF (Phase5ClearTimer >= tAmber5) THEN
    sg_green(8);
    sg_green(4);
    stop(Phase5ClearTimer);
    reset(Phase5ClearTimer);
END.

/*=====*/
/*End of 3-phase fixed */
/*=====*/

SUBROUTINE NoSignalControl;

```

```

sg_green(2);
sg_green(4);
sg_green(6);
sg_green(8);
sg_green(1);
sg_green(5).

/*****
/**** BEGIN MAIN SECTION ****
/****

START (QueueTimer);

IF QueueTimer = (QueueCountInterval + 1) THEN
  AvgOccup_OffRampR1Det := Occup_OffRampR1Det / QueueCountInterval;
  AvgOccup_OffRampR2Det := Occup_OffRampR2Det / QueueCountInterval;
  AvgOccup_ArtRightDet := Occup_ArtRightDet / QueueCountInterval;
  AvgOccup_ArtLeftDet := Occup_ArtLeftDet / QueueCountInterval;
  AvgOccup_BlockR1Det := Occup_BlockR1Det / QueueCountInterval;
  AvgOccup_BlockR2Det := Occup_BlockR2Det / QueueCountInterval;
  AvgOccup_ArtRightDetMid := Occup_ArtRightDetMid / QueueCountInterval;
  AvgOccup_ArtLeftDetMid := Occup_ArtLeftDetMid / QueueCountInterval;
  AvgOccup_OffRampR1DetMid := Occup_OffRampR1DetMid / QueueCountInterval;
  AvgOccup_OffRampR2DetMid := Occup_OffRampR2DetMid / QueueCountInterval;

  OffRampR1QueueSpill := AvgOccup_OffRampR1Det >= Queue_Threshold;
  OffRampR2QueueSpill := AvgOccup_OffRampR2Det >= Queue_Threshold;
  OffRampR1MidQueueSpill := AvgOccup_OffRampR1DetMid >= Queue_Threshold;
  OffRampR2MidQueueSpill := AvgOccup_OffRampR2DetMid >= Queue_Threshold;
  ArtRightQueueSpill := AvgOccup_ArtRightDet >= Queue_Threshold;
  ArtRightMidQueueSpill := AvgOccup_ArtRightDetMid >= Queue_Threshold;
  ArtLeftQueueSpill := AvgOccup_ArtLeftDet >= Queue_Threshold;
  ArtLeftMidQueueSpill := AvgOccup_ArtLeftDetMid >= Queue_Threshold;
  BlockR1 := AvgOccup_BlockR1Det >= Queue_Threshold;
  BlockR2 := AvgOccup_BlockR2Det >= Queue_Threshold;

  RESET (QueueTimer);
  Occup_OffRampR1Det := 0;
  Occup_OffRampR2Det := 0;
  Occup_OffRampR1DetMid := 0;
  Occup_OffRampR2DetMid := 0;
  Occup_ArtRightDet := 0;
  Occup_ArtRightDetMid := 0;
  Occup_ArtLeftDet := 0;
  Occup_ArtLeftDetMid := 0;
  Occup_BlockR1Det := 0;
  Occup_BlockR2Det := 0;

ELSE
  Occup_OffRampR1Det := Occup_OffRampR1Det + Occup_rate (OffRampR1Det);
  Occup_OffRampR2Det := Occup_OffRampR2Det + Occup_rate (OffRampR2Det);
  Occup_OffRampR1DetMid := Occup_OffRampR1DetMid + Occup_rate (OffRampR1DetMid);
  Occup_OffRampR2DetMid := Occup_OffRampR2DetMid + Occup_rate (OffRampR2DetMid);
  Occup_ArtRightDet := Occup_ArtRightDet + Occup_rate (ArtRightDet);
  Occup_ArtRightDetMid := Occup_ArtRightDetMid + Occup_rate (ArtRightDetMid);
  Occup_ArtLeftDet := Occup_ArtLeftDet + Occup_rate (ArtLeftDet);
  Occup_ArtLeftDetMid := Occup_ArtLeftDetMid + Occup_rate (ArtLeftDetMid);
  Occup_BlockR1Det := Occup_BlockR1Det + Occup_rate (QueueBlockR1Det);
  Occup_BlockR2Det := Occup_BlockR2Det + Occup_rate (QueueBlockR2Det);

END;

IF ControlType = 1 THEN
  IF Phasing = 3 THEN
    GOSUB Basic3PhaseFix;
  ELSE
    GOSUB TTI4PhaseFix;
  END;
END.

```

## B2. RAMP-METERING CONTROL

```

PROGRAM RampMeter;
/** This is the Ramp-Metering Code **/

CONST
/** select ALGORITHM to run **/

Integration = 1, /* 1 - Yes; 0 - No. Selecting "Yes" would flush meter when off-ramp
spillback */
Algorithm = 2, /* 1 - ALINEA; 2 - Fixed; 3 - No Meter; 4 - Ramp closure **/
QueueOverride = 1, /* 1 - queue override; 0 - no queue override **/

QueueCountInterval = 20,
OccupancyInterval = 20,
GreenInterval = 2.0,
KR = 70, /* ALINEA constant **/
MaxRate = 1800,
MinRate = 400,
FixedRate = 720, /* fixed metering, only rates at: 400, 450, 515, 600, 720, 900, 1200 */
NumberOfDetectors = 4, /* total num. of downstream detectors **/
ddl = 6, dd2 = 9, dd3 = 10, dd4 = 11, /*downstream detector numbers **/
NumberMeterLane = 1,
d_Presence1 = 5, /* presence detector-Lane 1 **/
/*d_Presence2 = 12,*/ /* presence detector-Lane 2 **/
QueueDetector_Advance = 4,
QueueDetector_OffRamp = 10,
QueueDetector_ArtRight = 30,
QueueDetector_ArtLeft = 40,
Occupancy_Opt = 0.16, /* optimal or target occupancy **/
Occupancy_Threshold = 0.010, /* threshold to metering **/
Queue_Threshold = 0.60, /* for ramp queue detection **/

/* Data Collection Parameters */
StartTime = 600,
EndTime = 12000;

SUBROUTINE ALINEA;

IF CountTimer = OccupancyInterval THEN
  TRACE (variable (MeterPrevious));
  IF OccupancyInterval = 1 THEN /* set interval to 1-sec for reporting **/
    AverageOcc := (Occup_rate (ddl) + Occup_rate (dd2) + Occup_rate (dd3) +
      Occup_rate (dd4))/NumberOfDetectors;
    AvgOccup_DownStreamDet := AverageOcc;
  ELSE
    AvgOccup_DownStreamDet := Occup_DetDownStream / (OccupancyInterval);
  END;

  IF AvgOccup_DownStreamDet < Occupancy_Threshold THEN
    MeterRate := 80000;
  ELSE
    MeterRate := MeterPrevious + KR*(Occupancy_Opt -
      AvgOccup_DownStreamDet)*100;
  END;

  IF MeterRate >= MaxRate THEN
    MeterRate := MaxRate;
    RedInt := (3600/MeterRate)*NumberMeterLane - GreenInterval;
    MeterPrevious := MeterRate;
  ELSE
    IF MeterRate <= MinRate THEN
      MeterRate := MinRate;
      RedInt := (3600/MeterRate)*2 - GreenInterval;
      MeterPrevious := MeterRate;
    ELSE

```

```

        RedInt := (3600/MeterRate)*2 - GreenInterval;
        MeterPrevious := MeterRate;
    END;
END;

SumVeh := rear_ends(dd1) + rear_ends(dd2) + rear_ends(dd3) + rear_ends(dd4);
FlowRate := (SumVeh/OccupancyInterval) * 3600;

TRACE (variable (AvgOccup_DownStreamDet, FlowRate));
TRACE (variable (MeterRate, RedInt));

RESET(CountTimer);
Occup_DetDownStream := 0;
clear_rear_ends(dd1);
clear_rear_ends(dd2);
clear_rear_ends(dd3);
clear_rear_ends(dd4);

ELSE
    AverageOcc := (Occup_rate (dd1) + Occup_rate (dd2) + Occup_rate (dd3) +
        Occup_rate (dd4))/NumberOfDetectors;
    Occup_DetDownStream := Occup_DetDownStream + AverageOcc;

END.

/*****
SUBROUTINE FixedMeter;

    MeterRate := FixedRate;
    RedInt := (3600/MeterRate)*NumberMeterLane - GreenInterval.
*****/

SUBROUTINE MeterOperation;

/*****
/**** METERING OPERATIONS *****/
/*****
/*Single-lane meter */

IF t_green(1) >= GreenInterval THEN
    IF (QueueOverride AND QueueSpill) AND (Integration = 0) THEN
        MeterPrevious := MaxRate; /** Do not start red **/
        IF (SimuTime >= StartTime) AND (SimuTime < EndTime) THEN
            MeterFlushTime := MeterFlushTime + 1;
            TRACE (variable (SimuTime,MeterFlushTime));
        END;
    ELSE
        IF (OffRampSpill OR ArtRightSpill OR ArtLeftSpill) AND (Integration) AND
            (QueueSpill) THEN
            MeterPrevious := MaxRate; /** Do not start red **/
            IF (SimuTime >= StartTime) AND (SimuTime < EndTime) THEN
                MeterFlushTime := MeterFlushTime + 1;
                TRACE (variable (SimuTime,MeterFlushTime));
            END;
        ELSE
            sg_red(1);
        END;
    END;
END;

IF (t_red(1) >= RedInt) THEN /*Red has the desired metering rate */
    IF Occupancy(d_Presencel) > 0 THEN
        sg_green(1);
        START (greenTimer1);
    END;
END;

IF greenTimer1 >= GreenInterval THEN

```

```

IF (QueueOverride AND QueueSpill) THEN
    MeterPrevious := MaxRate; /** Do not start red **/
ELSE
    IF (OffRampSpill OR ArtRightSpill OR ArtLeftSpill) AND (Integration) AND
        (QueueSpill) THEN
        MeterPrevious := MaxRate; /** Do not start red **/
    ELSE
        sg_red(1);
    END;
END;
RESET (greenTimer1);
STOP (greenTimer1);

END.

/*****
/**** This is the main routine ****
*****/

START(QueueTimer);
START(CountTimer);
SimuTime := SimuTime + 1;

IF QueueTimer = (QueueCountInterval + 1) THEN
    AvgOccup_AdvanceQueueDet := Occup_AdvanceQueueDet / QueueCountInterval;
    AvgOccup_OffRampQueueDet := Occup_OffRampQueueDet / QueueCountInterval;
    AvgOccup_ArtRightQueueDet := Occup_ArtRightQueueDet / QueueCountInterval;
    AvgOccup_ArtLeftQueueDet := Occup_ArtLeftQueueDet / QueueCountInterval;
    QueueSpill := AvgOccup_AdvanceQueueDet >= Queue_Threshold;
    OffRampSpill := AvgOccup_OffRampQueueDet >= Queue_Threshold;
    ArtRightSpill := AvgOccup_ArtRightQueueDet >= Queue_Threshold;
    ArtLeftSpill := AvgOccup_ArtLeftQueueDet >= Queue_Threshold;
    RESET (QueueTimer);
    Occup_AdvanceQueueDet := 0;
    Occup_OffRampQueueDet := 0;
    Occup_ArtRightQueueDet := 0;
    Occup_ArtLeftQueueDet := 0;

ELSE
    Occup_AdvanceQueueDet := Occup_AdvanceQueueDet + Occup_rate
        (QueueDetector_Advance);
    Occup_OffRampQueueDet := Occup_OffRampQueueDet + Occup_rate
        (QueueDetector_OffRamp);
    Occup_ArtRightQueueDet := Occup_ArtRightQueueDet + Occup_rate
        (QueueDetector_ArtRight);
    Occup_ArtLeftQueueDet := Occup_ArtLeftQueueDet + Occup_rate
        (QueueDetector_ArtLeft);
END;

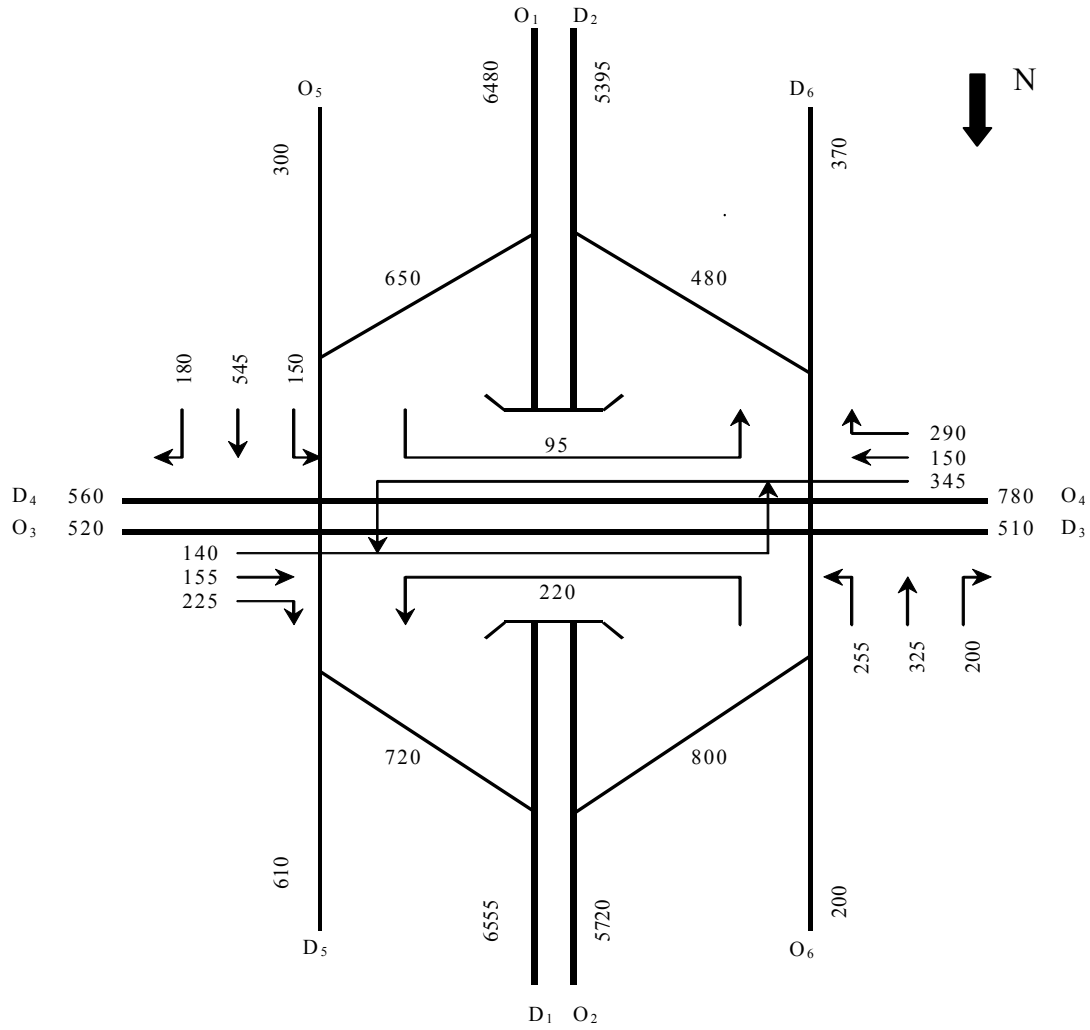
IF Algorithm = 1 THEN
    GOSUB ALINEA;
    GOSUB MeterOperation;
ELSE
    IF Algorithm = 2 THEN
        GOSUB FixedMeter;
        GOSUB MeterOperation;
    ELSE
        IF Algorithm = 3 THEN
            GOSUB NoMeter;
        ELSE
            IF Algorithm = 4 THEN
                GOSUB RampClose;
            END;
        END;
    END;
END;

END.

```

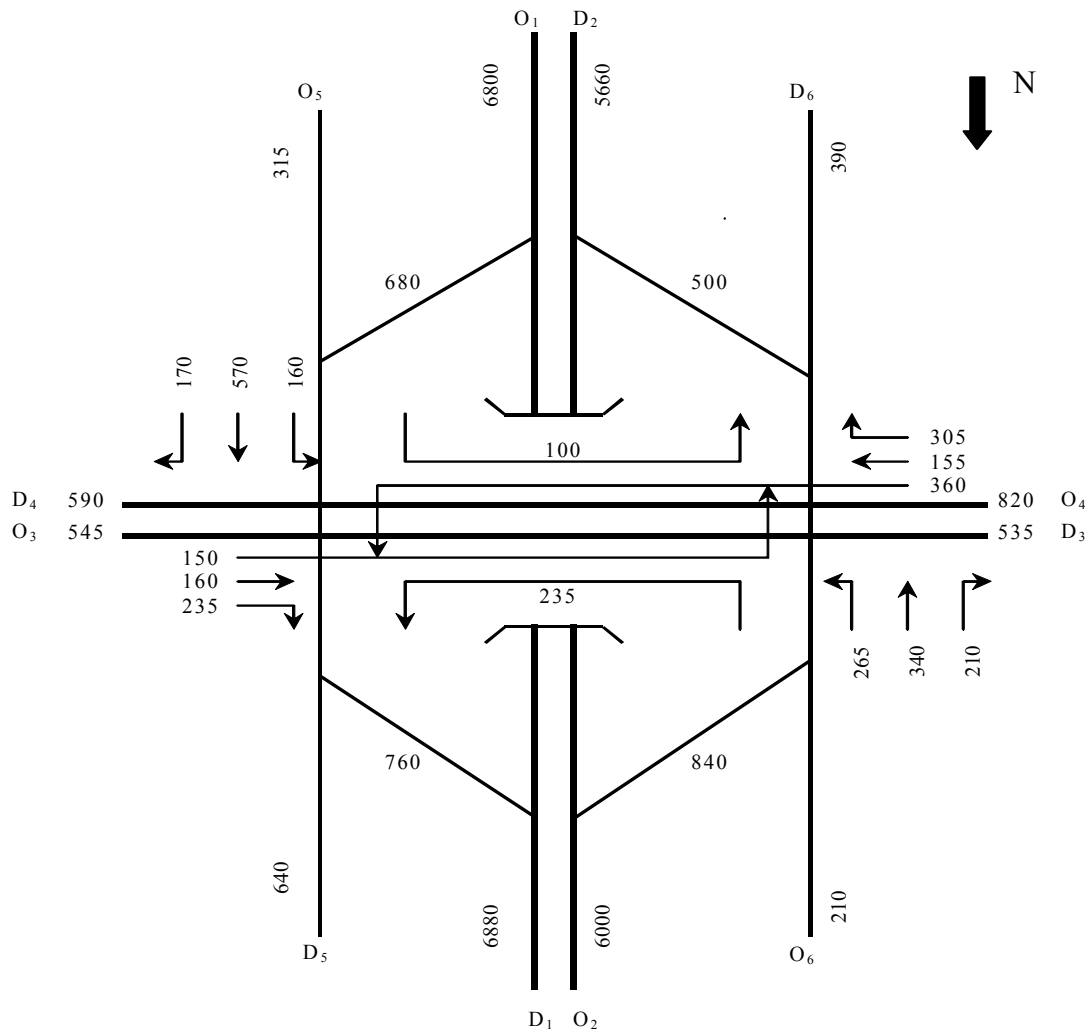
APPENDIX C

TRAFFIC DEMAND SCENARIOS



O/D	D1	D2	D3	D4	D5	D6	Total
O1	5833	0	130	130	324	65	6480
O2	0	4918	172	229	172	229	5720
O3	192	120	156	0	31	21	520
O4	296	250	0	148	47	39	780
O5	189	27	21	30	30	3	300
O6	44	82	30	24	6	14	200
Total	6555	5395	510	560	610	370	14000

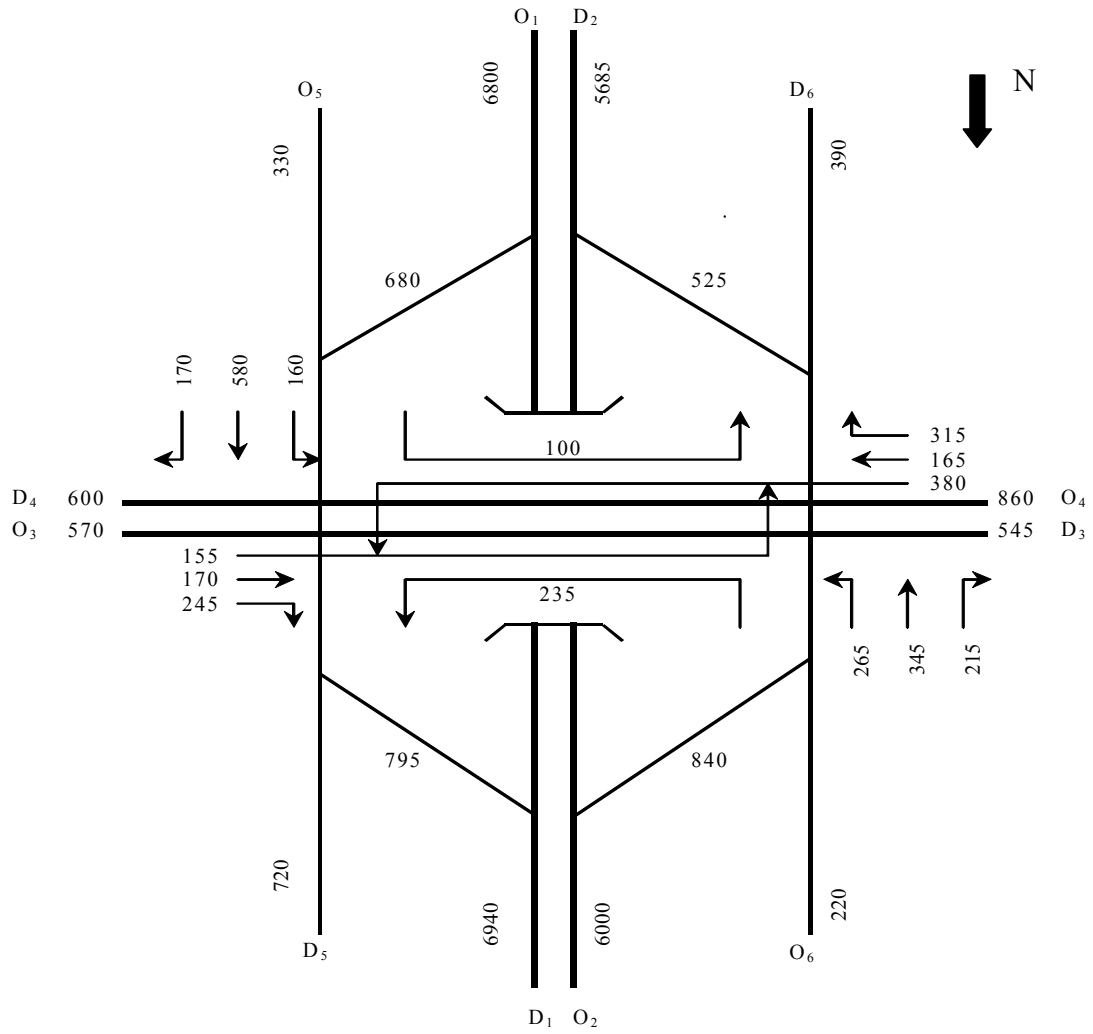
FIGURE 126 Low demand scenario.



O/D	D1	D2	D3	D4	D5	D6	Total
O1	6120	0	136	136	340	68	6800
O2	0	5160	180	240	180	240	6000
O3	202	126	164	0	33	22	545
O4	311	262	0	156	49	41	820
O5	198	28	22	32	32	3	315
O6	46	86	32	25	6	15	210
Total	6880	5660	535	590	640	390	14690

**FIGURE 127 Medium demand scenario.**





O/D	D1	D2	D3	D4	D5	D6	Total
O1	610	0	136	136	340	68	6800
O2	0	5160	180	240	180	240	6000
O3	212	132	172	0	34	23	570
O4	326	275	0	163	51	43	858
O5	208	30	23	33	33	3	330
O6	48	90	33	26	7	15	220
Total	6915	5685	545	600	645	390	14780

**FIGURE 128 High demand scenario.**

## APPENDIX D

### FUNCTIONAL DIAGRAMS OF THE ICS ALGORITHM

Functional diagrams provide detailed descriptions of the systems engineering process in functional terms, which are considered critical elements for implementing the proposed ICS in IDIRMS. Functional diagrams include the process of translating top-level system requirements into specific qualitative and quantitative design requirements. Figure 129 shows the top-level function diagram for the proposed ICS algorithm, and the lower-level function diagrams are depicted in Figure 130 through Figure 133.

The first function (Function 1.0) is to simply get and process the detector information. More specifically, the 20-second occupancy data are retrieved from the various detectors, including the ramp queue spillback detector, the intermediate queue detector, and the boundary queue detector. These detector occupancy values are compared with the predefined queue occupancy threshold (e.g., 60 percent) to determine whether a traffic queue exists at a particular detector location. Any occupancy exceeding the threshold value is considered to have the presence of a traffic queue. The reason for using occupancy instead of detector presence is that a traffic queue might be a moving queue such as in the case of ramp metering. Presence is also not a good indicator of traffic queues if the gaps between vehicles leave the detector unoccupied.

The second function (Function 2.0) is to determine whether integration control is needed. This is assessed based on the conditions of the traffic queues. To warrant the integration control, two conditions must be satisfied: (a) no queues exceed any boundary queue locations and (b) at least one ramp has detected a queue by the queue spillback detector. When the queuing conditions do not warrant integration control, the traffic signal and the ramp-metering signal remain in normal operations.

Top Level

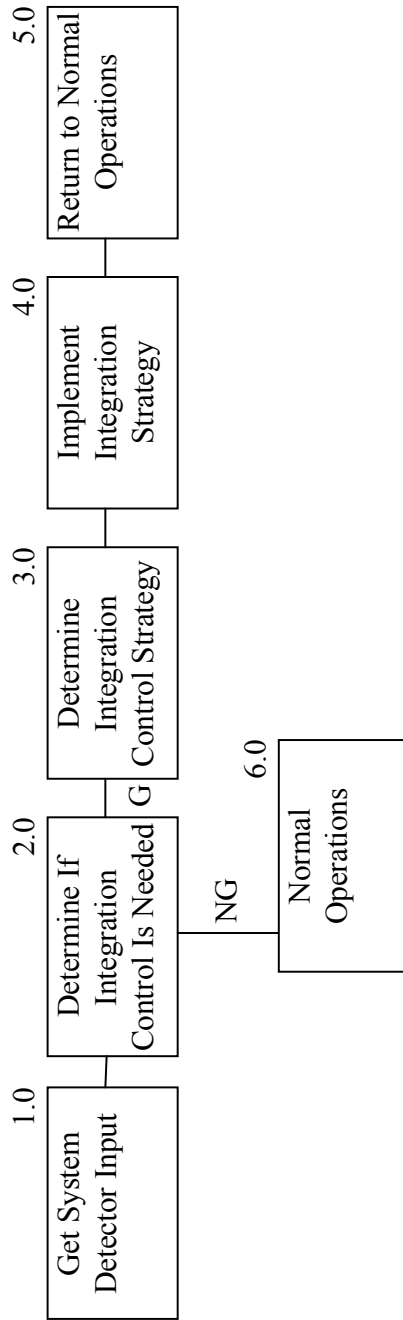
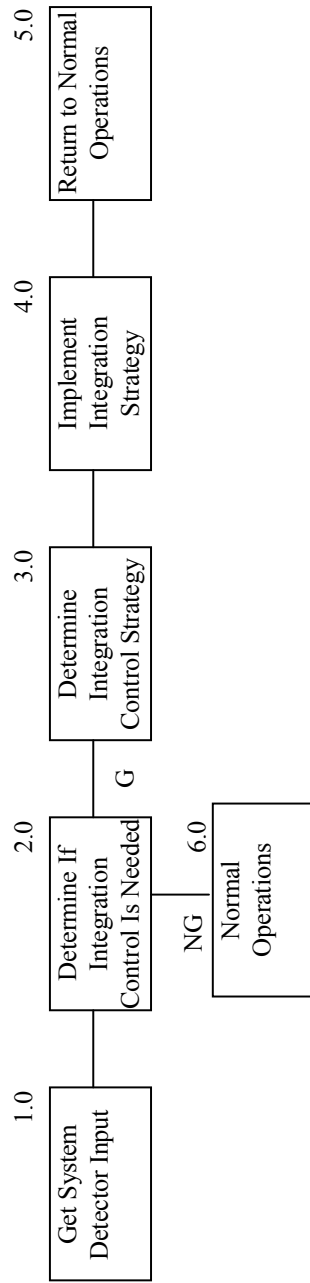


**FIGURE 129** Top level function diagram of proposed ICS algorithm.

Top Level



Second Level

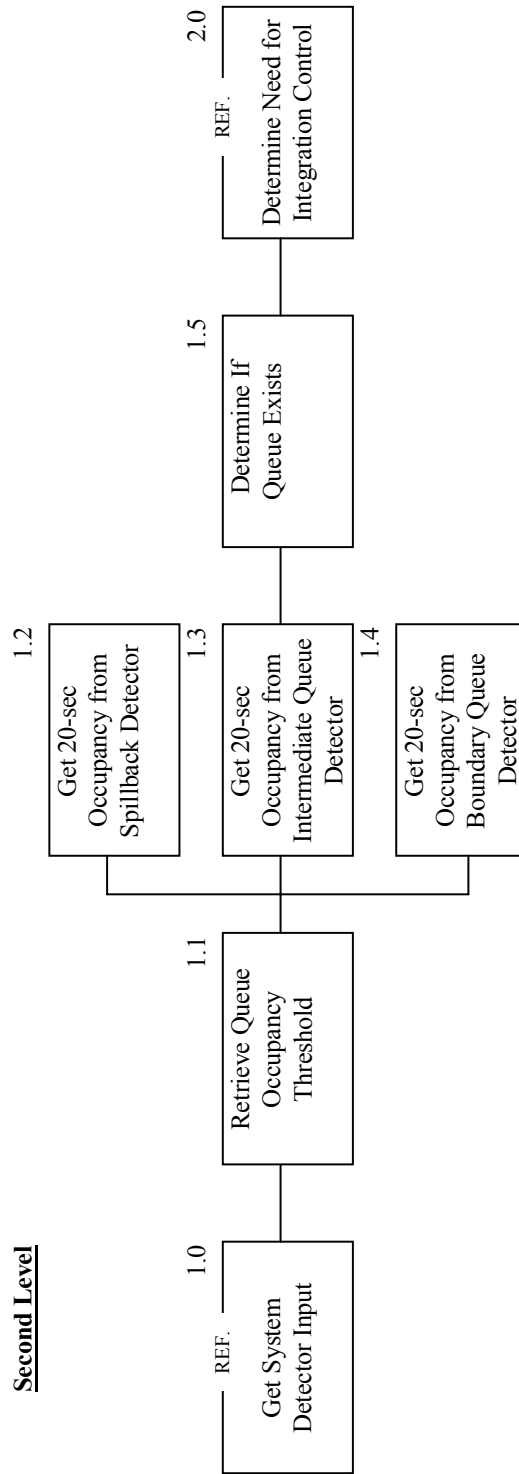


**FIGURE 130** Diagram of functions for getting and processing detector information.

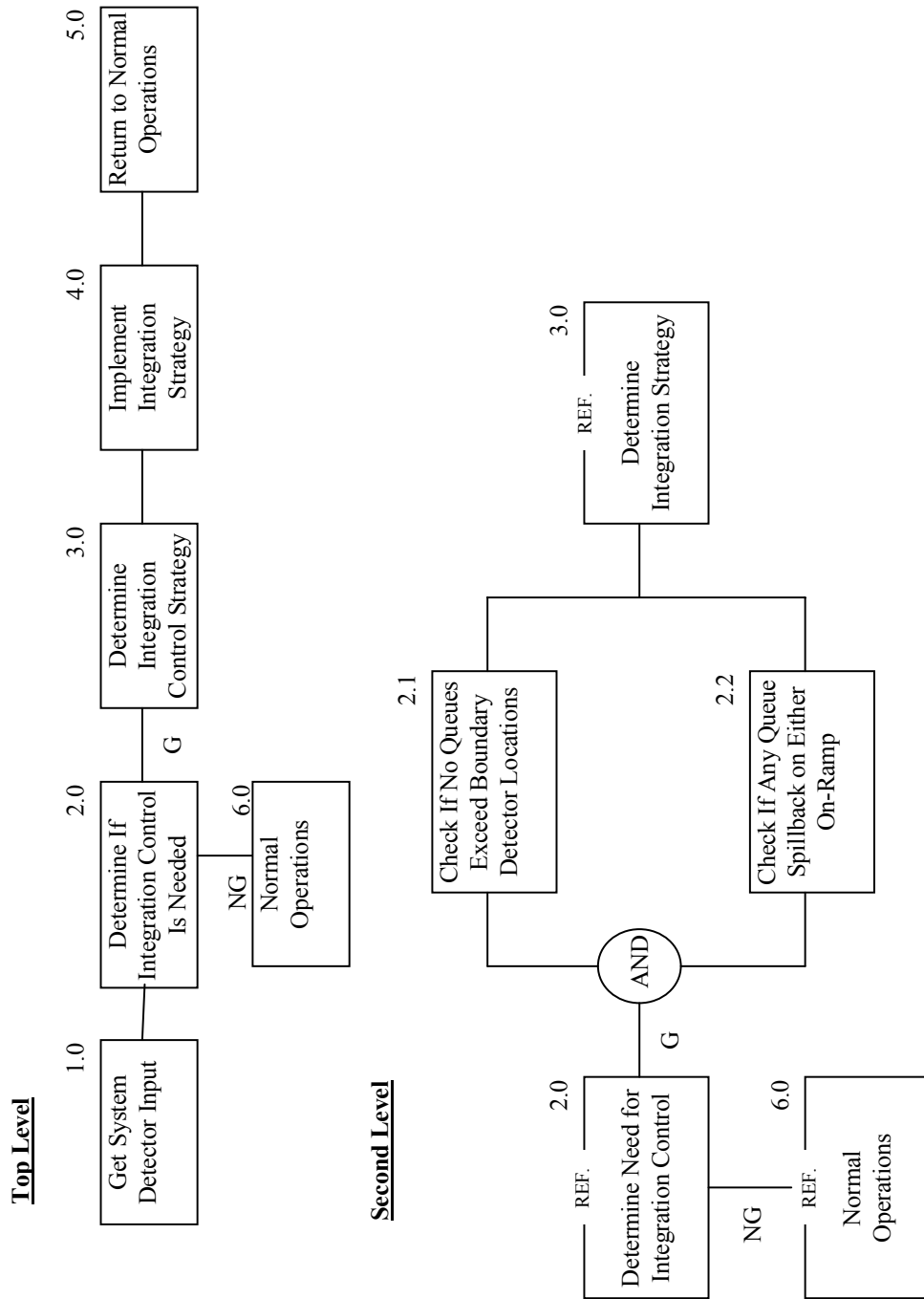


**FIGURE 131** Diagram of functions for determining need for integration control.

The third function (Function 3.0) is to determine what integration strategy should be implemented, i.e., which phase(s) need(s) to hold to control vehicles from further entering the ramp(s). Selection of the holding phase(s) is based on the queuing conditions at the intermediate queue detector locations and the diamond control mode. Details of the control logic have been depicted in the flow charts shown in Figure 91 and Figure 94.

The fourth function (Function 4.0) is to implement the control strategy, which involves the processes of signal transition between normal operation and integrated control as well as issuing appropriate commands to the diamond signal and the ramp-metering signal. Once the candidate phase(s) to hold has(have) been determined, the algorithm needs to retrieve the phase status from the diamond signal controller. The phase status should include parameters such as the minimum green times of each phase, the current phase, and the next phase. A force-off call or phase omit call may then be issued to terminate the current phase if it is not the candidate phase for holding, and either omit the following phases or allow minimum green times until transition to the holding phase(s) occurs. During the phase-holding period, the queuing conditions on the relevant queue detector locations are continuously monitored. When the conditions no longer satisfy the requirements for integrated operation, the phase holding will be terminated, and the diamond signal will return to normal operation. The ramp-metering signal will turn to queue flush mode if traffic queues are detected by any of the queue spillback detectors and traffic queues are detected by any of the boundary queue detectors.

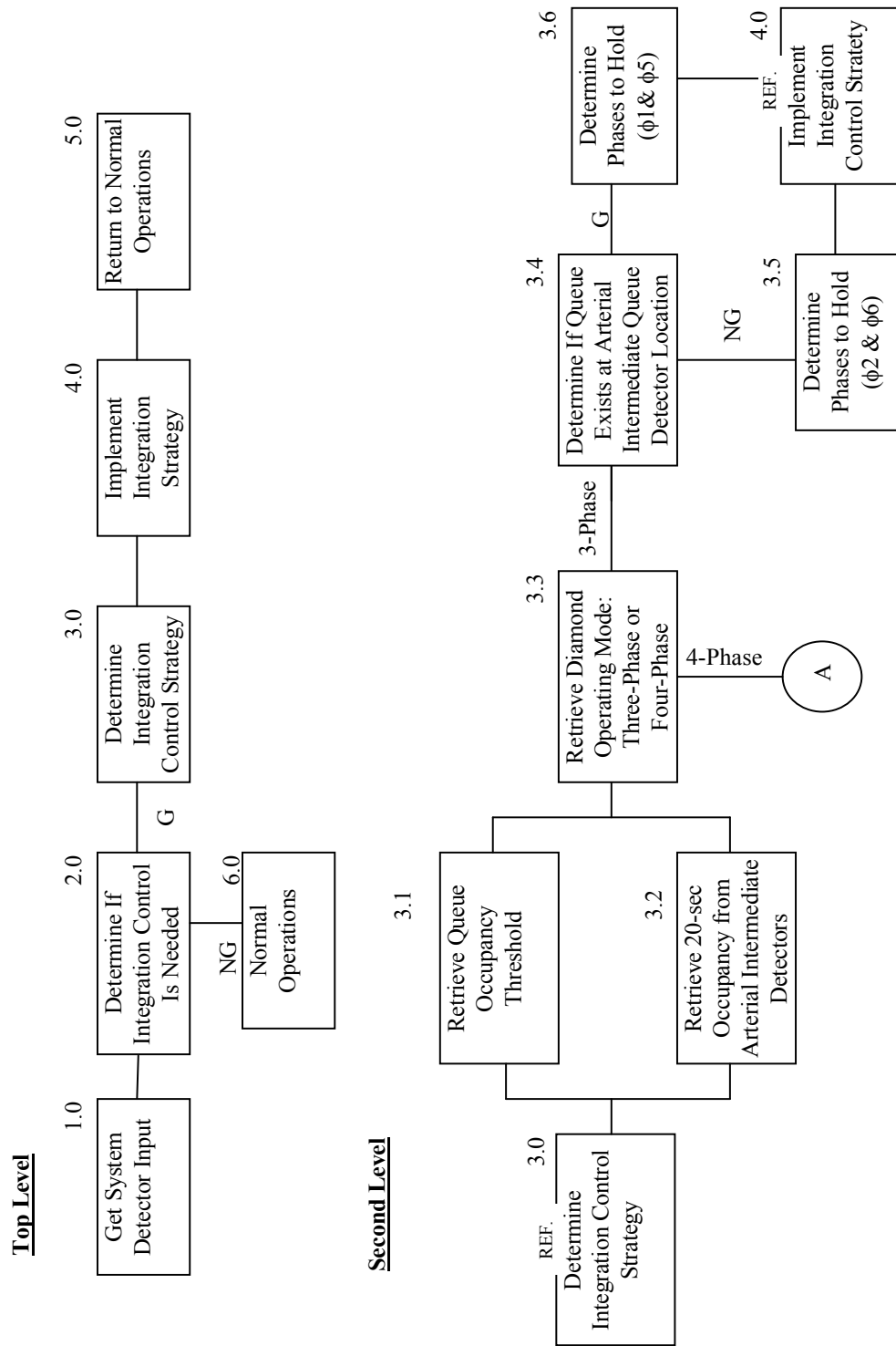


FIGURE 132 Diagram of functions for determining integration control strategy.

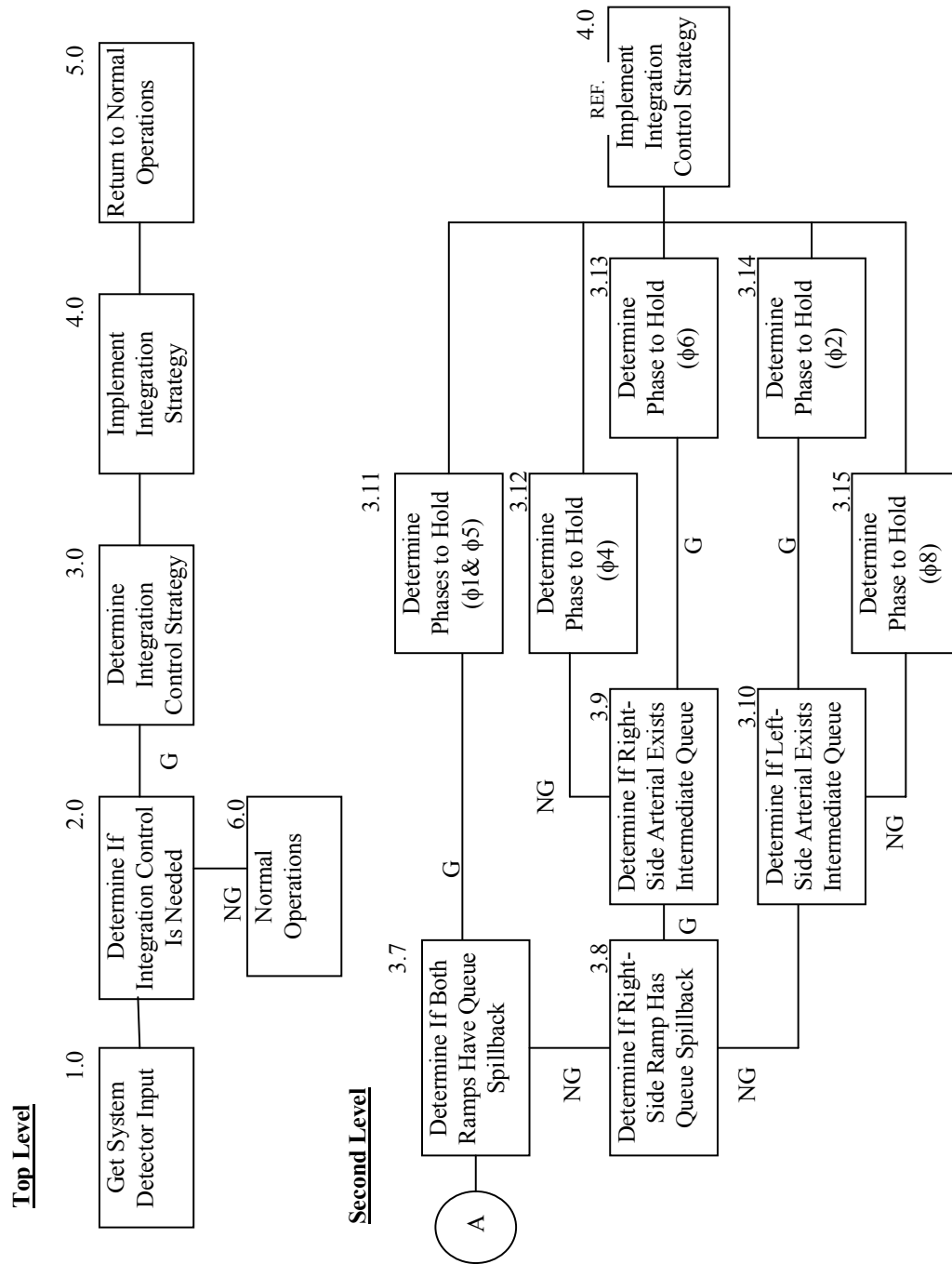


FIGURE 132 (Continued)



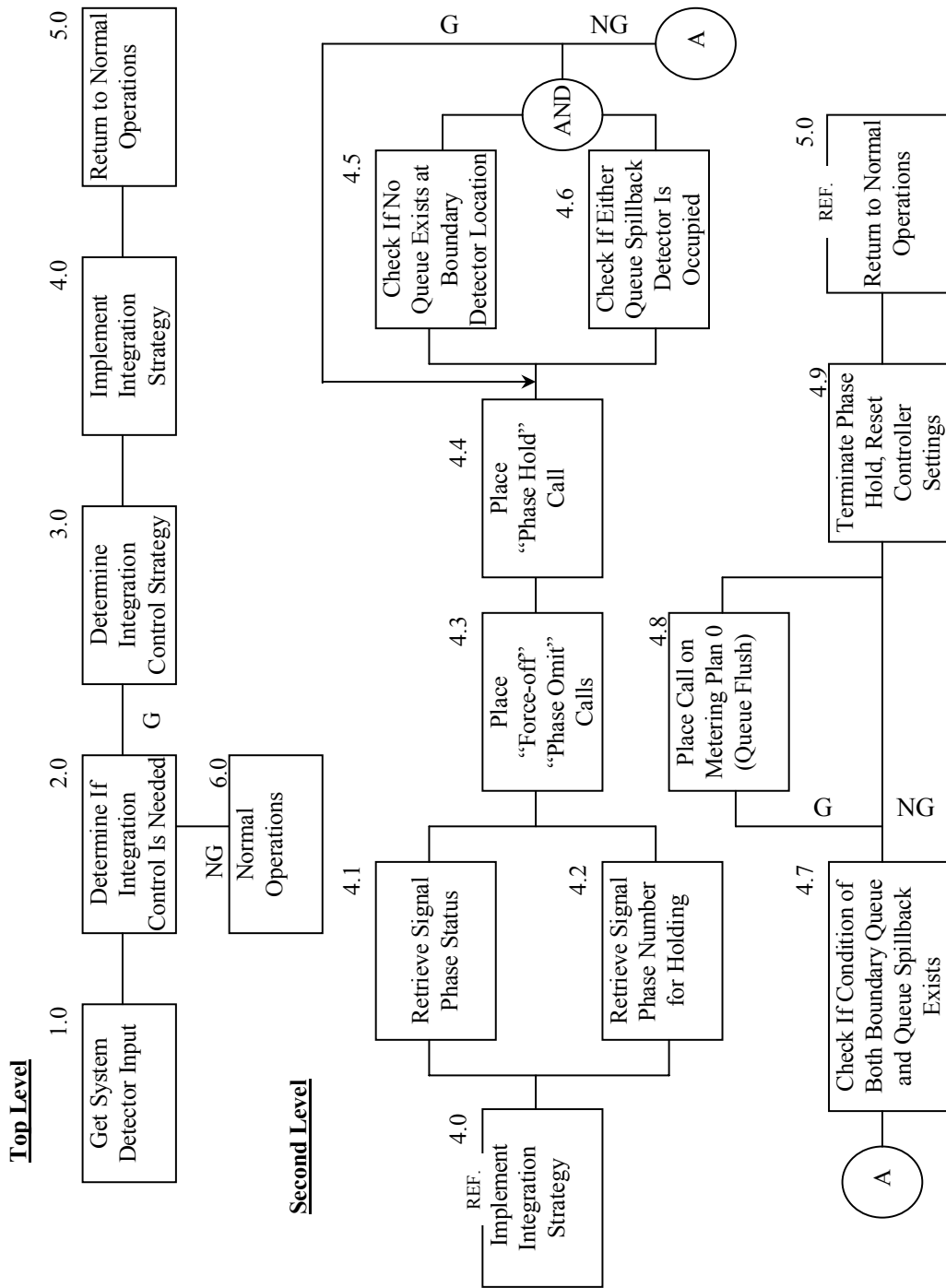


FIGURE 133 Diagram of functions for implementing integration strategy.

## VITA

The author of this dissertation, Mr. ZongZhong Tian, was born on August 24, 1962, in a rural village in China.

The author attended elementary school, middle school, and high school in Luan Nan County, Hebei Province, China, and graduated from Luan Nan High School in 1979. Mr. Tian attended Northern JiaoTong University (NJTU) in Beijing, China, and received a B.S. degree in 1983 and an M.S. degree in 1986 with majors in railroad engineering and operations. He was on the faculty at NJTU between 1986 and 1992.

Mr. Tian attended the University of Idaho and obtained an M.S. degree in 1996 with a major in transportation engineering. He worked at Kittelson & Associates, Inc., in Portland, Oregon, between 1995 and 1999 before joining the Texas Transportation Institute. He has been pursuing a Ph.D. degree in transportation engineering since 2000 in the Civil and Environmental Engineering Department at Texas A&M University.

Mr. Tian's permanent address is Gao Miao, LuanNan, Tangshan, Hebei Province, People's Republic of China, 063500.